FLUID POWER
FUTURE TECHNOLOGY!

CONFERENCE PROCEEDINGS

12.iFK

FLUID POWER

October
12 - 14, 2020
Dresden
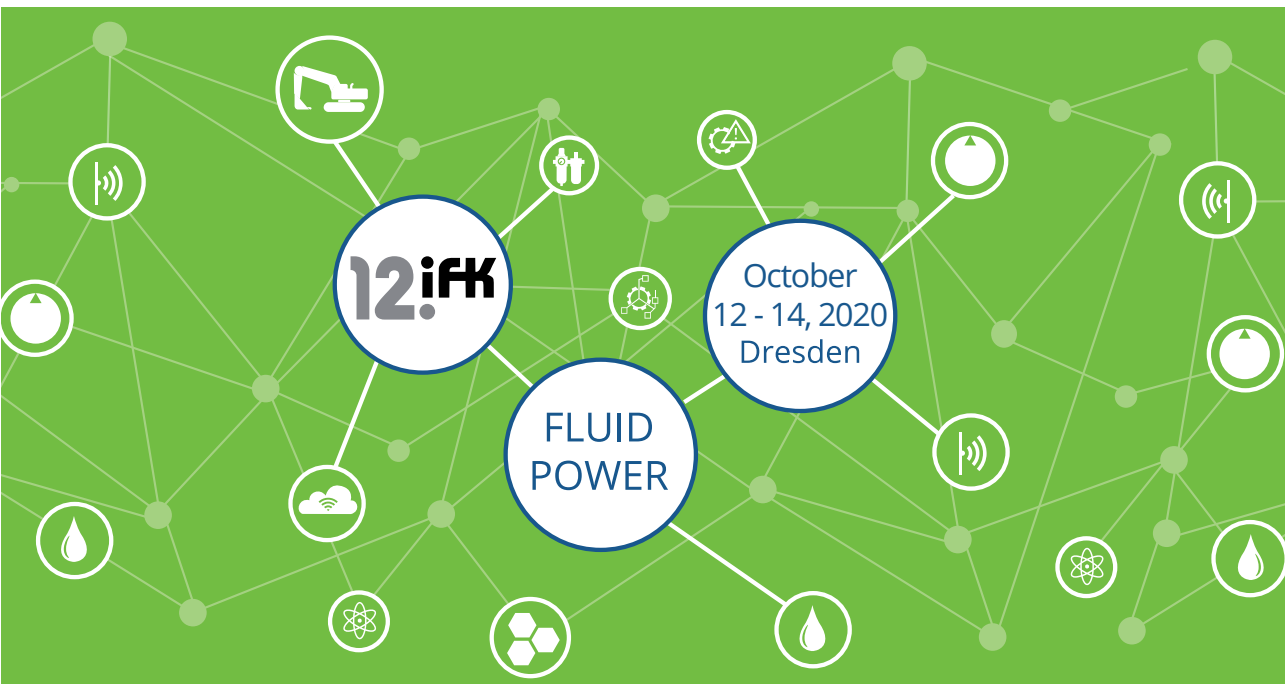
12th International Fluid Power Conference (12. IFK)

October 12 – 14, 2020

in Dresden

Volume 2 – Conference

Group 1 | 2:   **Digital systems**

Group 3:   **Novel displacement machines**

Group 4:   **Industrial applications**

Group 5:   **Components**

Group 6:   **Predictive maintenance**

Group 7:   **Electro-hydraulic actuators**

https://nbn-resolving.org/urn:nbn:de:bsz:14-qucosa2-386614

WELCOME TO THE 12TH IFK

Dear Sir or Madam,

we are pleased to present the conference proceedings for the 12th edition of the International Fluid Power Conference (IFK). The IFK is one of the world's most significant scientific conferences on fluid power control technology and systems. It offers a common platform for the presentation and discussion of trends and innovations to manufacturers, users and scientists.

The Chair of Fluid-Mechatronic Systems at the TU Dresden is organizing and hosting the IFK for the sixth time. Supporting hosts are the Fluid Power Association of the German Engineering Federation (VDMA), Dresdner Verein zur Förderung der Fluidtechnik e. V. (DVF) and GWT-TUD GmbH. The organization and the conference location alternates every two years between the Chair of Fluid-Mechatronic Systems in Dresden and the Institute for Fluid Power Drives and Systems in Aachen.

The symposium on the first day is dedicated to presentations focused on methodology and fundamental research. The two following conference days offer a wide variety of application and technology orientated papers about the latest state of the art in fluid power. It is this combination that makes the IFK a unique and excellent forum for the exchange of academic research and industrial application experience.

A simultaneously ongoing exhibition offers the possibility to get product information and to have individual talks with manufacturers.

The theme of the 12th IFK is "Fluid Power – Future Technology", covering topics that enable the development of 5G-ready, cost-efficient and demand-driven structures, as well as individual decentralized drives. Another topic is the real-time data exchange that allows the application of numerous predictive maintenance strategies, which will significantly increase the availability of fluid power systems and their elements and ensure their improved lifetime performance.

We create an atmosphere for casual exchange by offering a vast frame and cultural program. This includes a get-together, a conference banquet, laboratory festivities and some physical activities such as jogging in Dresden's old town.

I hope you enjoy reading the conference proceedings.

Prof. Dr.-Ing. Jürgen Weber

PROGRAM COMMITTEE

Achten, P.	Dr. ir., INNAS B.V., Breda NL
Bauer, F.	Dr.-Ing., Hydac Technology GmbH, Sulzbach/Saar
Boes, C.	Dr.-Ing., MOOG GmbH, Böblingen
Fabianek, M.	Dipl.-Ing., Liebherr Machines Bulle S.A., Bulle CH
Faß, U.	Dr.-Ing., Volvo Construction Equipment Germany GmbH, Konz
Fedde, T.	Dr.-Ing., CLAAS Tractor, Paderborn
Fiedler, M.	Dr.-Ing., Norgren GmbH, Fellbach
Fischer, M.	Dr.-Ing., Argo-Hytos Management + Consulting GmbH, Zug CH
Hahmann, W.	Dr.-Ing., Hydac International GmbH, Sulzbach/Saar
Hunger, I.	Lic. oec., Hunger DFE GmbH, Würzburg
Huster, G.	Dipl.-Ing., KraussMaffei Technologies GmbH, München
Igelhorst, W.	Dipl.-Ing., SMS Group, Mülheim an der Ruhr
Jähne, H.	Dr.-Ing., Hydrive Engineering GmbH, Freital
Kempermann, C.	Dr.-Ing., Fluitronics GmbH, Krefeld
Klug, D.	Dr.-Ing., Schuler Pressen GmbH, Waghäusel
Knobloch, M.	Dipl.-Ing., HAWE Hydraulik SE, München
Krallmann, J.	Dr.-Ing., Thomas Magnete GmbH, Herdorf
Krieg, M.	Dr.-Ing., Bosch Rexroth AG, Lohr am Main
Langen, A.	Dr.-Ing., Linde Hydraulics GmbH & Co. KG, Aschaffenburg
Legner, J.	Dipl.-Ing., ZF Friedrichshafen AG, Friedrichshafen
Leonhard, A.	Dr.-Ing., Parker Hannifin Manufacturing Germany GmbH & Co. KG, Chemnitz
Lindemann, L.	Dr., Fuchs Petrolub SE, Mannheim
Luther, R.	Dipl.-Ing., Fuchs Schmierstoffe GmbH, Mannheim
Lüüs, H.	Dipl.-Ing., Bucher Hydraulics GmbH, Klettgau
Martens, O.	Dr.-Ing., KOMATSU Mining Germany GmbH, Düsseldorf
Mundry, S.	Dr.-Ing., Caterpillar Global Mining Europe GmbH, Lünen
Neumeier, R.	Dipl.-Ing., Bürkert Werke GmbH, Ingelfingen
Pfab, H.	Dr.-Ing., Liebherr-Werk Bischofshofen GmbH, Bischofshofen AUT
Post, P.	Prof. Dr.-Ing., Festo AG & Co. KG, Esslingen
Rahmfeld, R.	Dr.-Ing., Danfoss Power Solutions GmbH & Co. OHG, Hamburg
Saffe, P.	Dr.-Ing., Aventics GmbH, Laatzen
Schmitz, K.	Prof. Dr.-Ing., RWTH Aachen
Schultz, A.	Dr.-Ing., Magnet-Schultz GmbH & Co. KG, Memmingen
Tappe, P.	Dr.-Ing., Magnet-Schultz GmbH & Co. KG, Memmingen
Sondermann, G.	Dipl.-Ing., Siempelkamp Maschinen- und Anlagenbau GmbH & Co. KG, Krefeld
Synek, P.	Dipl.-Ing., Fachverband Fluidtechnik im VDMA, Frankfurt am Main
Weber, J.	Prof. Dr.-Ing., TU Dresden

INTERNATIONAL ADVISORY COMMITTEE

Professor Eric Bideaux
INSA de Lyon, France

Professor Kalevi Huhtala
Tampere University of Technology, Finland

Professor Petter Krus
Lingköping University, Sweden

Professor Andrew Plummer
University of Bath, United Kingdom

Professor Kazushi Sanada
Yokohama National University, Japan

Professor Rudolf Scheidl
Johannes Kepler University Linz, Austria

Professor Kim Stelson
University of Minnesota, USA

Professor Huayong Yang
Zhejiang University, China

Professor Andrea Vacca
Purdue University, USA

Professor Takao Nishiumi
Shibaura Institute of Technology, Japan

PEER REVIEW AT THE 12TH IFK

peer reviewed

Many public institutions that support research projects require regular publication of the results. To ensure that the results are of scientific value, peer review is often required. Therefore we offer all authors the opportunity to have their work evaluated in order to be able to prove the scientific value.

A paper that has been chosen by the author to be reviewed will be subjected to an independent examination by a total of three specialized experts among the Program Committee as well as the Institute of Mechatronic Engineering at the TU Dresden, or the Institute for Fluid Power Drives and Systems at RWTH Aachen University. After this initial evaluation, the authors have the opportunity to revise their paper as needed and resubmit it with the necessary changes. If the reviewers accept the changes, the paper will be included in the conference proceedings as peer reviewed.

This extensive assessment process serves the purpose of quality assurance in terms of content and form, and would not have been possible without the expert support of the Program Committee. The organizers of the IFK want to thank all reviewers for their support.

The IFK traditionally is a colloquium where both scientists and representatives of industry come together to exchange their knowledge and experience. Accordingly, a peer review is only meaningful for some of the speakers, with the associated additional effort for both sides. Therefore the peer review is not intended to classify the paper but rather to support the need for it.

GROUP 1 | 2
Digital systems

GROUP 3
Novel displacemant machines

GROUP 4
Industrial applications

GROUP 5
Components

GROUP 6
Predictive maintenance

GROUP 7
Electro-hydraulic actuators

GROUP 1 | 2

Digital systems

GENERAL LECTURE:

DIGITAL MOBILE MACHINES – FROM CLOUD TO EARTH

Jürgen Weber

Institute of Mechatronic Engineering, Technische Universität Dresden, Helmholtzstrasse 7a, 01069 Dresden
* Corresponding author: Tel.: +49 351 46333559; E-mail address: fluidtronik@mailbox-tu-dresden.de

The term „industry 4.0" describes the transition from a classic value-added chain to dynamic value-added networks. It is driven by four main design principles:

- interconnection of machines and humans
- information transparency
- technical assistance to support humans
- decentralized decisions

This approach and its connected technologies, like IoT or cloud computing, enhance in the context of industrial production further flexibility and an increase in productivity through growing self-organisation and interlocking with logistics and planning processes. Extensive activities can be recorded in this field.

Construction processes and the associated operations and logistics differ fundamentally from the conditions concerning industrial goods production. In a complex, locally and temporally changing environment, a large number of individual contractors, which are characterised by a diverse and inhomogeneous use of technology, act in a collaborative way. The unique character of construction projects, the massive fragmentation of the construction industry and the lack of standardized interfaces for the documentation and coordination of the current construction process mean that huge efficiency and quality potentials remain unused under classical conditions.

A powerful wireless communication based on 5G enables for the first time the consistent, digital mapping of all construction processes and participants due to massive availability of real-time information, which had not been possible with previous wireless communication and its technical restrictions. At the same time, 5G can act as an anchor of common standards for a heterogeneous building landscape. As a result, the construction progress becomes transparent for all involved parties. This is a prerequisite and basis for future automation and assistance systems, which will enable humans to act efficiently in a highly digital, self-organizing environment.

Increasing the efficiency of construction processes, especially concerning the handling of mobile machinery, requires extensive support from assistance systems. The increasing integration of planning and process data via suitable communication channels and the trend towards electrohydraulic control systems open up the potential for innovative assistance and automation solutions. Manufacturers and suppliers of mobile working machines and work equipment are now confronted with new, partly unexplored technological topics. In addition to

automatable, interlinked mobile machinery

sensor technology
assistance systems
automation
remote handling
digital twins of mobile machinery

5G maschine and construction site networking

cloud solutions
distributed intelligence
reliable & secure exchange of data

digital construction site

logistics, data
remote management
environment recognition systems
digital twins of construction processes

the development and adaptation of algorithms of mobile robotics, drive technology has to be refined in an appropriate way.

Against this background, the so-called digital twin is of central importance. In the field of digitalization of the construction site and its running processes, the construction project is represented as a digital twin, which allows the holistic simulation-based optimization of the process sequence. By mirroring the construction progress, the digital twin leads to transparency regarding adherence to schedules as well as in quality management and in case of unplanned process changes, it enables the evaluation of suitable, alternative construction process and workflow scenarios. The digital twin of the construction project is also a prerequisite for efficient interactions of all involved construction site actors.

This inevitably results in the necessity of digital twins of all the mobile working machines involved in the construction process, the mutual exchange of desired trajectories as well as the achieved work progress. The specific machine characteristics with regard to kinematics, loads, wear condition, thermal budget, degree of automation, suitability for attachment, which are represented in the digital twin of the mobile machinery, enable transparency and decision possibilities for necessary maintenance and repair cycles as well as for expected efficiency and quality.

The requirement or availability of digital twins has to be transferred in a hierarchical way to subsystems and components of the drive and control systems as well as to the attachment of the construction machines or leads automatically to comparable potentials and increasing knowledge for the components and supplier industry.

What all digital twins have in common is the necessity of highly developed, robust and secure communication technologies, which meet the requirements of low latencies for safety-relevant real-time applications, such as remote handling of mobile machinery in imponderable terrain.

Therefore, the survey lecture will highlight the diversity, hierarchy and some exemplary potentials of digital twins suited for mobile machinery. Furthermore, particularly significant use cases will be illustrated.

GENERAL LECTURE:

INDUSTRIAL HYDRAULICS: NOW – NEXT - BEYOND

Dr. Steffen Haack*, Dr. Mark C. Krieg

Bosch Rexroth AG, 97816 Lohr am Main, Germany
* Corresponding author: E-mail address: steffen.haack@boschrexroth.de

Industrial hydraulics is often perceived as an old fashioned technology at the end of its innovation cyle. Despite its indiscussable technical benefits as well as its economical importance it is not seen as a promising future technology so that influencing people like to talk about and to promote. This results in disadvantages when it comes to customer choices comparing solutions, bidding processes, and – maybe most important – in a difficult position concerning the war for talents in the long run.

Partly, this situation is even home-made. For decades hydraulic people have told others how complicated industrial hydraulics are with its "hydraulic computers" made out of orifices, adjusting screws and that expert knowledge is needed to set it up and to maintain it. Even if that may be true – and of course there are challenges – it should be the job of all hydraulic people to make industrials hydraulics as easy as possible to configure, to buy, to set-up, to use as well as to maintain, repair and overhaul.

The challenges for industrial hydraulics are widespread. There are traditional challenges such as energy efficiency, environmental demands concerning material, oil, noise and, of course, safety related issues overlaying everything. New challenges are functional integration and especially the field of digitalization which offers multiple opportunities for additional digital service along the life cycle for both machine builders and end-users.

Depending on the requirements, products themselves will have everything from simple digital interfaces (e.g. IO-Link) to real-time-capable multi-Ethernet connections. Uniform standards such as OPC-UA and TSN will come and change the existing ones. Another upcoming technology is 5G communication. Its impact on industrial hydraulics is not clear yet, however due to the performance step in e.g. latency new topologies and services are possible.

Coming to digital services and ease of use, industrial hydraulic users are increasingly expecting the same level of convenience they are accustomed to from the "IT consumer world". This applies to the complete customer journey, from design via commissioning and production to maintenance.

Configurators, digital twin including product lifecycle management (PLM) will make selection and sizing process easier or even automated dependent on the customers' needs. Virtual commissioning allows plug and produce and - if required at all - start-up wizards and autotuning algorithms reduce the on-site efforts to a minimum. The production in general is characterized by small batches with different requirements. Here online parameter adjusting of the industrial hydraulic equipment either via industrial Ethernet or Bluetooth offer opportunities for the end-users facing changing customer demands on short notice.

Continuous condition monitoring and predictive analysis reduces unplanned downtime. Digital service assistants and globally available AR supported remote services helps to keep high productivity if maintenance or repair is needed even for the robust and long lasting industrial hydraulics components and systems.

GENERAL LECTURE:

DIGITIZATION OF THE HYDRAULICS -
UNIFORM SEMANTICS ONLY ALLOWS INTEROPERABILITY

Martin Hankel

Bosch Rexroth AG, 97816 Lohr am Main, Germany
E mail: Martin.Hankel@boschrexroth.de

Machine builder integrate products from different suppliers in their machines or production lines. Today, most of the information is supplier-specific. The major challenge is to extract the necessary information from all products from different suppliers. The information exchange is over the complete lifecycle of the machine from design, simulation, installation, operation and service phase.

At least, every supplier needs a Product Lifecycle Management from which he can manage the Digital Product Twins and produce the standardized data for the different lifecycle phases in machines.

The Industrie 4.0 Platform has defined two models. The Reference Architecture Model Industry 4.0 (RAMI4.0) and the Industry 4.0 component with its Administration Shell. They describes the important fields of action for identification, communication and for semantics. Both models describe a common language with vocabulary and structuring of the data to get an open exchange across the industry. Currently various working groups at national and international level are specifying this vocabulary for the various product groups and bring them into standardization.

This lecture shows the challenges, the current state of implementation, gives hints specifically for the implementation of the fluid technology and shows some opportunities for new services. (Sizing, Digital Nameplate, Product Dashboards, Oscilloscope)

Digitization hydraulics - Uniform semantics only allows interoperability
Important Topics for Industrie 4.0
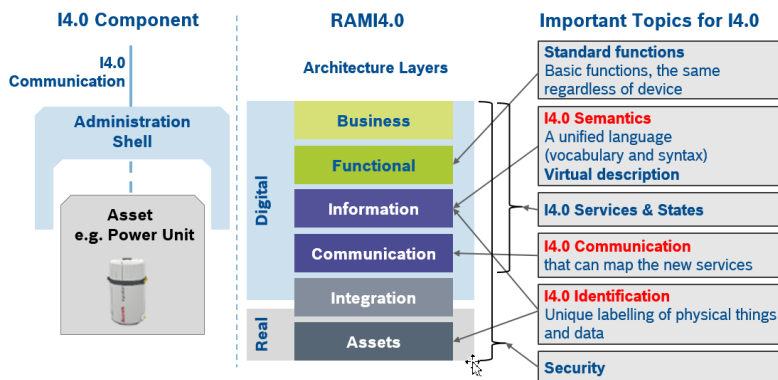
INTEROPERABLE INFORMATION MODEL OF A PNEUMATIC HANDLING SYSTEM FOR PLUG-AND-PRODUCE

Raphael Alt[1]*, Peter Wintersohle[1], Hartmut Schweizer[2],
Martin Wollschlaeger[2], Katharina Schmitz[1]

1: Institute for Fluid Power Drives and Systems, RWTH-Aachen University, Campus-Boulevard 30, 52074 Aachen
2: Institute for Applied Computer Science, TU Dresden, Nöthnitzer Str. 43, 01187 Dresden
* Corresponding author: Tel.: +49 241 80 47729; E-mail address: raphael.alt@ifas.rwth-aachen.de

ABSTRACT

Commissioning of a machine is still representing a very challenging operation and most steps are still executed manually by commissioning engineers. A future goal is to support the commissioning engineers and further automate the entire integration process of a newly installed system with a minimum of manual effort. This use case is known as plug-and-produce (PnP). In this contribution a concept of the Industrial Internet of Things is presented to improve the commissioning task for a pneumatic handling system. The system is based on a service-oriented architecture. Within this context, information models are developed to meet the requirements of PnP to provide relevant information via virtual representations, e.g. the asset administration shell, of the components to the commissioning process. Finally, a draft of the entire PnP process is shown, providing a general understanding of Industrial Internet of Things fluid power systems.

Keywords: IIoT, Plug-and-Produce, Pneumatic, Interoperability, Industry 4.0, Service-oriented architecture, Orchestration, Commissioning

1. INTRODUCTION

"Industrie 4.0" (I4.0) represents an initiative, introduced by the German government to maintain the competitiveness of the manufacturing industry in 2011 [1]. In this context, classical production systems are enhanced by new Information and Communication Technologies (ICT) to increase the productivity, flexibility and efficiency as well as enabling new digital and thus scalable business models to raise the profitability of the manufacturing sector [2]. Internationally, similar concepts are known under the expression Industrial Internet of Things (IIoT). [3]

Pneumatic fluid power systems state an important role in many automation lines. Handling and Pick-and-Place systems for example, which are usually built-in in an automation line, can contain several pneumatic rotational and linear actuators as well as grippers. The commissioning process of such automation lines, which includes the integration of the pneumatic system, is still posing a challenging operation. For the first time in a product life cycle, various subsystems of different domains and manufacturers need to work together in a machine. Due to the vast variety of different system configurations and the occurrence of unforeseen events, the commissioning represents an error-prone and complex task that is mostly executed manually by specialized commissioning engineers (CE) today. This makes the process time-consuming and costly. [4, 5]

Increasing international competition and changing market trends require to reconsider the requirements of commissioning with regard to economical and technical aspects. The current trends, like manufacturing individual products at low costs (mass customization), shortening of product life cycles, demands for effective maintenance, higher functionality and higher reliability of machines, all result in an increasing complexity of automation lines as well as frequent reconfigurations to continuously meet the changing requirements [3, 6]. Consequently, due to recurrent setups and reconfigurations of machines during lifetime, the economic importance of the commissioning process becomes more important in the product life cycle.

Additionally, the rising complexity of the machines challenges and overwhelms the CE. Assistant systems can support the personnel to a certain point [7], but an almost entirely automated commissioning process states the desired goal to meet the upcoming market demands.

Such a system requires two elements. First and for most, it requires a framework to provide and process knowledge about the commissioning of the system in order to derive steps that need to be performed. The automated sequencing of tasks is known as orchestration and is based on a semantic and interoperable information structure for the pneumatic systems that can be interpreted by different ICTs. This aspect will be focused in this contribution. Secondly, the system requires actuators to perform the required commissioning steps to fully automate the process. Here, many different solutions, depending on the component can be realized by the manufacturers. [8]

In this contribution, an approach based on concepts of distributed systems (e.g. the internet) is developed and modified to fit industrial applications in order to support the commissioning of a pneumatic handling system. This use-case is known as "Plug-and-Play", "Plug-and-Produce" (PnP) or "Plug-and-Work" [4].

After presenting the commissioning of the pneumatic handling demonstrator, the main aspects are identified, which need to be reflected by an automated assistant system. Basic elements of an IIoT system are introduced in general. As one important element, a virtual representation, serving as an information model for the commissioning of the pneumatic system, is derived. Based on that, a draft for the orchestration process is given. Finally, the implementation at the demonstrator represents a prove of concept and provides a general understanding of the main aspects of IIoT systems and its implications to the automated integration of fluid power devices.

2. COMMISSIONING OF A PNEUMATIC HANDLING SYSTEM

A pneumatic reference system is used to analyze the commissioning. It consists of a pneumatic handling system, a valve terminal and a pressure supply. As an example pneumatic handling systems are used in industrial packaging systems.

Figure 1 depicts the pneumatic handling system in detail.
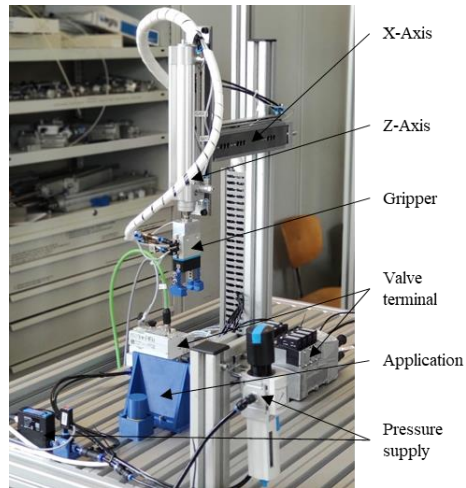
Figure 1:   Pneumatic handling system

The pneumatic handling system consist of three pneumatic actuators: x-axis, z-axis and a gripper. Each axis consists of a pneumatic drive which can be further subdivided into a linear pneumatic cylinder and two end position sensors. The pressure supply consists of a constant pressure source, a pressure sensor, a mass flow sensor and a manually adjustable pressure regulating valve. The system is operated via a programmable logic controller. This controller provides the sensor signals and functions of all the installed system components.

The commissioning of pneumatic systems is a complicated process, consisting of different commissioning tasks, which start after the completion of its assembly. The assembling and the commissioning are often executed by different people. Consequently, the CE needs detailed information on the system such as a system overview, a pneumatic circuit diagram and individual datasheets of its components. The CE derives an individual commissioning procedure depending on the structure of the pneumatic system and its components. Furthermore, the CE needs to identify and solve problems that result from the assembly process and ones that occur unforeseen during the commissioning. Therefore, expert knowledge is required to safely conduct the commissioning process.

Analysing the commissioning of the reference system shows that the commissioning process of a pneumatic systems can be divided into three sequential phases. During the first phase of commissioning the pneumatic system is unpressurised. All commissioning activities during this phase have the objective to put the system into a fail-safe state to avoid critical errors when the system gets pressurised later on. These activities include gathering information and visual inspection of the components. The pneumatic circuit scheme provides an overview of all components and their interactions. After checking all sensor signals for plausibility, the pneumatic end position dampers and throttle check-valves are adjusted according to the manufacturer specifications. The next phase begins via adjusting the pressure regulation valve of the power supply to an overall system minimum pressure level. The pressure level is chosen based on the required minimum pressure to safely operate relevant components to avoid severe collisions and damage resulting from uncontrolled movements of the system. All sensors are checked repeatedly to ensure valid values, followed by various tests regarding pneumatic functions. The tests include the switching of all valves and checking for the correct movements of the intended actuators and the sequence of the working cycle. The third commissioning phase starts by setting the system pressure to the intended operating level. In this phase, the cycle-times of the actuators are set via adjusting the throttle check-valves. After the pneumatic end position damping is tuned correctly, the system performs an entire working cycle to ensure correct interactions with other modules of the automation line. With the successful completion of all tasks, the system is commissioned and ready to operate. The analysis of the commissioning process shows that it can be time-consuming, prone to errors and thus specialist knowledge is indispensable.

Summarizing, the commissioning process can be divided into three different phases according to the pressure level: unpressurized, low pressure and operating pressure. This serves as a general frame for the CE or an automated system to sort specific system and component commissioning activities. To do so, both must be aware of all the required tasks, their correct sequential order and the corresponding relevant parameters.

3. BASIC ELEMENTS OF IIOT SYSTEMS

The concepts of the Internet of Things (IoT) in general as well as the IIoT in specific originate from the field of distributed systems. In contrast to classical systems, which are controlled via hierarchical and centralized patterns (e.g. automation pyramid), they consist of different collaborating assets to solve a task in a more flexible way. To do so, the individual assets offer encapsulated functionalities, which can easily be used by other system participants. The so-called services can then be combined to solve different system tasks. The process of combining services in such a service-oriented architecture (SOA) is called orchestration and represents a key element of IIoT systems.

The SOA leads to implications for the assets, as shown for a pneumatic component in **figure 2**. The smart IIoT component consists of the real object, combining the former proprietary hard- and firmware of the pneumatic asset. In addition, the real object is enhanced by the following aspects, building the virtual representation of the asset.
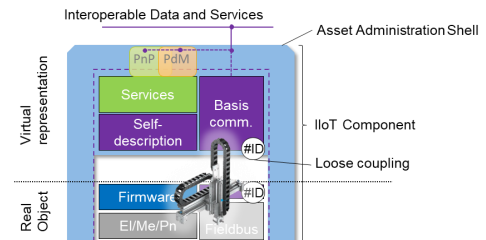
Figure 2: IIoT component using the AAS, after [3]

Services: Encapsulated functionalities of the asset to facilitate the usage for other system participants. Only inputs and outputs of the service interfaces are known and provided externally. The internal function remains untouched and resembles as a black box for the user.

Self-description: Part of an information model and provides data and information to other system participants about its identification, properties and functions. Additionally, it contains relevant aspects of different use-case scenarios, e.g. PnP or predictive maintenance (PdM).

Basic communication and interoperability: To collaborate system-wide, every IIoT component requires an open communication that is independent on proprietary and physical

communication interfaces (e.g. OPC UA, MQTT). Additionally, the broadcasted data needs to be interpreted correctly by every other interacting system participant. Thus, standardization and semantic description of data and information enables system-wide interoperability.

The asset administration shell (AAS) represents a concept to combine the mentioned aspects of the virtual representation in order to enable a consistent interaction of all different kinds of assets and thus to integrate them into an IIoT system. [9, 10, 11]

4. INFORMATION MODEL OF THE PNEUMATIC IIOT COMPONENT

The pneumatic IIoT component consists of the asset (physical pneumatic component) and the corresponding virtual representation, the asset administration shell (AAS). All relevant information and real-time data of the components are represented via properties within the AAS. Properties are grouped according to their objectives and assigned to a submodel. To ensure interoperability to a certain part, submodels and properties are currently defined by different industrial associations. [12]

Figure 3 shows a class diagram of the AAS for a pneumatic drive. The depicted class diagram focuses only relevant aspects for PnP of the corresponding asset. Submodels, which are relevant for other parts in the component's

lifecycle, e.g. condition monitoring, can be added to the existing model.

The submodel 'AssetIdentification' includes properties to identify the asset like the asset identifier and other unique identifiers such as the manufacturers name and serial number. These properties are used to find the AAS inside a digital network. Properties that describe the technical aspects of the asset are assigned to the submodel 'Datasheet'. It resembles a standardized digital version of today's existing datasheets and can be used to further derive more information. For example, the cylinder's velocity can be derived using the cylinder's stroke and the switching-time of the end position switches. Properties of the operational phase are assigned to the submodel 'Operating'. In contrast to properties of the datasheet, they can vary with time and reflect the current state of the component. For example, the current cycle times of the drive can be measured and compared to the target cycle times, which were set beforehand during the engineering phase of the system.

The submodel 'Topology' contains properties to reflect different kinds of dependencies of the assets in the system. The different topologies can give functional, structural, fluidic, electric, business and other views on the system. In this case, a functional and a fluidic view are focused for the commissioning process. The fluid power topology describes the airflow through the pneumatic system similar to the pneumatic circuit
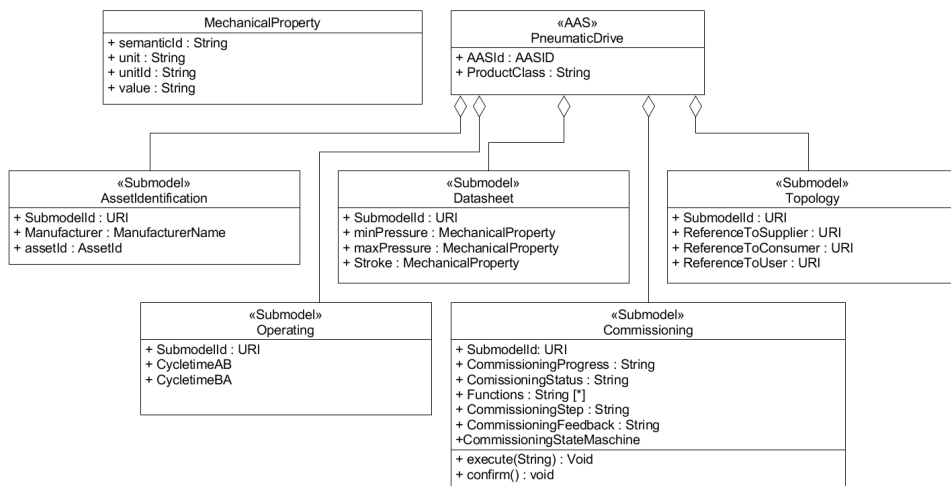

Figure 3: Class diagram asset administration shell pneumatic drive

diagram. Within the properties 'ReferenceToSupplier' and 'ReferenceToConsumer' the up- and downstream connected pneumatic components can be referred.

Figure 4 shows the fluid power topology of the reference system. The functional topology describes functional interactions between the components which can be derived from the system control. System-wide topologies can be derived from different engineering documents which are created during the design phase of a system. Afterwards they are stored distributed in the information models of different AASs and can be used during the assembly, commissioning, operation or other phases. During PnP, both topologies are used to directly interact with other relevant AASs in order to exchange information on the current commissioning progress or use services.
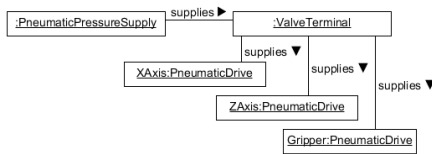
Figure 4: Fluid power topology of the pneumatic system

All other properties which are required for PnP and the corresponding orchestration are listed in the submodel 'Commissioning'. It includes all individual commissioning steps that need to be carried out, their preconditions and the available functionality of the assets.

To further detail the submodel for PnP, all previously analyzed commissioning activities are structured and grouped into commissioning steps. Each commissioning step has a precondition that determines when it can be carried out. It ends, when all necessary commissioning activities of this step are competed. Preconditions either refer to their own or to other component's PnP parameters, e.g. the commissioning progress. Commissioning steps and preconditions are implemented in a state machine. It is not visible to the outside world, thus not shown in the class diagram.

Figure 5 gives a brief overview of the state machine. Each state machine of a component has four generalized governing states INIT, Pre-Op, Safe-Op, Op, that indicate the progress of

commissioning. Each state can contain additional component specific commissioning steps. Component specific error handling can also be implemented in each step. Depending on the sensors installed, each component can detect errors during commissioning and operation.
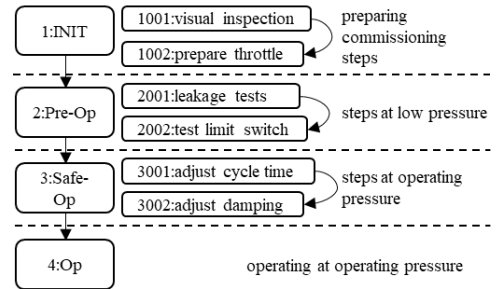
Figure 5: Diagram of the commissioning state machine inside an AAS

The AAS only exposes the next, respectively the currently running commissioning step within the property 'CommissioningStep'. A status property tells whether a commissioning step is currently running.

The property 'CommissioningFeedback' states a required precondition or an action that needs to be performed by other components in order to complete the running commissioning step. It is used to interact with other components or with the CE. The AAS gives out the required information or functionality. For example, a pneumatic drive requires the adjustment of end-damping.

The property 'Functions' lists functionalities that can be used by other components. This property is continuously updated, since the asset can provide additional functions as it increases its commissioning state towards OP state.

Two basic services are implemented in the AAS. 'Execute' is used to start a function or a commissioning step, 'confirm' is used to confirm that a requested function has been executed by another component or by the CE.

In the pneumatic reference system, the AASs are deployed on the PLC. Thus, a direct interaction between AAS and asset takes place. The AAS can directly access functions that are mapped in the control system and record real-time data of the asset.

5. PLUG-AND-PRODUCE SEQUENCE AT THE DEMONSTRATOR

The PnP commissioning starts after the assembly of the pneumatic handling system. A PnP-module is used to orchestrate and monitor the automated commissioning process. The orchestration, monitoring and error handling is done based on a state machine inside the PnP-module. In addition, it is used to guide the CE through the commissioning process. All necessary information are displayed on a human machine interface (HMI). Buttons of the HMI are used to confirm error messages and manual adjustments that had been carried out by the engineer.

The module is implemented on a single board computer and can therefore be used to commission various systems. OPC Unified Architecture (OPC UA) is used for communication between the AASs and the PnP-module.

Figure 6 shows a commissioning cycle of the PnP-module during the orchestration of the commissioning.
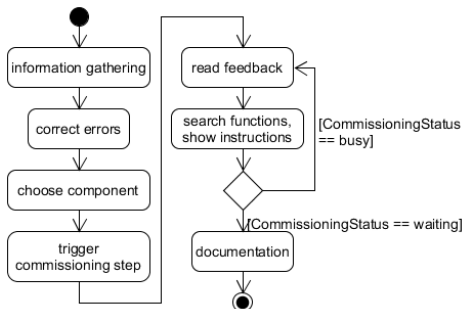
Figure 6: Activity diagram of a commissioning cycle during the orchestration of the PnP-module

Each cycle of the commissioning process starts with the collection of information. The PnP-module reads properties of the commissioning submodel of each AAS. If an error occurs the PnP-module starts an error handling sequence, showing the error massage and a trouble shooting hint on the HMI. Then, the component and its commissioning step is chosen based on the collected information. After the commissioning is triggered, the PnP-module reads the feedback property. If the required commissioning step of a component exceeds its own capabilities, the PnP-module searches for the appropriate functionality in the function property of the other AASs. The

CE is not excluded from this procedure and will additionally be consulted for backup if no other component can provide a suitable function. In this case the instructions will be displayed on the HMI. The CE confirms the activities that he carried out and the commissioning step continues. Once the commissioning step is finished, the commissioning status of the component switches to 'waiting'. The cycle ends with documentation of the commissioning step. It includes the component's identifier, a time stamp and the actions carried out. The documentation is automatically stored in a txt-file.

Figure 7 shows the simplified sequence diagram of a commissioning step to adjust the cycle time of the pneumatic drive.

The PnP-module orchestrates the process as
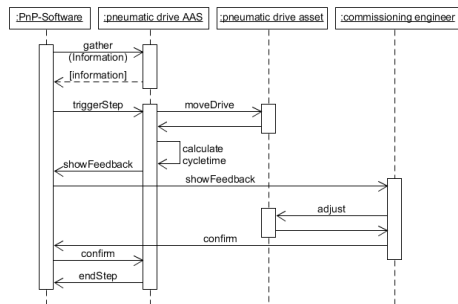
Figure 7: Sequence diagram of a commissioning step

shown in **Figure 5** and interacts with the pneumatic drive, its AAS and the CE. The CE carries out adjustments at the components according to the instructions displayed on the HMI of the PnP-module. Since the AAS is deployed on the PLC, it can directly execute functions like a movement of the drive. At the same time, a function determines the cycle time from the real-time data. The opening or closing of the throttle check-valve is determined based on the deviation of the current vs. the target cycle time and gets displayed for the CE. He makes the adjustment and confirms it via the HMI afterwards. This routine is repeated continuously until the cycle time is set correctly. At this point, the commissioning step is completed and the subsequent step is selected by the PnP-module. This process is repeated as well until the system archives the final commissioning state and goes into operational mode.

6. VALIDATION

The implementation and validation of the presented concept at this early stage have been successfully conducted on the demonstrator and can be summarized as follows. The introduced information model represent a key element to shift the task of instructing the commissioning from the engineer towards an automated information system. This sets the basis for further steps towards the automation of the entire process. In the current configuration of the demonstrator, improvements towards PnP have already been achieved.

First, the structuring of all commissioning tasks have been improved. No important commissioning steps have been forgotten, nor have been executed at the wrong time. Those faults happened before to an inexperienced commissioning engineer. The improvement with regard to the structure of the process, also increased the safety and repeatability of the commissioning and made it less dependent on the skills of the commissioning engineer. Second, all required information and parameters have been correctly and automatically provided to the system and engineer. In comparison to the former procedure, the engineer had to look up values, i.e. in the data sheets or the stakeholder requirements. This was a time consuming and error-prone process.

Some commissioning steps have already been automated, i.e. checking for leakage and mapping the valve spool configurations. Some steps still require manual effort, i.e. adjusting the end-damping or the throttle-check-valves. In those cases, additional actuators are required to automatically adjust the screws of the orifices.

Finally, a robust error handling hasn't been implemented up to this point. If unforeseen events or errors occur, the commissioning engineer gets a message and needs to solve the problem itself.

7. CONCLUSION AND OUTLOOK

In this contribution, basic enhancements of a classical pneumatic handling system towards an IIoT system are presented. The automated commissioning of this system is focused and serves as a use-case to demonstrate relevant elements of an IIoT system. A flexible and automated orchestration of different components for the commissioning requires the concept of a virtual representation of the assets, represented by the AASs. AASs have been detailed for the pneumatic system components and been implemented on the demonstrator to proof the concept. The proof-of-concept reveals that the concepts of IIoT systems can significantly structure and support the processes during the commissioning. Although it must be mentioned that the pneumatic system still relies on a commissioning engineer, since some commissioning activities can only be automated if the required functions or additional actuators are added to the system.

Consequently, developing and equipping systems with additional functionalities will be a further step for researchers and industrial manufacturers in the fluid power sector.

Additionally to approach the architecture of a distributed system, the centralized PnP-module, as presented in this paper, will further be deployed distributed on every AAS.

As a starting point, the presented concept and the information model represent a valid proof-of-concept. But it is still in an ongoing process of iterative changes and adaptions. To have an impact on daily industrial applications the concepts needs to be further enhanced and detailed to fulfill various requirements set by different kinds of stake holders.

NOMENCLATURE

AAS	Asset Administration Shell
CE	Commissioning Engineer
HMI	Human Machine Interface
I4.0	Industry 4.0
ICT	Information and Communication Technology
IIoT	Industrial Internet of Things
IoT	Internet of Things
OPC UA	Open Platform Communications Unified Architecture
PLC	Programmable Logic controller
PnP	Plug-and-Produce
SOA	Service-oriented architecture

ACKNOWLEDGMENTS

REFERENCES

[1] Kagermann H., Wolf-Dieter L., Wahlster W. (2011) Industrie 4.0: Mit dem Internet der Dinge auf dem Weg zur vierten industriellen Revolution, VDI Nachrichten (Nr. 13), 01.04.2011

[2] Abele E., Bauernhansl T., Reinhart G., Schuh G., (2016) WGP-Standpunkt Industrie 4.0, 2016

[3] Alt R., Schmitz K. (2019) Basic requirements for Plug-and-Produce of I4.0 fluid power systems, Fluid Power and Motion Control FPM 2019, Wuhan

[4] Schleipen M., Lüder A., Sauer O., Flatt H. Jasperneite J. (2015) Requirements and concept for Plug-and-Work, at – Automatisierungstechnik 63, Heft 10, 2015

[5] Alt R., Mahlzahn J., Murrenhoff H., Schmitz K. (2018) A Survey of Industrial Internet of Things in the field of Fluid Power - basic concept and requirements for Plug-and-Produce, Proceedings of the BATH/ASME 2018 Symposium on Fluid Power and Motion Control - FPMC 2018, September 12-14, 2018, Bath, UK

[6] Piller F. (2004) Mass Customization: Reflections on the State of the Concept, The International Journal of Flexible Manufacturing Systems, Volume 16, Springer, October 2004

[7] Dürkop L.; Jaspernite J. (2017) „Plug & Produce" Anwendungsfall von Industrie 4.0, Handbuch Industrie 4.0 Bd. 2

[8] Alt R., Murrenhoff H., Schmitz K. (2018) A survey of "Industrie 4.0" in the field of Fluid Power, The 11th International Fluid Power Conference, 11. IFK, 2018

[9] Adolphs, P. et al (2016) Structure of the Administration Shell - Continuation of the Development of the Reference Model for the Industrie 4.0 Component, Federal Ministry for Economic Affairs and Energy, Berlin, Germany

[10] Barnstedt E. et al (2018) Details of the Asset Administration Shell: Specification, Federal Ministry for Economic Affairs and Energy, Berlin, Germany

[11] VDI / VDE / ZVEI (2016) Fortentwicklung des Referenzmodells für die Industrie 4.0 – Komponente Struktur der Verwaltungsschale, Conclusionpaper

[12] Bedenbender H., Bock J., Boss B. et al (2019) Verwaltungsschale in der Praxis Wie definiere ich Teilmodelle, beispielhafte Teilmodelle und Interaktion zwischen Verwaltungsschalen. Bundesministerium für Wirtschaft und Energie

B2MML AS AN EXCHANGE FORMAT FOR ASSET ADMINISTRATION SHELLS AS PART OF A PLUG-AND-PRODUCE PROCESS FOR A FLUID POWER ENGINEERING APPLICATION

Hartmut Schweizer[1]*, Raphael Alt[2], Katharina Schmitz[2], Martin Wollschlaeger[1]

[1]*Institute for Applied Computer Science, TU Dresden, Nöthnitzer Str. 43, 01187 Dresden*
[2]*Institute for Fluid Power Drives and Systems, RWTH-Aachen University, Campus-Boulevard 30, 52074 Aachen*
* Corresponding author: Tel.: +49 351 463 38068; E-mail address: hartmut.schweizer@tu-dresden.de

ABSTRACT

One development in the course of industrial digitalisation, which is being driven forward particularly in the German-speaking countries and will gain in importance in the future, is that of the Asset Administration Shell (AAS) [1]. The present work deals with the distribution, instantiation and use of those AASs for assets within the domain of a fluid power engineering application, which by themselves do not currently have the corresponding hardware and software for harbouring an AAS. The Business to Manufacturing Markup Language (B2MML) is used here for the deployment and instantiation of these AASs. In the present work, B2MML is extended with the concept definitions of AAS using its enhancement mechanisms. The distribution of the AASs to computing resources then takes place using B2MML and its transaction definitions. Furthermore, B2MML is used in a submodel to orchestrate process queues. In the course of the FL4 research project, B2MML is integrated as a partial model into the AAS and is used for orchestrating the Plug-and-Produce processes one the business and on subordinate levels.

Keywords: Asset Administration Shell, B2MML, Automation

1. INTRODUCTION

The aim of the research project FL4 is a proof of concept for plug-and-produce in the field of fluid power by realizing an application based on industry 4.0 (I4.0) compliant components. For this purpose, a demonstrator consisting of two sets of components (hydraulics and pneumatics) is assembled.

The hydraulic application represents a positioning task under the influence of an external load. The hydraulic system consists of two modules, a constant pressure supply and a valve-controlled linear drive, which is tensioned by another valve-controlled linear drive. The pneumatic application is a 2D handling system for repositioning an object. The system consists of a pneumatic compressed air supply and a valve terminal with 5/3-way switching valves which actuate a gripper and two cylinders (X and Z direction) (**Fig. 1**).

Scope of the project is to proof interoperability of I4.0 compliant fluid components during commissioning. For this

purpose, the administration shells of the individual components are to be implemented in such a way that they function in the form of a service-oriented architecture (SOA) and partially und fully automate the commissioning of the plant together.

For this reason, both applications are brought together on a demo platform and are put into operation by the same commissioning logic and personnel. In addition, the systems were designed in such a way that an exchange and recommissioning of another actuator or valve can be carried out simply by switching over at the test bench. This simulates the replacement of one component with another, thus demonstrating that the commissioning of all fluid components is supported equally. For the realization of an industry 4.0 compliant PnP scenario, a virtual representation was created for the demonstrator using several Raspberry Pies (RP). Each Raspberry Pi hosts the AAS of one component (**Fig. 1**).

Since in the present case many fluid power components are non-smart components whose
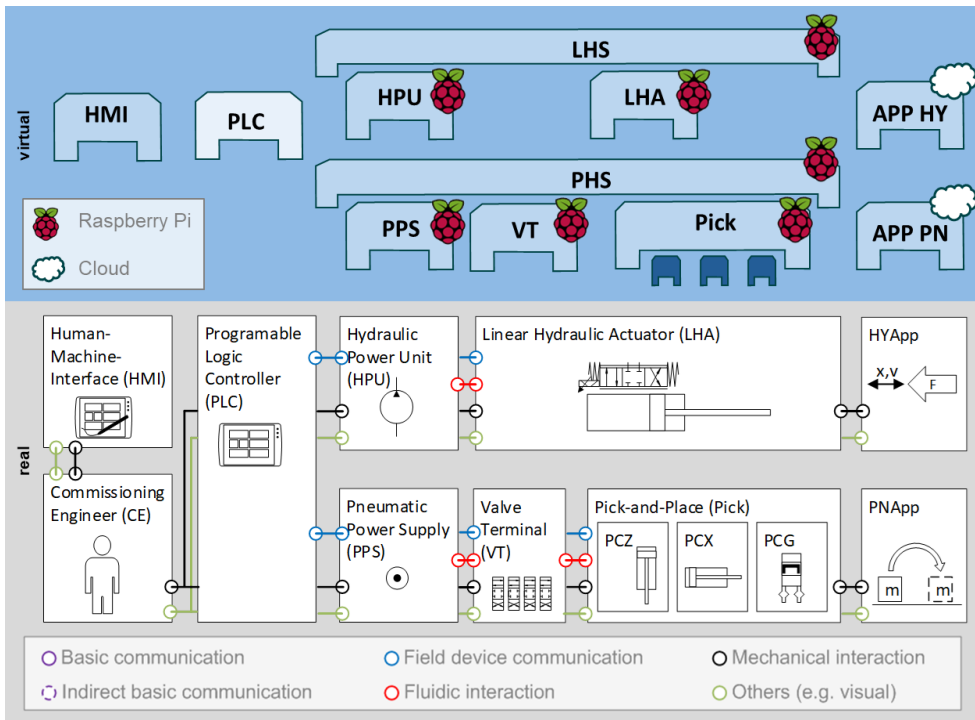
Figure 1: FL4 demonstrator (hydraulic and pneumatic components) with main virtual representation

AASs are not instantiated on the component itself, but on separate RPs, a standardized method is required to manage the deployment and exchange of the AASs. The present concept demonstrates an ERP-controlled approach using the IEC 62264 B2MML implementation for this processes. Furthermore, for partially and fully automated commissioning, the corresponding commissioning steps must be orchestrated. A solution approach with B2MML is also presented for this scenario. The runtime environment necessary therefor is currently being developed in form of a process engine for B2MML.

2. TECHNOLOGIES

In the following, the technologies of the Asset Administration Shell and the IEC 62264 implementation B2mml used in the present concept are briefly explained.

2.1. Asset Administration Shell

The AAS represents a decisive development in the field of automation. As a digital representative of an asset, it exposes its features in form of properties. The AAS integrates the physical object into Industry 4.0 communication, is addressable in the network and uniquely identifies the asset. It allows fine-grained access to all information of the object and provides standardized and secure communication interfaces.

It holds digital models of various aspects, so called submodels, and describes technical functionality exposed by the Administration Shell or respective assets (**Fig. 2**) [2].

A distinction can be made between passive and active AASs [11]. Passive AASs are data records in stored files are in databases (type 1), active AASs are instantiated and communicate with other AASs with properties in the form of functionality (type 2). The present work deals with the deployment and instantiation of AASs supporting a PnP procedure for fluid power
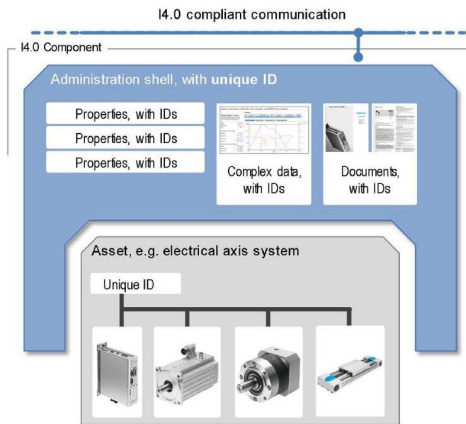
Figure 2: Asset Administration Shell [2]

applications and so AASs from type 2, e.g. a hydraulic power unit. This method is demonstrated with administration shell XML implementations, corresponding to the definition published in "The Asset Administration Shell in detail" (ZVEI) [2].

2.2. B2MML

The international standard IEC 62264 defines models, activities, and data exchange for Manufacturing Operations Management systems [5][7][8]. B2MML is an XML implementation of the IEC 62264 specifications in the form of XML schemas, which is designed as a link between ERP and materials management (supply chain) and to the production level [6]. Part 2 of IEC 62264 [7] defines objects and attributes for the integration of enterprise management and control systems. This includes the resource types *Personnel*, *Equipment,* *Material,* and *Physical Asset* as well as the production process type *ProcessSegment*. In the following, the equipment model, the process segment model and the transaction model (IEC 62264 Part 5 [8]) for the resources are explained in more detail.

The role-based equipment model of IEC 62264

Each *Equipment* resource can be composed of other *Equipment* resources and aggregates *Equipment Properties*. It can also be defined using one or more *Equipment Classes*, which can have any number of their own class

properties. Test specifications can also be defined for *Equipment* and *Equipment Classes* and their properties. Equivalent models are defined for the other resource classes *Personnel*, *PhysicalAsset,* and *Material* [7].

The process model of IEC 62264

Process segments in IEC 62224 are defined as the smallest elements of manufacturing activities that are visible to business processes. The process model is hierarchically structured, i.e., each process segment can contain further subordinate process segments. The interdependencies between the process segments are realized by references in the form of *ProcessSegmentDependencies.* These are e.g. *AtStart*, *NotFollow*, *PossibleParallel* and others. All resources like *Equipment* or *Material* can be aggregated from process segments as resource specifications via references. The processes in turn can correspond with *operation* or *product definition segments* [7].

The transaction model of IEC 62264

Part 5 of IEC 62264 defines transactions for the exchange of information between applications of business processes and applications of manufacturing processes. The extensive transaction specifications are one of the main reasons for using B2MML as a data model in this concept. The *GET/SHOW* transaction mechanism is the one that is used in presented concept. The transaction model for GET and SHOW is the *PULL transaction model*. It is used when a user submits a data request to an information provider [8]. A complete list of the transactions defined in the IEC 62264 is listed Table 1.

Table 1:   Transactions in IEC 62264-5 [8]

Transaction	Transaction model
Sync (Change)	PUBLISH
Sync (Delete)	PUBLISH
Sync (Add)	PUBLISH
Get	PULL
Show	PULL
Confirm, Cancel, Acknowledge, Process, Respond, Change	PUSH

3. DEPLOYMENT AND ORCHESTRATION WITH B2MML

In the present concept B2MML fulfils two functionalities.
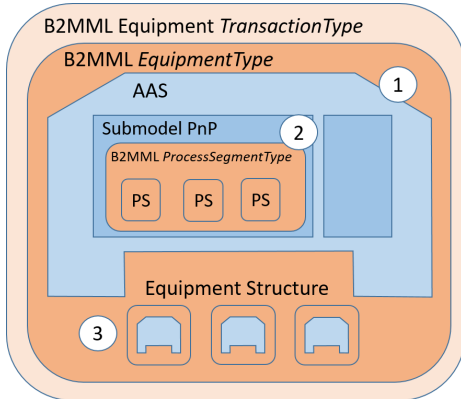

Figure 3: B2MML in combination with AAS

Firstly, it is used as a deployment container for the AAS from the ERP side. The AAS is integrated into the Equipment Type and communicated within the Transaction Types (**Fig. 3**, ①).

On the other hand, the associated processes and process chains are modeled in B2MML and integrated into the AAS as submodels for the orchestration of the commissioning (**Fig. 3**, ②). This structure can be interconnected at any depth (**Fig. 3**, ③).

Communication in this concept is realized via Message Queuing Telemetry Transport (MQTT) [3] for deployment of the AAS and with OPC Unified Architecture (OPC UA) [4] as communication protocol between the different AASs in the Plug-and-Produce procedures. Both approaches are explained in more detail below.

3.1. Deployment

As described in the introduction, the components of the demonstrator are non-smart components as defined in chapter 2.1 and [11].

When a component is replaced, the corresponding AAS must also be replaced due to the technical conditions in the corresponding hardware and software, in this case the associated RP and the process engine installed on it. For this, an appropriate procedure is necessary to exchange and instantiate the AAS. For a simulated ERP-controlled deployment, the model of the resource type *EquipmentType* of B2MML (IEC 62264) [6][7] was extended by the model of the administration shell as XML schema. The extension points provided were used for this purpose (**Fig. 4**). Equivalent to this, the other B2MML resource types (source) *PhysicalAsset*, *Material* and *Personnel* can be extended in the same way.

In this way, the XML representation of the AAS can be integrated unchanged into the data record of an *EquipmentType* and communicated in a corresponding *TransactionType*, in this case the *ShowEquipmentTransactionType* (**Fig. 5**). The submodel with the B2MML commissioning process queue for the asset is included in the referenced file.

When a new asset is installed, the corresponding administration shell can be read from the equipment data record in parallel, and can be instantiated on the corresponding hardware. To do so, the equipment data, including the administration shell, which is embedded in the transaction types, is transferred using MQTT [3]. The prerequisite for this is that the appropriate software with implemented MQTT is available. In the present approach, this task is performed by the B2MML process engine.

3.2. Orchestration

B2MML is also used to orchestrate the commissioning processes in the submodel "PnP" of the AASs. For this the *ProcessSegmentType* of B2MML is used (chapter 2.2 [7]). **Figure 6** shows such a commissioning sequence from the X-axis of the pneumatic handling system.

The individual commissioning steps are

```
<xsd:group name = "Equipment">
        <xsd:sequence>
                <!-- add extended elements here -->
                <xsd:element name="assetAdministrationShell" type="aas:assetAdministrationShell_t"
                minOccurs="0" maxOccurs="unbounded" />
        </xsd:sequence>
</xsd:group>
```

Figure 4: B2MML EquipmentType extension with AAS type

```xml
<?xml version="1.0" encoding="utf-8"?>
<xsi:ShowEquipment releaseID="{CFC4363D-92C6-4887-B19D-C244E785078B}" xmlns:xsi="http://www.mesa.org/xml/B2MML-V0600">
  <xsi:ApplicationArea>
    <xsi:CreationDateTime>2019-11-05T09:00:00</xsi:CreationDateTime>
  </xsi:ApplicationArea>
  <xsi:DataArea>
    <xsi:Show />
    <xsi:Equipment>
        <xsi:ID>ID_01_PPS</xsi:ID>
        <xsi:Description>Pneumatic Power Supply</xsi:Description>
        <assetAdministrationShell xmlns="http://www.mesa.org/xml/B2MML-V0600-AllExtensions">
          <assetRef xmlns="http://www.admin-shell.io/aas/1/0">
            <keys>
....
          </keys>
          </assetRef>
          <submodelRefs xmlns="http://www.admin-shell.io/aas/1/0">
            <submodelRef>
              <keys>
                <key type="SubmodelElement" idType="URI" local="true">IBN_PPS_01.xml</key>
              </keys>
            </submodelRef>
          </submodelRefs>
        </assetAdministrationShell>
    </xsi:Equipment>
  </xsi:DataArea>
</xsi:ShowEquipment>
```

Figure 5: B2MML *ShowEquipmentType* transaction with integrated AAS

modeled using the *ProcessSegment-Dependencies* of the B2MML process type in accordance with the commissioning requirements for the sequence of the commissioning steps. Since in this concept the dependencies are referenced using the IDs of the processes, the processes must be known among themselves [7]. This is not the case with the commissioning of a complex plant consisting of several components with their different AASs. Therefore the external dependencies are modeled in B2MML parameter types in the form of pre and post conditions, which are assigned to the processes.
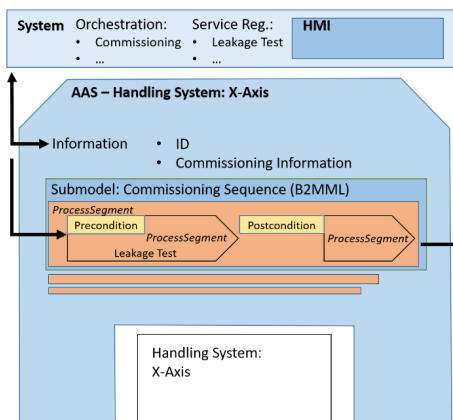
Figure 6: Orchestration of commissioning with B2MML *ProcessSegmentType* [7]

In order to instantiate and run the defined processes, a process engine for B2MML is required, which must be installed on the respective RPs and PLC. Such a process engine is currently being developed as part of the FL4 project. The (very extensive) details of the process modeling as well as the implementation of the B2MML process engine would exceed the scope of this publication and will therefore be focused separately in a following publication.

4. TRANSFERABILITY OF THE OVERALL CONCEPT

The presented concept can be applied with restrictions to the complete life cycle of an administration shell within a company [14] (**Fig. 7**). The concept is based on non-smart components (chapter 1), which will probably be in operation for several more years. Currently, the concept is applied for type 2 administration shells for fluid power components, but it can also be very useful for assets like cylinders or material, which have typical type 1 administration shells.

Procurement and Inventory

Once an asset has been acquired, it will first be inventoried. In the present concept, the AAS, which is supplied by the manufacturer, is directly maintained in the system as part of the associated asset in a B2MML type and is therefore directly available at all times.

Attention has to be paid to ensure that the AAS has to be unpacked before, according to the rules after [2].

Production and Process Planning

In production and process planning, the added or changed data can be entered natively in the domain specific models. This information can then be used in the AASs. This applies to both, information directly in the AAS, and information regarding communication, topology or orchestrated processes as B2MML in the submodels.

With regard to the submodels, this concept offers the advantage that these can also be integrated natively, provided they are XML-based, into the B2MML structure [12]. This is especially true for topology information in AutomationML [9], programming information in PLCopen XML [13] or communication specifications for OPC UA [4].

Engineering and Configuration

In the engineering and configuration phase, the data from the submodels, especially topological planning information and communication (OPC UA), are also available natively, and thus can be read and edited via the corresponding transactions (chapter 2.2, [8]).

Commissioning

Finally, when the system is put into operation, the AAS, which has been kept up to date by the processes described above, can be instantiated on hardware provided for this purpose. Then the processes, which are also modelled in B2MML, can be executed with the help of a Process Engine. Other information like OPC UA [10] or PLCopen XML can be used for the setup of the asset i.e. its managing hardware and software.

Production and monitoring

Finally, B2MML can be used in production equivalent to commissioning as a model for automated process chains. For the necessary monitoring, the approach offers the advantage that the AAS, since instantiated from the ERP-readable B2MML data record, is also known from the ERP and thus also for the upper levels of the company hierarchy. Therefore, it can be easier connected and monitored.

5. CONCLUSION

Through the combined use of B2MML and Asset Administration Shells it is possible on the one hand to manage and distribute the AASs of the respective assets consistently within an ERP system, or to deploy them. In addition, B2MML, as an implementation of IEC 62264, is very well
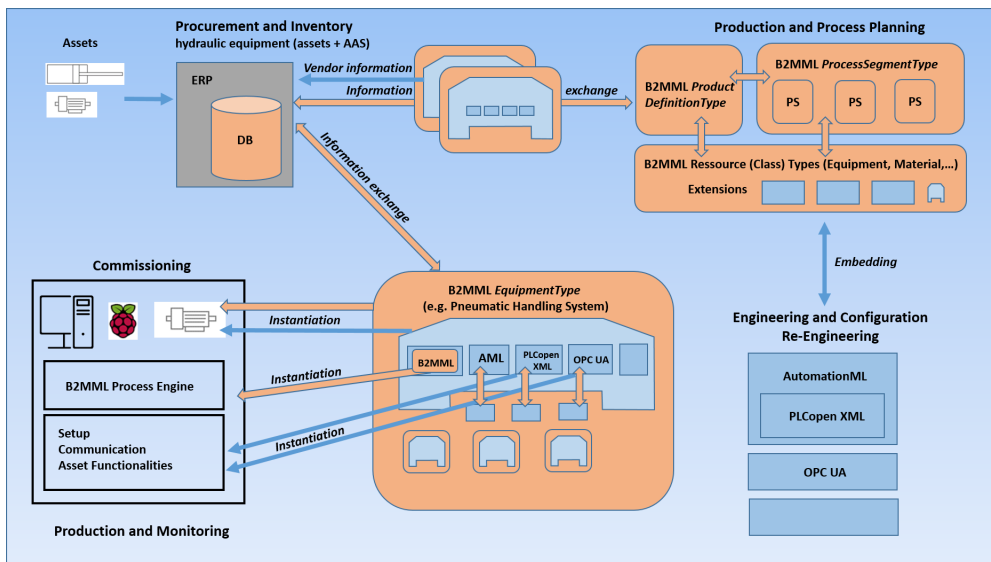

Figure 7: Overall concept of combination of AAS and B2MML

suited as a submodel for process queues, e.g. for partially and fully automated commissioning. Thus, this concept can support the entire life cycle of an AAS within a company, from the acquisition of the associated asset through installation and commissioning to production and monitoring. The concept was implemented within the project FL4. Of course, further tests and implementations in different contexts are necessary to prove the basic suitability.

ACKNOWLEDGMENTS

NOMENCLATURE

AAS	Asset Administration Shell
AML	Automation Mark-up Language
B2MML	Business to Manufacturing Mark-up Language
CE	Commissioning Engineer
HMI	Human Machine Interface
I4.0	Industry 4.0
MQTT	Message Queuing Telemetry Transport
OPC UA	Open Platform Communications Unified Architecture
PLC	Programmable Logic controller
PnP	Plug-and-Produce
SOA	Service-oriented architecture

REFERENCES

[1] VDI / VDE / ZVEI (2016) Fortentwicklung des Referenzmodells für die Industrie 4.0 – Komponente Struktur der Verwaltungsschale, Conclusionpaper

[2] VDI / VDE / ZVEI, Details of the Asset Administration Shell, November 2018

[3] http://mqtt.org/

[4] OPC Foundation: OPC-UA, https://opcfoundation.org/about/opc-technologies/opc-ua/, retrieved: November 2019.

[5] International Electrotechnical Commission (IEC). IEC 62264-1:2013 Enterprise-control system integration – Part 1: Models and terminology. International Electrotechnical Commission, Geneva, 2013.

[6] MESA International, Business To Manufacturing Markup Language (B2MML), http://www.mesa.org/en/B2MML.asp, retrieved: November 2019.

[7] International Electrotechnical Commission (IEC), IEC 62264-2:2013 Enterprise-control system integration-Part 2: Objects and attributes for enterprise control system integration, International Standard, Rev. 2.0, June 2013.

[8] International Electrotechnical Commission (IEC), IEC 62264-5:2016 Enterprise-control system integration – Part 5: Business to manufacturing transactions. International Electrotechnical Commission, Geneva, 2016

[9] IEC 62714 - Engineering data exchange format for use in industrial automation systems engineering - AutomationML, www.iec.ch, International Electrotechnical Commission, 2014.

[10] OPC Foundation: ISA-95 for OPC UA. https://opcfoundation.org/markets-collaboration/isa-95/, retrieved: November 2019.

[11] VDI / VDE / ZVEI, Verwaltungsschale in der Praxis, April 2019

[12] Schweizer, H.; Wollschlaeger, M.; Information Model Integration for Service-oriented Manufacturing Operation Management Systems; eKNOW 2019; Athens, February 2019.

[13] PLCopen, TC6-XML Schemes. http://www.plcopen.org/pages/tc6_xml/, retrieved: November 2019.

[14] Wagner, C. et al; The role of the Industry 4.0 Asset Administration Shell and the Digital Twin during the life cycle of a plant; ETFA 2017; Limassol, January 2017.

A REFERENCE ARCHITECTURE FOR CYBER-PHYSICAL FLUID POWER SYSTEMS: TOWARDS A SMART ECOSYSTEM

Dominik Martin[1]*, Johannes Kunze von Bischhoffshausen[2], Anna Hensel[1], Johan Strandberg[2]

[1]*Karlsruhe Institute of Technology, Kaiserstraße 89, 76133 Karlsruhe, Germany*
[2]*Trelleborg Sealing Solutions Germany GmbH, Schockenriedstr. 1, 70597 Stuttgart, Germany*
* Corresponding author: Tel.: +49 721 608-48967; E-mail address: dominik.martin@kit.edu

ABSTRACT

Technological advances (e.g., high speed communication, artificial intelligence) and affordable computing and sensor hardware have become a key driver of developments like "Industry 4.0" or the "Industrial Internet of Things" (IIoT). Large numbers of machines and products are equipped with sensors to constantly monitor their condition, log usage data or trigger control processes. IIoT has been largely adopted by OEMs in various industries (such as automotive, machinery industry, or healthcare and medical), turning their product into cyber-physical systems. However, the resulting potential is not yet accessible to component manufacturers. Overall, horizontal integration of the value chain is still in its infancy. Specifically, IIoT for fluid powers just started in recent years with first research projects and commercial solutions. This work presents a reference architecture for cyber-physical fluid power systems which depicts how horizontal integration can be achieved and which potentials thus can be released. The architecture is validated in an industrial use case. Furthermore, the paper at hand discusses which components of the architecture should be addressed by which actor in the fluid power ecosystem in order to leverage opportunities from the IIoT.

Keywords: Reference architecture, Fluid power systems, Cyber-physical systems, IIoT

1. INTRODUCTION

Due to rapidly advancing technological developments in a wide variety of areas (e.g., high speed communication, artificial intelligence) and at the same time the decreasing costs for hardware (i.e., sensor and computing), digitization and networking are shaping the current trends in the industrial landscape [1–3]. This development is discussed under different terms: Industrial Internet of Things (IIoT) and Industry 4.0 are the most common ones. All these terms are united by the idea that increasing networking holds the potential to create completely new products and services or establish data-based business models that allow companies to open up new business areas.

Many companies, especially OEMs (Original Equipment Manufacturer), focus on vertical integration, i.e., the flexible and seamless networking of production facilities, machines and products within their own company [4–6]. The aim is to equip physical assets, whether production machines or end products, with sensors and actuators. By integrating and, thus, leveraging networking and communication capabilities so-called cyber-physical systems (CPS) emerge [7,8].

However, horizontal integration, i.e., networking across company borders, is still at a very early stage of development [5,9]. It is precisely the fear of competition, data theft, the loss of the own supremacy and ultimately increased costs through innovation that prevents the research and development of new innovative products and solutions based on existing but so far insufficiently used data. Success stories of corporate giants such as Google, Apple and Amazon show the enormous potential of data-based business models. Yet, traditional industries still are reluctant to take this step towards horizontal integration and networking [10–12].

In view of this enormous business potential illustrated by concepts and initiatives in this context, there is a need for a uniform framework, standards and guidelines, which ideally represent

a future-oriented holistic picture of the industrial communication of tomorrow. This is of enormous importance in order to reduce the increasing complexity caused by an increasing number of devices and networks as well as to avoid isolated solutions. In addition, uniform approaches contribute to cost reduction in the medium and long term, since the development of individual solutions is avoided [13]. For this reason, we aim to propose a reference architecture which takes these issues into account.

While there has been extensive research on high-level architectures for the IIoT as well as for cyber-physical systems, no generalizable architecture for cyber-physical fluid power systems has been proposed yet. Thus, this work presents a reference architecture for cyber-physical fluid power systems addressing networking as well as cross-company integration aspects. The architecture is validated in an industrial use case. Furthermore, this work discusses which components of the architecture should be addressed by which actor in the fluid power ecosystem in order to leverage opportunities from the IIoT.

2. RELATED WORK

Two terms are of great importance in the Industry 4.0 and IIoT context: cyber-physical systems and reference architectures. Cyber-physical systems (CPS) are "intelligent system[s] connecting the physical and the digital/cyber word through influence and control using sensors and actuators" [7]. Connectivity as one of the main functions of a CPS enables real-time data acquisition from the real world and direct feedback from the cyber world. Analysis and intelligent data management shape the cyber world. The advantages of a CPS are manifold. For example, the presence of digital twins of physical components in the cyber world allows components to predict by themselves when they will fail or break down by comparing their status to the status of other components [14,15]. Consequently, components and machines have the ability to schedule maintenance for themselves. In practice, however, such applications are still rare [16].

Therefore, reference architectures in the area of Industry 4.0 strive to most ideally represent a generalized overview and serve as guidelines and best practices for the actors involved. Reference architectures serve as a kind of guide for system development. It provides basic definitions and specifies commonalities for all systems based on it.

An example of a well-known reference architecture—although not in the context of IIoT but rather from the area of network protocols—is the Open Systems Interconnection model (OSI model) of the International Organization for Standardization (ISO) [17]. However, since it focuses only on the pure communication mechanisms, it is not sufficient for the description and classification of specific aspects in the context of IIoT.

Therefore, we conducted an in-depth structured literature search looking for reference architectures that also address horizontal integration aspects in terms of data exchange and access management among different companies participating in a common value chain.

Actually, there are a number of architectures in the field of fluid power systems [18,19], but none of them addresses integration or data-related aspects.

In regard to IIoT-related reference architectures, in literature there exist various generic architectures, however, two particular ones actually dominate: The Reference Architectural Model Industrie 4.0 (RAMI 4.0) [20] proposed by the Working Group for Industry 4.0 and the Industrial Internet Reference Architecture (IIRA) [13] of the Industrial Internet Consortium (IIC). Both of them strive to define standards for communication and interaction in the IIoT context.

RAMI 4.0 covers essential elements of Industry 4.0 concept as a three-dimensional layer model. In RAMI 4.0 a production object can be recorded over its entire life cycle. This reference architecture offers a uniform wording and a common understanding across all actors involved in the Industry 4.0 context. On the vertical axis, production objects and their data are displayed in six layers. There are two horizontal axes on each of the six layers. On one axis, the production objects are arranged according to hierarchical levels in production. On the other axis data about the production objects are recorded over the life cycle. In this way, objects can be arranged precisely in the model along these three axes.

Similarly, the goal of the very generic IIRA is "to achieve broad consensus in driving device and product interoperability and deploying large

industrial control systems" [21]. The IIC aims to depict a comprehensive architecture generally applicable. Therefore, it does not formulate concrete guidelines or implementation aspects.

Both architectures are very high-level and therefore offer only limited applicability in practice. Since existing reference architectures neither do explicitly consider the involvement of e.g., suppliers to a sufficient extent nor provide applicability to a typical fluid power system use case, we propose a novel reference architecture described in Section 4.

This architecture should not only represent a pure architectural structure but should also provide practical recommendations for action regarding information and data exchange between the actors involved. We see our architecture as an extension to common reference architectures, such as RAMI 4.0. However, our proposed architecture starts at a different, more detailed level and should provide practical recommendations for actions in terms of the organization of the parties involved, data flows and access management. Above all, in comparison to RAMI 4.0, it does not classify components according to certain criteria. Our architecture allows for the derivation of different types of implementation. It is therefore designed to be general and extensible, covering a specific area of Industry 4.0: the interaction between the OEM, its customers and its suppliers—especially applicable to the context of fluid power systems.

3. THE FLUID POWER ECOSYSTEM

3.1. Fluid Power Today

Despite the potential of digitization and increasing networking, so far there has been little horizontal integration and networking along all industries, but also in the fluid power domain.

Traditionally, a value chain is characterized by bidirectional exchange between the actors along the chain. While product specifications are passed through the supply chain by the OEM or end customer via Tier 1 supplier to Tier 2 supplier and so forth, the manufactured components flow back in the opposite direction, which are assembled by the OEM to become an end product. However, data that arises during the production of components as well as domain expertise, for instance, is usually not passed on to neighboring actors in the supply chain. Similarly, data that is created or gathered by a product at the end customer is usually collected either by the end customer himself or by the OEM and is not made accessible to the suppliers. This problem is particularly prevalent in the area of fluid power solutions, since very few of the companies operating in this area actually manufacture end products.

3.2. Digitization Impact

The increasing development within the industry towards intelligent and networked products creates a number of new opportunities for companies to expand their portfolio. The competitive boundaries are blurring and expanding towards the inclusion of more and more functions. These additional functions do not necessarily correspond to the original core competence of a company that previously specialized in a pure core product [22]. For example, a wind power turbine can be serviced or maintained in reasonable time before damage occurs by enriching condition monitoring capabilities. Through networking and system-wide consideration, additional services can be created that allow the operator or manufacturer to offer, for example, weather forecasts based on the data collected.
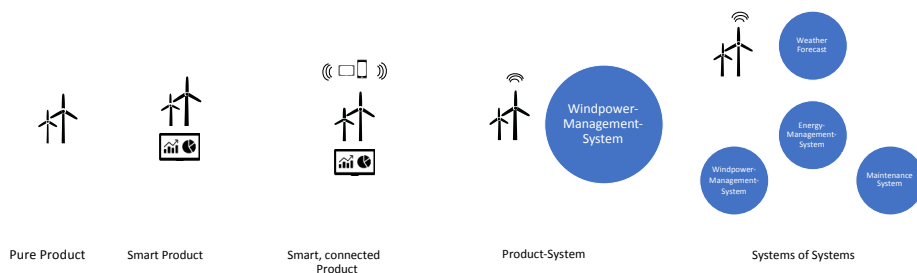

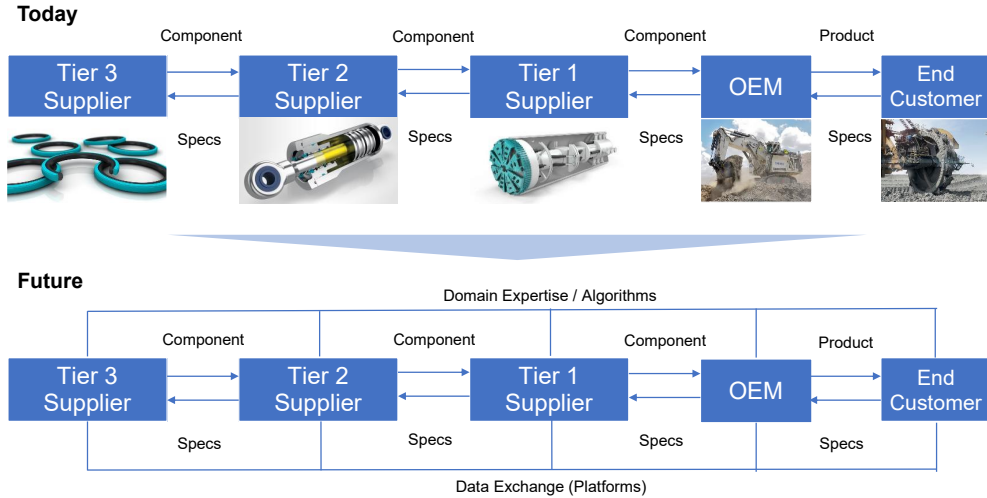**Figure 1:** Pure Products turn into Systems of Systems based on [25]

Figure 2: From Fluid Power Systems Today towards Fluid Power Systems in Future

Discrete isolated products are increasingly becoming complex systems of systems in which the company is only one player among many. The development shown in Figure 1 allows the manufacturer to offer bundles or packages of linked services or devices that increase the total value for the customer.

3.3. Fluid Power in Future

Thus, while some companies are trying to expand their portfolio and offer additional enriching products and services, others which do not follow this trend will certainly face threats. Even companies which have previously acted as OEMs can lose their role in favor of system integrators who specialize in linking several products and services to increase the overall product/bundle value [22].

Networked intelligent CPS thus provide the opportunity to rethink the existing value creation structure. It should be in the interest of all actors not to block each other through isolation, but to generate holistic added value for the customer through joint initiatives. The value chain of the future should therefore not be dominated by bidirectional exchange alone but should rather become a value creation network in which all stakeholders have the opportunity, through shared data access, to offer new services that benefit the overall product or system. Figure 2 depicts exemplarily the additional exchange of data and domain expertise—for instance

encapsulated in algorithms or findings based on the application of data analytics or artificial intelligence techniques.

4. REFERENCE ARCHITECTURE

Most CPS consist of multiple components manufactured by several suppliers and combined into the final product/cyber-physical system (CPS) by the OEM. The CPS are equipped with sensors to constantly monitor their condition, log usage data or trigger control processes. To make use of this data to the full extent it must be made available not only to the OEM, but also to the component manufacturers. Possible use cases include value-added services such as predictive maintenance or product optimization based on data of components in use. While there has been extensive research on reference architectures for cyber-physical systems in general, no generalizable architecture taking into account the component manufactures, especially in the context of cyber-physical fluid power systems, has been proposed yet.

Such a reference architecture must consider all parties involved from a data perspective. These parties are: The CPS itself, the OEM producing the CPS and the tiers of component manufacturers supplying their components to the OEM. Bearing in mind the complexity resulting from the multitude of suppliers, simplicity of implementation is crucial for the applicability of the pursued reference architecture.
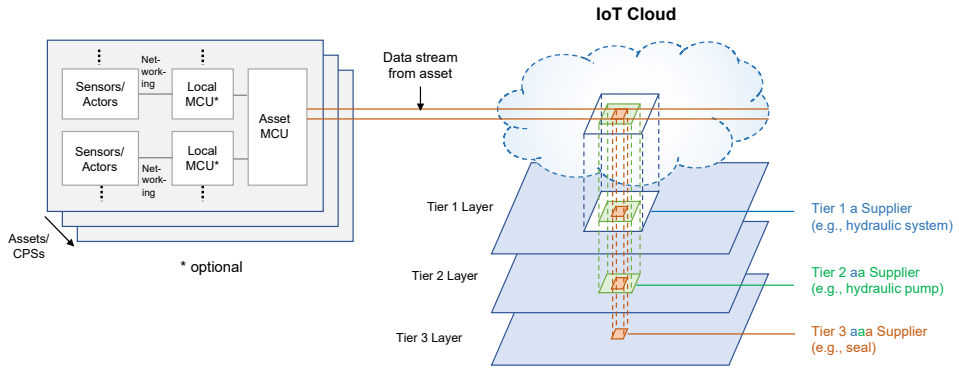
Figure 3:   Reference Architecture for Cyber-physical Fluid Power Systems

To realize this, we propose the reference architecture depict in Figure 3. The reference architecture aims to present a framework of actors around a cyber-physical fluid power ecosystem especially focusing on data exchange aspects.

It is based on the following key assumption: each party involved must make additional arrangements regarding data availability exclusively with those parties with whom the respective party is already in direct contact. This idea is already addressed by Schöggl et al. [23]. As we are looking at cyber-physical systems, we can assume that the data exists. For simplicity, we do not take into account legal issues, for example, concerning data privacy.

4.1. Structure of the Reference Architecture

The CPS consists of sensors and actors which collect data on different components. The sensor and actuators are controlled by either local MCUs (microcontroller units) or an asset MCU and made available to the IoT cloud. While the local MCU is mainly is used for sensor/actor control and edge analytics, the asset MCU acts as firewall and handles security and communication aspects. The OEM is responsible for the existence of the IoT cloud and the data transfer from the assets to the cloud. Additionally, the OEM has full access rights to all data in the IoT cloud and manages the access rights for the Tier 1 suppliers, however, explicitly not for any of the Tier 2 and Tier 3 suppliers. Managing also the access rights for the Tier 2 suppliers would violate the assumption made above. The Tier 1 suppliers, in turn,

manage the access rights for their corresponding Tier 2 suppliers and so on. In many use cases such as predictive maintenance, insights generated from e.g., a Tier 2 supplier might be of interest for the Tier 1 supplier, the OEM or even the customer owning the CPS [24]. Therefore, the insight generated by the Tier 2 supplier would be stored in the IoT cloud and made accessible to all corresponding players in the layers above.

Consequently, the reference architecture depicted in Figure 3 can be divided into three main parts: The data is stored in the IoT cloud; the horizontal axis describes the data transfer from the CPS into the IoT cloud and vice versa; and the vertical axis describes the availability management of the data.

4.2. IoT Cloud

The IoT cloud is the central storage point for all data. All data exchange between the CPS, the OEM, the Tier 1, the Tier 2 and the Tier 3 suppliers takes place indirectly via the IoT cloud. The OEM has full access to all data in the cloud. However, the Tier 1, 2 and 3 suppliers access a filtered/sliced version. Thus, they have limited access to the data in the cloud depending on their needs. The process of access rights management is described in Section 4.4. Having one central storage point for all data is beneficial in many aspects: Data validity is ensured because there exists only one version of the data and there are no copies of partial data. It is also advantageous because traceability and transparency is guaranteed and flexibility with regard to changing suppliers is ensured.
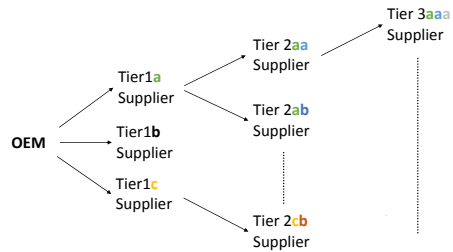
4.3. Horizontal Axis

The horizontal axis shows the interaction between the CPS, the OEM and the IoT cloud. The product a customer buys from the OEM is either named CPS or asset in this paper. Examples for assets in the field of mobile hydraulics are excavators or wind turbines. Each asset provides continuous data gathered through multiple sensors. However, some components do not directly provide sensor data themselves because they are not fitted with a sensor. Data on these components can be made available indirectly through sensor data of other components. For example, if a seal in a hydraulic pump is not fitted with a sensor directly, other sensors installed in the pump might provide relevant data concerning the seal. E.g., pressure data from the pump could provide information on the condition of the seal. Thus, all data needs to be transferred to the cloud by the OEM or its customer automatically. Thus, every asset generates a data stream into the cloud. The OEM determines which part of the data may be accessed by a certain Tier 1 supplier. The customer and the Tier 1 suppliers are not in direct contact in terms of data transfer and communication. Both are contractual partners of the OEM, but the reference architecture does not require any coordination between them. We call this property *independence*, which is expressed by the orthogonality of the horizontal axis (customers) and the vertical axis (tiers of suppliers) in Figure 3.

4.4. Vertical Axis

The vertical axis shows the interaction between the OEM, the IoT cloud and the suppliers. The OEM owns the admin rights and administrates the access rights for the Tier 1 suppliers. In other words, the OEM regulates which data a particular Tier 1 supplier can access. Each Tier 1 supplier administrates the access rights for the corresponding Tier 2 suppliers and so on (see Figure 4).

A Tier 1 supplier only grants a particular Tier 2 supplier access to data that is relevant or of interest for this particular Tier 2 supplier. Extending the example in Section 4.3, if a Tier 3 supplier is the seal manufacturer, a Tier 2 supplier passes the hydraulic pump data to the Tier 3 supplier. In order to obtain the greatest added

value from the data, the suppliers have access to data that is generated directly by their component and to indirect data. The grant of access rights being done by the party in the next highest level ensures that complexity is kept on a low level. In addition, the possibility of violations of data protection is minimized, since each party involved only has access to the data that is relevant and of concern to it. Again, we abstract from legal issues.

Figure 4:   Data Access Management

The parties have direct access to the data available to them. This means that a Tier 1 supplier does not forward the data to a Tier 2 supplier but grants him access to the specific data in the IoT cloud. The Tier 2 supplier thus accesses the data in the cloud directly. This is advantageous so that, for example, there are no duplicates of data and supports data validity. Figure 5 shows the vertical axis exemplarily for two layers and several suppliers.

Figure 5:   Vertical Axis of the Reference Architecture

This vertical axis does not only represent the data access rights management but also the handling of insights generated by the suppliers. A particular supplier is an expert for its product and, therefore, can create additional value, that we call insights. Based on the available data, a certain party such as a Tier 2 supplier might generate these insights. Examples include results of predictive models, descriptive analytics or other

data augmentations. In particular, insights that arise from the application of data analytics or artificial intelligence methods can have enormous added value for other actors in the value chain. Access to this knowledge is therefore exchanged for access to the necessary raw data. Insights generated by a certain party and relevant to other parties are stored in the IoT cloud and linked to data they are based on. A party automatically has access rights to insights if it has access rights to all data the insights are based on. This implies that a certain party always has access rights to the insights from the corresponding parties on the levels below. These insights could be used to generate further insights. Access rights to insights that do not fulfill the condition above can of course be assigned manually.

5. USE CASE

We evaluate the proposed reference architecture on an exemplary use case from the fluid power industry.

The value creation ecosystem around a certain CPS from the area of offshore infrastructure for oil and gas is exemplarily represented by three independently operating companies. While the OEM (acts in our use case also as Tier 1 supplier) manufactures the end product as well as the corresponding hydraulic system, the Tier 2 supplier is responsible for the hydraulic cylinders and the Tier 3 supplier for the included sealing systems.

The proposed reference architecture is applied exemplarily in a joint research project. The aim of the project is to research an AI-based algorithm for monitoring the condition of the sealing system assembled in the hydraulic cylinder. However, the domain expertise required to develop such an algorithm lies with the sealing system manufacturer (Tier 3), who is dependent on the usage data (pressures, velocities, etc.) and failure data of the entire system.

Finally, an AI-based condition monitoring system was successfully developed by the sealing system manufacturer based on the data provided by the OEM / Tier 1 indirectly via Tier 2. In return, these findings are transferred back to the OEM via Tier 2 by leveraging communication mechanisms provided by the IoT cloud, who can, for instance, offer a maintenance service based on this information. While the data exchange and preprocessing still required a significant amount of manual effort, the next step in this use case will be an automation of the entire data exchange.

6. CONCLUSION AND OUTLOOK

Today's potential, which results from the emerging networking capabilities of several products in the field of fluid power systems depicts the necessity for companies to agree on horizontal integration in order to exploit this potential and, consequently, to remain competitive in the future.

Thus, the paper at hand proposes a uniform, easy-to-implement reference architecture that allows companies in a value creation ecosystem around a core product / cyber-physical system to develop additional innovative products and services. This is achieved by the exchange of data and insights created through the application of data analytics and artificial intelligence techniques. An important aspect of the proposed architecture is the inclusion of the entire value chain or the entire value creation ecosystem. Only through value co-creation holistic benefits can emerge, which provide appropriate incentives to share data and the insights, respectively. Besides aspects of horizontal integration, the architecture also addresses the importance of seamless communication between the cyber-physical systems and a central IoT cloud.

The conducted evaluation based on an exemplary application from the field of fluid power systems shows the added value that results from the application of the proposed architecture. Especially when suppliers can contribute to the overall value of a product, by generating additional insights based on their domain expertise, a simple and structured data exchange between the players must be ensured.

However, this work also has limitations. On the one hand, it is in the nature of reference architectures to draw only an abstract picture of an ideal world. On the other hand, the implementation or application of our proposed architecture is primarily the responsibility of the OEM, who first has to transfer data to the suppliers before they can feed back their findings. In addition, the OEM is also responsible for moderating and providing an IoT cloud, but it can be assumed that in most cases this already exists anyway. In general, we are convinced that isolation in terms of data disclosure will not be a valid option in the future to remain competitive.

The realization of our proposed reference architecture, however, reveals new business opportunities.

REFERENCES

[1]	Civerchia, F., Bocchino, S., Salvadori, C., Rossi, E., Maggiani, L., and Petracca, M. (2017) Industrial Internet of Things monitoring solution for advanced predictive maintenance applications. *Journal of Industrial Information Integration*. 7 4–12.

[2]	Gubbi, J., Buyya, R., Marusic, S., and Palaniswami, M. (2013) Internet of Things (IoT): A vision, architectural elements, and future directions. *Future Generation Computer Systems*. 29 (7), 1645–1660.

[3]	Shanthamallu, U.S., Spanias, A., Tepedelenlioglu, C., and Stanley, M. (2017) A Brief Survey of Machine Learning Methods and their Sensor and IoT Applications. in: Int. Conf. Information, Intell. Syst. Appl., IEEE, pp. 172–175.

[4]	Wang, L., Törngren, M., and Onori, M. (2015) Current status and advancement of cyber-physical systems in manufacturing. *Journal of Manufacturing Systems*. 37 517–527.

[5]	Zhou, K., Liu, T., and Zhou, L. (2015) Industry 4.0: Towards future industrial opportunities and challenges. *2015 12th International Conference on Fuzzy Systems and Knowledge Discovery, FSKD 2015*. 2147–2152.

[6]	Gerrikagoitia, J.K., Unamuno, G., Urkia, E., and Serna, A. (2019) Digital Manufacturing Platforms in the Industry 4.0 from Private and Public Perspectives. *Applied Sciences*. 9 (14), 2934.

[7]	Martin, D., Hirt, R., and Kühl, N. (2019) Service Systems, Smart Service Systems and Cyber-Physical Systems—What's the difference? Towards a Unified Terminology. in: 14. Int. Tagung Wirtschaftsinformatik 2019 (WI 2019), Siegen, Ger. Febr. 24-27, pp. 17–31.

[8]	National Science Foundation (2012) Cyber-Physical Systems (CPS). 1–12.

[9]	Khan, M., Wu, X., Xu, X., and Dou, W. (2017) Big data challenges and opportunities in the hype of Industry 4.0. in: IEEE Int. Conf. Commun., IEEE, pp. 1–6.

[10]	Zhou, J. (2013) Digitalization and intelligentization of manufacturing industry. *Advances in Manufacturing*. 1 (1), 1–7.

[11]	Hunke, F., Seebacher, S., Schymanietz, M., Jonas, J., Genennig, S., Kühne, B., et al. (2019) Geschäftsmodelle 4.0. in: V. Stich, J.H. Schumann, D. Beverungen, G. Gudergan, P. Jussen (Eds.), Digit. Dienstleistungsinnovationen Smart Serv. Agil Und Kundenorientiert Entwick., Springer Berlin Heidelberg, Berlin, Heidelbergpp. 167–183.

[12]	Schüritz, R.M., Seebacher, S., Satzger, G., and Schwarz, L. (2017) Datatization as the Next Frontier of Servitization-- Understanding the Challenges for Transforming Organizations. in: 38th Int. Conf. Inf. Syst. Seoul, South Korea, 10th - 13th December 2017, .

[13]	Lin, S.-W., Miller, B., Durand, J., Joshi, R., Didier, P., Chigani, A., et al. (2015) Industrial internet reference architecture. *Industrial Internet Consortium (IIC), Tech. Rep*.

[14]	Lee, J., Lapira, E., Bagheri, B., and Kao, H. an (2013) Recent advances and trends in predictive manufacturing systems in big data environment. *Manufacturing Letters*. 1 (1), 38–41.

[15]	Martin, D. and Kühl, N. (2019) Holistic System-Analytics as an Alternative to Isolated Sensor Technology: A Condition Monitoring Use Case. in: Proc. 52nd Hawaii Int. Conf. Syst. Sci., pp. 1005–1012.

[16]	Dobbs, R., Manyika, J., and Woetzel, J. (2015) The Internet of Things: Mapping the Value beyond the Hype. *McKinsey*. 1–131.

[17]	International Telecommunication Union (1994) ITU-T X.200 (07/1994).

[18]	TechMiny.com (n.d.) Fluid Power System Types and their Components.

[19]	Achten, P., van den Brink, T., Potma, J., Schellekens, M.H., and Vael, G. (2009) A four-quadrant hydraulic transformer for hybrid vehicles. in: 11th Scand. Int. Conf. Fluid Power, Linköping, Sweden, pp. 1–15.

[20]	Hankel, M. and Rexroth, B. (2015) The Reference Architectural Model Industrie 4.0 (RAMI 4.0). *ZVEI, April*. 410.

[21]	Limited, I. (2018) interoperability between IIC & Industriy 4.0 for industrial assets.

[22]	Porter, M.E. and Heppelmann, J.E. (2014) How Smart, Connected Products Are Transforming Competition. *Harvard Business Review*. 92 (11), 64–88.

[23]	Schöggl, J.P., Fritz, M.M.C., and Baumgartner, R.J. (2016) Toward supply chain-wide sustainability assessment: A

conceptual framework and an aggregation method to assess supply chain performance. *Journal of Cleaner Production*. 131 822–835.

[24] Pai, D.M. (2018) Interoperability between IIC Architecture & Industry 4.0 Reference Architecture for Industrial Assets. *Infosys*.

[25] Porter, M.E. and Heppelmann, J.E. (2014) How Smart, Connected Products Are Transforming Competition. *Harvard Business Review*. 92 (11), 64–88.

ON THE USE OF SINGULAR PERTURBATION BASED MODEL HIERARCHIES OF AN ELECTROHYDRAULIC DRIVE FOR VIRTUALIZATION PURPOSES

Philipp Zagar*, Rudolf Scheidl

Institute of Machine Design and Hydraulic Drives, Johannes Kepler University Linz, Austria
* Corresponding author: Tel.: +43 732 2468 6537; E-mail address: philipp.zagar@ jku.at

ABSTRACT

Virtualization of products means the representation of some of their properties by models. In a stronger digitalized world, these models will gain a much broader use than models had in engineering so far. Even for one modelling aspect different models of the same product will be used, depending on the specific need of the model user. That need may change in the course of product life, between first product concepts till over the different phases of development, to product use, maintenance, or even recycling. Since a digitalized world use of these diverse models will not be limited to experts model consistency will play a much stronger role. Model hierarchies will play a stronger role and can serve also as means for teaching product users a deeper understanding of product properties. A consistent model hierarchy leading from a simple to a more advanced property representation can support this learning process. In this paper perturbation methods are analyzed as a means for setting up model hierarchies in a consistent manner. This is studied by models for the behavior of a electrohydraulic drive, which consists of a variable speed motor, a pump, a double stroke cylinder and a counterbalance valve. Model hierarchy is achieved by model reduction in the sense of perturbation theory. The use of these different models for different questions in a system design context and their interrelations are exemplified.

Keywords: model hierarchies, virtualization, singular perturbation, electrohydraulic drive, digital twin, model order reduction, stability.

1. GENERAL INSTRUCTIONS

Since decades, formal models represented by data structures and processed by simulation programs in computers are indispensable means in modern engineering. So far, those models have been set up for a well-defined use in certain phases, like, for instance, for product planning, development, manufacturing, for control development, and for maintenance. Mainly experts created and used those models or gave assistance to users with lower modelling and simulation expertise. The trend towards a stronger digitalization of the technical world - currently heavily emphasized in the public and in industry and promoted by various political initiatives, like the German Industrie4.0 - gives models an additional role: to be virtual representatives of conventional products, e.g., of mechatronic systems. The word "digital twin", see e.g. [1], is the most popular term to express this model role. The

corresponding activity is virtualization, one of the strong consequences of digitalization in the engineering world. More persons than today will become stakeholders of the models. Centering digitalization to persons is one of the pillars of Industrie 4.0 (see [2]). Different models of a certain system or component will serve these stakeholders' different needs concerning the qualitative model purpose or the expected model accuracy. Model management will become much more challenging than today due to the diversity of use cases and to guarantee consistency between models and as well as a correct use which cannot longer be fully controlled by experts.

Models serve a certain purpose ([3]). In the envisaged product virtualization context, purposes are manifold, e.g.: to represent its building structure, its physical behavior, its functional decomposition structure, or its communication capabilities. These diverse

models of one system have something in common: a CAD model of the mechanical structure shares some information with a dynamical model of its vibration properties; the hydraulic schematic of the electrohydraulic drive in this paper is related to topological properties of a hydraulic system model. A coarse model of the basic hydraulic performance characteristics of this hydraulic drive, like its maximum force, pressure, speed, size and motor speed relations is in some way also included in a much more refined model of the nonlinear system dynamics. The refined hydraulic drive model may be used to derive the steady state characteristics as well, but requires many more input data than the simple model. Some users might miss some of these data but may have sufficient information for the coarse model. They even might be too demanded understanding the results of the detailed model and drawing the right conclusions. Computing effort, numerical stability issues, model robustness properties are further aspects which, in general, are more challenging for more complex models. Therefore, it makes sense to provide different system models.

These models should give comparable answers to the same question, e.g., concerning the influence of system parameters on results. This vaguely characterized property might be called model consistency in a weak sense. Furthermore, it is helpful if the model differences can help understanding the system properties and which parameters influence certain properties strongly. Systematic approaches for establishing such models with strongly overlapping purpose which provide also a means to assure or validate consistency are desirable. Model hierarchies have been discussed to some extent in the mechatronic system development context often in a more general sense than in this paper, e.g., by [4], [5], [6], [7], since hierarchies provide a simple ordering and ease the understanding of relationships. In this paper a perturbation approach is discussed for this purpose. It works for model classes which have a common base in form of a most complex model from which simpler models can be derived by setting certain and typically small parameters zero. This is a quite natural approach, since most used models disregard certain effects which play a negligible role for the specific model purpose. Further on, perturbation theory is a highly developed discipline which can help to systematically compare models, hence quantify model consistency, and it defines a model hierarchy in a natural and consistent way. That is done in an exemplary fashion for a nowadays very popular electrohydraulic drive.

2. EXAMPLE ELECTROHYDRAULIC DRIVE

2.1. Governing Equations

This drive concept (see Fig. 1) uses a speed variable electric motor to rotate a constant displacement pump (displacement volume V_P) and to move the cylinder piston. The different oil flows of both cylinder ports are compensated by a counterbalance (CBV) and a check valve (CHK). Closed loop control is achieved by measuring the velocity of the piston, comparing it to the command variable and feeding back the difference to a PI-controller. The drive is loaded by a process force F which is assumed being constant enabling rigorous stability statements. Those would be also feasible if F is slowly time dependent with a sufficient frequency gap between $F(t)$ and the fast dynamics of the self excited oscillations of the Hopf-bifurcation instability. The assumptions for the mathematical model of the overall system are that the compressibility of the hydraulic oil can be represented in linearized form, there is no stiction between piston and cylinder, all mechanical parts can be described sufficiently accurate as rigid bodies, nonlinear effects of the electric motor (as e.g. stray flux) can be neglected, there are no spatial pressure gradients in the two volumes of the chambers A and B, the valve's flow rates can be described by a quadratic relation between pressure and flow rate and that the inertia of the hydraulic oil is neglected. With these assumptions effects like cavitation, wave propagation, elasticity of the piston and the poppet in the CBV are ignored and the mathematical model reduces to a system of eight coupled nonlinear ordinary differential equations.

$$\dot{p}_A = \frac{E_{Fl}(-A_A w - q_A + q_P)}{A_A x + V_{A0}} \tag{1a}$$

$$\dot{p}_B = \frac{E_{Fl}(A_B w + q_B - q_P)}{-A_B x + V_{B0}} \tag{2b}$$

$$\dot{x} = w \tag{3c}$$

$$\dot{w} = \frac{-F(t) + p_A A_A - p_B A_B - d_W w}{m_F} \tag{4d}$$

$$\dot{z} = v \tag{5e}$$

$$\dot{v} = \frac{-c(z + z_0) + p_A A_{P1} + p_B A_{P3} - d_V v}{m_P} \tag{6f}$$

$$\dot{\omega}_M = \frac{M_N - (p_A - p_B)V_P/(2\pi) - d_P \omega_M}{\theta_{tot}} \tag{7g}$$

$$\dot{e}_I = \frac{w_d - w}{\varepsilon_I} \tag{8h}$$

Equations (9a) and (10b) describe the pressure build-up in chambers A and B respectively which is affected by inflowing oil and by the movement of the piston using a linearized compressibility relation. Equations (11c) and (12d) account for the motion of the piston which results from the external force F and the weighted pressure difference between chamber A and B. The equations of motion for the poppet of the CBV are illustrated in Equations (13e) and (14f). The model of the CBV consists of a simple mass-spring system with a damping coefficient d_V proportional to the velocity of the poppet. The equation of motion for the electric motor (15g) incorporates the torque M_N delivered by the electric motor, the resulting torque on the displacement pump due to the pressure difference and a damping factor d_P which models effects as viscous friction of the bearings and other dissipative actions. The internal state of the PI-controller is described in Equation (16h) where ε_I stands for the inverse I-coefficient of the PI-controller. The torque M_N (which is the PI-controller output) and the flow rate q_P of the displacement pump as well as the flow rate q_A through the CBV are algebraic functions of the state variables (Eq. (2)). A square root relation between flow rate and pressure drop which is scaled by the opening z of the valve is used to model the CBV. This is motivated by the assumption that the electrohydraulic drive is used for long (and fast) stroke actuation which involves large flow rates through the CBV.
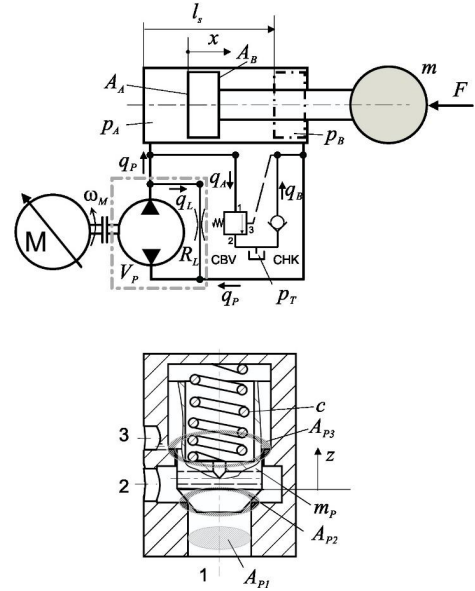

Figure 1: Hydraulic schematic of the electrohydraulic drive and sketch of the counterbalance valve

$$M_N = k_P(w_d - w) + k_I e_I \tag{2a}$$

$$e_I = \int (w_d - w)\, dt \tag{2b}$$

$$q_P = \frac{\omega_M V_P}{2\pi} - \frac{p_A - p_B}{R_L} \tag{2c}$$

$$q_A = \frac{q_N \sqrt{p_A - p_T}}{\sqrt{p_N}} \left(\frac{z}{z_{max}}\right) \tag{2d}$$

2.2. Dimensionless Equations

To identify small parameters for a perturbation analysis the equations are transformed into dimensionless form. To this end, following transformations of the states and of the time t are performed: the pressures in chamber A and B $p_A = P_A p_S$ and $p_B = P_B p_S$ are scaled by the system pressure p_S, dimensionless position $x = X l_S$ is scaled by the piston's stroke length l_S, dimensionless piston velocity $w = W w_{ref}$ is scaled by a reference velocity $w_{ref} = l_S/T_{ref}$, dimensionless poppet position of CBV $z =$

Zz_{max} is scaled by the maximum poppet position z_{max}, dimensionless velocity of CBV $v = Vv_{ref}$ is scaled by $v_{ref} = z_{max}/T_z$ with $T_z = 2\pi\sqrt{m_P/c}$, dimensionless angular velocity of motor (gear transmission ratio of clutch is $i = 1$) $\omega_M = \Omega\omega_N$ is scaled by the nominal rotation speed of the electric motor ω_N, dimensionless internal PI-controller state $e_I = E_I l_S$ is scaled by l_S and time $t = \tau T_{ref}$ is scaled by a reference time $T_{ref} = A_A l_S/q_N$ where q_N is the normal flow rate at nominal pressure p_N bar. These transformations and the substitution of equations (2a) – (2d) into (1) result in the dimensionless set of nonlinear differential equations.

$$\varepsilon_P\dot{P}_A = \frac{\frac{-\sqrt{P_A - P_T}Z}{\sqrt{P_N}} + \frac{(\Omega r_L + P_A - P_B)v_P}{r_L} - W}{X + v_{A0}} \quad (3a)$$

$$\varepsilon_P\dot{P}_B = \frac{-\gamma W + \frac{(\Omega r_L + P_A - P_B)v_P}{r_L}}{\gamma(X - v_{B0})} \quad (3b)$$

$$\dot{X} = W \quad (3c)$$

$$\varepsilon_F\dot{W} = -W\delta_w - P_B\gamma - f + P_A \quad (3d)$$

$$\varepsilon_Z\dot{Z} = V \quad (3e)$$

$$\varepsilon_V\dot{V} = -CV\delta_V + P_A\alpha_{P1} + P_B - C(Z + Z_0) \quad (3f)$$

$$\varepsilon_M\dot{\Omega}_M = v_P\big((E_I + K_P(W_d - W))m_N - \delta_P\Omega - P_A + P_B\big) \quad (3g)$$

$$\varepsilon_I\dot{E}_I = W_d - W \quad (3h)$$

Where following parameters were used:

$$v_{A0} = \frac{V_{A0}}{A_A l_S} \qquad v_{B0} = \frac{V_{B0}}{A_B l_S}$$

$$\gamma = \frac{A_B}{A_A} \qquad D_P = \frac{d_p p_S V_P}{2\pi\omega_N}$$

$$C = \frac{c z_{max}}{A_{P3} p_S} \qquad \alpha_{P1} = \frac{A_{P1}}{A_{P3}}$$

$$m_N = \frac{M_N 2\pi}{V_P p_S} \qquad q_N = \frac{A_A l_S}{T_{ref}}$$

$$r_L = \frac{R_L \omega_N V_P}{2\pi p_S} \qquad v_P = \frac{V_P T_{ref} \omega_N}{2\pi A_A l_S}$$

$$K_P = k_P \omega_N/M_N \qquad K_I = k_I \omega_N T_{ref}/M_N$$

where k_P and k_I are the parameter of the proportional and the integral term of the PI-controller respectively and

$$\varepsilon_P = \frac{p_S}{E_{Fl}} \quad \varepsilon_F = \frac{m l_S}{A_A T_{ref}^2 p_S} \quad \varepsilon_V = \frac{z_{max} m_P}{A_{P3} T_{ref}^2 p_S} \quad (4)$$

$$\varepsilon_I = \frac{1}{K_I} \quad \varepsilon_Z = \frac{2\pi\sqrt{m_P/c}}{T_{ref}} \quad \varepsilon_M = \frac{\theta_{tot}\omega_N^2}{A_A l_S p_S}. \quad (5)$$

Eq. (4) and (5) are the perturbation parameters which – when their values are small – lead to a differential-algebraic system of equations. The process of reducing the system of ordinary differential equations is described in the next paragraph.

3. MODEL REDUCTION USING SINGULAR PERTURBATION THEORY

The mathematical model of a physical system always comes along with simplifications by, e.g., dimensionality reduction. A consistent theory which constitutes the process of simplification of a certain class of dynamical systems is the singular perturbation theory for ordinary differential equations in a form introduced by [8]. It basically states that a dynamical system which consists of two coupled subsystems with slow and fast dynamics has an invariant manifold close to the solution of the reduced problem. The latter is obtained if the fast dynamics is neglected.

The dimensionless state space model (3) exhibits the structure of a singular perturbation model. Due to proper scaling the right hand side of these equations are of order 1 so that the coefficients (ε_i with $i = \{P, F, Z, V, M, I\}$) in front of the state's time derivatives determine how fast the states are changing in time. As $\varepsilon_i \to 0$ the change of the corresponding state happens instantaneously and the differential equation degenerates to an algebraic equation. If the algebraic equation is fulfilled at isolated points for the fast state variables the singular perturbation model is said to be in standard form.

3.1. System Reduction: $\varepsilon_P, \varepsilon_F, \varepsilon_Z, \varepsilon_V \to 0$

The variable ε_P is the ratio between system pressure p_S (typical 300 bar) and bulk modulus of the hydraulic oil E_{Fl} (typical 14000 bar) and therefore, its value is in the order of 10^{-2}. The value of ε_F is in the order of 10^{-4}. As the ratio

between $\varepsilon_F : \varepsilon_V$ is $\varepsilon_F / \varepsilon_V = (m/m_p)(l/z_{max})/$ (A/A_{P3}) where each factor in brackets scales approximately with size of the actuated piston compared to the size of the CBV and the overall effect ($m \sim scale^3$, $A \sim scale^2$ and $l \sim scale$) ends up being $\varepsilon_F / \varepsilon_V \sim scale^2$. The scaling factor $scale$ is in the range of $scale \approx 10^4$, therefore, ε_V is negligible as $\varepsilon_F \to 0$. The value of ε_Z is defined by $\varepsilon_Z = T_Z / T_{ref}$. T_Z is the inverse resonance frequency of the mass-spring-system of the poppet CBV which is in the range of several milliseconds and T_{ref} is the time that is needed to drive the piston from one end to the other when the CBV delivers nominal flow rate. Therefore, ε_Z is in the range of 10^{-3}. Taking these small values into account it is a valid simplification to reduce system (3) to the slow model (6) with the singular perturbation parameters $\varepsilon_{\{P,F,Z,V\}} = 0$ and to algebraic equations (7) which further simplify to the following form if leakage is neglected, i.e. leakage resistance $r_L \to \infty$.

$$\dot{X} = W \tag{6a}$$

$$\varepsilon_M \dot{\Omega}_M = v_P((E_I + K_P(W_d - W))m_N - \delta_P \Omega - P_A + P_B) \tag{6b}$$

$$\varepsilon_I \dot{E}_I = W_d - W \tag{6c}$$

$$V = 0 \tag{7a}$$

$$W = \frac{\Omega v_P}{\gamma} \tag{7b}$$

$$Z = \frac{-C\gamma^2 Z_0 + \gamma^2 P_A \alpha_{P1} + \gamma P_A - \Omega \delta_W v_P - f\gamma}{C\gamma^2} \tag{7c}$$

$$P_B = \frac{-\Omega \delta_W v_P - f\gamma + \gamma P_A}{\gamma^2} \tag{7d}$$

$$\sqrt{P_A - P_T} = \gamma \Omega v_P \sqrt{P_N} C(\gamma - 1) / \tag{7e}$$
$$((CZ_0 - P_A \alpha_{P1})\gamma^2 + (f - P_A)\gamma + \Omega \delta_W v_P)$$

Equation (7b) describes a relation between velocity W and rotational velocity Ω of the pump representing an idealistic view on system behavior, i.e. a rotational movement of the pump immediately results in a linear actuation of the piston. P_A is expressed in an implicit formula (7e) which basically equates the flow rate through the valve and the flow rate of the pump q_P out of chamber A.

3.2. Additional system reduction: $\varepsilon_M, \varepsilon_I \to 0$

Many users of the presented drive appreciate its simple handling, including those control tasks which they have to provide in the course of system integration. What they expect is a kind of perfect gearbox which transmits the desired speed signal w_d (or W_d) with an acceptable accuracy into the actual piston speed w (or W). In other words, their model concerning system response is $w \equiv w_d$. Of course, that requires acceptable signals w_d and process forces $F(t)$ as well as a sufficient drive performance. This system behavior corresponds to a further reduced system, by setting also ε_M and ε_I zero. The dimensionless state equations degenerate to a system of algebraic equations, given by (8), if $\delta_W = 0$.

$$V = 0 \tag{8a}$$

$$W = W_d \tag{8b}$$

$$\Omega = \frac{\gamma W_d}{v_P} \tag{8c}$$

$$Z = \frac{-C\gamma Z_0 + \gamma P_A \alpha_{P1} + P_A - f}{C\gamma} \tag{8d}$$

$$P_B = \frac{-f + P_A}{\gamma} \tag{8e}$$

$$P_A = \frac{W_d(1 - \gamma) + \dfrac{\sqrt{P_A - P_T}}{\sqrt{P_N}} Z}{X + v_{A0}} \tag{8f}$$

The simple algebraic expressions in (8) as well as the corresponding slow model shall help the stakeholder to get a comprehensive understanding of the system behavior. Of course, the simple models are restricted to certain constraints like system stability which for the system under study is decided by the fast dynamic subsystem. The following section shall lead the reader through a rough concept phase and highlights the limits of the reduced models.

4. USING THE REDUCED MODEL FOR DESIGN

4.1. Exploitation of reduced models in a virtualization context

Equation (8f) is basically a third order polynomial in P_A if Z is inserted from (8d). A compact approximate solution is

$$P_A \approx \frac{\gamma f_{PL} + f}{1 + \gamma \alpha_{P1}} + \frac{(\gamma-1)\gamma \sqrt{\frac{\gamma f_{PL} + f}{\gamma \alpha_{P1} + 1}} W_d \sqrt{P_N}}{\gamma f_{PL} + f} C \qquad (9)$$

In this relation the tank pressure P_T is set to zero and the spring preload distance Z_0 of the CBV is replaced by its equivalent dimensionless preload force f_{PL}: $Z_0 = f_{PL}/C$ which is an essential adjustment parameter.

This relation provides adjustment rules for the CBV: For the considered retraction ($W_d < 0$) scenario, a positive load ($f>0$), and the requirement $P_B > 0$ the following approximate design rule for f_{PL} results

$$f_{PL} > \alpha_{P1} \max f \qquad (10)$$

Spring stiffness C leads to an increase of P_A, since $\gamma < 1$. A small C reduces this effect but this is traded-off by a higher Z_0, i.e. a longer counterbalance spring, and a slower CBV dynamics. The relation seems to require a preload $f_{PL} > -\min f/\gamma$. But this is technically an erroneous conclusion. For $f < 0$ and a small f_{PL} Z goes to its limit, $Z = 1$. The equilibrium is handled by an end stop contact force. P_A computes to

$$P_A = P_N W_d^2 (\gamma - 1) \qquad (11)$$

Similar design considerations can be made for the CBV area ratio α_{P1}. Also approximate expressions for the efficiency η of stationary retraction motion can be derived from the reduced problem, if the terms of basic formula

$$\eta = \left(\frac{Fw}{\omega_M M_M} \right)^{-sign(f)} \qquad (12)$$

are successively replaced by their dimensionless counterparts and solutions of the reduced problem. For pulling forces ($f<0$) the following series approximation of η in W_d results:

$$\eta \approx \frac{f v_p (\gamma \alpha_{P1} + 1)}{\gamma (v_p (\alpha_{P1} + 1) f + f_{PL} v_P (\gamma - 1))} \qquad (13)$$

$$- \frac{f a (C \sqrt{P_N} (\gamma - 1)^2 ab + \gamma \delta_p a (\gamma f_{PL} + f))/v_P}{\gamma (f(\alpha_{P1} + 1) + f_{PL}(\gamma - 1))^2 (f_{PL} \gamma + f)} W_d$$

with

$$a = \sqrt{\frac{\gamma f_{PL} + f}{\gamma \alpha_{P1} + 1}} \qquad b = \gamma \alpha_{P1} + 1 \qquad (14)$$

For the CBV opening the following approximate solution can be derived

$$Z \approx \frac{(\gamma - 1)\sqrt{\gamma \alpha_{P1} + 1} W_d \sqrt{P_N}}{\sqrt{\gamma f_{PL} + f}} \qquad (15)$$

Obviously, $f > \gamma f_{PL}$ must hold true, otherwise the valve goes to its fully open state $Z = 1$. That gives another formula, which is not presented here because of the page limits.

Figure 2 shows the efficiency values for a retraction with vanishing speed ($W_d \to 0$) in those force regions where the formula above is valid. The reduced system (Eq. (8)) describe algebraic relations between all the system states. In the end, the curves describe how much power is dissipated in the CBV as this is the only loss which exists in the reduced model. The loss is characterized by the flow rate through the CBV (which corresponds to the desired speed of the piston) and the pressure combination in chamber A and B which is needed to, firstly, compensate
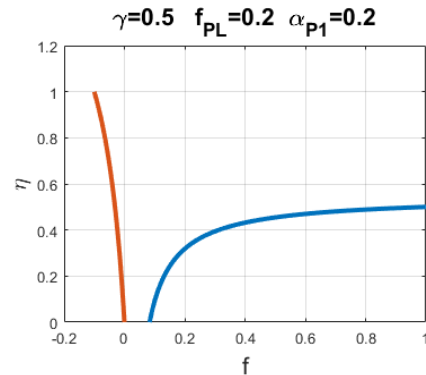

Figure 2: Efficiency η for different external force f.

the external force f and, secondly, open the CBV such that the right flow rate is reached. It is clear that for pulling forces (red curve) the pressure in A becomes low which results in a small pressure drop in the CBV and hence in a good efficiency.

4.2. Comparison between reduced and full model

In the previous section the use of the reduced problem was shown exemplary. In this section the reduced model, i.e. the dynamics of the slow model, shall be compared to the full model always having in mind a system design task. When applying a reduced model it is necessary to notice under which circumstances it is a valid approximation of the complete model. Validity of the reduced model cannot be checked directly by looking at the formulas of the reduced model.

One condition is that the fast system has to be stable on the so-called slow manifold, which basically is a subset in phase space where the solutions of the reduced system live. This condition can be shown by linearizing the fast subsystem and checking the Routh–Hurwitz stability criterion for all possible slow states and parameters. In most cases the inequalities that result from this procedure cannot be solved for certain parameters analytically because the expressions become very cumbersome when the number of fast states increases. In case of the electrohydraulic drive, the first two criteria are trivially fulfilled for physical meaningful quantities. The remaining inequalities are cumbersome and only two approximations are presented here.

$$\alpha_{P1} < \frac{Z}{2(P_A - P_T)(X + v_{A0})} \tag{16a}$$

$$\begin{aligned} &\alpha_{P1} \\ &> \frac{k_1(-C(1 + k_1{}^2 k_2{}^3) - k_1 k_2{}^2 k_3 k_4 - \gamma k_4)}{k_3(\gamma k_1{}^2 k_2{}^2 k_4 + 1)} \end{aligned} \tag{16b}$$

with

$$k_1 = 1/(\sqrt{P_A - P_T}\sqrt{P_N})$$

$$k_2 = 1/(X + v_{A0})$$

$$k_3 = \sqrt{P_A - P_T}/\sqrt{P_N}$$

$$k_4 = 1/(-X + v_{B0})$$

The two inequalities in (16) represent necessary conditions for stability, thus, for the reduced system to be valid. Such conditions restrict the derived relationship (10) for f_{PL} (including parameter C) and α_{P1} further and highlight limitations that come along when using only the reduced model for design purposes. Equation (16a) is derived by neglecting dissipative effects ($\delta_V = \delta_W = 0$). It shows the explicit connection between the pilot ratio α_{P1} and the position variable X as $1/(X + v_{0A})$ is decreasing rapidly when X grows to its maximum value. Similar sensitivity of the expression originate from pressure P_A in chamber A. This dependence is particularly interesting for fast transients rather than for quasi-static dynamics as P_A is kept low by large α_{P1} in steady state operation.

Another aspect is the validity of the model itself (e.g. the value of the valve opening Z can only take values between 0 and 1) if such boundary conditions are not explicitly integrated into the model. In the next paragraphs we take a closer look at the design parameter α_{P1} and analyze how the the eigenvalues behave on the slow manifold.

Figures 3 and 4 show the velocity w of the piston calculated from the full and the reduced model described by (6) and (7) and the desired velocity w_d for different values of the pilot ratio α_{P1}. The graphs can be interpreted as showing the pistons velocity with different level of detail which ranges from the velocity of the full model (blue) to the instantaneous step response $w = w_d$ (green) which results from the reduced system
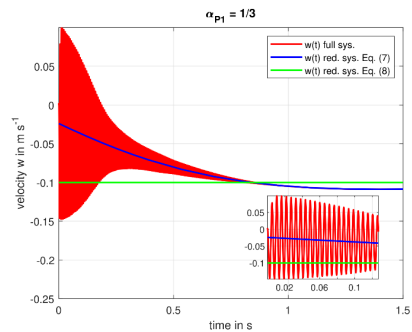

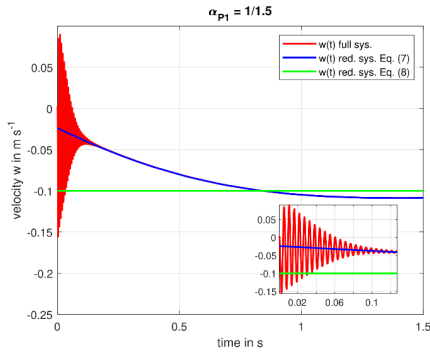**Figure 3:** Dynamic step response of velocity W with $\alpha_{P1} = 1/3$.

Figure 4: Dynamic step response of velocity W with $\alpha P1 = 1/1.5$

Figure 5: Largest eigenvalue max λ_i on a trajectory.

(8). It can be seen that the reduced model is not capable of predicting weak stability issues but rather approximates the qualitative behaviour of the fast states. In general increasing the pilot ratio α_{P1} in the electrohydraulic drive stabilizes the system which might result in longer life time due to fewer wear in the moving parts. A down-side is the increase on working pressure in both chambers which might negatively affect e.g. the pump's life-time.

Another important system property which is indirectly influenced by α_{P1} is the maximum load the hydraulic actuator can hold because the CBV acts as a simple pressure relief valve when the piston is in steady state.

Besides the severe effect of α_{P1} on the stability of the overall system the position of the piston is a further crucial parameter in the sense of the fast system. A low stiffness of the hydraulic oil in chamber B which is decreased by increasing chamber B's dead volume is positively influencing the stability of the actuator. This can be seen in **Figure 5** where the largest eigenvalue at each point on the slow manifold for a given trajectory is plotted for different values of the piston position x and the parameter α_{P1}. Notice that for some pairs (x, α_{P1}) the fast system is becoming unstable, i.e. max $\lambda_i > 0$. The area of the fast system's instability happens for piston position around the mechanical end stop x ≈ 1 and for small $\alpha_{P1} < 0.5$.
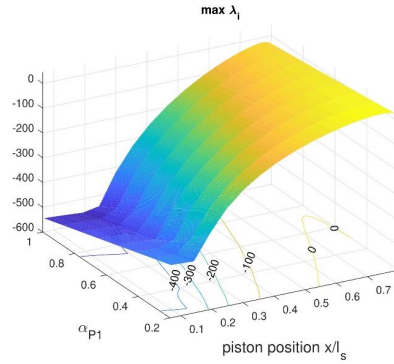
5. CONCLUSION

Mathematical modelling of physical systems is a standard approach engineers are using for centuries to gain insights and predict the system's behaviour. Nowadays, in context of digitalization and political trends as Industrie4.0 there is the need for a variety of models which perhaps describe different aspects of the same physical system. At the same time it is crucial to keep consistency within such models. One attempt for preserving consistency and simultaneously obtaining model hierarchies which is discussed in this paper is to use the well-known method of singular perturbation. It was shown that simple, sometimes even algebraic equations lead to a useful model for the fast states of the system. Subsequently, this model was used to derive simple approximations, limitations for key parameters as well as a basic formula for the efficiency of the exemplary system of an electrohydraulic actuator. Besides showing the usefulness of such a model for design approach it was highlighted that due to the reduction procedure the static model might not even predict qualitative system behavior. This is for example the case when the fast subsystem loses its stability. Necessary bounds for preserving stability were derived by using Routh–Hurwitz stability criterion which implied further limitations on the parameter space.

NOMENCLATURE

θ_{tot}	Effective moment of inertia of pump and motor
$\omega_M (\Omega)$	Angular velocity of electric motor
$A_{A,B}$	Piston area A, B side
A_{p1}	Area of piloted poppet from side 1 of CBV
A_{p3}	Area of piloted poppet from side 3 of CBV
c	Spring constant of poppet preload spring
$d_v, (\delta_v)$	Damping factor of poppet (dimensionless)
$d_w, (\delta_w)$	Damping factor of piston (dimensionless)
E_{fl}	Bulk modulus oil
$e_i (E_i)$	Internal state of PI-controller (dimensionless)
$F (f)$	Process force (dimensionless)
$k_I (K_I)$	I-coefficient of PI-controller (dimensionless)
$k_P (K_P)$	P-coefficient of PI-controller (dimensionless)
m_F	Mass of piston
$M_N (m_N)$	Torque of electric motor (dimensionless)
m_P	Mass of poppet of CBV
$p_{A,B} (P_{A,B})$	Pressure chamber A, B (dimensionless)
p_N	Nominal pressure drop of CBV
$P_T, (P_T)$	Tank pressure (dimensionless)
$q_A (Q_A)$	Flow rate through CBV (dimensionless)
$q_B (Q_B)$	Flow rate through CHK (dimensionless)
q_N	Nominal flow rate through CBV
$q_P (Q_P)$	Pump flow rate (dimensionless)
$R_L (r_L)$	Leakage resistance (dimensionless)
$v (V)$	Velocity of poppet (dimensionless)
$V_{A0,B0}$	Dead volume chamber A, B
V_P	Displacement volume
$w (W)$	Piston velocity (dimensionless)
$w_d (W_d)$	Desired velocity of piston (dimensionless)
$x (X)$	Piston position (dimensionless)
$z (Z)$	Position of poppet (dimensionless)
$z_0 (Z_0)$	Preload deflection of poppet spring (dimensionless)
Z_{max}	Maximum poppet displacement of CBV
γ	Area ration between piston side B and A
$\varepsilon_{P,F,V,Z,M}$	Perturbation parameter for pressure, piston, poppet displacement, poppet velocity, rotary parts (pump and motor)
α_{Pl}	Inverse pilot ratio of CBV
η	efficiency

ACKNOWLEDGEMENTS

REFERENCES

[1] Abramovici, M. (2016). Engineering im umfeld von industrie 4.0: Einschätzungen und handlungsbedarf. Herbert Utz Verlage, München.

[2] Lanza, G., Nyhuis, P., Fisel, J., Jacob, A., Nielsen, L., Schmidt, M., and Stricker, N. (2018). Wandlungsfähige, menschzentrierte Strukturen in Fabriken und Netzwerken der Industrie 4.0. Herbert Utz Verlage, München.

[3] Vajna, S., Weber, C., Bley, H., and Zeman, K. (2009). CAx für Ingenieure, 2nd Ed. Springer Verlag, Berlin Heidelberg.

[4] Hehenberger, P. and Zeman, K. (2008). The role of hierarchical design models in the mechatronic product development process. Proc TMCE international symposium series on tools and methods of competitive engineering.

[5] Hehenberger, P., Poltschak, F., Zeman, K., and Amrhein W. (2010). Hierarchical design models in the mechatronic product development process of synchronous machines. Mechatronics, 20(8), 864-875.

[6] Munch, E., Adelt, P., Kruger, M., Kleinjohann, B., and Trachtler, A. (2008). Hybrid planning and hierarchical optimization of mechatronic systems. Control, Automation and Systems, ICCAS 2008, 1047-1054.

[7] Paredis, C.J., Diaz-Calderon, A., Sinha, R., and Khosla, P.K. (2001). Composable models for simulation-based design. Engineering with Computers, 17(2), 112-128.

[8] Fenichel, N. (1979). Geometric singular perturbation theory for ordinary differential equations. Journal of Differential Equations, 31, 53-98.

GROUP 3

Novel displacement ment machines

GENERAL LECTURE:

DISPLACEMENT MACHINES - KEY ELEMENTS OF FUTURE TECHNOLOGY

Dr.-Ing. Robert Rahmfeld

Danfoss Power Solutions, Columbus Haus, Am Sandtorkai 38-41, 20457 Hamburg
* Corresponding author: Tel.: +49 40 73675 119; Mobil: +49 173 6288132; E-mail address: rrahmfeld@danfoss.com

Fluid Power displacement machines are still by far the dominant power transfer principles in mobile machinery. Power density, simple continuous variability for rotary and linear drives as well as straight forward repair and service concepts have enabled this technology a very successful development in the last decades. This general lecture will critically analyze if and how those drive line elements will be Key Elements of Future Technology in this market in the future, especially under the view that battery technologies are facing many challenges for powerful machines with intense duty cycles (see also automotive industry). Considering for example the fork lift, it is an application where various technologies can be found inside today, focused on different application conditions and sales channels. But the more powerful and heavy mobile machines are, it is still mainly the traditional concept powered by a combustion engine. However, this can be also seen as a circle of devil, because it is well known that the total efficiency (power-in/power-out) for hydraulic drives is in many cases quite low. I.e. not improving this energy balance or not creating synergies between hydraulics and other technologies, will hinder even hybrid systems to enter the market and to foster advanced technologies. That is why a change usually starts as a combination or extension with the somehow existing technology, and not with a drastic revolution, for which the market including distributors, service/repair centers, etc. in various regions are not prepared. For mobile machines in the field, still reliability and up-time are key to success, what needs to be carefully regarded when considering new technologies into a conservative and cost competitive market.

One aspect or even advantage of hydraulic displacement machines, in particular for motors, is the immediate availability of torque.

Nevertheless, as all mechanical rotary components, there is friction basically following the Stribeck curve. The lecture will also explain that special attention needs to be paid to loss modeling, in particular in the low speed area, in order to ensure that the prediction is well suited as Key Elements of Future Technology. Due to the multi-dimensional and non-linear loss behavior, other physical behavior based modeling approaches are required for a reliable performance picture - than advanced mathematic inter- or extrapolation.
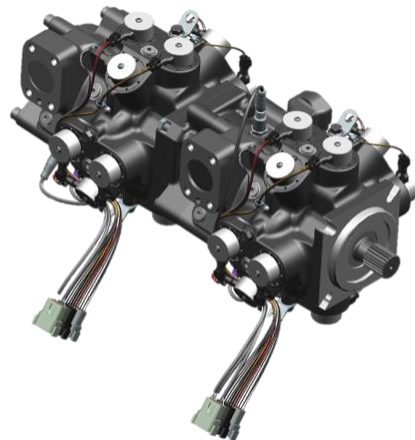
APPLYING A MULTI-SERVICE DIGITAL DISPLACEMENT® PUMP TO AN EXCAVATOR TO REDUCE VALVE LOSSES

Matteo Pellegri*, Matthew Green, Jill Macpherson, Callan McKay, Niall Caldwell

Artemis Intelligent Power Limited, Unit 3, Edgefield Industrial Estate, Loanhead,EH20 9TB, United Kingdom
* Corresponding - author: Tel.: +44 (0)131 440 6268; E-mail address: m.pellegri@artemisip.com

ABSTRACT

Reducing the energy consumption of off-highway machinery due to poor system efficiency is an urgent challenge. Several advanced and innovative architectures have been proposed over the years to tackle this problem, but very few of them found fertile ground for commercial applications due to increased complexity and cost. In this paper, the design, implementation, and testing of a multi-service Digital Displacement ® Pump architecture applied to an excavator are presented. The Digital Displacement ® Pump allows for a dynamic physical displacement allocation to services at different pressure levels, thus reducing throttling losses required to operate multiple actuators simultaneously. A feed-forward control logic is implemented and applied to the system using a closed-centre architecture. The results indicate a fuel reduction of more than 30% compared to the baseline excavator.

Keywords: Digital Displacement®, Digital, Pumps, Excavator, Hydraulics

1. INTRODUCTION

As climate change accelerates, the inefficient energy usage of hydraulic off-highway machinery becomes a matter of global importance. Official estimates are that fluid power systems consume 2 – 3% of the USA's total energy [1], while estimates of typical hydraulic system efficiency range from 21% [1] to 30-50% [2]. The main reasons for this low efficiency are excessive dissipation in control valves, poor pump/motor efficiency, sub-optimal engine utilisation, and lack of recovery of kinetic and potential energy [3].

In previous work [4], the authors investigated the effect on an excavator of swapping the analog axial-piston pumps for Digital Displacement® pumps, thereby reducing the pump energy losses from 10.4kW to 3.6kW for a digging cycle, reducing the fuel consumption per cycle by 21.2% while increasing productivity by 10.4%.

This work showed a substantial improvement for a relatively simple change to the system, and is now being commercialised [5]. However there is limited further potential of this approach, as the DDP pump losses (3.6kW) are such a small fraction of the dominant valve throttling losses (19.3kW), which cannot be significantly improved without changing the system architecture.

Ultimately, throttling losses may be avoided by eliminating proportional valves completely, and instead digitally connecting multiple displacement-controlled DDP pump outlets directly to the actuators [6]. Other authors have also investigated unconventional architectures to reduce throttling losses, such as displacement controlled (DC) circuits [7,2], independent-metering systems and decentralized electro-hydraulics [8,9], 2-pressure level hybrid systems such as STEAM [10], and multi-chamber linear actuators [2].

The efficiency advantages of these approaches are in general counter-balanced by increased complexity and cost, uncertainty over safety, and reduced operator controllability. Vehicle manufacturers have typically taken a more evolutionary approach.

This work describes an evolutionary system which significantly reduces the throttling losses while preserving the same overall system architecture, safety and operator control characteristics.

The concept is demonstrated on a 16-ton excavator, by installing a 'multi-service' DDP, a switching valve block and associated system controllers. The original Negative-Flow (Negacon) control system is replaced by a closed-centre feed-forward control architecture in which

the boom and bucket actuators are decoupled from the arm and swing, thus allowing each group of functions to work at a different pressure level. In this paper, the control system, test method, data analysis, and results are described.

2. SYSTEM DESCRIPTION

2.1. DEXTER: The Digital-Displacement® Excavator

The Digital-Displacement® Pump (DDP)

The Digital-Displacement® Pump (**Figure 1**) is a radial piston machine which enables and disables cylinders in real-time, using ultra-fast mechatronic valves controlled by an embedded computer. The advantages of DDP over traditional swash-plate pumps are mainly [11]:

1. Increased part-load efficiency due to the principle of displacement control by disabling cylinders
2. Faster response (typically less than 30 ms)
3. Lower high-frequency noise
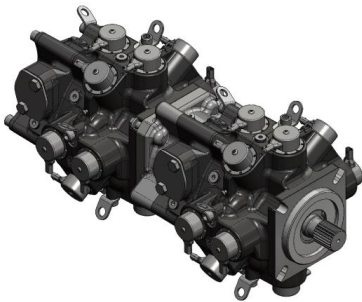
Figure 1: Tandem configuration of a Digital-Displacement® Pump 'E-dyn 96'

The pump installed on the excavator is a tandem configuration of an 'E-dyn 96'. The E-dyn 96 has 12 x 8cc cylinders. The output of these cylinders can be combined to form one 96cc/rev output, or multiple smaller outputs (for example 4 x 24cc/rev), each output being independently controllable. In the tandem configuration used, the DDP has a total of 8 x 24cc/rev outputs, which are referred to as "Pumplets".

The DEXTER hydraulic system

The target machine is a JCB JS160, a 16 tonne tracked excavator property of Artemis Intelligent Power Limited. The specifications of the machine are summarized in **Table 1**. During the 'DEXTER' project, the axial piston pumps were replaced with a tandem E-dyn 96 DDP with two 96cc/rev outputs [4]. The combination of the DDP and standard Negative-Flow control system that was developed during the DEXTER project will be referred to as 'System Architecture 1' (SA1).

Table 1: DEXTER Excavator (JCB JS160) Specifications

Machine parameter	Value
Operating weight [kg]	17774
Engine Max Power [kW]	93
System Max Pressure [bar]	343
Pump Displacement [cc/rev]	2x96

2.2. Concept of the 'Elastic Pump'

In a traditional 2 pump negative flow control system like the JS160, the displacement of each pump is determined by the pressure across the 'Negacon' orifice, which is in series with the spool valve open centres. The boom and bucket functions are primarily serviced by Pump 1, while the arm and swing functions are primarily serviced by Pump 2. This allows two independent pressure levels, reducing the losses due to throttling compared to single pump systems. However, when the boom or arm functions require high flow, the flow from a single pump is insufficient, and the outputs of Pump 1 and 2 are combined via secondary spool valves. This results in a single flow source and therefore a single pressure level – and more throttling losses when multiple functions are operating.

In previous work [4], the authors measured the energy flow through the DEXTER SA1 system. The efficiency when grading was around 30%. As shown in **Figure 2** the most significant losses are due to throttling (shown as 'system losses'). Of these, 70% are associated to delivery and exhaust losses in the arm function.
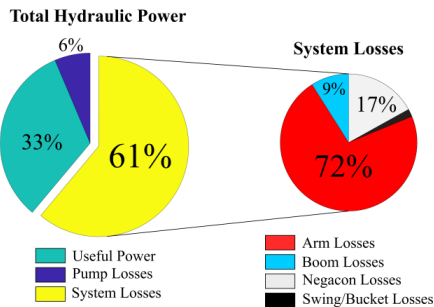
Figure 2: Losses in the grading cycle.

Much of the valve throttling losses for both digging and grading were found to be generated during periods of high flow of either boom or arm functions, when both Pump 1 and 2 were combined and operated at the highest pressure required by any actuator.

By working back from the actuator pressures, it was possible to calculate what the Pump 1 and Pump 2 pressures and flows would be if they were never combined in the valve block. The average mechanical power drawn from the engine could was determined to be 17.5% less (see **Figure 3**).
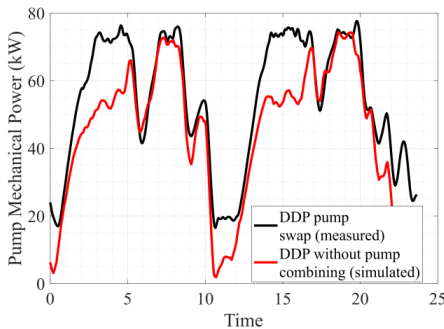
Figure 3: Simulation of effect of inhibiting pump combining

Of course the reason for the pumps combining is that the flow from a single pump is sometimes insufficient, so simply inhibiting the combining function would result in much lower productivity unless pump capacity was increased - which would significantly increase cost, space requirements and pump losses.

It was realised that the total pump capacity installed would not need to be increased if the apportionment of that capacity to each of Pump 1 and Pump 2 could be varied over the course of the

duty cycle. Such a conceptual pump was termed "Elastic" because the capacity of each fluid supply could be stretched or shrunk as required.
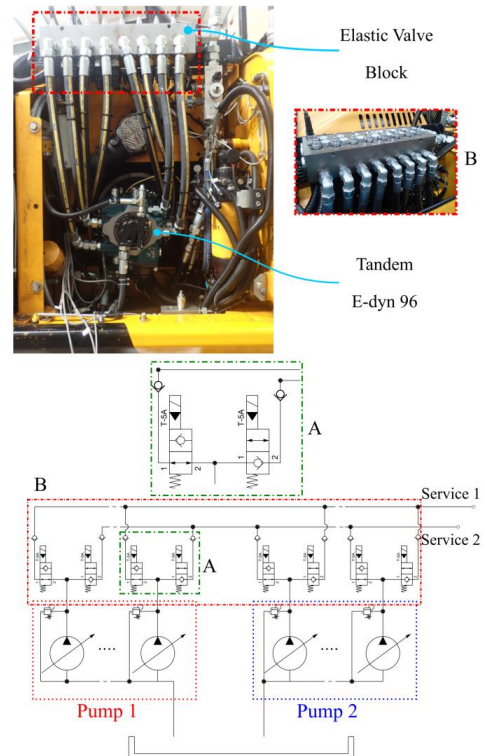
2.3. The 'Elastic Pump' System

Figure 4: Physical implementation and schematic of the Elastic Pump System. The schematic shows the connection between the Pumplets and the two services using 2/2 directional poppet valves working in parallel (detail A). There are four Pumplets per Pump, but only two are shown above for clarity.

Each 'Pumplet' of the 'E-dyn 96' can be controlled as a single variable displacement unit of 24cc/rev or combined to obtain fractions of a tandem unit of 192cc/rev. For the current study, considering that the original circuit of the excavator has two pressure lines, the Pumplets can be combined to obtain two separate units of different possible sizes. A few examples, other than the obvious 96/96 cc/rev, could be a 48/144 cc/rev or 0/192 cc/rev configurations.

The flow redistribution to the two services is obtained using a valve block comprising 16 x 2/2 solenoid-operated directional poppet valves, 8 normally open and 8 normally closed as shown in **Figure 4**. This valve block will be referred to as the 'elastic valve block'.

Each Pumplet is connected to both services using one normally-open valve and one normally-closed: in the normal configuration 4 Pumplets are delivering flow to service 1 and 4 to service 2. When a change of pump 'size' is requested, both valves connected to a single Pumplet are activated and the flow is diverted to the desired service. This operation happens in synergy with the pump controller which now will have bigger and smaller physical displacements available for the two pumps with respect to the previous state.

The combination of the DDP and the Elastic Valve Block will be referred to as the Elastic Pump System, and also 'System Architecture 2'.

Simulation model

In order to verify the feasibility and worthiness of the new architecture, a backwards-facing simulation model aiming at quantifying the benefits in terms of potential fuel savings has been developed. This extends the previous model developed during the 'DEXTER' project [4], which was validated against experimental results. The model takes as inputs measured data of the original system and simulates what the fuel consumption would be with the modified system.

The flows the pumps need to provide are calculated from the ideal active flows requested by the actuators. Assuming a unitary efficiency for the linear actuators the flow required is calculated as

$$Q_{la} = v \cdot A \qquad (1)$$

For the hydraulic motors (e.g. swing motor) the required flow is calculated as

$$Q_m = V_{d_m} \cdot \omega + Q_{loss} \qquad (2)$$

The volumetric losses for the hydraulic motors are calculated using the 'Polymod' approach described in [12], in which the losses are estimated using a polynomial fitting of experimental data together with scaling factors for different sized machines.

The flows are then combined to obtain the total flow associated with each service as follows

$$Q_{s1} = Q_{boom} + Q_{bucket} + Q_{rtrack} \qquad (3)$$

$$Q_{s2} = Q_{swing} + Q_{arm} + Q_{ltrack} \qquad (4)$$

The mechanical power required by the DDP to satisfy the total flow is calculated using a backward-facing simulation model described in [13] in which pressures, speed, and flows are fed as input and the fraction of displacement required to satisfy the flow request, fluid and mechanical power are the output. The volumetric displacement of the two pumps varies dynamically as described in the previous section and is calculated as

$$V_{d_s} = \text{ceil}\left(\frac{Q_s}{\frac{n}{1000}} \cdot \frac{1}{24}\right) \cdot 24 \qquad (5)$$

with V_d in cc/rev, Q_s in L/min and n in rpm. In this way, the flow will be always satisfied even if the total size of the machine is greater than 192cc/rev. It has to be clarified that even though the machine size can be greater than 192cc/rev, the actual flow will be at most 192cc/rev due to the fraction of displacement $F_{ds} \cdot V_{ds}$. To take into account the losses generated by non-working Pumplets the volumetric displacement of the idling portion of the DDP is simply calculated as

$$V_{d_{idle}} = V_{d_{s1}} \cdot \left(1 - F_{d_{s1}}\right) + V_{d_{s2}} \cdot (1 - F_{d_{s2}}) \qquad (6)$$

The pressure for each service is defined by the function at the highest pressure.

Once the mechanical power is calculated for the tandem pump, the total torque is passed to an engine model containing the BSFC map of the engine. In this way, an accurate estimation of fuel consumption can be made.

The simulation model showed good potential for fuel savings with the new architecture. The simulation results are presented together with the experimental results in the results section.

2.4. Modification to the DEXTER Hydraulic System

As previously described, in the original Negacon system, the boom and bucket actuators are connected primarily to Pump 1, whilst arm and swing primarily to Pump 2. To minimise the number of modifications to the system, the original layout has been maintained. The communication between boom and arm and Service 2 and 1 respectively is prevented by blocking the secondary control valves. In the

standard system, this would imply that the boom and the arm can now access only up to 96 cc/rev. This problem can be tackled by the service switching capability of the DDP.

Secondary directional control valves replacement

The concept just presented allows for a complete separation of the two pressure lines allowing each actuator to be fed by a single service whilst satisfying the flow requirements. Modifications are required on the original hydraulic layout for the new control and hydraulic structures to work as intended.

First of all, as the Negacon pressure signal is not required, the Negacon lines can be blocked by turning the open-center system into a closed-center one using solenoid-operated 2/2 discrete position valves.

Secondly, the secondary valves which allow arm and boom to access Pump 1 and Pump 2 respectively, must be by-passed. Removing those valves is not possible as they are integrated into a complex valve block. This problem has been circumvented using two external solenoid-operated valves in parallel to the original secondary valves and by inhibiting the opening of the secondary spools. The new external valves are then controlled in order to achieve the same $\Delta p - Q$ pairs as the original valves for the same joystick signal.

2.5. The Control Structure

In the DEXTER system, the pump displacement was controlled using the signal from a pressure sensor positioned on the 'Negacon' line, previously described [4]. This strategy was conceived to mimic the original swashplate hydraulic control system. In this project a Feed-Forward (FF) control strategy similar to a Positive-flow control system has been implemented.

The controller structure is shown in **Figure 5**. Pilot pressures of each function are imposed by the joystick commands of the operator. Look-up tables are used to convert the pilot pressures (p_{pilots}) into displacement demands (V_{di}) for each function. The displacement demands of the functions connected to each service are summed (V_{dtot1} and V_{dtot2}) and pumplets are allocated to the two services to best satisfy the displacement demands of all functions using a Pumplet allocation algorithm. The Pumplets assigned to each service have limited displacement capacity, so the displacements to each service are saturated (V_{sat1},V_{sat2}). The hydraulic circuit is configured for this Pumplet allocation by acting on the solenoid valves (i_{valves}) in the elastic block. The displacement commands (V_{tot1} and V_{tot2}) are limited if the pressure difference between the pump and the active actuator at the highest pressure exceeds a pressure threshold (which is a function of p_{pilots}, V_{d_i} and shaft speed). The pressure limited displacements (V_{lim1}, V_{lim2}) are further limited using engine anti-droop and torque limiter logic [4] to respect the available engine torque. The torque limited displacements are converted to final fractions of displacement of each service (F_{d1} ,F_{d2}). The maximum displacement of each service is a function of how many pumplets are allocated to each service.

3. TESTING

Tests have been conducted to evaluate the effect of the Elastic Pump architecture on fuel consumption on dig-and-dump and grading operations. In particular, for the digging operation, both 90° Dig-and-Dump and JCMAS air-test [14] cycles were carried out.
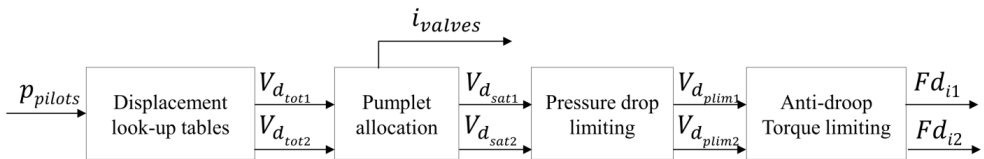

Figure 5:   Simplified block-diagram of the control architecture implemented on the excavator using dynamic allocation of the pumps' physical displacement.

3.1. Test Cycles

According to a study of 2015 [15], tracked excavators spend 60% of their time digging and 15% grading. Grading is a simple operation in which the soil is flattened using mainly the arm and boom actuators, with the bucket tracing a horizontal line parallel to the ground level. Digging is instead a complex operation that changes over time, depending on the depth of the trench, soil and working conditions. A dig and dump cycle, which is representative of an operation in which material is transferred to a truck, is often used to measure the performance of an excavator, although there are again many parameters that can be varied either intentionally (e.g. angle through which the machine rotates) or unintentionally (e.g. the amount which the bucket is filled). In this project a 90° dig and dump cycle was used. The JCMAS H020-2007 [14] standard defines a dig-and-dump cycle where the operation is carried out in air only. It is divided into 4 main operations: a grading operation is followed by the tucking of the bucket, boom lift and swing rotation, and terminated with bucket opening. The pressure of each function varies, and when more than one function is supplied by a single flow source throttling is required to control the functions velocities. This cycle was used in this project and will be referred to as 'JCMAS'.

3.2. Test Set-up

The tests were conducted at Artemis Intelligent Power (**Figure 6**) by both employees (internal) and external contractors. The testing ground was soil with some mixed industrial debris (mixed rocks and broken concrete). Any large pieces of debris (>40x30x20 cm^3) were removed before testing to ensure consistent test cycles. A 2.5m tall metal frame 'hurdle' is used to set a minimum height limit for dig-and-dump and JCMAS Air Loading. The control cabin is used for test engineers to adjust the parameters within the excavator's system controller through remote control features. In particular, the engineers can switch between System Architecture 1 (SA1, DDP with Negative Flow Control) and System Architecture 2 (SA2, Elastic Pump System) while the machine is operating. This remote access can also be used for live fault checking through the Pump controller and DAQ software.

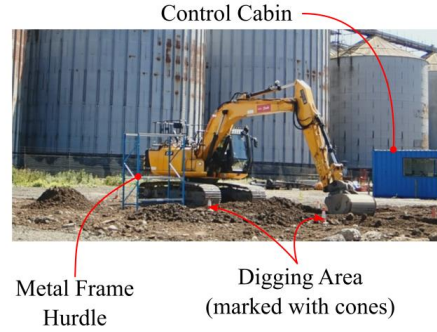Test data for comparison are recorded within 2 hours to ensure similar ground conditions.

Figure 6: DEXTER excavator during test cycle at Artemis Intelligent Power Ltd.

3.3. Test Procedure and Validation

Several tests were performed for each cycle type. During each test, several cycles were repeated. For example, the grading consisted of a circular pattern covering 360 degrees of swing rotation, during which more than 50 full boom/arm extension and retraction were performed. In the case of the JCMAS/digging test, the test was stopped after 20 cycles.

Keeping consistency during the cycle was very hard and the two main factors affected were productivity and end effectors trajectories. In order to select cycles that can be used to perform fair comparisons, a post-processing tool was developed. With this tool, it is possible to evaluate the productivity in terms of useful work/power from experimental data. The useful work for each actuator was defined as

$$W = \sum_i \int \left(Q_{in_i} \cdot p_{in_i} - Q_{exh_i} \cdot p_{exh_i} \right) dt \qquad (7)$$

Tests exceeding 5% difference of useful work for the same architecture were discarded.

As will be discussed in the results section, keeping the useful work the same with the change of architecture was not easy for the digging cycle and the grading. However, in the JCMAS cycle, it was possible to keep the same productivity between tests performed with different architectures.

In order to visualize the motion, a 3D kinematic model based on the Denavit-Hartenberg parameters of the machine was developed.
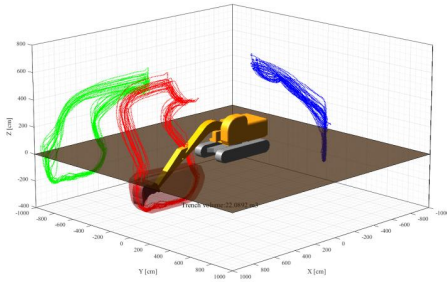
Figure 7: Graphical visualization of a JCMAS air loading cycle. In red, the actual traces, in green and blue the projections on the z-x and z-y axis. In red, the volume covered by the bucket is shown.

The model is capable of estimating the volume of the trench, assuming an initially flat surface and non-collapsing walls (**Figure 7**). The estimation is performed by triangulating the boundary points defined by the bucket and applying a discrete form of the Gauss' theorem. With this tool, the authors were able to perform a qualitative visual inspection of the trajectories in order to spot mistakes of the operators and/or inconsistent cycles. A quantitative approach is also possible; however, the approach is sufficient for the current analysis.

3.4. Test list and description

Table 2:   Test list and description

Operator	Eng. Speed	Cycle Type	N. of Tests	N. Cycles Tot.
External 2	1500	Dig-Dump	4	100
External 3	1500	Dig-Dump	6	72
Internal	1500	JCMAS	2	40
External 3	1500	JCMAS	4	75
External 2	1500	Grading	4	206
External 3	1500	Grading	5	152
External 3	1200	Grading	1	25

All the tests were performed at 1500rpm which is the engine maximum-torque speed except for one grading test performed at 1200rpm. Although several tests were conducted for each cycle type and speed, as shown in **Table 2**, only a limited amount fulfilled the requirements and have been

used for the comparison and presented in the results sections.

4. RESULTS

The results are presented in this section for grading and JCMAS air-loading. Unfortunately, the 90° Dig-and-Dump results were too inconsistent and hence they will not be included. The results show the improvements in terms of fuel consumption, in L/cycle, and productivity, in kW, comparing the System Architecture 1 (SA1-Negacon system) with the System Architecture 2 (SA2-Elastic Pump system). Productivity is calculated as

$$P = \frac{W}{T} \tag{8}$$

Where W is the useful work defined in equation (7) and T is the cycle time. In this way, the improvement in terms of cycle time can be included. The improvement is calculated as

$$\%_{improvement} = \frac{X_{SA1} - X_{SA2}}{X_{SA1}} \tag{9}$$

The test results are also compared with the simulation results. A more thorough analysis is carried on for the results showing significant fuel reduction.

4.1. JCMAS air-loading

The Dig-and-Dump test represents the most realistic situation the excavator will incur in the field [15]. The interaction between the machine and the soil represents a significant obstacle for performing a rigorous analysis of this type of cycle so it is common practice to use standardized gravel for consistency, or to test using a JCMAS air-loading cycle where the uncertainties created by the material being moved are eliminated: in this test, the machine structure serves as the load. **Figure 8** shows the results obtained comparing measured and simulated data for two tests.

The results summarised in **Table 3** show significant improvement in the fuel consumption of up to 16% with a negligible reduction of productivity of 0.8% in the first test as well as an improvement of 13.7% in fuel consumption and 3.3% in productivity for the second test. It should be emphasised that these results are in addition to any savings achieved by the SA1 system over the standard excavator.

The simulation and the measurements are closer to each other thanks to very consistent productivity, thus giving confidence in the model output.
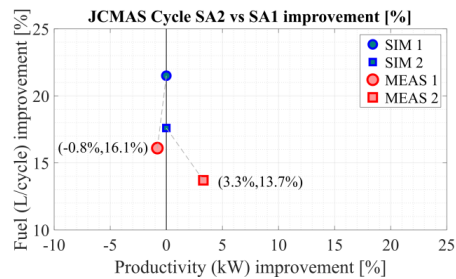

Figure 8: Productivity and Fuel/Cycle improvement for the JCMAS cycle. SIM indicates simulation and MEAS measured data.

Table 3:   Summary of the JCMAS tests results

Test	Fuel Improvement [L/cycle]	Productivity Improvement [kW]
1	16.1%	-0.8%
2	13.7%	3.3%

4.2. Grading

Grading is a low power cycle and it involves only two functions working simultaneously: arm and boom. The ground is scraped trying to keep the penetration depth to a constant level which tests the skills of the operator and the controllability of the machine. Considering the separation of arm and boom pressure, a significant improvement in terms of fuel consumption was expected. In **Figure 9** the results obtained comparing measured and simulated data for two tests are shown.

As expected, the results summarised in **Table 4** show a great improvement in terms of fuel savings, up to 30.5% with an associated productivity increase of 15.9%. Even though the results showed a positive improvement for both parameters, it is clear that keeping the productivity consistent between SA1 and SA2 was a difficult goal to reach. This is probably because the control of the machine differs in the SA1 and SA2 cases: in the SA2 case, the velocities of the arm and boom functions do not depend on their relative pressures.
In Test 4, in order to achieve a similar productivity, the engine speed has been reduced during the SA2 tests until the productivity of the

SA1 case was matched. Similar productivity was reached at 1200 rpm. In this condition, 43.8% of reduction in fuel consumption has been achieved without compromising productivity.
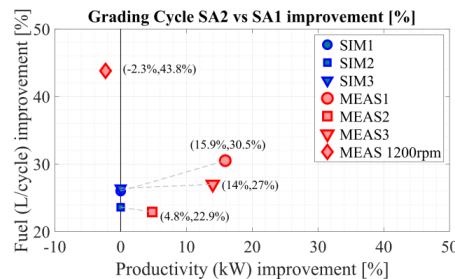

Figure 9: Productivity and Fuel/Cycle improvement for the Grading test cycles. SIM indicates simulation and MEAS measured data.

Table 4:   Summary of the Grading tests results

Test	Eng. Speed [rpm]	Fuel Improvement [L/cycle]	Productivity Improvement [kW]
1	1500	30.5%	15.9%
2	1500	22.9%	4.8%
3	1500	27.0%	14.0%
4	1200	43.8%	-2.3%

4.3. Results Analysis

To understand the reasons for such a decrease in fuel consumption whilst keeping useful power the same (in JCMAS test 2 and Grading test 4), several aspects can be analyzed. Amongst these, the main reasons for a decrease in fuel consumption can be associated to an increase in system efficiency due to a reduction of throttling (delivery) losses, the pump working in a higher efficiency region, and possibly an improved working point on the BSFC map for the engine combined with decreased ancillary loads.

In **Table 5** and **Table 6** the breakdown of the different sources of losses is shown. It is clear that the biggest portion of the fuel savings has to be attributed to a lower engine power demand caused by a significant reduction in system losses. The decrease of pump losses is marginal, together with the reduction of engine accessory power.

**Table 5:   JCMAS Air cycle analysis**

Parameters	SA1 (1500RPM)	SA2 (1500RPM)	Variation
Fuel [L/cycle]	0.066	0.057	-13.7%
Avg. Engine Power [kW]	52.64	45.83	-11.2%
System Useful Power [kW]	17.7	18.24	+3%
Avg. System Losses [kW]	23.4	16.32	-30% (96.3% of total)
Avg. Pump Losses [kW]	2.99	2.77	-7% (3% of total)
Engine Accessory Power [kW]	8.55	8.50	0% (0.7% of total)
Engine BSFC [g/kWh]	201.8	204.3	+1.2%
Cycle Time [s]	18.6	18.17	-2.3%

Table 6:   Grading cycle analysis

Parameters	SA1 (1500RPM)	SA2 (1200RPM)	Variation
Fuel [L/cycle]	0.039	0.0219	- 43.8%
Avg. Engine Power [kW]	59.37	33.53	- 43.5%
System Useful Power [kW]	16.68	16.3	-2.3%
Avg. System Losses [kW]	30.87	8.31	-73% (88.6% of total)
Avg. Pump Losses [kW]	3.23	1.82	-43% (5.5% of total)
Engine Accessory Power [kW]	8.59	7.1	-17% (5.9% of total)
Engine BSFC [g/kWh]	200.2	207.1	+3.4%
Cycle Time [s]	9.85	9.46	-4%

When grading, the power reduction allowed by the DDP enabled a lower engine speed. The fuel consumption is reduced because the total power required from the engine is also reduced. It is important to highlight that BSFC at 1200 rpm is not improved as shown in **Table 6** and it is actually slightly worse (+3.4%). This shows that, if the system losses would have been kept the same, the fuel consumption would have increased in order to achieve the same amount of work.

During the Dexter project the baseline excavator was tested over a trenching, digging and dig-and-dump cycle [4] but unfortunately not over the JCMAS cycle as is used in this project. However, an estimate of the fuel saving of the SA2 system over the baseline system can be made by combining the average fuel saving over the Dexter test cycles and the SA2 JCMAS result, As shown in **Figure 10** the combined saving is more than 30%, which will be verified by direct comparison of the two systems in future.
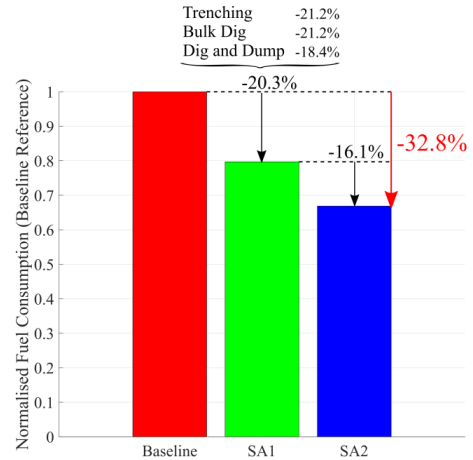
Figure 10: Fuel saving prediction for SA2 system with respect to the baseline machine.

5. CONCLUSION AND OUTLOOK

In this work, the conversion of the hydraulic system of a Digital Displacement excavator from a Negacon flow control architecture to a novel dynamic multi-service Digital Displacement® architecture is presented. The new 'Elastic Pump System' exploits the controllability and dynamic service displacement allocation capability of the DDP technology. Field tests showed significant improvements in terms of fuel consumption, in particular, for the JCMAS and grading cycles. The achieved fuel saving was up to 30% for the same speed with increased productivity and 43% for reduced speed and the same productivity. This is in addition to the already significant improvement made by the simple pump swap system previously presented [4]. These results show the potential of Digital Displacement® to enable unconventional, yet feasible architectures capable of significant reduction of fuel consumption and increased productivity.

In the future, additional tests over a wider range of operating conditions will be performed by directly comparing the Elastic Pump System with the standard baseline machine. This will allow a deeper understanding of the potential and limitations of the new architecture enabling a system design optimization in order to move towards the development of a commercially viable solution.

NOMENCLATURE

A	Area
Fd	Fraction of Displacement
i	Control Signal
n	Speed
p	Pressure
P	Productivity
Q	Volumetric Flow Rate
s	Service
SA	System Architecture
v	Linear Velocity
Vd	Volumetric Displacement
W	Work
X	General Quantity
ω	Angular Velocity

REFERENCES

[1] Oak Ridge National Laboratory (2012) Estimating the Impact (Energy, Emissions and Economics) of the US Fluid Power Industry.

[2] Heybroek K (2017) On Energy Efficient Mobile Hydraulic Systems, Phd Thesis, Linköping University.

[3] Lynch L, Zigler B (2017) National Renewable Energy Laboratory report: "Estimating energy consumption of mobile fluid power in the United States", NREL.

[4] Green M, Macpherson J, Caldwell N, and Rampen WHS (2018) DEXTER: The Application of a Digital Displacement® Pump to a 16 Tonne Excavator. In BATH/ASME 2018 Symposium on Fluid Power and Motion Control. American Society of Mechanical Engineers Digital Collection.

[5] Budden J, Williamson C, Danfoss Digital Displacement Excavator: Test Results and Analysis, ASME/BATH 2019 Symposium on Fluid Power and Motion Control. American Society of Mechanical Engineers Digital Collection.

[6] Rampen W, Caldwell N, Stein U, Joly P, and Fielding M, Fluid Power Distribution and Control System, International Patent Application PCT/GB2007/002747.

[7] Zimmerman J D (2012) Toward optimal multi-actuator displacement controlled mobile hydraulic systems (Doctoral dissertation, Purdue University).

[8] Weber J et al. (2016) Novel System Architectures by Individual Drives. The 10th International Fluid Power Conference.

[9] Minav T, Heikkinen J, Pietola M, (2017) "Direct driven hydraulic drive for new powertrain topologies for non-road mobile machinery", Electric Power Systems Research.

[10] Vukovic D (2016) STEAM–a hydraulic hybrid architecture for excavators.

[11] Caldwell N, Review of early work on Digital Displacement Hydrostatic Transmission Systems, In BATH/ASME 2018 Symposium on Fluid Power and Motion Control. American Society of Mechanical Engineers.

[12] Ivantysynova M (2001) Energy losses of modern displacement machines–a new approach of modelling. The Seventh Scandinavian International Conference on Fluid Power, Linköping.

[13] Caldwell N J (2007). Digital displacement hydrostatic transmission systems. Phd Thesis, The University of Edinburgh.

[14] JCMAS H020:2007 (2007) Earth-moving machinery – Fuel consumption on hydraulic excavator – Test procedure.

[15] Fecke M (2015) Standardisierung definierter Lastzyklen und Messmethoden zur Energieverbrauchsermittlung von Baumaschinen. Proceedings of the 5th Fachgaung Baumaschinentechnik, Dresden, Germany, 17-19.

Digital Displacement® is a registered trademark of Artemis Intelligent Power Ltd.

DIGITAL PUMPS IN SPEED-CONTROLLED SYSTEMS – AN ENERGY STUDY FOR A LOADER CRANE APPLICATION

Samuel Kärnell*, Amy Rankka, Alessandro Dell'Amico, Liselott Ericson

Division of Fluid and Mechatronic Systems, Linköping University, 581 83 Linköping, Sweden

* Corresponding author: Tel.: +46 700 896196; E-mail address: samuel.karnell@liu.se

ABSTRACT

Imagine a system with a pump driven by a speed-controlled electric motor. What and how much can be gained by using a pump with discretely variable displacement instead of a conventional fixed pump in such a system? This question is the focus in this paper, in which a simulation study based on a drive cycle for a loader crane is presented. The results indicate that the system efficiency from inverter input to pump output can increase by a few percentages. This might be considered small in relation to the increasing complexity that comes with discrete displacement. However, the results also show that a system with discrete displacement substantially reduces torque and cooling requirements on the electric motor. The required maximum torque can be reduced by 30 to 50 % and the motor can generate up to 40 % less heat since it can work in more efficient conditions. These potential benefits will be obtained with only a few discrete displacement settings available.

Keywords: Digital pumps, Loader crane, Speed-controlled system

1. INTRODUCTION

There is an increasing interest in implementing electric drives in mobile machines. A consequence is that speed-controlled systems are receiving more attention. Such systems have been used in industrial applications for some years, and several pump suppliers are offering solutions with fixed pumps and variable pumps as well as so-called dual-displacement pumps that are basically variable displacement pumps but with only two pre-set displacement settings [1][2][3]. Arguments for having adjustable displacement in speed-controlled systems are that the electric motor can be downsized and that the total efficiency can be increased.

When it comes to systems with discrete displacement pumps, several researchers have studied the performance of novel architectures, see e.g. [4][5][6]. However, these studies use fixed-speed prime movers and mainly focus on the system architecture, unlike the focus of this study.

1.1. Contributions

The idea behind this paper is to quantify the amount of energy that can be saved and how the requirements on the electric motor changes when discretely variable displacement is used instead of fixed displacement in a speed-controlled system. This study does not consider how the pump should be controlled in real-time applications and it does not take dynamic aspects of the system into account.

The system boundary is set from the input of the frequency converter to the outlet of the pump, as illustrated in **Figure 1**. The flow from the pump as well as the pressure increase over it is always considered to be positive. This means that regeneration possibilities are not considered.

1.2. Digital Pumps

The title of this paper includes the term "digital pump", but there is no widely accepted definition of what a digital pump is. Some might think of the Artemis Digital Displacement pump, but that is not necessarily the type of pump considered here. In this paper, a digital pump is defined as a pump with discretely variable displacement that is built up from several pump elements. Each pump element can be either active or not. The principle layout is illustrated in **Figure 1**.
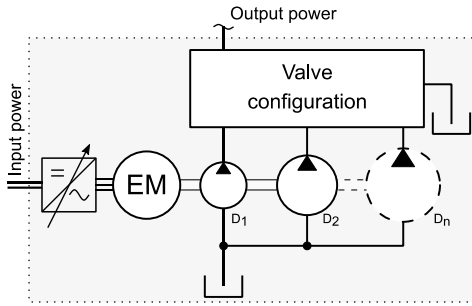
Figure 1: Principle layout of a digital pump with n number of pump elements driven by one frequency controlled electric motor. The large box illustrates the system boundaries for this analysis.

Looking at **Figure 1**, it is reasonable to regard a digital pump as several stacked pumps, but there are other possible solutions. For example, some types of piston pumps can be turned into pumps with a discrete number of displacement settings by grouping the pistons in the pump [7]. When grouping pistons, digital pumps do not have to be much larger than fixed pumps and cost-wise it is only the additional valve configuration and its control, which is required to switch between displacement settings, that differs. Therefore, digital pumps can be an interesting alternative to fixed pumps.

Valve configuration

There are different ways of realising the valve configuration in a digital pump. For example, through use of a check valve in combination with a 2-way valve for each pump element, as shown in **Figure 2**. Characteristics of different valve combinations are discussed in [7]. However, how they differ is not important for the analysis presented in this paper.
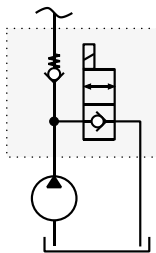
Figure 2: An example of a by-pass valve configuration.

Scaling of pump elements

The pump elements that the pump is built up from can be of arbitrary size and optimized for a specific case. However, another alternative is to use so-called binary scaling. That means that the second element is twice the size of the first, the third element is twice the size of the second and so on. Binary scaling results in an equally distributed displacement setting range. This is illustrated in **Figure 3**. All results presented in this paper are based on binary scaling.
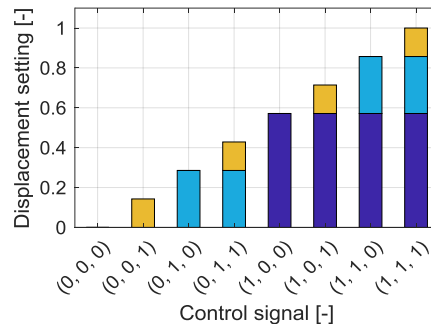
Figure 3: Control of a binary scaled digital pump with three pump elements.

1.3. Synchronous machines

There are many types of electric machines. However, permanent magnet synchronous machines (PMSM) are starting to get common in mobile systems due to their high efficiency and high power density. Therefore, this kind of electric machine has been considered in this analysis. The working range of a PMSM is usually divided into an intermittent region and a continuous region. An example of a typical working range is illustrated in **Figure 4**. As a rule of thumb, when dimensioning the motor for a drive cycle, the point where the root mean square of the torque meets the root mean square of the speed should be within the continuous region [8]. However, the size of the continuous region is highly dependent on the cooling capacity. Better cooling means higher continuous torque. The peak torque of the motor is principally defined by its physical size.

In addition to the intermittent and continuous region, a flux weakening region is also illustrated in **Figure 4**. Flux weakening must be achieved at speeds above the rated speed to reduce the back

emf voltage, which increases with speed. Flux weakening costs energy, which means reduced efficiency. Nevertheless, in this study the rated speed is never exceeded.
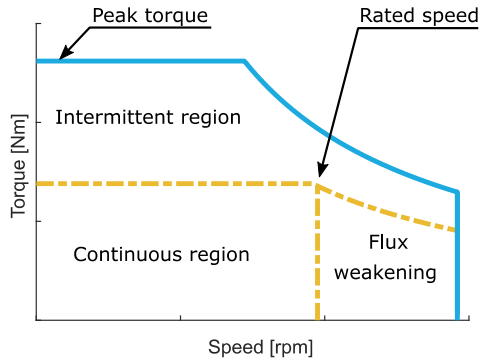

Figure 4: Example of working range for a liquid cooled synchronous motor.

2. SIMULATION MODEL

The simulation model that has been developed for this analysis is static. The input to the model is pressure and flow and from this, the required electric power is calculated. An overview of the model is illustrated in **Figure 5**.

2.1. Model initialisation

Before running the model, some parameters are initialised, primarily pump displacement, peak torque for the motor and inverter power rating. The parameters are based on the drive cycle and the rated motor speed. Throughout this analysis, the rated speed is set to 2400 rpm. The required pump displacement is calculated from the highest flow in the cycle and the rated speed. To compensate for the flow losses, the displacement is iteratively increased until it fulfils the required flow in the cycle. For the torque dimensioning, two different initialization methods have been used: one where the torque is calculated from the corner power and one where it is based on the maximum cycle power. The different power levels are shown later in **Figure 10**, where the drive cycle is presented.

2.2. Control

In this model, the most efficient displacement setting is used at all times. All possible displacement settings are evaluated for each point in the drive cycle and the one with the lowest losses is chosen. Restrictions are set to avoid speeds over the rated speed as well as torque over the peak torque. This control is inappropriate in a real system since it means a lot of switchings and requires much computational power. However, it gives the best possible energy efficiency, assuming switching losses due to compression and decompression of the oil are small.

2.3. Pump model

The pump model is based on look-up tables for the losses, which in turn are based on measurements provided by the manufacturer. The layout of the pump model is illustrated in the top block of **Figure 5** and the efficiency map for the reference pump is shown in **Figure 6**.

The first steps in the pump model are to calculate the ideal speed and to determine the pressure for each pump element. This means that the inactive elements get the pressure that corresponds to their pressure drop over the bypass valve. For the active elements, the pressure drop is added up to the system pressure. The actual speed is then calculated by iterating the flow losses. When the actual speed is determined, the torque losses are calculated. Additionally, the actuation power required for the bypass valves is summed up to the power consumed by the system. The valves can be either normally pumping or normally bypassing. In these simulations normally pumping valves have been used, which means that no actuation power is required for an active pump element.

The losses from the look-up tables for the flow and torque losses are scaled with the displacement of the pump, which often is the case for analytical loss modelling in pumps [9].

2.4. Electric motor model

Like the pump model, the motor model is based on look-up tables, but with speed and relative torque as input variables and required input power as output. The model structure is shown in the middle block in **Figure 5** and the efficiency of the reference motor is shown in **Figure 7**.

When rescaling the motor parameters, the relative power losses are based on the relative torque. This assumption is based on efficiency maps in data sheets [8].
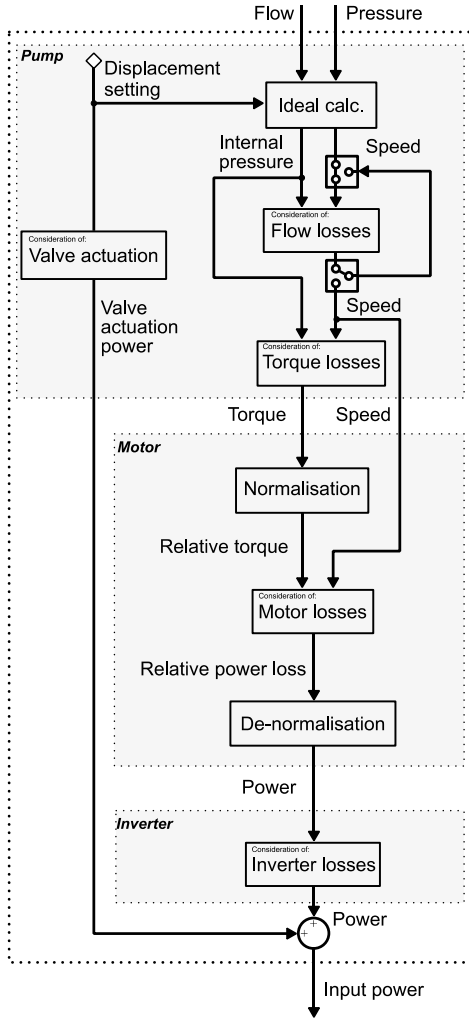

Figure 5: Layout of the simulation model. The arrows show the direction for the calculations, which is opposite to the energy flow. The model basically consists of three blocks; the pump, the motor and the inverter.
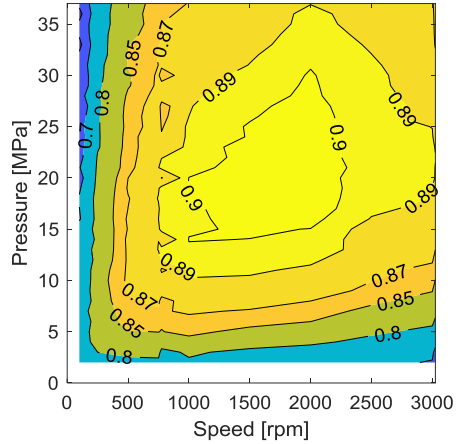

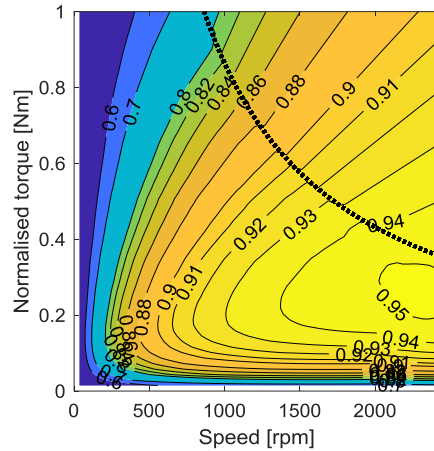**Figure 6:** Measured total efficiency for the reference pump, which is a 34 cc bent-axis pump.

Figure 7: Provided synchronous motor efficiency with normalised torque. The dotted line represents the border between measurements and the described loss model.

In the motor data provided, measurements for the efficiency over a certain power were missing. To make the model more general, that region was filled with data from a simple loss model described in Equation 1:

$$P_{loss} = T^2 R + n^\alpha c \tag{1}$$

T is the torque and n the speed. The other parameters are constants based on the provided measurements. The first term represents the copper losses and the second the core losses. The

representation of the core losses is a result from lumping of parameters in the modified Steinmetz equation [10]. The efficiencies above the dotted line in **Figure 7** are based on this loss model. However, note that these efficiencies imply a high cooling capacity and that they only will be reached in simulations where the motor is dimensioned for the cycle power.

2.5. Inverter model

The losses in the inverter are mainly conduction and switching losses. The simulations are based on data for a typical inverter [11], which is shown in **Figure 8**.
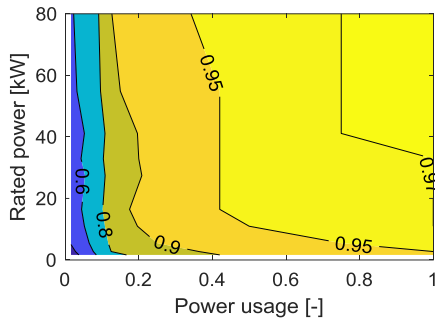
Figure 8: Inverter efficiency used in the model.

3. DRIVE CYCLE

As mentioned, the drive cycle corresponds to the input to the simulation model and is defined in terms of pump flow and pump pressure. It is based on long term field-measurements made on a crane. The pressure is measured, and the flow is derived from the cylinder positions. See [12] for more information about the drive cycle generation. Note that regeneration is not considered in this study since the required flow is defined as positive at all times.

    Figure 9 shows histograms for the pressure, flow and power in the drive cycle. It can be seen that the crane is operating at very low power most of the time. The drive cycle is also represented in a pressure/flow-diagram in **Figure 10**.
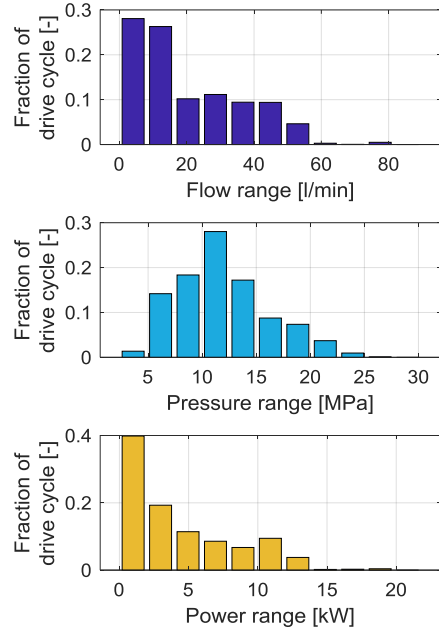
Figure 9: Flow, pressure and power distribution of the drive cycle.
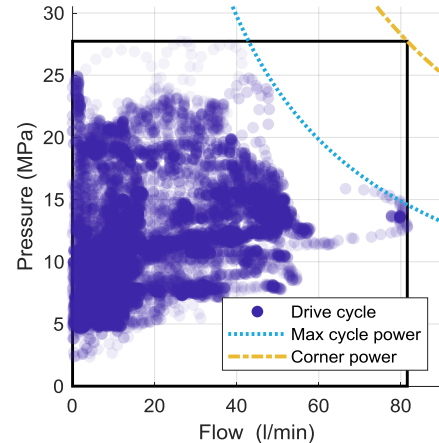
Figure 10: Pressure/flow-diagram of the drive cycle. The max cycle power-line shows the highest power used in the cycle and the corner power is the required power when using maximum flow at maximum pressure.

4. RESULTS

As earlier stated, there are two main reasons to consider a digital pump; downsizing possibilities and energy savings. However, before going into the results, the general simulation setup is described.

4.1. Simulation setup

If nothing else is stated, the presented results are based on the following setup:

- Number of pump elements: 2.
- Rated motor speed: 2400 rpm.
- Valve size: 120 l/min at 10 bar pressure drop. The pressure drop is the same over the bypass line as for the line to the system for all pump elements.
- Valve configuration: normally pumping.
- Valve actuation power: 33 W.

The efficiency of the system will also be affected by the size of the motor as well as the rated inverter power. As earlier mentioned, two different dimensioning methods are applied when dimensioning these components. One where the they are dimensioned strictly by the cycle. This method allows for downsizing of the electric motor and inverter. The other method is to dimension for the corner power. This means that the motor and the inverter must keep the same size for all simulated cases.

4.2. Downsizing

The downsizing possibilities for the analysed drive cycle, when only considering the peak torque, are illustrated in **Figure 11**. It shows that 67 % of the reference peak torque is required to be able to run the whole cycle with 2 pump elements. With 3 pump elements it is instead 62 % and with 4 it is 56 %. This should be compared to a continuously variable pump where 53 % of the torque is needed. Bear in mind that this relation is the same as the ratio between the maximum cycle power and the corner power illustrated in **Figure 10**.
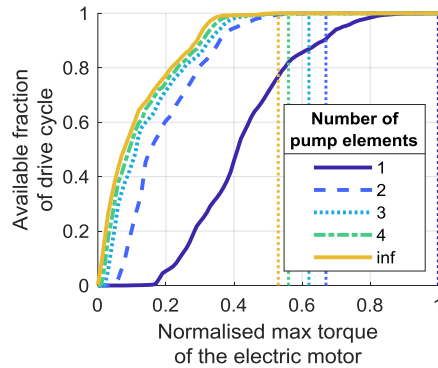
Figure 11: Drivable fraction of the drive cycle as a function of motor torque for different number of binary scaled pump elements. Inf corresponds to a continuously variable pump. The vertical lines are placed at the torque level where 100 % of the cycle can be performed.

As mentioned in the introduction of the paper, it is not only the peak torque that is of interest when dimensioning the motor, but also the rms torque for the cycle, which can give an indication of the required continuous torque. The required peak torque and the rms torque for different numbers of pump elements are shown in **Figure 12**. The figure shows that the rms torque decreases slightly in relation to the peak torque when downsizing the motor. It also shows how the rms speed is increasing.
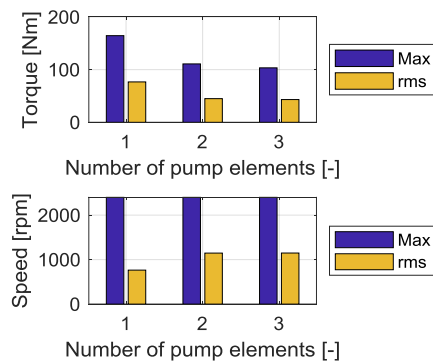
Figure 12: Relation between maximum values and root means square values torque and speed when using different numbers of pump elements.

4.3. Loss analysis

The efficiency is defined as the output energy for the whole cycle divided by the input energy. **Figure 13** shows how the efficiency varies with the valve size for different numbers of pump elements in both dimensioning cases. Note that the reference line is slightly higher than the curve for a digital pump with one pump element. The reason is the additional losses that comes with the bypass valve. When comparing the both dimensioning cases, one can first note that the efficiency is generally lower in the corner power case. This is mainly due to the fact that the inverter losses increase when the inverter is working at a lower relative power. Apart from that, the results are very similar. The total efficiency gains correspond to about two to three percentages for a 120 l/min valve.

Dimensioned for cycle power

Dimensioned for corner power
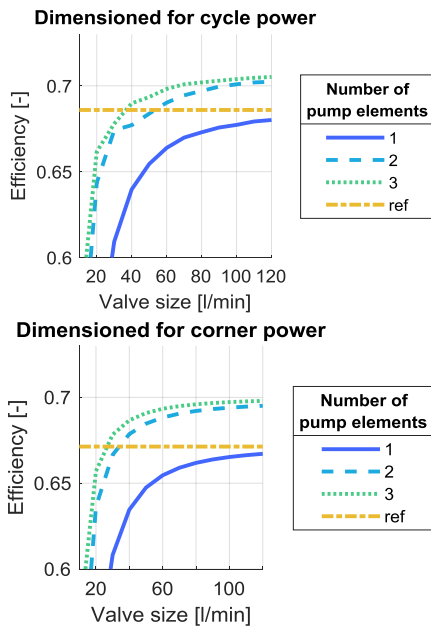
Figure 13: Efficiency for different valve sizes when varying the number of pump elements. The line labelled ref corresponds to a fixed pump without bypass functionality. In the upper figure components are dimensioned for the required cycle power whilst the lower shows components dimensioned for the corner power.

The loss distribution between the different components is illustrated in **Figure 14**. It shows that the introduction of more pump elements reduces the total losses by about 10 %. However, note that the motor losses can be reduced by up to 40 %.

Dimensioned for cycle power

Dimensioned for corner power
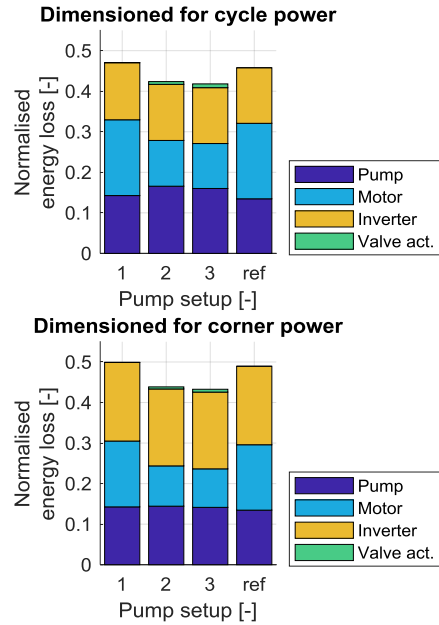
Figure 14: Energy losses in the different components over the full drive cycle. The losses are normalised with the output power, which is defined by the drive cycle and equal for all pump setups. The pressure drop over the valve configuration is included in the pump losses.

In **Figure 15**, it is illustrated how the working points for the motor changes when increasing the number of pump elements without downsizing the motor. It can be seen how the points are moving towards a more efficient region. The downsizing possibilities are also visible since the required torque is reduced when the number of pump elements is increased. If the motor is downsized, the results will be similar, but the efficiency maps will be rescaled and the motor will have to work in its high-power corner, where the losses are modelled according to Equation 1.
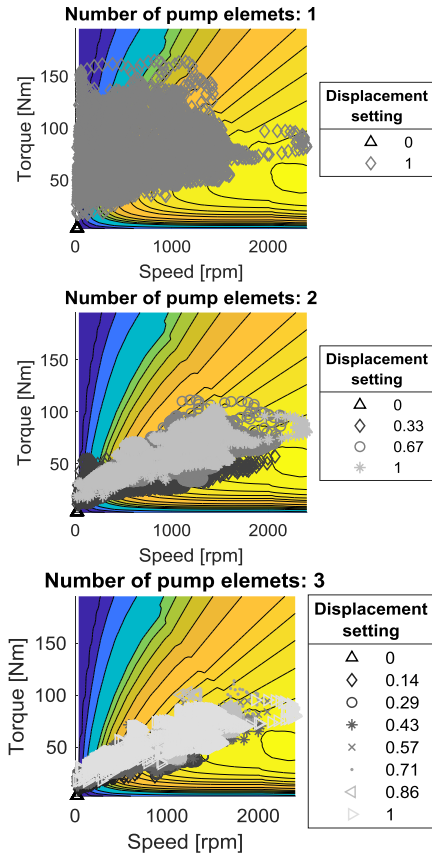
Figure 15: Drive cycle scattered over the motor efficiency map for different numbers of pump elements when dimensioning the components for the corner power.

4.4. Drive cycle variations and generalisability

The results presented so far are based on the specific drive cycle. However, it is of interest to see to what extent the results are applicable to other cases. To illustrate how sensitive the results are to variations in the drive cycle, random noise of different amplitudes was added to the cycle. **Figure 16** shows how the efficiency varies with added noise. The implementation method of the noise signal is shown in **Figure 17**. The results indicate that the difference in efficiency between

a digital and a fixed pump is almost independent of the noise. The inclination of the efficiency can be explained by that fact that the average power increases when adding noise this way since the output values are saturated between zero and the maximum cycle value.
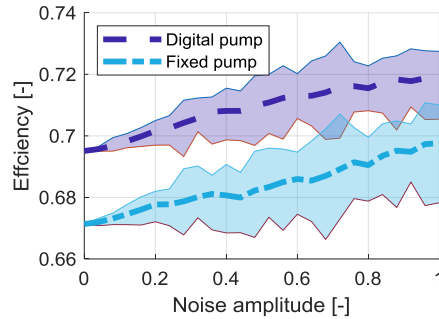
Figure 16: Sensitivity to changes in the drive cycle. 25 simulations were run for all analysed noise level amplitudes. The shaded areas corresponds to the efficiency variations and the lines shows the average efficiency. The implementation of the noise signal is shown in **Figure 17**.
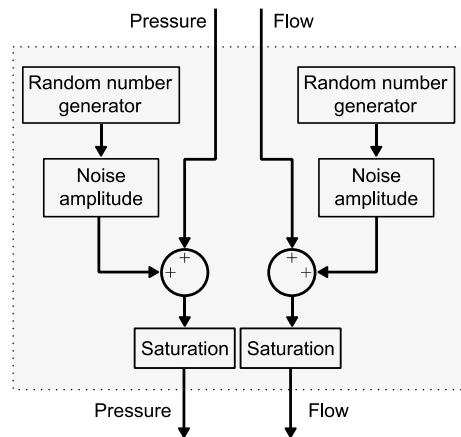

Figure 17: Implementation of the noise signal. The random number generator generates a number between the negative and positive maximum cycle value. This is multiplied by the noise amplitude factor and the product is added to the original signal. The saturation block limits the output to be between zero and the maximum cycle value.

To determine if a drive cycle is applicable for a digital pump, the absolute power loss reductions for each work condition is of interest. **Figure 18** shows the difference in power consumption between a digital pump with two pump elements dimensioned for the corner power and a fixed pump. It shows that the highest loss reduction possibilities are in the high-pressure/low-flow region, when the lowest displacement setting is in use. This means that drive cycles working much in that region will have high efficiency gain possibilities. This is because the motor does not have to work much in high-torque/low-speed conditions. However, when the highest displacement is in use, the losses will be slightly higher for a digital pump than a fixed because of the additional pressure drops over the additional valves.
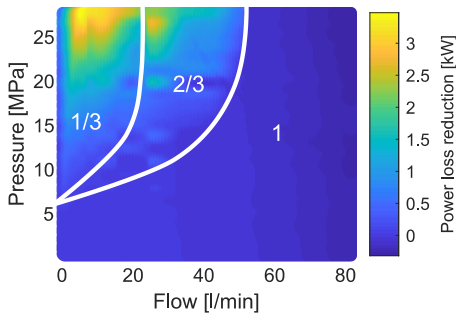
Figure 18: Difference in power consumption for a corner power dimensioned digital pump with two pump elements and a fixed pump. The figure also shows the most efficient displacement setting for each working condition.

5. DISCUSSION

The increase in efficiency for the analysed case is only a few percentages since the drive cycle mostly is in the moderate pressure region, where the difference in power losses are small, as illustrated in **Figure 18**. The impact will be greater for a drive cycle that rarely requires high flow but low flow at high pressure often. A related notice is that it, from an energy perspective, could be interesting to only have two available displacement settings since displacement settings in the higher region does not affect the efficiency much.

Nevertheless, this study shows that the total efficiency is not increased much, but when looking at energy losses, the numbers are larger, especially the energy losses in the motor, which can be reduced by about 30-40 %. This means that the lifetime of the motor can be increased, since it will be exposed to less heat. Alternatively, the cooling restrictions of the motor can be lowered. It has also been stated that the peak torque of the motor can be reduced if one allows dimensioning for maximum cycle power instead of corner power. However, note that these downsized motors must be able to run at high power in relation to their peak torque.

Anyway, smooth switching behavior is a criterion for digital pumps if they should be considered as relevant for loader cranes and similar applications. To achieve this, research is required. Furthermore, digital pumps must also be cheaper and/or have better efficiency than variable pumps since variable pumps allows for the same or even better performance than digital pumps can do.

6. CONCLUSIONS

It has been shown that the differences in potential loss reductions and downsizing possibilities are small between a digital pump with two and three pump elements. Regarding the total efficiency, it can be increased by a few percentages for the analysed drive cycle, but the potential benefits are higher for cycles that often requires low flow at high pressure. The results also show that even if the total efficiency is not increased much, the motor losses can be reduced substantially. The requirement of the peak torque can also be significantly reduced. This means that digital pumps mainly are relevant if downsizing of the electric motor is of interest or if the cooling requirements of it should be reduced, alternatively if the drive cycle often requires low flow at high pressure.

7. ACKNOWLEDGEMENTS

NOMENCLATURE

P_{loss}	Power loss [W]
T	Torque [Nm]
R	Lumped constant [(sNm)-1]
n	Speed [rad/s]
α	Constant [-]
c	Lumped constant [Nm]

REFERENCES

[1] Moog Inc. (2017) Electrohydrostatic pump unit. CDL49052-en, Rev. D.

[2] Eaton (2015) Variable speed drive pump solution. E-PUIO-CC002-E.

[3] Parker Hannifin Corporation (2017) Drive Controlled Pump Effiziente hydraulische Antriebe mit System. HY11-3351/DE.

[4] Moorhead JR (1984) Saving energy with digital pump systems. Machine Design, 56(4): 40–44

[5] Heitzig S, Sgro S, Theissen H (2012) Energy efficiency of hydraulic systems with shared digital pumps. International journal of fluid power 13(3): 49–57

[6] Locateli C, Teixeira P, De Pieri E, Krus P, De Negri V (2014) Digital hydraulic system using pumps and on/off valves controlling the actuator. In 8th FPNI Ph. D symposium on fluid power, pages V001T01A009–V001T01A009. American Society of Mechanical Engineers.

[7] Kärnell S, Ericson L (2019) As Simple as Imaginable - an Analysis of Novel Digital Pump Concepts. 16th Scandinavian International Conference on Fluid Power

[8] Parker Hannifin Corporation (2018) Global Vehicle Motors GVM Series. PVD 3668_GB.

[9] Huhtala K, Vilenius M (1997) Comparison of steady state models of hydraulic pump. 5th Scandinavian International Conference on Fluid Power

[10] Reinert J, Brockmeyer A, De Doncker R. W (2001) Calculation of losses in ferro-and ferrimagnetic materials based on the modified Steinmetz equation. IEEE Transactions on Industry applications, 37(4), 1055-1061

[11] U.S. Department of Energy (2012) Adjustable Speed Drive Part-Load Efficiency. DOE/GO-102012-3730

[12] Rankka A, Dell'Amico A, Krus P (2019) Drive Cycle Generation for a Hydraulic Loader Crane. The 16th Scandinavian International Conference on Fluid Power

DESIGN AND TESTING OF PISTONS AND CUPS FOR LARGE HYDROSTATIC PUMPS AND MOTORS

P.A.J. Achten*, R.F.H. Mommers, H.W. Potma, J.J. Achten

INNAS BV, Nikkelstraat 15, 4823AE Breda, The Netherlands
*Corresponding author: E-mail: pachten@innas.com

ABSTRACT

A new transmission is being designed for a next generation of large, offshore wind turbines, based on floating cup pumps and motors. The machines have a fixed displacement of around five liter per revolution. The objective of this study is to design, manufacture and test the pistons and cups of these machines. To this end, a new test bench has been designed and build, to measure the leakage and friction of the pistons up to a pressure level of 350 bar. Several sets of pistons and cups have been tested against a reference set which was proven to have very little friction at rated and peak operating conditions. The leakage between the pistons and cups was measured at different piston positions at stationary conditions. The friction between the piston and the cup has been measured continuously. From the tests it can be concluded that the friction force is below 0,01% of the piston force. The leakage losses are less than 0,5% of the total effective flow output.

Keywords: Floating Cup, Transmission, Turbine

1. INTRODUCTION

The Dutch company Hydrautrans is developing a transmission for large scale wind turbines. The target of the new design is to combine high efficiency, reduced nacelle weight, increased lifetime, and reduced maintenance costs. A key element of this transmission is a 4919 cc hydrostatic pump or motor that uses floating cup technology [1]. The pistons and cups were considered to be the most critical components in this design. To test these core components, a separate test bench has been designed and build. This new test bench needed to give evidence of the low friction and wear behavior. The test results are also expected to be a good indication of the efficiency of the complete hydrostatic drivetrain components.

2. DESCRIPTION OF THE TEST BENCH

With a diameter of 66 mm, the dimensions of the pistons and cups in the 4919 cc pump are much larger than the dimensions of any floating cup pump tested before. At this size, the deformation of the components as a result of the oil pressure will be much larger than with smaller components. **Figure 1** shows an exaggerated illustration of how the two components will expand. The figure shows that the cup will expand uniformly, while the piston, which is positioned at an angle, will deform to an oval
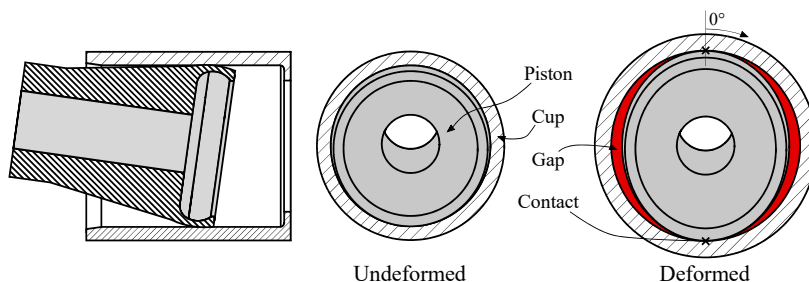

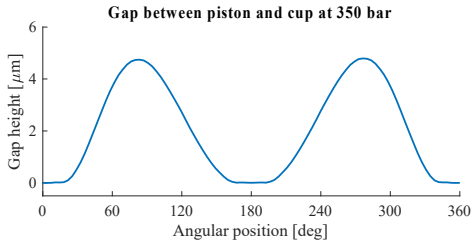**Figure 1:** Deformation of the piston and the cup as a result of the oil pressure.

Figure 2: Simulated gap between piston and cup at an oil pressure of 350 bar (0° corresponds with definition in **Figure 1**).

shape. **Figure 2** shows the distance between the two components from a contact simulation of the two components with an oil pressure of 350 bar.

Friction forces

As a result of the oval expansion, the friction between the piston and cup will increase where the piston expands more than the cup (points indicated with 'x' in **Figure 1**, and gap height = 0 in **Figure 2**). The friction was expected to be less than 100 N. Since this is merely 0.08% of the hydrostatic forces on the piston at a pressure of 350 bar, the main design challenge was to isolate the friction from the other forces. This was realized by having two sets of pistons and cups being applied in opposite directions, thereby balancing the main piston forces.

The cups are placed back-to-back in a central block that is held in place by a force sensor, while the pistons are connected via a moveable construction around the central block. During experiments, oil is supplied to the pistons and cups under various pressure levels. The pistons can be moved by a linear actuator, while the remaining forces on the central block are being
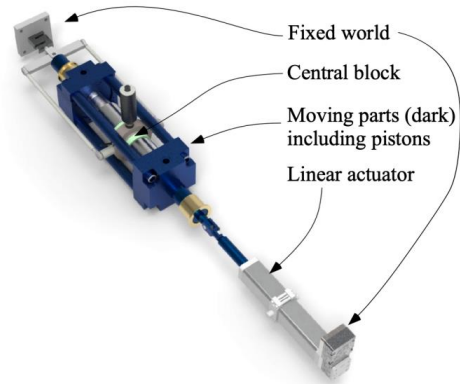

Figure 3: Main components of the test bench.

measured. The main components of the test bench are shown in **Figure 3** and **Figure 4**. Since one of the piston-cup sets will be a reference set with near zero friction, the force that is measured between the central block and the fixed world will be the friction force between the other piston-cup set: the test specimen.

Leakage flow

Another result of the oval expansion of the piston is that a gap forms where the piston expands less than the cup (red areas in **Figure 1**, and gap height > 0 in **Figure 2**). An additional feature of the test bench is that it is designed such that the leak flow at the contact between the piston and cup is separated from the other leakages, as illustrated in the cross-section shown in **Figure 4**. The separated leak flow rate was measured in a separate experiment to exclude the resistance of the flow sensor from the friction force measurements.
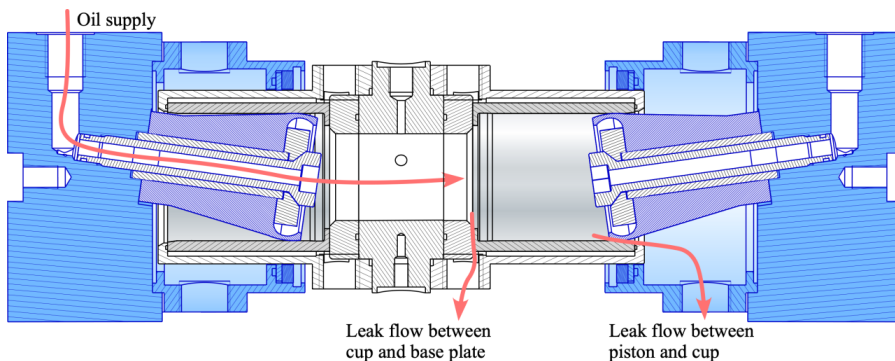

Figure 4: Cross-section of the centre of the test bench (blue parts are moving) with separated leak flow paths.

3. CUPS AND PISTONS

State of the art manufacturing techniques were used to produce two unhardened reference piston-cup sets, and nine hardened piston-cup sets for testing. Each of the components has a diameter of 66 mm, and was manufactured to a precision of less than 3 µm. **Figure 5** shows how the minimum and maximum fitting inside diameter of the cups was measured at five positions. From this figure it can be concluded that the cup had a slightly smaller diameter in the bottom dead center (BDC), which was true for all of the cups. This was an unintentional result from the used production method.
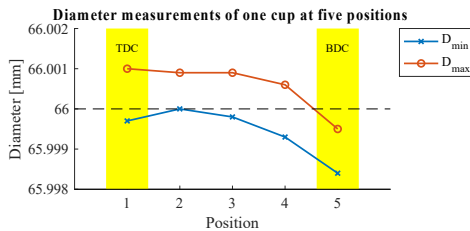
Figure 5:   Minimum and maximum fitting diameter measured at five positions in one cup.

Small differences in the diameters of each piston and cup made some sets fit tighter than others. To specify how tightly each piston fits in its cup, the gap between them was defined as the difference between the largest fitting inner diameter of the cup and the smallest fitting diameter around the ball shaped crown of the piston. Since the friction forces will be larger for tighter fitting sets, some of the tightest fits were chosen as the test specimens to measure the worst-case scenario.

By combining pistons and cups from different sets, a total of five sets were selected with decreasing difference in diameter between the piston and the cup: -1.9, -2.7, -3.9, -5.2, and -7.0 µm. Note that all of these sets have a negative diameter difference. This means that the piston crown at some point is larger than the largest fitting inside diameter of the cup. An advantage of negative tolerances is that the deformation of the piston will be less oval, since the expansion of material is limited by the slightly smaller cup. This means the leakage between the piston and cup will decrease, while only slightly increasing the contact friction forces.

4. MEASUREMENT DESCRIPTION

Two types of measurements were done:
1. dynamic, measuring the friction forces, and
2. static, measuring the leak flow.

For each piston-cup set, all measurements were done at a pressure level of 50 to 350 bar in steps of 50 bar, using Shell Tellus 46 oil at a measured temperature between 49.5°C and 50.5°C.

4.1. Positioning

The pistons in the design of the full 4919 cc machine will make a stroke of 51.5 mm. The testbench was set up such that the pistons would make a stroke of 54.0 mm, to make sure the extreme positions were included. The position of the piston inside the cup was defined as the distance to the bottom of the cup, with 0 being the top dead center (TDC) and 54.0 mm the BDC. The position was measured at the motor of the linear actuator.

4.2. Friction forces

The friction between the piston and the cup has been determined by measuring the forces acting on the central block. During these measurements, the chambers surrounding the cups to collect the leaked oil were removed on both sides of the test bench to exclude the friction between these chambers and the central block from the measurements.

Figure 6 shows the position profile that was used for the friction tests. the actuator moved the pistons back and forth for two full cycles. This is done at a speed of 0.010 m/s, with an acceleration and deceleration of 0.1 m/s^2 at the turning points, resulting in a frequency of 0.091 Hz. Since the speed of the pistons in the turbine will be much higher, this is considered the worst-case scenario
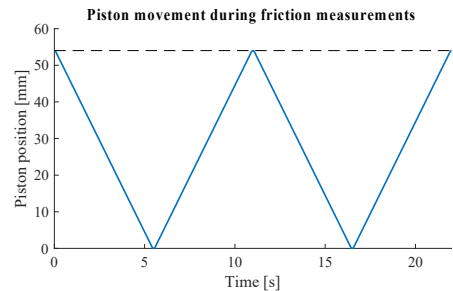

Figure 6:   Piston position during the friction tests.

when determining the friction forces, as there is no hydrodynamic friction yet.

Leak flow

The leakage of oil between the piston and the cup has been determined by measuring the flow rate during static measurements at incremental piston positions. In these static measurements, the linear actuator moved the piston block from position 0 to 54.0 mm in steps of 6.0 mm. At each position, the flow sensor output during a period of 10 seconds was stored, the average of which is shown in the results section.

5. MEASUREMENT RESULTS

5.1. Friction force

Reference sets

During a dynamic measurement, the force sensor measures the combined friction of both piston-cup sets. If one of the sets is known to have very little friction, the measured force is more or less equal to the friction of only the other set. To this end, the two reference sets were measured first. **Figure 7** shows the measured forces at four different pressure levels.

The reference force measurements shown in **Figure 7** clearly have an offset at all pressures. This is caused by a slight difference in area between the two piston-cup sets that are placed opposite to each other in the test bench (a difference of 0.01% between the two piston surface areas will already result in 12 N at 350 bar). Assuming that the friction is equal (but switched sign) in both directions, this offset equals the average value of the measured force during the two full cycles. **Figure 8** shows the same results, but after subtracting these average values. This correction seems to remove the offset properly, as the forces are now close to mirrored around the 0 N axis.

The results in **Figure 8** show that while there is very little friction force at lower pressure (up to 8 N), there is almost no friction in the reference sets when operating at higher pressures (less than 2 N for most part of the stroke). This force was found to be negligible with respect to hydrostatic forces acting on the pistons. Please consider that during the measurements with the hardened sets, the measured friction force will be the combined
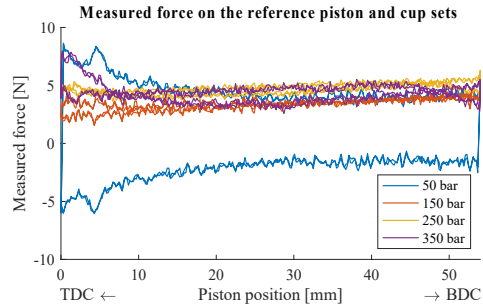

Figure 7:   Measured force during dynamic measurement using both reference sets.
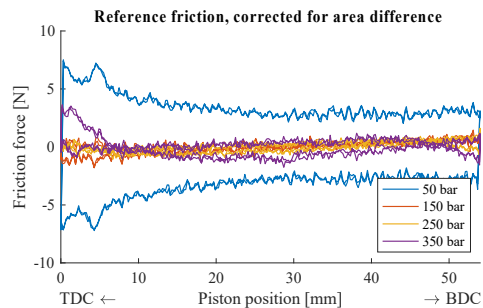

Figure 8:   Friction forces of the reference sets after correcting for area differences.

friction of this test subject and one of the reference sets.

Test specimens

The results of the dynamic measurements using the hardened sets, at a pressure of 50 and 300 bar are shown in **Figure 9**. Similar to the reference results, these results were first corrected by the average value of the measured force to account for the shape differences.

Overall, **Figure 9** shows relatively small amounts of friction during most of the stroke. At 50 bar, the maximum friction of each set was measured when the piston was in BDC. The tightest fitting set (-7.0 μm) measured just under 80 N of friction force under these conditions. This is in accordance with the slightly smaller diameter of the cups shown in **Figure 5**. During most part of the stroke however, the friction was less than 10 N for each set.

At 300 bar, the maximum friction was measured when the piston was in TDC. This side of the cup contains an additional edge on which the cup stands. Due to this extra material, the stiffness of the cup is higher on this side, making
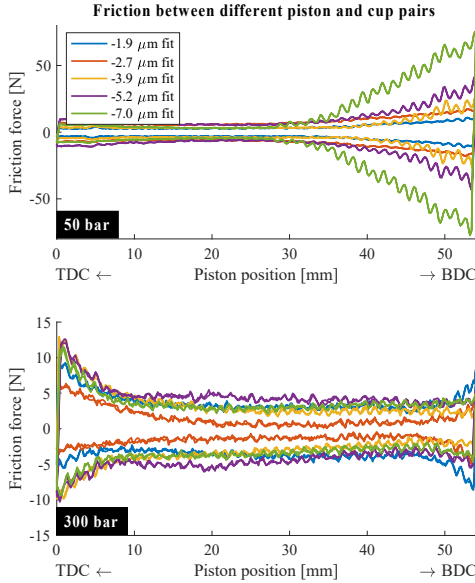
Figure 9: Friction force between the different piston-cup sets at two pressure levels.

Figure 10: Leak flow between the different piston-cup sets at two pressure levels.

it less sensitive to pressure caused deformations in the TDC. In other words, the cup does not expand as much as the piston does in the TDC, resulting in a contact between the piston and the cup and thus an increased friction force. The maximum measured friction force under these conditions was less than 13 N for all pairs. During most part of the stroke however, the friction was measured to be roughly 5 N or less.

5.2. Leak flow

The results of the static incremental leakage experiments at a pressure of 50 and 300 bar, are shown in **Figure 10**. In this figure, we see that the flow was generally lowest when the piston was in the BDC position, and increased as the pistons moved towards the TDC. The results at 300 bar show that the leak flow was highest at roughly one third of the stroke, and this was found to be true for all sets at pressures above 150 bar.

This leak flow pattern is again in accordance with the shape seen in **Figure 5**, as well as with the results of the friction measurements; at low pressures the cups are tighter near the BDC, and at higher pressures the cups are tighter near the TDC due to different deformation behavior between the piston and the cup.
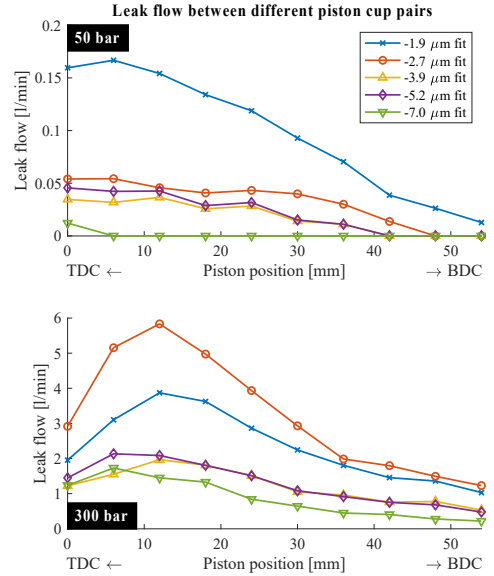
6. PERFORMANCE PREDICTIONS

To predict the effect of the measured friction and leak flow on the performance of a full 4919 cc pump or motor, the measurement results needed to be scaled up. This was done by accounting for the sinusoidal stroke of a piston, and, in the case of leakage, multiplying by the total number of pistons. These predictions are discussed around 277 bar, which is the nominal operating pressure for the wind turbine application.

6.1. Friction losses

To overcome the friction force, a small portion of the piston force will no longer be pushing the piston. Therefore, the estimated loss due to friction is quantified by ϵ_f:

$$\epsilon_f = \frac{F_f}{pA} \tag{1}$$

in which F_f is the average friction force during a stroke, p is the pressure level, and A is the surface area of the piston.

The estimated friction loss for the different piston-cup sets is shown in **Figure 11**, which shows the full pressure field, as well as a close-up around the nominal operating pressure. The figure shows that even at low operating pressures, where friction forces were found to be highest,

the friction is never more than 0.15% of the piston force. Looking at the losses around the nominal operating pressure, the friction losses are estimated to be less than 0.006% during a full stroke. It can thus be concluded that the friction forces are negligible.

6.2. Leakage losses

Leak flow will reduce the amount of oil displaced by the pump or motor. Therefore, the estimated loss due to leakage is quantified by ϵ_l:

$$\epsilon_l = \frac{z \, Q_l}{n \, V_g} \qquad (2)$$

in which z is the number of pistons, Q_l is the average leak flow rate during a stroke of a single piston, n is the rotational speed of the machine, and V_g is the geometrical displacement of the machine per revolution. At nominal operating conditions, the motors will rotate at four times the speed of the pumps, due to a 4:1 transmission ratio. Therefore, a full pump is estimated to have four times as much performance loss as a result of leakage, when compared to a full motor.

The estimated leakage losses for the different piston-cup sets are shown in **Figure 12**. The figure shows these losses both when operated as a pump (left axis) and as a motor (right axis). A pump at nominal operation pressure is expected to have a 1.8% performance loss for the loosest fit, while the tightest fit is expected to lose 0.5%. Although these losses are also not very large, they cannot be neglected like the friction losses.

7. IMPROVED DESIGN

To decrease the expected loss in performance, the design of the piston was slightly altered. Since the deformation behavior of the piston and the cup under higher pressures was found to be an important factor, the new design allowed the piston crown to better follow the deformation of the cup as well as any inconsistencies in the internal diameter. This was realized by removing some material on the inside of the piston crown, as shown in **Figure 13**.

The improved design was tested on the piston of the tightest fitting set. **Figure 14** shows that this improved design reduced the leak flow, especially at higher pressure levels. The expected leakage loss was reduced to around 0.32% at nominal operating pressure for pump operation, and 0.08% for motor operation.
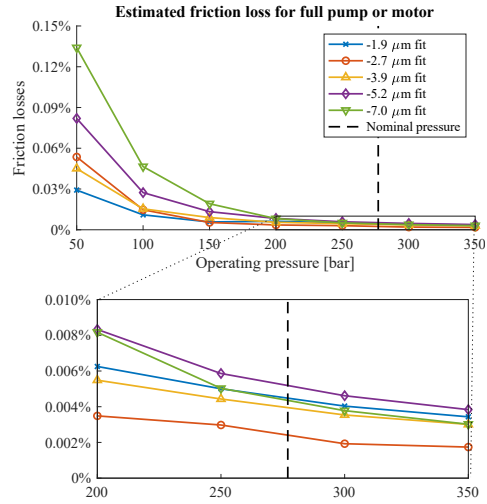

Figure 11: Estimated performance loss due to friction $\left(\epsilon_f \cdot 100\%\right)$, for a full pump or motor.
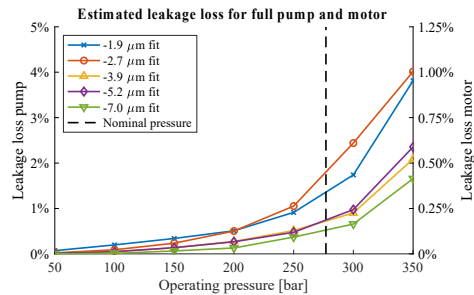

Figure 12: Estimated performance loss due to leakage $\left(\epsilon_l \cdot 100\%\right)$, for a full pump and motor.
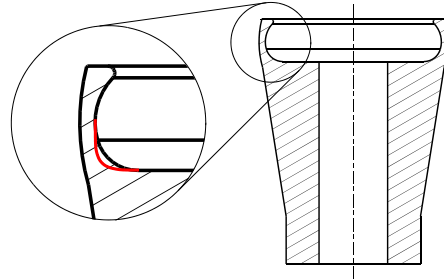

Figure 13: Removed material from the inside of the piston crown to reduce its stiffness.

The estimated performance loss due to friction as a result of this improved design is shown in **Figure 15**. This figure shows the friction loss reduced significantly at pressures below 200 bar for the improved design. The close-up in **Figure 15** shows that the improved design did introduce some additional friction losses near and above the nominal operation pressure. However, the friction loss is still found to be negligibly small for this tightly fitting set.

The results suggest that the leakage losses can be further reduced by using an even tighter fitting piston-cup combination or removing more material from the inside of the piston crown. The effect of these design changes on the friction and

Figure 14: Comparison between expected leakage loss for the -7.0 μm fitting piston of the original design and the improved design.

Figure 15: Comparison between expected friction loss for the -7.0 μm fitting piston of the original design and the improved design.

evident wear of the components could be the topic of future research. Durability measurements should furthermore show how the leakage patterns evolve over time.

8. CONCLUSION

The new test bench for individual pistons and cups of a 4919 cc floating cup pump and motor was created and used on five sets of pistons and cups. On each of the sets, a series of dynamic and static tests were conducted to measure the friction and the leak flow at the contact between the piston and the cup at different operating conditions. In the dynamic measurements, the piston moved back and forth over more than the length of a full stroke to determine which parts of the stroke will cause most friction during pump or motor operation. In the static measurements, the leak flow was measured at incremental positions of the piston inside the cup to determine how much the leakage is influenced by the different deformations of the two components.

The results show that even for sets with a very tight fit, the friction force between the piston and cup was very low and the performance loss due to friction was found to be negligible. The performance loss due to leakage between the piston and cup however, was not found to be negligible. The leakage was estimated to account for up to 1.8% of the total output flow of a full pump for the loosest fitting piston-cup set and 0.52% for the tightest fitting set.

The friction force and leak flow both depended on the part of the stroke the piston was in. This dependency was found to be partly explained by the shape of the produced cups, and partly by a difference the deformation behavior between the piston and the cup.

To improve the pistons ability to follow the shape of the cup, an improved piston design was proposed. In this design, some material was removed from the inside of the piston crown such that it would become less stiff. The new design was tested on the piston of the tightest fitting set. For this new design, the estimated performance loss due to leakage between the piston and the cup decreased from 0.52% to 0.32%, while the friction losses remained negligible.

Future research could focus on finding the optimum design with respect to leakage and friction, while also measuring the effect of wear by means of durability tests.
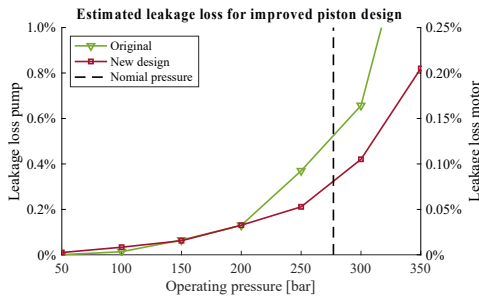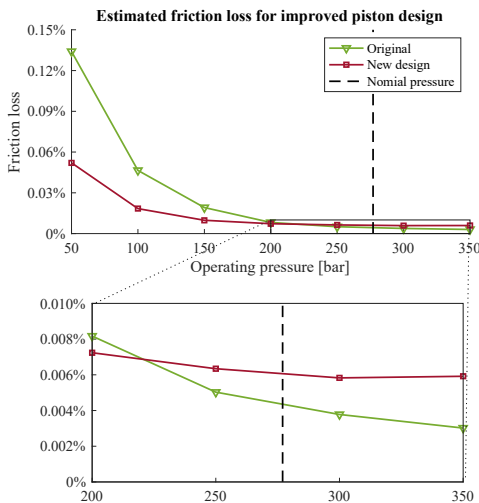
NOMENCLATURE

ϵ_f	Performance loss due to friction	[-]
ϵ_l	Performance loss due to leakage	[-]
A	Surface area of piston	[m^2]
F_f	Friction force	[N]
n	Rotational speed	[1/s]
p	Operating pressure	[Pa]
Q_l	Leak flow rate	[m^3/s]
V_g	Displacement volume per rotation	[m^3]
z	Number of pistons	[-]

REFERENCES

[1] Achten PAJ, Van den Brink TL, Paardenkooper T, Platzer T, Potma HW, Schellekens MPA, Vael GEM (2003) Design and testing of an axial piston pump based on the floating cup principle, Proc. SICFP 2003, Vol. 2, Tampere University of Technology, pp. 805-820

GROUP 4

Industrial applications

USER-ORIENTED SYSTEMATIC OF CONTROL CONCEPTS FOR FLUID-MECHATRONIC SERVO DRIVES

Prof. Dr.-Ing Peter Anders[1]*, Dr.-Ing Simon Ströbel[2]

[1] *Hochschule Furtwangen Universit8iy, Kronenstraße 16, 78532 Tuttlingen, Germany*
[2] *X-Dot Engineering, Blumenstraße 36, 72355 Schömberg, Germany*
* Corresponding author: Tel.: +49 7461 15026620; E-mail address: an@hs-furtwangen.de

ABSTRACT

This paper aims to show that controlled hydraulic drives, when properly considered and approached, are a technology that allows for a systematic and safe system design with regard to performance and energy efficiency. Controlled hydraulic drives are predestinated to be an indispensable alternative to electromechanical drives for many fields of application, especially against the background of Industry 4.0. But hydraulic drives will only be able to play this role if they see themselves as a part of mechatronics, speak the language of mechatronics and recognize the increasing importance of electric drives as part of the hydraulic toolbox as a chance.

Keywords: servo drive, mathematical model, transfer behaviour, characteristic map, model-based control, energy efficiency

1. INTRODUCTION

Although other topics have been more prominent in recent years, there are many quite interesting developments and trends in the field of controlled hydraulic drives. With the possibilities of digital technology available today, there are good prospects that hydraulic servo technology (at least in some application areas) will be the better alternative to electromechanical drives, so that it can maintain and even expand its current position in the world of mechatronic systems and components. The present article presents some of these developments without claiming to be complete. Due to time constraints, we will focus on the following topics in this article:

- More accurate models for controller design.
- Transparent systematics of the control concepts.
- Model-based control concepts.
- Automated model identification, optimization and tracking.
- Energy efficiency.
- Pump-directed drives / compact drives.
- Variable-speed electric drives.
- The role of computers.

The aim of this presentation is to show that hydraulic servo drives can be designed much more simply than is often claimed, especially with regard to aspects such as performance and energy efficiency. An important point here is to look at hydraulics from a more mechatronic perspective. Modern hydraulics has everything it takes to be a perfect and indispensable complement to drive solutions in the mechatronic world of *Industry 4.0*, especially for high load forces or special motion requirements. This article ends with some comments on what steps hydraulics should take to achieve these great prospects in the future

2. MORE ACCURATE MODELS FOR CONTROLLER DESIGN

2.1 Weaknesses of conventional models

The still most widespread and historically probably oldest type of controlled hydraulic drives is the valve-controlled hydraulic one, composed of a cylinder (or rotational motor), a constant pressure supply and a 4/3 proportional directional valve. The following discussion in this chapter are mostly formulated for the cylinder drive case but can of course be directly transferred to the rotatory equivalent.

If the traditional methods for system and controller design are often criticized as being quite fuzzy, this is certainly also due to the limited accuracy of the traditionally used steady-state models (= characteristics representing all possible steady-state operating points) and the dynamic model for controller design (= second-order transfer function), which together form the basis for system design. However, most users of these models are not aware of the background of the mathematical derivation of these models (see [1], [2] for details of this paper's chapters 2 and 3). The models are based on assumptions that one would never make in practical cases. Or, to put it more clearly: a real drive with the assumed properties would be unsuitable for real applications. The stationary model concretely is based on the assumptions that

- the servo valve has zero overlapped metering edges.
- the servo valve has linear characteristics.
- a synchronous double rod cylinder is used.
- friction is neglectable.

And for the dynamic model it is additionally assumed that

- the used piston stroke is only a small range around the neutral hydraulic centre position.
- the control valve is "infinitely fast" in relation to the dynamics of the motor itself and can therefore be dynamically regarded as a simple proportional (P-) element.
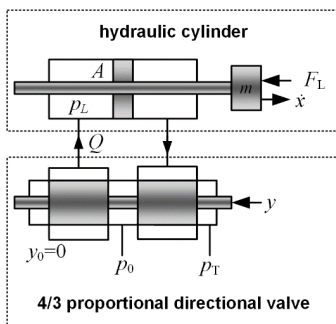

Figure 1: Simple scheme of a very idealized valve-controlled servo drive.

However, most users of these models are not aware of the background of the mathematical derivation of these models (see [1], [2] for details of this paper's chapters 2 and 3). The models are based on assumptions that one would never make in practical cases. Or, to put it more clearly: a real drive with the assumed properties would be unsuitable for real applications.

Stationary model

For the stationary model, the relationship between the valve opening y (or control signal u), load force F_L (or load pressure p_L), and speed $\dot{x}$ (or volume flow Q) is shown in equation (1) (and equation (2) respectively) and graphically in Figure 2.

$$\frac{\dot{x}}{\dot{x}_{max}} = \frac{y}{y_{max}} \cdot \sqrt{1 - \frac{F_L}{F_{max}}} \qquad (1)$$

$$\frac{Q}{Q_{max}} = \frac{u}{u_{max}} \cdot \sqrt{1 - \frac{p_L}{p_{max}}} \qquad (2)$$

A closer look reveals the consequences of these rough assumptions. As can be seen in the diagram, there is no longer a defined operating point for a very low speed or standstill at a given load. On the other hand, this is not a big surprise, as low speeds are caused by very small valve openings, but it is precisely these small openings within the negative overlap that have been neglected by the assumptions made. At higher speeds with correspondingly large valve openings, this overlap is in any case no longer significant, so that the corresponding operating points are approximately correct. This simple model is therefore suitable for rough estimations, i.e. to decide whether a concrete configuration *pressure supply – valve – cylinder* is sensibly dimensioned or not. The additional assumption of a symmetrical system is only approximately fulfilled for differential cylinders with a rather thin piston rod ($\alpha = A_B/A_A \geq 0.7$). With smaller area ratios ($\alpha \ll 1$) the differences between the model-based estimated behaviour and the real behaviour become more and more significant.
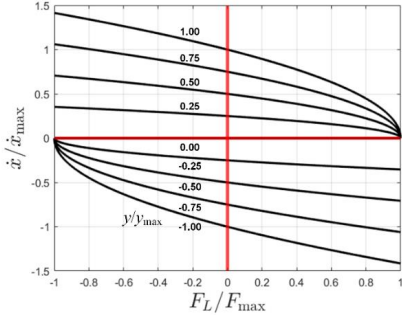
Figure 2: Static transfer behaviour of the idealized system.

Dynamic model

Concerning the dynamic transfer behaviour from the independent input signals valve opening y or load force F_L to the output signal cylinder speed $\dot{x}$, the named assumptions lead to the well-known second-order transfer functions $G_y(s)$ and $G_{FL}(s)$ with the corresponding block diagram shown in Figure 3.

$$G_y(s) = \frac{\dot{x}(s)}{y(s)} = \frac{K\omega_0^2}{s^2 + 2D\omega_0 \cdot s + \omega_0^2} \tag{3}$$

$$G_{FL}(s) = \frac{\dot{x}(s)}{F_L(s)} = \frac{-b_1 \cdot s - b_0}{s^2 + 2D\omega_0 \cdot s + \omega_0^2} \tag{4}$$

$$K = \frac{V_{Qy}}{A + \frac{V_{Qp}d_N}{A}} \tag{5}$$

$$\omega_0 = \sqrt{\frac{2}{C_H m}\left(A^2 + V_{Qp}d_N\right)} \tag{6}$$

$$D = \frac{d_N\sqrt{\dfrac{C_H}{2m}} + V_{Qp}\sqrt{\dfrac{2m}{C_H}}}{2\sqrt{A^2 + V_{Qp} \cdot d_N}} \tag{7}$$

$$b_1 = \frac{1}{m} \quad b_0 = \frac{2AV_{Qp}}{C_H m} \tag{8}$$

Above all, the parameters V_{Qy} and V_{Qp} may be considerably influenced by the linearization of the real non-linear mathematical model equations. Therefore, they are in principal operating point dependent. These parameters result as the gradients of equation (2).

$$V_{Qy} = \left.\frac{\partial Q(p_L, y)}{\partial y}\right|_{OP} = \frac{Q_{max}}{y_{max}} \cdot \sqrt{1 - \frac{p_{LOP}}{p_{Lmax}}} \tag{9}$$

$$V_{Qp} = \left.\frac{\partial Q(p_L, y)}{\partial p_L}\right|_{OP} = \frac{-Q_{max}y_{OP}}{2p_{Lmax}y_{max}} \cdot \sqrt{1 - \frac{p_{LOP}}{p_{Lmax}}} \tag{10}$$

As in the stationary case, the erroneous assumptions in the dynamic model become immediately apparent. For example, the assumed zero overlap leads to a gradient that defines pressure gain V_{Qp} to zero, i.e. the load pressure p_L would not play any role at low speeds or standstill situations, which is of course simply nonsense. Larger deviations between the theoretical model behaviour and the actually observed drive behaviour are caused by to the neglected area ratio and the center position requirement, that often isn't fulfilled in reality. The literature recommends here the application of "correction steps", i.e. via the *eigenfrequency correction curve*, as shown in Figure 4 and equation (11). However, practice shows that these corrections are of little help if the deviation from the
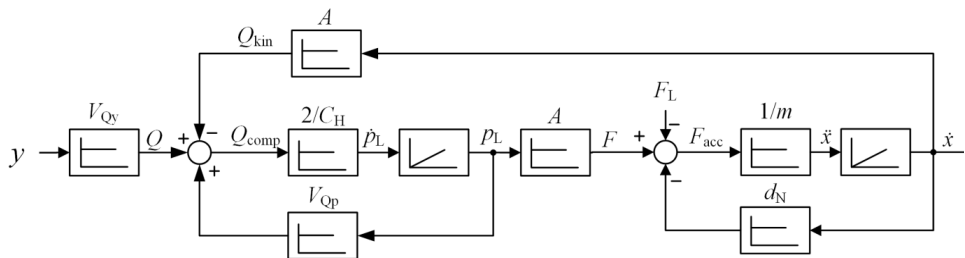

Figure 3:   Block diagram of the idealized system.

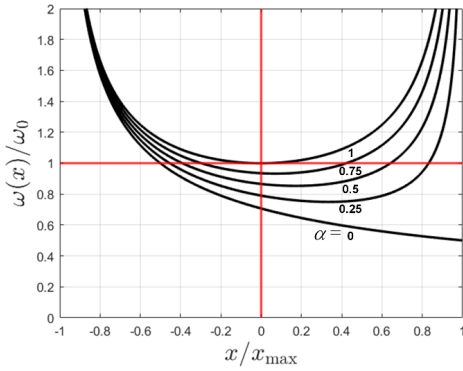assumptions becomes larger and especially with higher accuracy requirements.

Figure 4: Eigenfrequency correction curve (dead volumes neglected).

$$\frac{\omega(x)}{\omega_0} = \sqrt{\frac{x_{\max}}{2} \cdot \left(\frac{1}{x_{\max} + x + \frac{V_{dead\,A}}{A_A}} + \frac{\alpha}{x_{\max} - x + \frac{V_{dead\,B}}{A_B}} \right)} \quad (11)$$

2.2 More accurate models

It is no surprise that controller designs based on such simple models often only show a rough coincidence between the theoretical expected and the real observed behavior. On the other hand, there are more suitable models that do not make such radical assumptions and are therefore more accurate.
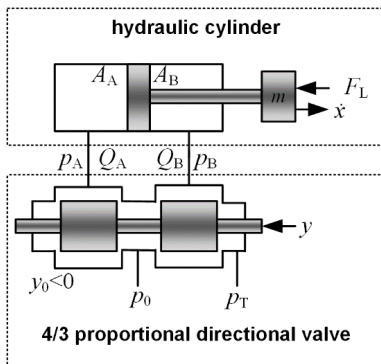

Figure 5: Simple scheme of a slightly more realistic valve-controlled servo drive.

Stationary model

A better stationary model is based on the chamber pressure diagram, which describes the pressures occurring in the cylinder chambers during stationary (= unaccelerated) motion and at standstill. With the usually available nominal data of the control valve and the cylinder, quite usable chamber pressure diagrams can be calculated.
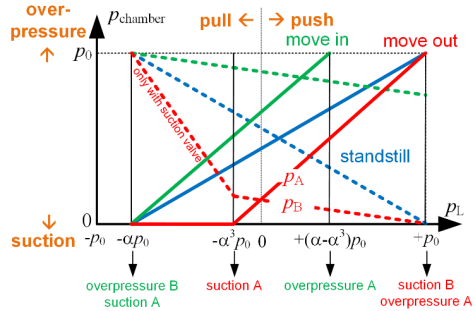

Figure 6: Pressure diagram (qualitative). Solid line = chamber A, dotted line = chamber B.

The operating point dependent volume flows and thus the speeds of the cylinder as well as the load-dependent neutral position within the overlap can also be determined via the known pressure differences across the control edges. However, this means that the complete stationary characteristic map of the drive system consisting of pressure supply-valve-cylinder is known.
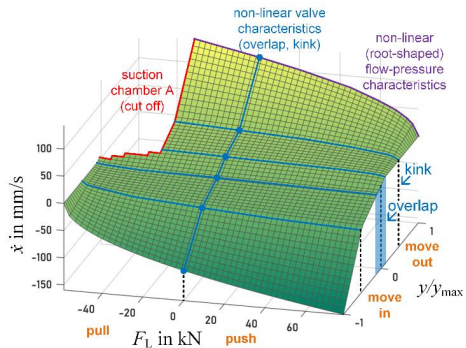

Figure 7: Characteristic map of entire system supply-valve-cylinder, representing all reachable stationary operating points (quantitative example configuration with kinked valve characteristics and cylinder ratio α = 0.75).

The pressure diagram or the characteristic map is also helpful to detect in advance critical operating conditions such as *suction* ($p < 0$) or *overpressure* ($p > p_0$) states in a cylinder chamber due to the area ratio. The calculation shows that the dangerous suction of air in differential cylinders with pulling loads in the large chamber occurs already at a load pressure of $p_L = -p_0/\alpha^3$. With an area ratio of e.g. $\alpha = 0.5$, the maximum possible load force in the pull-in case is thus reduced to 12.5% (!) compared to the push-out case. This makes it clear how restrictive the practical effects

This model also correctly considers the area ratio and movements over the entire stroke. This model is a third-order system, as it has three integrators (two for the stroke-dependent pressure build-up and one for the movement) and six linearized parameters V_{QyA}, V_{QyB}, V_{QpA}, V_{QpB}, C_{HA} and C_{HB}, see Figure 8. The first four parameters are again derived from the non-linear valve characteristics, the last two from the piston position. Based on an operating point-dependent linearization of a real nonlinear system it is a much better description of the actual dynamic transfer behavior.

$$G_y(s) = \frac{\left(\dfrac{A_A V_{QyA}}{C_{HA} m} - \dfrac{A_B V_{QyB}}{C_{HB} m}\right) \cdot s + \left(\dfrac{A_B V_{QpA} V_{QyB} - A_A V_{QpB} V_{QyA}}{C_{HA} C_{HB} m}\right)}{s^3 + \left(\dfrac{V_{QpB}}{C_{HB}} + \dfrac{V_{QpA}}{C_{HA}}\right) \cdot s^2 + \left(\dfrac{A_A^2}{C_{HA} m} + \dfrac{A_B^2}{C_{HB} m} + \dfrac{V_{QpA} V_{QpB}}{C_{HA} C_{HB}}\right) \cdot s + \left(\dfrac{V_{QpB} A_A^2 + V_{QpA} A_B^2}{C_{HA} C_{HB} m}\right)} \tag{11}$$
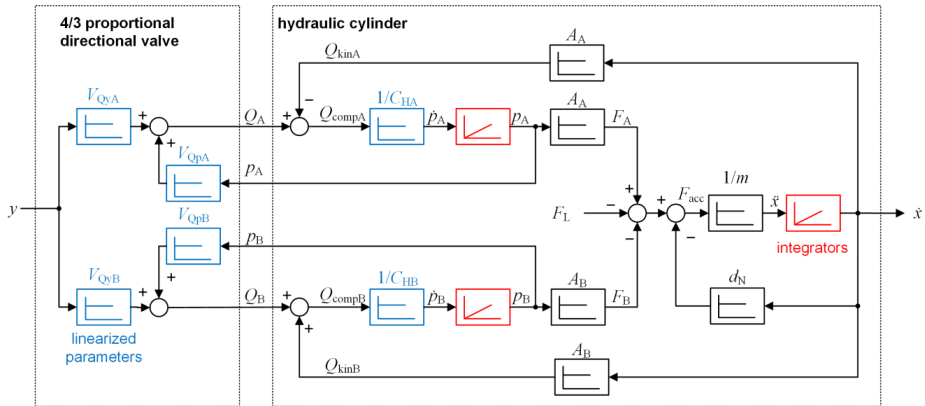

Figure 8: Linearized block diagram of more realistic system.

of the asymmetry of a cylinder drive can be.
In many cases, the real characteristic map of the specific control valve can be provided by the manufacturer on the basis of test bench measurements, which considerably simplifies the determination of a meaningful characteristic map of the overall system.

Dynamic model

A much more accurate version of the dynamic LTI model, which is important for controller design, is also available. It is obtained by describing the pressure build-up in both cylinder chambers separately and explicitly formulating the force generation over the two piston areas.

In order to apply the classical methods of control engineering, such a (linearized) LTI system description is always needed. Of course the transfer functions $G_y(s)$ and $G_{FL}(s)$ can be derived for this model, the former is given e.g. in equation (11). Even if friction is neglected in this equation, it is hardly useful to perform these calculations manually, but with the help of suitable computer algebra systems this is easily possible. Such programs can, for example, be created by the user himself with Matlab using the Control System Toolbox [3], or you can use service providers who offer such programs or perform these not quite trivial calculations.

In this context, however, the question immediately arises as to how the classic dynamic
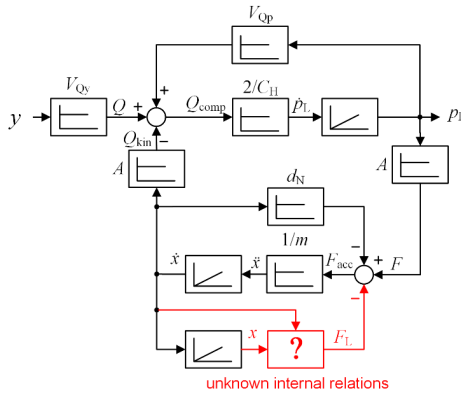
model as a second-order system *without a zero* in $G_y(s)$ is compatible with the expanded dynamic model as a third-order system *having a zero* in $G_y(s)$. The explanation is this: For the simple classic model, it was assumed that the piston was in the volumetric middle position (same volume in both cylinder chamber sides), but in this very constellation, a zero point and a pole position of the more accurate model become cancelled, and so in exactly this one position, the results of both models match. With increasing distance from this ideal position, the weaknesses of the simple model become apparent with the correction calculations mentioned (eigenfrequency correction curve etc.) due to increasingly significant deviations in the transfer behaviour and consequently also in the expected control behaviour.

If the position is considered as the controlled variable instead of a velocity, only one integrator has to be added in series to the output of the model, since the position is the integral of the velocity over time.

Figure 9: PT2 and IT1 step response (qualitative).

However, if an internal process signal is selected as the control variable, e.g. here the (load) pressure as the output variable, dynamic elements (those ones containing at least one integrator) of the model lie in a feedback path and act in the opposite direction to the direct forward direction between the input signal (control voltage at the valve) and the output signal (here now pressure or driving force). Such branches inevitably generate zeros in the transfer function $G_y(s)$, see figure (10) (here again, for simplicity and clarity, the idealized LTI model is used). These zeros, in turn, can have unusual and usually unpleasant effects on the transmission behaviour if they are located near pole points and/or near the imaginary axis of the *s*-plane. For example, if a zero point is closer to the origin than the nearest pole, the system will show overshoots in the step

response, even if the poles do not allow any oscillations at all, see figure (11).

Figure 10: Idealized block diagram with load pressure as control variable.

Figure 11: Characteristic pole/zero constellations (qualitative).

In many cases, the load force is not an external force (not an input signal), which is given from outside independently of the system, as is the case with a lifting movement, for example. In forming processes, the load force depends decisively on the motion state of the forming piston, i.e. specifically on its position and speed. However, these relationships are often rarely known in such detail that they can be described mathematically unambiguously and used meaningfully in a model, see Figure (12). In such cases this fact has far-reaching consequences for the controller design and is often the background to many unsatisfactory solutions.

Figure 12: Idealized block diagram with unknown internal relations.

3. CLASSIC CONTROL CONCEPTS FOR SERVO DRIVES

3.1 Basic Rules

Controlled hydraulic drives are often said to be complicated in terms of control technology, the control concepts are very diverse and case-specific, and there is no transparent systematic approach. However, if one takes a closer look at the subject, one must contradict this assertion, at least in this drastic form.

Of course, the situation with electric drives is comparatively simple. Electrical positioning axes are usually controlled by a three-loop cascade controller, sometimes also by a three-loop (state space) controller [3]. Here it is assumed that they have sufficiently high-dynamic output stages, so that there are almost recipe-like instructions for the controller design that lead to fixed design formulas. In contrast to the hydraulic case, electric drives as controlled systems are by nature mostly over-damped ($D \gg 1$), which simplifies the control task, since it is easier to reduce the damping of an over-damped system than to calm a system that is susceptible to oscillations. Perhaps it can be said that the basic conditions of the hydraulic case (parameter dependency, actuator dynamics etc.) are somewhat more difficult than in the electrical case. Nevertheless, control structures and control parameters also result quite systematically for hydraulics if some elementary basic rules of control engineering are observed. Non-compliance with these basic rules

is often the cause of the difficulties mentioned. Such basic rules are [8]:

1) The actuator (= control valve) should be as fast as possible, otherwise its dynamics must be considered when designing the controller.
2) If the controlled system itself has an integral behaviour, the controller must not have any pure integral parts.
3) Integral controller components serve on the one hand to correct disturbance variables and on the other hand to provide stationary control signal components, so that these have not to be generated permanently via a remaining control error or the proportional control component respectively.
4) Integral controller components generally have a destabilizing effect because they reduce the phase margin in the frequency response.
5) Stationary control signal components should be generated by appropriate offset or feedforward instead of integral feedback controller components. In this way, the operating point is adopted more quickly via the feedforward signal components without having the destabilizing effects of a closed feedback circuit. However, this compensatory measure requires more precise knowledge of the structure and parameters of the controlled system in the form of an appropriate mathematical model.
6) Zeros in the transfer function are caused by dynamic components in the feedback or by branches parallel to the forward branch of the controlled system. Depending on the position of the zeros, they can have a strong influence on the dynamic behavior, which is why they should be compensated by an upstream filter element. This compensation, which may depend on the operating point, requires knowledge of the structure and parameters of the mathematical model of the controlled system.
7) State controllers of higher than third order are usually problematic, since the generation of the additional state variables necessary via measurement, observer models or (possibly adaptive) differentiation algorithms is usually not easy.
8) The three-loop control is a special version of the state control for positioning drives with a sufficiently highly dynamic actuator. The

advantage is that you can assign a defined effect to the inner return loops directly (and not only via the pole positions).

9) The control signal limitations that for energy reasons always do exist limit the possibility of correcting the eigendynamics of the system by means of controls. Multi-loop controls are particularly vulnerable here. Approaches to convert these controller structures into single-loop pole compensation algorithms can be helpful here [8].

3.2 Case Studies

Position control of the hydraulic cylinder drive

The situation for the position control of a hydraulic cylinder drive is as follows: Because of the free integrator at the end of the controlled system, this has an integrating behavior in the position control and there is no fundamental control error in the reference behavior with a simple P-controller ($y = K_P \cdot e$), provided that static friction is negligible.
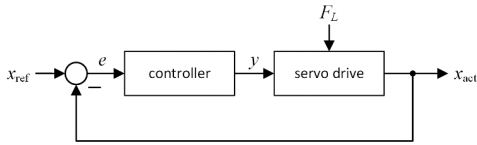
Figure 13: Single-loop position control.

However, a permanent control error e_{stat} follows under load or during movement, namely in proportion to the respective cause load force and/or speed.

$$e_{\text{stat}} = \left(\frac{V_{Qp}}{V_{Qy} A} \cdot \frac{1}{K_p} \right) \cdot F_L + \left(\frac{A}{V_{Qy}} \cdot \frac{1}{K_p} \right) \cdot \dot{x} \qquad (12)$$

However, with the controller coefficient K_P as the only degree of freedom of the P-controller, at best the requirement for a sufficiently safe stability of the controlled positioning drive can be met. For further requirements, controllers with more degrees of freedom (poles and zeros) are required.

If the actuator is sufficiently fast, the three-loop controller with speed and acceleration feedback is ideal. In particular, the tendency to oscillate can be relatively well suppressed here via acceleration feedback.
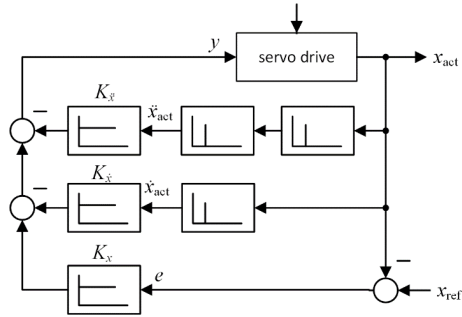
Figure 14: Three-loop position control.

A significant increase of the eigendynamics finds its limits quite quickly in the control signal limitation, but such an increase is not a primary goal for the mostly quite highly dynamic hydraulic drives. However, this control with additional speed and acceleration signal requires the availability of the necessary auxiliary control variables. Here, the speed can usually be determined by differentiation of the position signal, but for acceleration this procedure is much more difficult, due to several A/D quantization effects. Alternatively, a fading feedback loop with the difference pressure is possible. This is a direct equivalent to current feedback in the cascade control of electric drives. One way to completely bypass this procurement of the two auxiliary control variables is to implement this variant of pole assignment control by means of an extended single-loop compensation controller. Ideally, however, this requires real time computers that can handle floating point operations and a somewhat more sophisticated implementation of the control algorithm.

Even with the three-loop controller, there is a remaining permanent control error in the disturbance behavior. Pure integral controllers are not possible for reasons of stability. A PI-controller as a way out creates a parallel branch and thus as mentioned above a system-related zero. This zero is even dominant and creates a characteristic overshoot. These can be avoided by a switching integrator (i.e. type of anti-windup integrator), which only becomes active within a relatively narrow band around the setpoint.
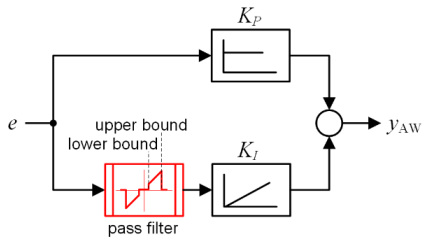
Figure 15: Anti-windup PI-controller structure.

Alternatively, the zero can be compensated by an upstream filter element. To dimension this compensating element, however, the system model must again be well known with high parameter accuracy.
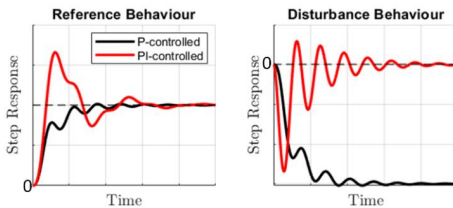

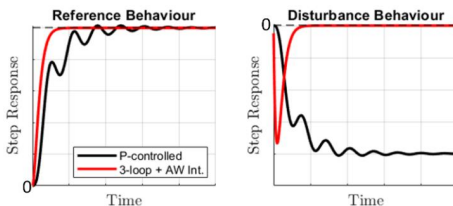**Figure 16:** P- and PI-controlled step response (qualitative).

Figure 17: P-controlled and three-loop + anti-windup controlled step response (qualitative).

If actuator (= valve) dynamics cannot be neglected in relation to the main system dynamics, a frequency response based controller design using the bode diagram of the open loop system is recommended. This is somewhat more complex to carry out than the other methods mentioned so far, but can be applied practically without any restrictions in regard to the controlled system. With the design strategy often referred to as *PT2 analogy* according to Lunze [4], a purposeful and relatively design-safe design process based on the bode plot is available, that can theoretically be applied to any transfer function, even with dead time. With the appropriate use and combination of basic LTI-elements (P- and I-elements) and amplitude and

phase shaping elements (lead-lag-compensators or PDT1- and PPT1-elements respectively) the following design criteria should be met:
1) Provide an integrator if the system itself has none.
2) Phase margin of about 70°.
3) High crossing frequency (frequency at which magnitude crosses 0dB line).
4) Magnitude slope of about -30dB/dec at crossing frequency.
5) High magnitude attenuation for frequencies >> crossing frequency.

In principle, this leads to single-loop controls and does not require the reconstruction of auxiliary variables, but can lead to control algorithms of quite high order if system dynamics are changed too far. However, such changes are restricted quite narrow due to the control signal limitations anyway. State space control using pole placement is a much discussed and often propagated high-end solution. The three-loop controller just mentioned is (for positioning drives with a sufficiently fast actuator) nothing else than a special case of this state space control using pole placement. A big advantage of this controller is the existence of clear and easily algorithmizable design calculations. However, a general application of the state space control via pole placement often is not without problems. This concept requires the availability of all state variables, some of which, however, often cannot be measured or can only be reconstructed with a great deal of effort. The possibility of apparently being able to define "freely" the eigendynamics of the controlled system often leads to the design of "overbred" and highly sensitive controllers, which then result in malfunction of the control circuit and even instability. Last but not least, with model-based controllers based on the Two-Degree-of-Freedom principle, which has emerged strongly in recent years, a powerful and extremely promising alternative to state space controllers is available [8], see next chapter.

Speed control of the hydraulic cylinder drive

The basic principles for the controller design mentioned above are generally valid and therefore also applicable to other control modi of the drive systems. In the case of speed control, the integrator at the plant output is missing. The concept presented below is therefore useful

according to the basic rules mentioned. To improve the transfer behaviour, an integral component is unproblematic here and should be used for load and disturbance compensation. However, the required control signal component should not be generated mainly based on the control error by means of this integrator, but via a forward branch/offset using the reference signal and the inverse stationary model equations (discussed in more detail in the next chapter). A possible overall configuration is shown in Figure 18
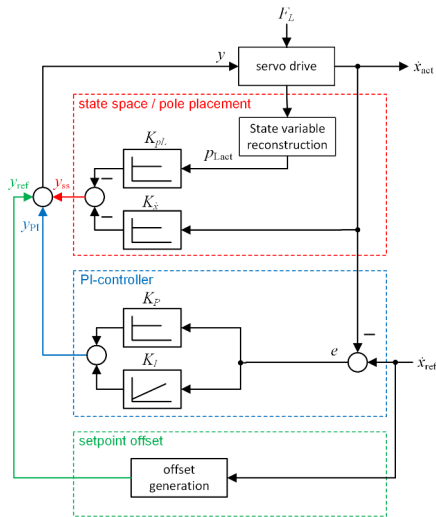
Figure 18: Structure of velocity control using a PI-controller, a state space controller and a velocity offset in parallel.

Pressure control of the hydraulic cylinder drive

The basic problem with pressure control is that the compression volume flow required for the desired pressure profile is usually orders of magnitude smaller than the kinematic volume flow required for superimposed piston movement. Since any kind of volume flow can only be generated in the controlled drive via the control deviation, this situation leads to dramatic deviations of the actual pressure from the target pressure in case of superimposed piston movement. As already mentioned in the chapter about modeling, the causal relationship between load force and piston speed/position cannot be described in most cases in simple and transparent mathematical way. As a result, a reliable determination and thus compensation of the

disturbance volume flow resulting from this piston movement is analytically impossible. However, the magnitude of this disturbance volume flow can be determined and calculated indirectly via the piston speed, which means that compensation of the disturbance volume flow is now possible by means of a corresponding control signal offset. With a sufficiently fast valve as the actuator element, this special form of feedforward control provides sufficiently good compensation of the movement, so that from a control engineering point of view, only one PT1 element effectively remains as the system to be controlled, see block diagram Figure 19. Due to the variable piston position (the variable hydraulic capacity of the chamber respectively), the time constant of the PT1 element is variable. However, since this position-dependent time constant can thus be determined via the position sensor, an adaptive PI algorithm can be easily implemented here. This concept is ideally suited, for example, for high-precision pressure control of die cushions.
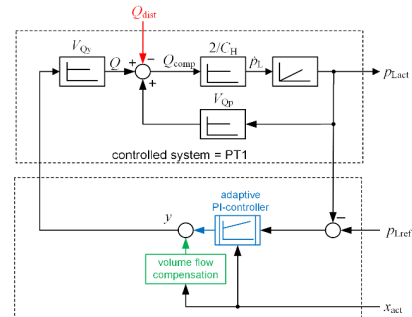
Figure 19: Structure of pressure control using an adaptive PI-controlled and qualitative control results.

Chapter summary

Using the example of the valve-controlled hydraulic cylinder drive, these examples show that control design for these drives is a transparent task that can be solved relatively

purposefully, provided that a corresponding accurate model is available. With this knowledge, an adaptation of the controller to changed operating parameters and thus a turn away from a worst-case parametrization is also quite feasible. In principle, this also applies to fundamentally different drive concepts, such as pump-controlled drives.

These considerations show that the controllability of the systems goes hand in hand with the availability of structurally correct and correctly parameterized system models. If these models can be generated computer-aided with reasonable effort and with sufficient accuracy, the model-based control based on the Two-Degree-of-Freedom principle is a modern method that will complete or replace the classic approaches in many areas, especially when higher dynamics are demanded. This concept will be briefly discussed in the next chapter.

4. MODEL-BASED CONCEPTS

4.1 Model-based control according to the Two-Degree-of-Freedom concept

Developments that have been unstoppably on the rise in recent years and that will replace or supplement the classic control concepts in many areas are model-based control concepts. At its core, this is a more sophisticated and systematic variant of the well-known pilot control. On the control theory side, it was motivated and scientifically proven by the theory of so-called *dynamic flat systems*. The simple basic idea of these concepts is that it does not matter where the correct control signal required for the desired course of the controlled variable comes from, the system to be controlled does not notice its origin anyway. The control signal has only to be correct in the sense that it meets the control requirements. This control signal is generated in classic control loops based on the control error. The term control *error* already makes it clear that one inevitably accepts that the system is at least temporarily not at the operating point that is specified as the current target via the command signal. If you want to keep this error small, the controller, as the coupling element between the control error and the control signal, must be set to "armed", i.e. the loop gain must be driven up. Therefore, the

stability limit is increasingly being approached. In order to avoid the impending instability, higher-quality controllers (e.g. pole placement using state space controllers) are used that strongly intervene in the system's own dynamic. With increasing complexity, these higher-quality controllers are of course becoming more and more susceptible to signal errors or parameter fluctuations.

This is where the model-based concepts come into play. On the one hand, today one has (or should have) very precise knowledge of the real system behaviour. On the other hand, also excellent mathematical computing tools that allow such models to be calculated and evaluated even in real time are available. In the model-based method, target trajectories are generated in a so-called trajectory generator, from which, based on a mathematical model of the system, a feedforward pilot controller calculates control signals that "impress" the desired output trajectories as precisely as possible.
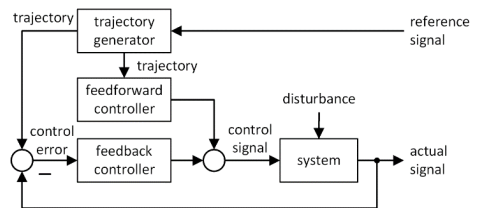

Figure 20: Basic structure of the Two-Degree-of-Freedom control concept.

If the system is to be guided at least in part via this input based control branch, only such trajectories may be generated which can be realized by the physical drive system: limits and operating point-dependent power restrictions must therefore be considered when specifying sensible target trajectories. Therefore, step signals as a command signal are of course pointless, or they must be smoothed out sensibly by the trajectory generator. If this requirement is met, the problem of signal limitations that is always present in conventional controller design processes, is avoided or at least largely mitigated. The design goal is achieved when the control signal profile provided by the feedforward pilot control branch produces the desired target curve in good approximation even without feedback control. With this structure, the feedback

controller only has the task of correcting the effects of inaccuracies of the model used in the pilot control system, as well as supressing the remaining influence of disturbance signals. Without disturbance signals and with an ideally exact model, the control signal based on the model-based feedforward branch would force the desired trajectory. The feedback controller would recognize no control deviation and would not intervene.

Some big advantages of this approach are:
- Nonlinearities have no or only a minor effect, provided that they are considered sufficiently precisely in the model used in the feedforward pilot branch.
- Parameter fluctuations do not have a major impact.
- A comparatively simple feedback control structure can be selected, and the feedback control parameters can be weighted moderately.
- The problem of stability is reduced, only feedback components of the control signal can cause instability.

In order to be able to use this approach for the position control of valve-controlled servo drives e.g. effectively, the following basic conditions must be met (see [5], [6] for further details e.g.):
- A target trajectory that can be differentiated three times must be generated.
- The chamber pressures p_A and p_B must be measured.
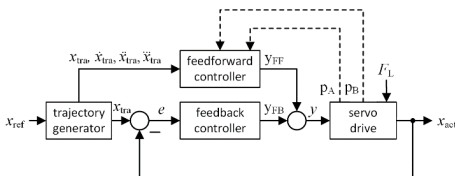
Figure 21: The Two-Degree-of-Freedom concept applied to the position-controlled servo drive.

As Ströbel has shown [5], implementing this idea in accordance with the control of dynamically flat systems in the case of the hydraulic cylinder drive is not without problems. On the one hand, the real physical dependencies can often hardly be described exactly and reliably using a parametric (=formula-based) mathematical model.

Examples are the real flow conditions over the control edges as well as the influences of friction and leakage. On the other hand, the necessary case distinctions when describing the flow behaviour via the control edges of the control valve make the creation of a real time capable algorithm considerably more difficult. Although Ströbel was able to create a suitable algorithm, he also had to recognize that the resulting complexity of a generally applicable approach would significantly hinder the widespread dissemination of this theoretically good concept.

4.2 Practical alternative using a characteristic map

So in [5] a slightly different, more pragmatic approach is taken. The basis for this was the following principle consideration: Ideally, the pilot control branch should determine an actuating signal that generates the entire volume flow required, i.e. both the *kinematic volume flow* for moving the piston and the *compression volume flow* for building up pressure in the cylinder chambers. On the other hand, when the system state changes, the compression volume flow is usually orders of magnitude smaller than the kinematic volume flow. There is also no convincing reason why the pilot control branch must generate the *entire* volume flow required, as the feedback controller did previously. It would already relieve the feedback controller dramatically, and thus allow a much weaker and therefore more stable controller parameterization if the pilot branch could at least generate the signal component for the kinematic volume flow.

The entirety of the operating points belonging to purely stationary states of motion (or kinematic volume flows respectively) is exactly represented by the characteristic map of the drive. The creation of the same was based on the boundary condition that the current pressure changes and thus the compression volume flows were zero, or in other words: compared to a general dynamic movement, the respective compression volume flow is generally missing in the characteristic map. Conversely, this fact means that significant parts of the control signal can be determined from the characteristic map of the drive if this is known, that is to say if this is somehow available by calculation or measurement technology. The

characteristic map represents the stationary solution of the corresponding mathematical model equations of the drive and can therefore be derived from construction plans and catalogue data of the drive components mostly in good approximation. On the other hand, it can in principle also be determined by measurement from the data triplet $(F_L, y, \dot{x})$ or (p_L, u, Q) respectively: each operating point that is taken up when passing through a trajectory represents such a data triplet.

If the map is in a form in which the control signal y of interest is the output variable, the important -because dominant!- stationary control signal component for the displacement volume flow can be interpolated in real time depending on the operating point and used to control the valve. Since only stationary components can be generated in the pilot control branch by means of the characteristic map, a trajectory that can be differentiated once is sufficient to determine the control signal y, whereby a smoother trajectory of higher order still remains meaningful in order not to demand impossible accelerations. The gradient of this trajectory directly corresponds to the variable stationary speeds or the kinematic volume flow to be realized and, from the feedforward controller's point of view, is thus the reference variable. The load force F_L or the load pressure p_L as the disturbance variable is reconstructed online based on the two chamber pressures.
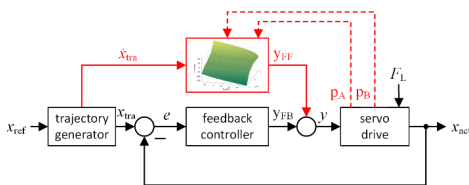
Figure 22: Characteristic Map based implementation of the Two-Degree-of-Freedom concept applied to the position-controlled servo drive.

This concept was tested on valve-controlled hydraulic cylinder drives and on die cushion presses. Together with a subordinate classic feedback controller, this concept according to the Two-Degree-of-Freedom concept delivered excellent results, see [5] and [7] for example. The concept in this form is of course also transferable to other drive variants and offers a number of additional expansion options.

With this map-based approach, the term *Two-Degrees-of-Freedom* can be also assigned a clearly specified meaning:

- *Feedforward part* (model-based): takes care of the most exact possible implementation of the stationary process components, which are traditionally realized by a high loop gain. For this, the most exact possible representation of the stationary transfer behavior, i.e. the characteristic map, is necessary.
- *Feedback part* (physical state based): takes care of the non-considered dynamic process components. Should realize a dynamically acceptable, i.e. above all a well damped (stable and robust), dynamic transfer behavior by constant feedback monitoring and correction. The better the feedforward part, the smaller the corrective interventions.

The two parts can thus be meaningfully and independently dimensioned according to their respective areas of responsibility.

4.3 Characteristic map optimization

Whether as the basis for a conventional controller or as the basis for a model-based control based on the Two-Degrees-of-Freedom principle, the availability of more suitable, i.e. sufficiently accurate and easy-to-use mathematical models is a basic prerequisite for realizing highly precise dynamic drive controls. Of course, the question immediately arises as to how these models are determined in terms of structure and parameters. It is very common to define model equations that appear sensible on the basis of physical considerations and to first set all unknown or uncertain parameters here as variables. The specific values of the present case are then determined experimentally, for which there are a number of different identification methods. The equations parameterized in this way form the mathematical model of the system and then e.g. the basis for the controller design.

With the Two-Degrees-of-Freedom principle according to the theory of dynamically flat

systems, the control signal for desired trajectories is determined analytically (= formula-based) at the current operating point by evaluating these in general non-linear system equations. A certain weakness of this method is that the analytical model equations are structurally fixed, based on physical considerations and assumptions, and only their parameters can be experimentally determined or optimized in the sense of a curve fitting. Structural errors in the model cannot be corrected. In the case of the hydraulic cylinder drive, however, it is sufficient and sensible to determine the dominant control signal component for the displacement volume flows from the solution for stationary conditions. However, the entirety of all stationary solutions is nothing else than the characteristic map of the drive in question. Mathematically, this map forms a non-linear surface Y of a two-dimensional input space with input quantities X_1 and X_2.

$$Y = f_{nl}\left(X_1, X_2\right) \tag{12}$$

Or in the specific case of the cylinder drive:

$$\dot{x} = f_{nl}\left(F_L, y\right) \tag{13}$$

Every point of this surface is a possible stationary operating point of the drive. Conversely, every real occurring and thus measurable stationary operating point represents a point of the real surface. The totality of all real occurring stationary operating points thus defines a point cluster which, if the model is correct, should lie exactly on this surface. Ströbel uses this fact for an extended optimization process of the map. First, based on the known or roughly estimated model structures and parameters, a first, usually only partially accurate, steady-state characteristic field is determined by solving the model equations and stored as a non-parametric (= number-based) *white box model* (index W) in the form of a two-dimensional lookup table (LUT), which mathematically represents the corresponding surface **CM**$_W$.

$$\mathbf{CM}_W: \ \dot{x} = \mathbf{LUT}\left(F_L, y\right) \tag{14}$$

In a second step, the triples $(F_L, y, \dot{x})$ that occur during regular operation are measured. Since these are generally "contaminated" due to the dynamic processes that are actually taking place, for example due to oscillations and measurement

noise, they are first filtered by suitable measures and the stationary parts are extracted. As a result, there is a set of *black box observations* (index B) which represent N stationary operating points.

$$\mathbf{OP}_B = \begin{pmatrix} F_{L(1)} & y_{(1)} & \dot{x}_{(1)} \\ \vdots & \vdots & \vdots \\ F_{L(N)} & y_{(N)} & \dot{x}_{(N)} \end{pmatrix} \tag{15}$$

If the model is accurate, the operating points are exactly on the surface. If they are next to it, this is an indication of one or more possible model errors and in this case the surface should be corrected or optimized accordingly to bring the model and observation into line. For this correction, Ströbel developed a method based on a special variant of neural networks (radial basis function networks). Based on both the original white box model and the black box observations, a new optimized *gray box model* is synthesized in the form of another numerical lookup table.

$$\mathbf{CM}_G: \ \dot{x} = \mathbf{LUT}\left(F_L, y\right) \tag{16}$$

This method has proven to be extremely suitable and quickly converging in various tests, even if only a few (e.g. fewer than ten) reliable black box observations are available. See [5] and [7] for further theoretical and experimental details.
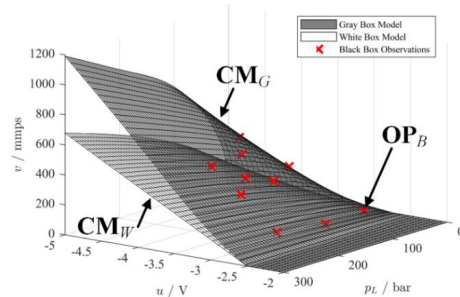

Figure 23: Illustrating the characteristic map optimization on the example of a die cushion press with positive overlapped valve control edges, taken from [7].

A major strength of this method is that the transition to a nonparametric model in the form of a lookup table, composed of many numerical data points, means that the model errors as a result of the mathematically rigid structure of the model equations can be easily compensated. In principle, each data point of the lookup table

forms a degree of freedom to correct the model qualitatively and quantitatively, regardless of whether these errors are due to a faulty model structure or faulty model parameters. Another advantage is that no additional sensors are required for this correction, position and pressure sensors are sufficient. Since this process can run online in the background of the operation of the system, changes in the model parameters due to wear or aging can also be detected. In terms of condition monitoring, this can provide important information about the current state of the drive and/or about possible impending faults or failures.

5. ENERGY ASPECTS

5.1 Concepts for continuous setting of hydraulic power

When evaluating drive concepts, energy efficiency is becoming more and more important. The energetic consideration of drives can be divided into two parts: One question is which losses occur when power is transferred from the hydraulic power source to the consumer and then converted into mechanic power or motion within the motor. The other question is whether, and if so to what extent, power can be fed back and made usable when the load drives the motor thus works in the generating 2nd or 4th quadrant. As far as the first question is concerned, as is generally known and apart from special solutions such as the hydro transformer etc., hydraulics knows

three well-known methods of power generation [1], [2]. The most important features of which are briefly listed in Figure 24.

5.2 Resistance control as an energetic problem case

As mentioned above, the resistance control is principally lossy. Nevertheless, it is interesting to compare the principal volume flow path of the valve-controlled servo drive with the electric circuit of the electric drive.
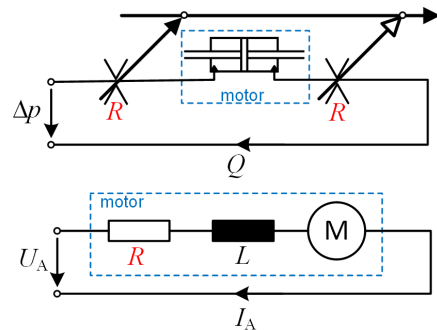
Figure 25: Principal comparison of the hydraulic and the electromechanical case.

Here a structural similarity is noticeable, but it is deceptive: In the electrical case of the circuit as well as in the hydraulic case resistors are in series with the force-generating element. But while in the hydraulic case the resistors are part of the actuator for power adjustment, in the electrical case they are part of the operating principle of the
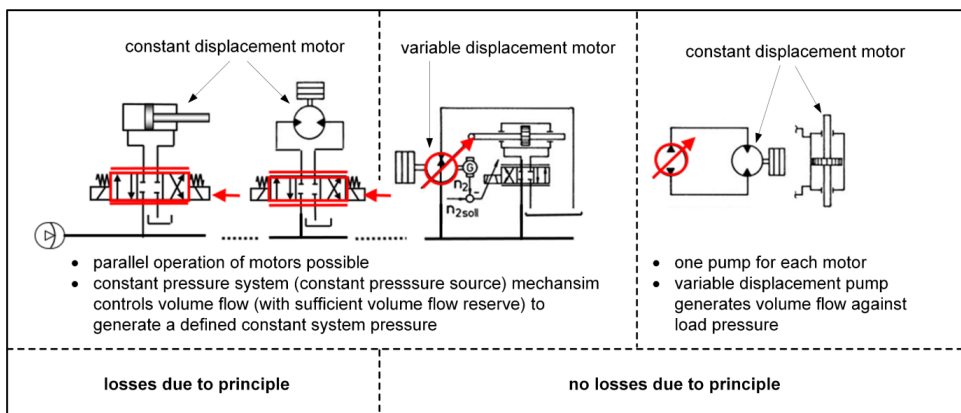
Figure 24: Practically relevant variants of the continuous hydraulic power setting.

motor. However, a real correspondence would be given there, if an adjustable ohmic resistor for power setting at the consumer (=motor) would be introduced into the electric circuit. This variant would be physically possible here too, but in practice it is de facto meaningless for various good reasons (power loss, unfavourable characteristic map, etc.). On the other hand, both drive variants take their power from a central supply unit, a constant pressure network (hydraulic) or a constant voltage intermediate circuit (electric). Parallel operation of several consumers at these power sources is only possible by adjusting the power flow in each consumer branch to the required power. The question remains as to why this is possible without any losses in the electric case, but not possible in the hydraulic case.

The torque-generating motor current is controlled for the electric motor via the drive or armature voltage (A = armature, M = motor, EMF = back electromotive force) [1].

$$U_A = U_M + U_{EMF} \qquad (17)$$

Whereas in hydraulics the power adjustment is achieved by reducing the supply pressure via pressure losses in resistors, the electrical drive technology has the advantage that with the inductance L of the coil in the current circuit there is an inertia-generating element which offers the possibility of generating the "correct" torque-generating motor current via the time average value of the current flowing between the switching states $U_A = U_{MAX}$ and $U_A = 0$. At $U_A = U_{MAX}$ the resistance in the "electronic switching valves" (transistors, thyristors, IGBTs etc.) and therefore the power loss is minimal and at $U_A = 0$ no current flows and the power loss is therefore zero. Due to the inductance of the coil as an inertia creator, the current "trembles" at a sufficiently high switching frequency f_S (usually several kHz), with a superimposed ripple, sufficiently smoothly around the value required to generate the torque.
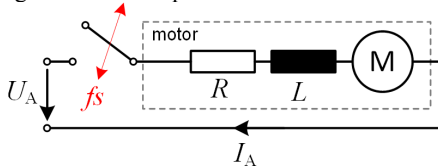
Figure 26: On-off switching of the electrical circuit.

In the output stage as a control element, therefore, no drive power is consumed, "only" the switching losses in the semiconductor components occur, whereby at high power levels and high frequencies the power losses can become so big that the corresponding components must be cooled with water and the energy advantage is at least partially lost again. This possibility of an at least in principle lossless voltage adjustment is a great advantage of electrical drive technology. In addition, even higher voltages than the existing supply voltage can be generated by special circuitry if required. (step-up converter). Unfortunately, there is no usable equivalent for this at hydraulics, because at electric case (= electron current) the flowing medium is practically massless and thus inertia-free but can be made inertial by inductors (e.g. coils). And the opening and closing of contacts is done by electric fields and not by movement of masses with corresponding impulse and thus permanently destructive forces due to the closing procedure.

This leaves the second question about the possibilities of energy recovery. This is unproblematic in the case of the electric drive, since the drive voltage $U_M = U_A - U_{EMF}$ because of

$$U_{EMF} = c\phi \cdot \Omega \qquad (18)$$

becomes negative at sufficiently high negative speeds Ω and thus feeds an electric current back to the power supply. Hydraulically, the power is generated in hydrostatic displacement units and these can in principle always also work as generators, so that one could think that power recovery (= recuperation) is possible with all three principles of hydraulic power setting mentioned. Unfortunately, this does not apply to the valve-controlled drive, and this is ultimately due to the rigid coupling of resistors, which are firmly attached to the slider as control edges and which prevent loss-free filling of the chamber on the inflow side when pulling forces. The fluid flowing into this chamber is then also fed by the pressure line and must be throttled via the control edges as throttle resistors, whereby the phenomenon of sucking already mentioned above can quickly occur. This critical condition can again be avoided using check valves. This solution to the suction problem is on the other

hand essentially a workaround of the fixed control edge configuration of conventional control valves. As the chamber pressure diagram shows, position control is not unproblematic with pulling loads because of the kink in the characteristic curve at the critical load pressure $p_L=-\alpha^3 \cdot p_0$ [1], [2]. However, the complete problem with all the case distinctions for the various operating situations becomes obsolete if the asymmetry caused by the unequal piston areas is compensated by a corresponding reciprocal asymmetry in the flow rate coefficients in the control valve [2]. However, the associated turning away from the use of classic 4/3 control valves does not necessarily mean to create a larger unwished variety of individual valve configurations that is hardly manageable in economic terms.
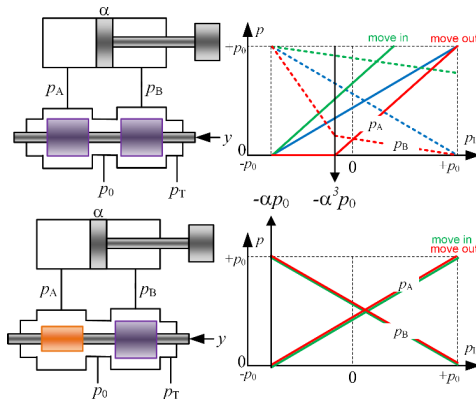
Figure 27: Symmetric and asymmetric valve control edges and corresponding qualitative pressure diagrams. The asymmetric case can possibly and easily be realized via two independent 3/2 proportional directional valves which are coupled electrically.

There are some more examples that conventional concepts with classical control valves may lead to useful but often suboptimal solutions. Possibilities of creating alternatives here by means of other valve designs are known but have not yet been pursued or have been pursued only half-heartedly. Such approaches under the heading of resolved control edges have already been investigated in various cases at universities [11], but despite numerous interesting perspectives, they have unfortunately not yet found any significant systematic implementation in practice except some quite special solutions. Even if the importance of valve-controlled servo

drives in hydraulics might decline further in the future, efforts should still be made to fully exploit the existing potential of this technology, which is unrivalled for some applications.

As far as power recovery is concerned, even in cases where it is possible in principle, it only makes sense if the energy generated can be used reasonably. This raises the question of storage, whereby in the case of a hydraulic drive on the engine itself, hydraulic power is initially generated, which in turn can only be stored directly as pressure energy in hydro accumulators. Here the possibilities are quite limited, not least for reasons of profitability. A conversion into other forms of energy that are easier to store is a possible way out, but it must not be neglected that each conversion of the form of energy is associated with losses. Here, the pump-controlled drive in principle has a slightly better position if it is driven directly by an electric motor as done in the so-called compact drive. Here there is the possibility of feeding back energy into an electric intermediate circuit (if existing and accessible), which makes it possible to supply other parallel running electric drives completely or partially with the energy fed back. It can also be expected that the latest developments in electrical power engineering e.g. by new battery technologies will bring new possibilities for the efficient use of regenerated electrical energy.

In view of the fundamental problems in energy recovery mentioned above, the current focus should be on avoiding unnecessary energy losses in hydraulic power supply control. Here there are comparatively simple approaches which are relatively simple and nevertheless very efficient and which, fortunately, are increasingly being used in practice. One approach that is becoming increasingly important, especially against the background of the digitalisation and Industry 4.0 concerns power adjustment on the supply-side. In the case of constant pressure supply, the hydraulic unit provides the volume flow which is required by the consumer as a resultant compression or kinematic volume flow. The aim must be to supply this volume flow as precisely as possible and to keep the excess volume flow required to maintain pressure as small as possible. This can be achieved by determining the volume flow over the pressure control valve using the

signals for pressure and control slider position available in modern digitised pressure control valves. This volume flow is the actual value in a control circuit, that is set up for the outflow to keep this at a reasonable small value. The whole thing becomes even more precise and thus energetically more efficient if the pump is given a sensible pilot control signal to provide the very volume flow which is nominally required currently as the sum of all volume flows of all connected consumers. Determining this target value should be no problem in a digitised and fully interconnected process environment. [2]
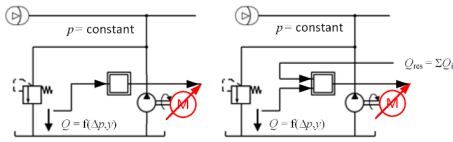
Figure 28: Energy saving solutions by smart hydraulic power supply.

5.3 Pump control as an alternative

According to what has been said above, two concepts with at least basically loss-free performance remain on the consumer side. However, since the realisation of a motor control is quite elaborate, especially if drives with differential cylinders are to be operated with it, only the pump control is left for the broad application. This umbrella term includes numerous variants, whereby the rotation of the pump drive shaft again can be generated by an electric motor [1], [2].
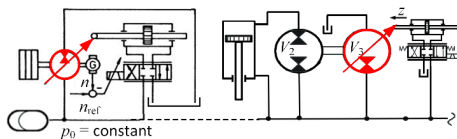
Figure 29: Rotary vs. linear motor control (hydro transformer).

Figure 30 shows the basic principle of the pump control, which as one knows is basically suitable for four-quadrant operation. However, some things must not be overlooked in this very simple representation of the concept. When operating under a torque load, the fluid on the driving side is naturally compressed. If this compression volume were simply taken from the low-pressure

side, negative pressures would be created there, and cavitation would threaten. At valve-controlled drives, both chambers on consumer side are pre compressed to half system pressure.
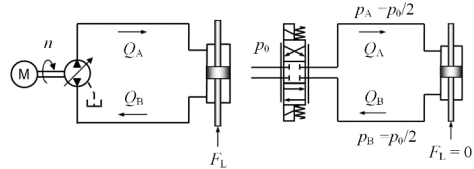
Figure 30: Comparison pump control vs. valve control.

In this case, an assembly with its own feed pump must be provided to generate the pressure on the low-pressure side. In addition to this unit for the load-dependent correct activation of the pressure on the low-pressure side, measures may be necessary, especially for drives that operate continuously with high loads, to feed the fluid stressed under load back into the tank for cooling and to replace it with fresh fluid from the tank [2].
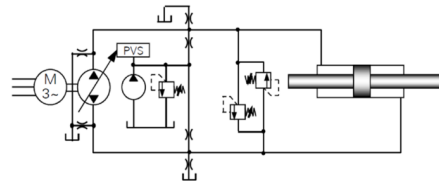
Figure 31: Closed circuit with preload pressure unit.
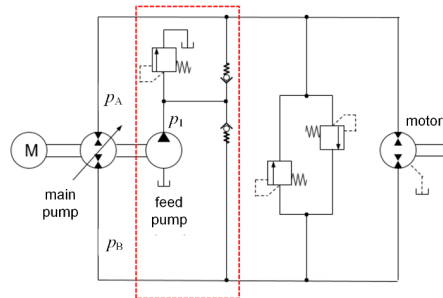
Figure 32: Closed circuit pump control with flushing and feeding unit.

Further circuitry measures are required if the motor is asymmetrical as in the case of a single rod cylinder. In this case the rod volume must be stored somewhere as a so-called pendulum volume depending on the stroke and fed back again during the return stroke. For this purpose, various more or less complex circuits have been developed, see Figure 33.
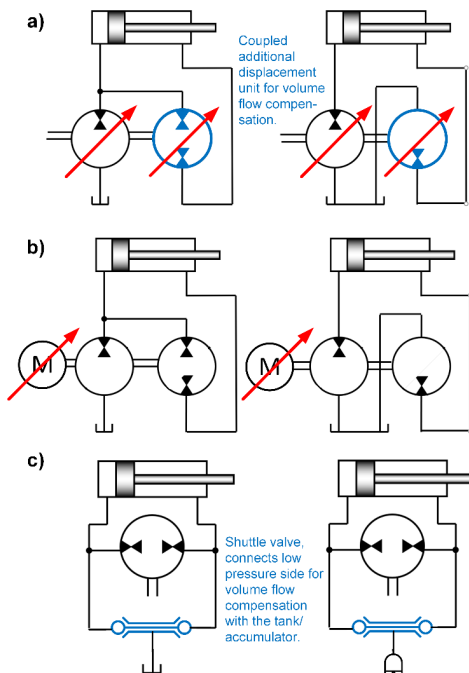
Figure 33: Differential cylinder drive with a) variable displacement pump control, b) variable speed motor directed pump control, c) shuttle valve

But a glance at the displacement units required in the case of a constant-speed electric motor a) clearly shows that these solutions were only used for very special applications for reasons of design and costs. However, when using constant displacement units and a variable-speed electric motor instead of displacement units b), the principle is basically the same but represents a more reasonable solution.

An even more simple and also cheap solution is to use a shuttle valve c). Here, however, there are certain switching effects when the low-pressure side is changed [1], [2], [12]. As an alternative to a tank, the pendulum volume can also be stored in an accumulator. Since the fluid volume to be stored is now stroke-dependent, the accumulator pressure increases with the stroke, starting with the withdrawn position. The actuator can be regarded as a plunger with a nonlinear hydraulic return spring. This effect must be considered when designing the controller. Figure 34 shows the dynamic model of such a pump-controlled cylinder drive. As can be seen, in comparison to the model of the valve-controlled cylinder drive, the servo valve has been replaced by a pump which generates a variable flow in both directions, either by varying the swivel angle at constant pump speed or, increasingly important, with a fixed displacement pump driven by a variable speed electric motor [1], [2], [12]. The model has only one motor chamber with an independent dynamic pressure build-up. If one defines the clamping pressure on the low pressure side with retracted piston and thus with minimum pendulum volume as the new zero pressure level, a structure for the cylinder results which differs from that of the valve-controlled drive only in two points: the term $1/C_H$ instead of $2/C_H$ and the stroke-dependent pressure in the driven chamber [1], [2], The halving of the proportionality factor expresses that now only one chamber (instead of two in case of valve-controlled actuators) is active as force generator. In cases with a sufficiently large accumulator and small pendulum volume, the stroke-dependent force effect of the low-pressure chamber (dashed force branch) can be neglected. Appropriate control concepts for this structure again result from implementing the basic rules presented above.
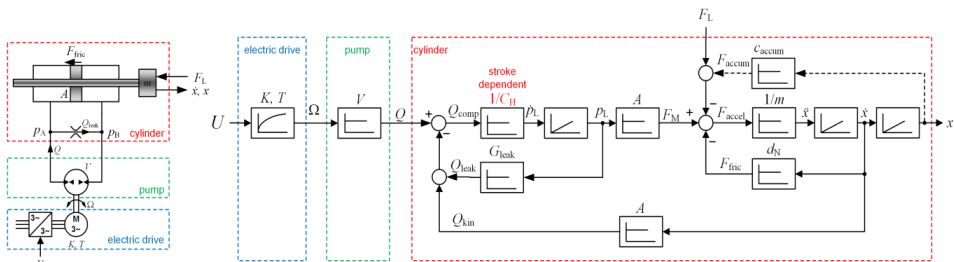
Figure 34: Pump-controlled system: simple scheme (left, switching valve and tank respectively accumulator for pendulum volume storage not drawn) and block diagram (right)

In the specific selection of the fixed displacement pump for applications with variable speed drive, special attention must be paid to operating points where no or almost no volume flow is required, for example when reversing direction. However, many pumps require some drag fluid due to the relative movement of rotor and stator for internal lubrication. Here, tribological aspects also play an important role in the selection of materials. A consciously accepted larger leakage can help here but is questionable from an energy point of view. On the other hand, a leakage "smears" somewhat the reversing point with the change of the low-pressure side. These detailed questions are currently a R&D-topic and there is certainly still potential for further developments.

5.4 Electrohydraulic compact drives as an alternative to electromechanical linear axes

With the pump-controlled cylinder drive with a variable-speed electric motor, a drive variant has been developed that is often referred to as a compact drive [12]. This attribute compact is perhaps less to be understood in the geometric sense, but rather expresses the fact that this is a standalone electro-hydraulic linear axis with the typical features that are otherwise only found in electromechanical drives. As an interface to the other process peripherals, it has an electrical power connector and a bus interface. The hydraulic transmission of the power generated in the electric motor can avoid numerous weaknesses of the electromechanical drives, where as you know, for example, the conversion of the rotary motor movement into a linear stroke movement via threaded spindles or similar converters is not unproblematic, especially with large strokes [12]. The possibility to store the pendulum volume in a hydraulic accumulator instead of in a tank has the advantage that the last component of the system, which requires a defined installation orientation, has been eliminated thereby. An electrohydraulic linear drive with an accumulator can be used in applications where the axis can swivel in all spatial directions. Even working in overhead positions is no problem any longer [9]. A disadvantage of the accumulator-afflicted version is that the pendulum volume to be stored increases with large strokes, which makes relatively large-volume hydraulic accumulators necessary. Here the multi-chamber cylinder as a special design variant can be a way out [9].
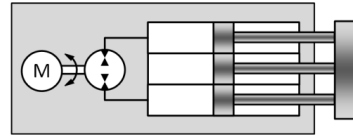
Figure 35: Simple scheme of a pump-controlled multi-chamber cylinder drive.

In this case five pressure chambers and one idle chamber are moved synchronously, whereby these chambers are connected in such a way that the drive has a resulting area ratio of $\alpha = 1$ like a synchronous cylinder and still has only one piston rod. In addition, this variant allows a rapid-motion mode in both stroke directions, whereby switching between rapid and power mode is possible in any position [10].
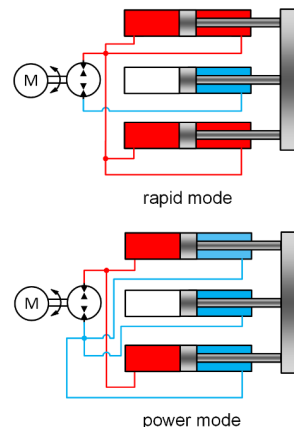

rapid mode

power mode

Figure 36: Multi-chamber cylinder drive connections for rapid mode and power mode.

Since there is no more pendulum volume, the hydraulic accumulator only needs to take up the compression volume and is correspondingly small, which in turn enables the realization of very long-stroke drives [9].

Of course, all these linear axes subsumed under compact drive do not normally have the flushing and refeeding unit which classic industrial pump-controlled drives do have. They are therefore

probably more suitable as positioning actuators than as servo drives, although the limits and possible remedies have not yet been researched. In any case, the heat input is significantly lower than with valve-controlled drives. Since the drive principle is not based on controlling pressure losses at control edges, there is nothing any more to be said against solutions in the low-pressure range. This could be interesting for numerous applications which are electromechanically problematic for one of the reasons mentioned above, but which are above the range covered by standard pneumatics in terms of performance. A perhaps still somewhat visionary aspect of such a low-pressure variant today are current research activities, that investigate whether and, if so, which components of such a drive could be made entirely or partially of plastic, what would open alternative new production possibilities.

5.5 The variable-speed electric drive as a component in hydraulic systems

The remarks of the last chapter made clear that in the future the electric motor will play an increasingly important role in hydraulic drive technology. For this reason, a brief look now shall be included at some relevant aspects of this increasingly important component in the modular building kit of a hydraulic engineer. As a representative example of an electric motor, the classic externally excited direct current motor will be considered below. This motor may seem antiquated, especially in its brushed elementary version, but apart from the reluctance motor it has the advantage of obeying the same physical laws in a very transparent form as all other electric servo motors in use today, what makes understanding basic laws and dependencies easier. In addition, its stationary and dynamic behaviour is almost ideal, so that, to put it simply, other electric motor principles to be used as servo drives attempt to impose to these motors the stationary and dynamic behaviour of this DC machine e.g. by vector based motion control concepts realised by sophisticated electronic circuitries.

Electrical DC drive basics

In the DC machine, the creation of torque is based on the Lorentz force as a force effect on moving electric charge carriers, i.e. the electrons of the

electric current flowing in the winding wires, which are permeated by a magnetic field with the flux density B. To drive this flux quantity, a armature voltage U_A is applied to the winding strands as a potential quantity [2].
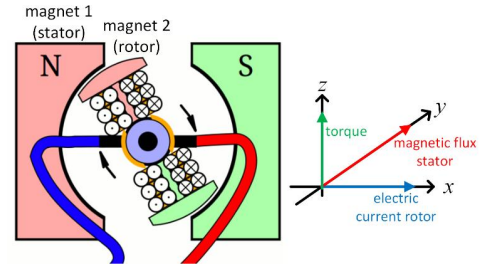
Figure 37: Operating principle of a DC motor.

However, as soon as the motor moves, this voltage U_A is reduced by the speed-proportional induction voltage U_{EMF}. At least, it is precisely the differential voltage $\Delta U = U_A - U_{EMF} - U_R$ driving the current I_A in the windings and thereby generating the torque $M_M = I_A \cdot c_\phi$. Nevertheless U_A is the power – directing variable.
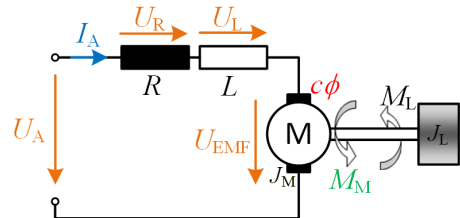

Figure 38: Scheme of a DC motor.

Based on the elementary equations for the Lorentz force on flowing currents in a magnetic field, for the voltage induction during the movement of charge carriers in a magnetic field and applying Newton's equation of motion, one obtains the well-known relationship as stationary model:

$$\Omega(M_L, U_A) = \frac{1}{c\phi} \cdot U_A - \frac{R}{(c\phi)^2} \cdot M_L$$

(19)

And again, under the assumption that the control element (output amplifier) is dynamically much faster than the drive itself, one obtains the dynamic model of the DC motor also quite simply but in contrast to the hydraulic case without the necessity of such questionable idealizing

assumptions and without operating point dependent linearization. The corresponding block diagram is shown in Figure 40 [1], [2].

Some selected comparisons between the electric and the hydraulic drive

In this approximate view, the characteristic map of the DC motor according to equation (19) represents a linear plane and is therefore very simple compared to the (multiple) non-linear plane of the characteristic map of a real hydraulic cylinder drive.
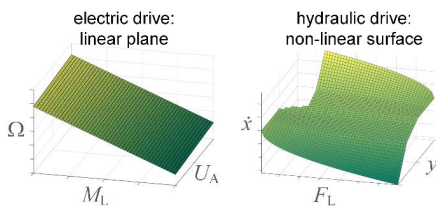

Figure 39: Principal comparison of the characteristic maps of electric and hydraulic drives.

As can be seen in the comparative block diagram in Figure 40, there is a structural similarity between the electric and the (idealised) hydraulic case of the dynamic model. However, despite this structural similarity, there are also a few significant differences:

- The parameters of the hydraulic case are partly strongly dependent on the operating point and are the result of linearization calculations, whereas the parameters of the electrical case are largely constant.
- Both models are second order systems that can in principle oscillate. However, with the parameters usually occurring in everyday practice, this oscillatory case is rather rare in the electrical case in contrast to the hydraulic case.

- In the electric case the force or torque generating variable is the current, i.e. a power *flow* variable, and in the hydraulic case the pressure, i.e. a power *potential* variable. However, since a potential variable can occur alone, but a flow variable requires a simultaneously occurring driving potential, the well-known fact results that to maintain a force in the hydraulic case, in principle, no power flow is required, but in the electrical case it is.

There is another difference between the hydraulic and the electric servo drive: with hydraulic drives as hydrostatic drives, the pressurized fluid is completely enclosed ("chambered"). During the movement of the chambers, there are relative movements between moving and still standing parts. At these contact points, leakage must be prevented by means of appropriate seals without unacceptably high frictional forces occurring. With increasing relative speed, however, the frictional forces do increase, and speed becomes a limiting factor.

With electrical drives, there are no contact points between bodies with relative movement, apart from the bearing of the rotor shaft. With electric drives, however, the force density in relation to a given available installation space is 5-7 times lower than in the hydraulic case and thus the force or torque here is the limiting factor.

Hydraulic drives generate power as a product of force and speed mainly via the factor force at comparatively low speed, whereas electric drives, apart from special designs (torque motors), generate power mainly via the factor speed at comparatively low force. Since the speed is then often far higher than required on the load side of the application, reduction gears with a transmission ratio i are usually introduced into the drive train. This measure apparently only
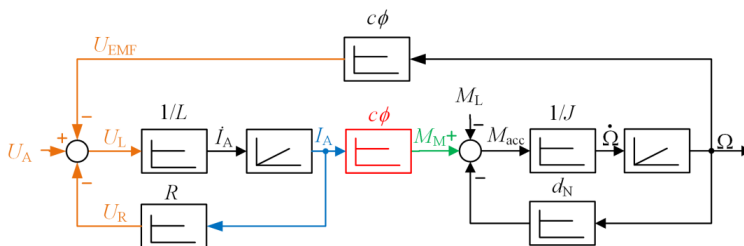

Figure 40: Block diagram of the DC drive.

mechanically relevant has considerable control engineering consequences. The inertial mass of the load J_L is added to the total inertial mass to be driven by the motor J_M only with a factor of $1/i^2$ as reduced moment of inertia. At the usual transmission ratios (usually $i > 10$), the driven load mass changes the eigenfrequency of the drive train only marginally, whereas in the case of hydraulic drives without gears it is fully taken up, see equations in Figure 41 (index M = motor, L = load).
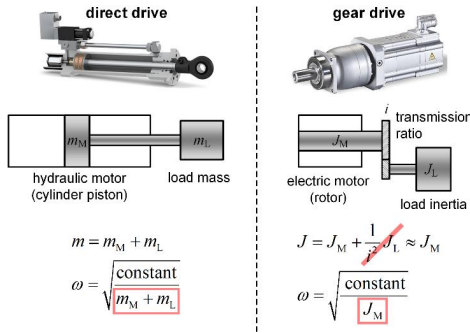

Figure 41: Mass influence on eigenfrequency.

Since the controller parameterization is significantly dependent on the eigenfrequency of the controlled system, the consequence of this fact is that the controller parameterization of a servo axis in the electrical case can be carried out without any knowledge of the load mass, whereas in the hydraulic case the controlled system can often only be optimized at the customer's system.

Due to the typical parameters of electric motors suitable for servo operation, the electrical time constant T_E is usually many times smaller than the mechanical time constant T_M, i.e. the electric motor as the possibly oscillating second-order system can be simplified to a non-oscillating first-order system in the model. If, as in the case of the compact drives mentioned above, the fixed displacement pump is driven by a variable-speed servo drive, the latter can be regarded as the actual actuator of the entire drive system whose (only) task is to generate a desired speed Ω_{ref} as fast and error-free as possible. The variable-speed drive itself is here a closed mechatronic subsystem consisting of the motor, the required encoder and current sensors, the power output stage and necessarily the implicitly required PI control loops for current (torque) and speed. This actuator subsystem can under the precondition of a well-adapted controller be regarded as a dynamic first-order system again with a specific time constant T_{SD}. This second reduction of order is legitimized by the fact that, due to the cascade control normally used in electric servo drives, the outer speed control loop is slower than the inner current control loop and thus is the dominant link in the chain $\Omega_{ref} \rightarrow \Omega_{act}$. If this electric servo drive is integrated into the overall hydraulic system as the actuating element, a further control loop is required for the actual controlled variable, for example the cylinder position x [1], [2], see Figure 43 and Figure 44.
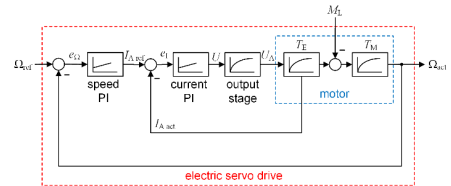

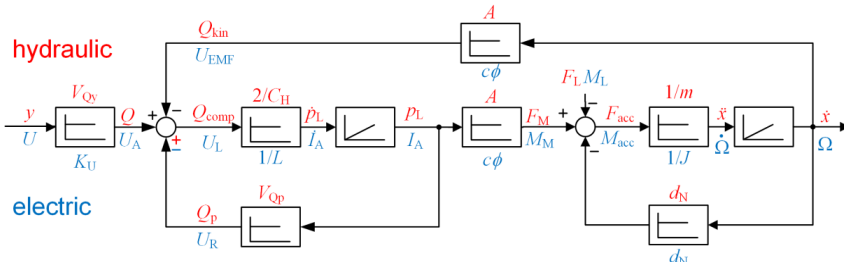**Figure 43:** Simplified block diagram of the controlled electric servo drive.

Figure 42: Block diagram of the DC drive and the idealized valve-controlled cylinder drive.
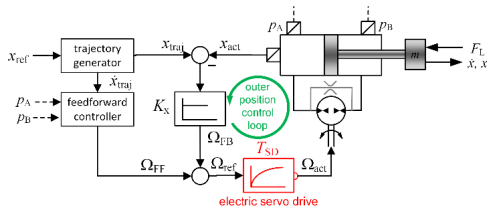
Figure 44: Use diagram of the electric servo drive as the actuating element for a pump-controlled cylinder drive.

For this outer control loop, a simple P-controller is usually sufficient here which continuously "corrects" the reference velocity for the electric servo drive. Additional model-based feedforward controllers are also possible and conceivable, of course. It should be mentioned in this context that, especially at slow speeds or when the cylinder is at a standstill, the speed of the electric drive is usually not zero, which is mainly due to the significant leakage within the pump in these operating conditions. These effects could in turn be identified and corrected with the characteristic map based control and optimization methods mentioned straight forward, whereas the desired cylinder speed and the measured pressures are the necessary input quantities.

6. THE ROLE OF COMPUTERS

The explanations in this paper show that the design and calculation of servo-hydraulic drive systems can be carried out systematically and purposefully. At the same time, however, it also became clear that due to the peculiarities of hydraulics, which are caused, for example, by asymmetries and non-linearities, the corresponding mathematical calculations and relationships are often not trivial. For this purpose, the possibilities of the computer-aided calculation and simulation tools available today should be used sensibly. The authors' view is that these tools should neither be used blindly nor over-automated, or that they degenerate into an end in themselves. This means that these tools are seen as pure aids (CAE = Computer *Aided* Engineering), but not as tools that release the engineer from his core tasks, i.e. the analysis and solution of corresponding problems. All too often, overflowing simulation programs are created that may very well reflect the real system

behaviour, but do not really allow a true insight into the system's inherent relationships. A simple look at a chamber pressure diagram, a characteristic map or a transfer function can often produce an "aha!" effect to explain and understand the phenomena observed in reality. Such a manufacturer-independent and mathematically oriented *fluid-mechatronic toolbox* tool is currently being created by the authors as a Matlab Toolbox.

Nevertheless, current development trends in model-based engineering do offer possibilities for controller design that were unthinkable just a few years ago. In simulation environments, for example, controller designs can be tested and then implemented directly on the target hardware at the push of a button using appropriate code generation tools. Recently, this has even become largely platform- and manufacturer-independent (e.g. keyword FMI = Functional Mockup Interface [13], [14]). Due to the memory capacity and real-time computing performance available today and in the future, there are virtually no limits to the engineer and the possibilities associated with it.

Due to the aforementioned principle-based properties of hydraulics, this computer-based tool chain, supporting the engineer from design to implementation, seem to be made for help catapulting servo-hydraulic drive technology into the digital 21st century. Nevertheless, a sound knowledge of mathematics, physics and technology must still be the basis for the meaningful application of these techniques.

7. CONCLUSION AND OUTLOOK

This paper has examined a number of current aspects of hydraulic servo drives in more detail. Although the individual points may appear somewhat heterogeneous at first glance, they all convey the same message: hydraulic drive technology may be a niche discipline, but in the mechatronic toolbox for building high level technical solutions it is indispensable and offers many unexpected perspectives. However, it can only take on and fill this important role in drive technology if it no longer considers itself as an independent discipline but defines itself rather as a fluid mechatronic part of *Industry 4.0*. In order

to be competitive in the future, it is only necessary to make consistent use of the available opportunities. What is needed are not new revolutionary ideas and devices, what it needs is a new self-image. Hydraulic drive technology is the ideal solution for many tasks with high demands on motion sequences, especially in the higher power range, such as drive solutions for multi-body systems or with load masses with their own dynamics. This new self-image requires an interdisciplinary new start or better a complete reset in engineering education, where at present the signs point more to retreat than to reorientation.

NOMENCLATURE

A	area
α	area ratio
c	electric motor constant
C_h	hydraulic capacity
CM	characteristic map (lookup table)
G	transfer function
d	friction coefficient
D	damping
e	control error
F	force
i	gear ratio
K	system gain, controller gain
m	mass
OP	operating point
p	pressure
ϕ	magnetic flux
Q	volume flow
u	control signal
U	voltage
V	system gain, volume
x	position
$\dot{x}$	velocity
y	valve opening, control signal
ω	eigenfrequency
Ω	angular velocity

REFERENCES

[1] Anders P (2019) *Elektrohydraulische Industrieantriebe*. Lecture Notes, IFD, TU Dresden

[2] Anders P, Ströbel S (2019) *Servomechanismen*. Lecture Notes, Faculty of Industrial Technologies, Hochschule Furtwangen University

[3] Lutz H, Wendt W *Taschenbuch der Regelungstechnik, mit MATLAB und Simulink*. Europa-Lehrmittel Haan

[4] Lunze J (2016) *Regelungstechnik 1: Systemtheoretische Grundlagen, Analyse und Entwurf einschleifiger Regelungen*. Springer Vieweg

[5] Ströbel S (2018) *Modellbasierte Vorsteuerung ventilgesteuerter hydraulischer Linearantriebe im Lageregelkreis*. Dissertation, TU Dresden

[6] Wey T, Lemmen M (1997) *Flachheitsbasierte Regelung – Folgeregelung eines hydraulischen Differentialzylinders*. Forschungsbericht Nr. 11/97 MSR, Universität Duisburg

[7] Helmke M, Ströbel S, Anders P, Schulze T. (2018) *Computer-assisted modeling and automatic controller adjustment for hydraulic drives based on an innovative nonparametric identification method*. 11th International Fluid Power Conference. March 19-21, 2018, Aachen, Germany

[8] Anders P, Ströbel S (2019) *Regelungstechnik*. Lecture Notes, Faculty of Industrial Technologies, Hochschule Furtwangen University

[9] Anders, P, Scheidt M, Bauer F (2017) *Applikationsabhängig anpassbar - Antriebskonzept bietet Lösung bei Problemkonstellationen von Linearachsen*. In: Antriebstechnik, Nr. 1-2, pp. 32-34

[10] Kolks G, Weber J (2018) *Single Rod Cylinders with Variable Piston Area? A Comprehensive Approach to the Right Solution*. In: Proceedings of the ASME/BATH Symposium on Fluid Power & Motion Control. Bath, UK

[11] Kolks G, Weber J (2018) *Getrennte Steuerkanten für den Einsatz in stationärhydraulischen Antrieben*. In: O+P Fluidtechnik, Nr. 6, pp. 42-51

[12] Michel S, Weber J (2012) *Energieeffiziente elektrohydraulische Antriebe kleiner Leistung*. Abschlussbericht zum Vorhaben TU Dresden, Institut für Fluidtechnik

[13] Modelica Association (2020): *Functional Mockup Interface*. https://fmi-standard.org/, Accessed 03 Feb 2020

[14] Beckhoff GmbH & Co. KG (2020): *TC3 Target for FMI*. https://www.beckhoff.de/TE1420/, Accessed 03 Feb 2020

CYTROCONNECT – A CLOUD-BASED IOT-SERVICE AS CONNECTIVITY SOLUTION FOR ELECTROHYDRAULIC SYSTEMS

Martin Laube[1]*, Andreas Günder[1], Jan Bierod[1], Volker Jesberger[2], Stefan Rauch[2]

[1] *Bosch Rexroth AG, Zum Eisengiesser 1, 97816 Lohr a. Main*
[2] *grow platform GmbH, Postfach 30 02 40, 70442 Stuttgart*
* Corresponding author: Tel.: +49 9352 183619; E-mail address: martin.laube@boschrexroth.de

ABSTRACT

Conventional electrohydraulic solutions integrate easily into modern machine concepts by utilizing field bus technology. Nevertheless, most use cases are limited to machine automation concepts. Integration into higher-level data and IoT systems is the key for positioning of electrohydraulic solutions within the factory of the future. CytroConnect is a new approach for the integration of electrohydraulic systems into IoT environments and the corresponding market offerings. Bosch Rexroth decided not only to integrate IoT-ready features like pre-installed sensor packages but also a modular automation concept providing decentralized intelligence with an open multi-ethernet interface. An edge-to-cloud connectivity stack operated by Bosch turns the target into a Connected Product. The convergence of physical and digital product can be realized. Based on that the digital service CytroConnect solves concrete holistic use cases like visualization and condition monitoring by offering a web-based dashboard of all relevant sensor data that is accessible everywhere. Modular paid add-ons offered as risk-free monthly subscriptions address further smart maintenance and prediction use cases.

Keywords: CytroBox, IoT, Connectivity, Industry 4.0, electrohydraulic systems

1. STATE-OF-THE-ART

Pulled by the increasing complexity and variances in products and pushed by the progressive capabilities in communication technology the internet and automation systems are getting more and more connected to reach a new level of efficiency.

The traditional way of industrial communication is described in the automation pyramid (**Figure**). The exchange of data is mainly between the adjacent levels. Due to the diverse manufacturers related standards it is taking a lot of effort to realize level crossing communication. With standards like OPC-UA and Ethernet TNS, it is possible to exchange data between different systems and automation levels efficient and in real time, which is important for M2M communication in an industry 4.0 environment.

The communication of traditional electro-hydraulic drive systems is mainly field bus based and only connecting the different components of the drive system to the machine control. It is a clear focus on realizing the machine

functionalities and required performance. The data is not leaving the machine border and only basic and no scalable condition-monitoring concepts are integrated.
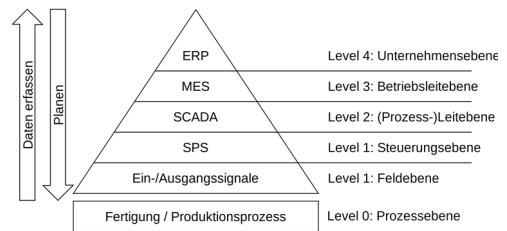

Figure 1:   Automation Pyramid [1]

2. MOTIVATION FOR NEW CONNECTIVITY SOLUTIONS

Physical products and digital services merge into hybrid solutions. Physical products become carriers of digital services, also known as Smart Components, for which services and business models are offered on a "Smart Service Platform" in the form of "Smart Services".

These "Smart Services" for example, can

enable fast machine service or other business models such as pay-per-use for machines and components. It should be possible to use engineering data and live data from the machines and components to develop the "Smart Services". In order to be able to add quickly new functionalities and services to the systems, it is essential to collect and prepare data in a cloud and to use a suitable device management. This platform approach enables the scalable further implementation of technical features and the integration of new use cases. By means of a standardized building block of physical products and systems, digital services can be transferred to
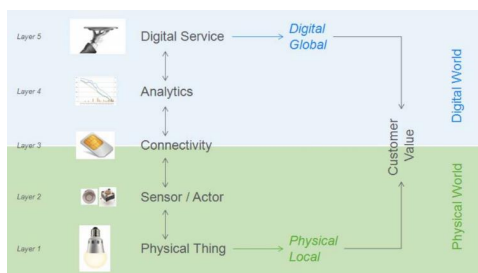
different hardware products with little effort.

Figure 2: Value-creation Layers in an Internet of Things Application [2]

As shown in the figure below (**Figure 3**), physical products with their digital services are thus establishing themselves as drivers for new maintenance and service concepts and for new business models. The targeted collection and analysis of data is becoming increasingly

important and is a key capability for product and business model design. Examples are provided here by the business model patterns subscription, flat rate, freemium, pay per use and performance-based contracting.

As an additional benefit of collected data, the conditions of use and business models also change in physical services (**Figure 4**). For example, in the event of a fault, service technicians can use the data to carry out a faster diagnosis and data-supported business models can also be offered here.
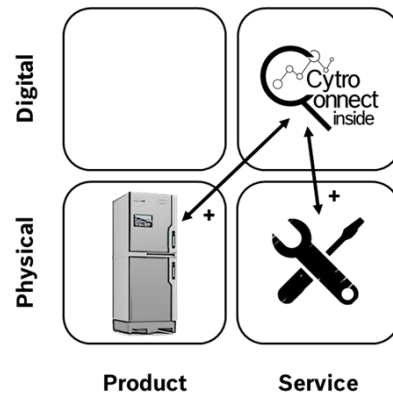
Figure 4: Digital Add-ons enlarge customer benefits

To leverage the potential in IoT technologies, it is crucial that the number of systems sold is decoupled from the size of the team responsible for developing and operating the solution. It is therefore crucial to consider the scaling aspect in
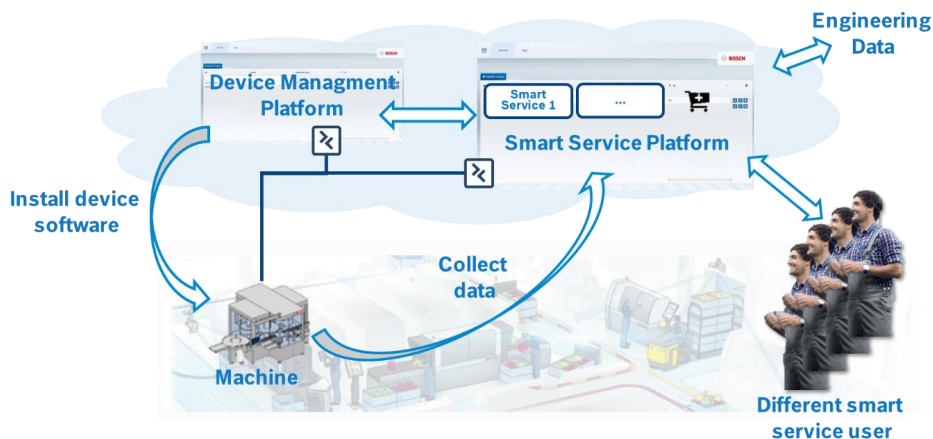
Figure 3: Concept Smart Service [2]

the solution from the very beginning in the design. The project planning and commissioning processes must also be taken into account. The goal must be to automate them completely. Another aspect that also contributes to the topic of "Non-Human-Scaling" is the topic of Plug and Play. If products do not generate any commissioning effort and the customer does not have to make any adjustments to the configuration for commissioning (because this all happens automatically), the service and support effort (both scaled by humans) can also be minimized on the manufacturer side.

3. CYTROCONNECT AS A NEW APPROACH

Based on the requirements driven by the technical concepts for convergence of physical and digital products Bosch Rexroth has developed and implemented a new solution for the integration of electrohydraulic systems into IoT environments and the corresponding market offerings which is described in the following:

3.1. Hardware Concept

The concept is physically divided into the hardware integrated in the target product (sensor technology, data acquisition unit) and corresponding edge devices (communication module) **Figure 5**.

A PLC integrated in the target product is the main control system. Sensors in the system exposing their data via IO-Link to an IO-Link-Master, that communicates with the PLC via Fieldbus. For decoupling- and IT-security-

purposes, a dedicated industrial PC (IPC) is used as the edge device for the IoT services. This also brings the advantage, that a different (Linux based) software platform can be used to realize data streaming and IT security requirements.
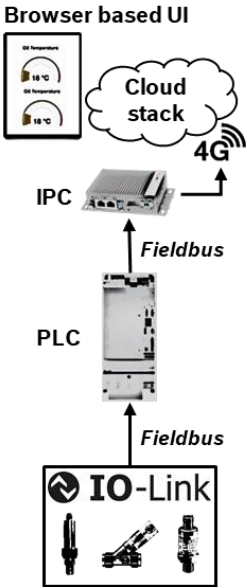
Figure 5: Hardware Topology (Product, Edge Device, Cloud, User Interface) [3]

3.2. Software Topology

Each target product is equipped with a dedicated Industrial-PC for exposing data to IoT-Services. This device is capturing sensor- and condition data from the control system (PLC) of the target product and pushes it via 4G-Link to a cloud
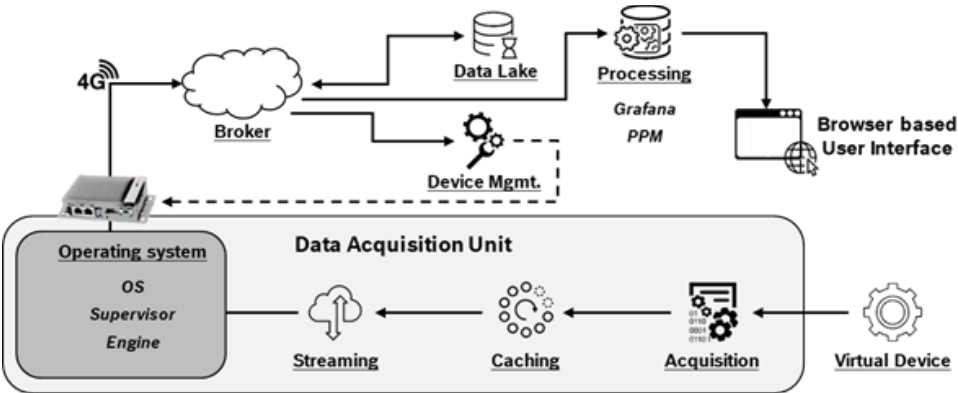
Figure 6: Software topology CytroConnect

endpoint. The data of all devices in the deployed fleet is streamed to a broker that is used as the central data hub. To make the data available in the customer facing systems, filtering rules and data transformations are applied on the data streams **Figure 6.**

Beside the customer facing solutions (a customizable Grafana Dashboard and the Bosch Nexeed Production Performance Manager - PPM), there are some additional systems, that are required for running such a platform. A Monitoring solution that allows to monitor the health of the infrastructure, a Device Management solution, which enables software updates and management of the edge devices and a Data Lake that is storing raw data for intended analytics use cases. The dashboard, showing the machine data is a web application, running in the cloud. That enables access to machine data by any device, every time and everywhere.

3.3. Digital Service as a business model

The integrated IoT service Bosch Rexroth CytroConnect is intended to ensure higher availability and to avoid unplanned downtimes. With this IoT service, operators can monitor operating state and plan maintenance in a cost-efficient manner. As a result, fluid technology has taken a further step towards the factory of the future.

With the CytroConnect digital service, operators have all information about their product all time available. Whether it is the visualization of the component and operation state or chargeable IoT services. This services – based on big data analytics – support the maintenance work during troubleshooting and provide warnings of upcoming events before they happen. In addition to the condition monitoring of the target product, maintenance personnel and maintenance managers can add extra solutions for various applications as add-ons. These pay-per-use payment models include additional IoT analytics tools and can be subscribed to on a monthly basis.

For optimizing maintenance processes, the CytroConnect Maintain module offers access to historical sensor data as well as instant messages if maintenance is required. Pre-defined rules - based on long time application experience - allows customers to improve their maintenance strategy on an ongoing basis. With that

combination of scalable software, Bosch IoT solutions and Bosch Rexroth domain specialists a high benefit can be offered to the customers.

One example of the used Bosch IoT solutions is the Nexeed Production Performance Manager (PPM). It is a software solution for systematic production optimization and allows easy processing of acquired data. With that tool, the different components and data can be set into correlation. Single sensor or data points like pressure, oil temperature or level for themselves don´t allow conclusions about the system. However, in correlation the data sources can be used to perform a condition diagnosis of the system.

Beyond this, the CytroConnect Predict service offers the possibility of using machine learning. Big data analytics and self-learning algorithms calculate the actual status and expected remaining lifetime of relevant components. Based on this the operator gets informed and can plan the downtime. Furthermore, this information allows changing the component in advance to prevent further damage on the complete system and ensures maximum availability.

4. MATURITY AND VALIDATION

To evaluate the entire concept a first target product was defined – the new standardized hydraulic power unit CytroBox. Looking on the hardware topology in **Figure 7** it shows why this product is perfectly suitable for a digital service. By means of the newest version of speed variable servo technology in combination with IO-Link sensors, it is possible to collect many different data points of all components. Based on this architecture the entire soft- and hardware stack was built, always focused on an open and scalable design.

Already in the CytroBox development process, CytroConnect could be used in order to detect unknown behavior of the sample units during testing and for troubleshooting. For example, the detection of a damaged pressure sensor allowed the development team to order and replace it, even before there was a failure of the system. Further issues during testing and validation of the units in customer prototype machines like system leakage caused by a defect cylinder could be detected and evaluated by CytroConnect. Fixing of these incidents could happen without having the development team on-
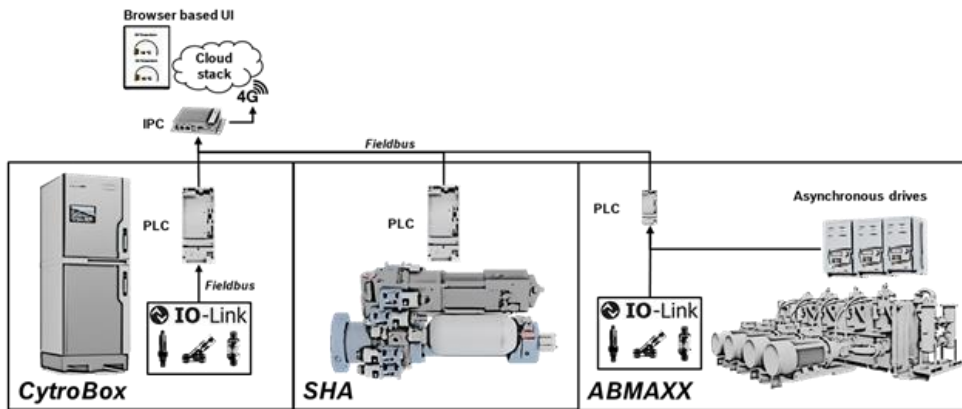
Figure 7:   Hardware Architecture CytroConnect portfolio extension

site, just by a phone call in most cases.

Depending on this experience, the actual target for CytroConnect is to extend the supported product portfolio. Due to the open design and scalability it´s easy to implement into different electrohydraulic system solutions, like the Servo Hydraulic Actuators (SHA) or Modular Large HPU (e.g. ABMAXX). **Figure 7** shows the needed hardware architecture for different target products. PLC and edge device integrated in the target products are kept identical throughout all possible use cases. To implement the different products on the cloud no main software changes are required. Only the dashboard for visualization and the product specific rules need to be configured and adjusted.

5. SUMMARY AND BUSINESS OUTLOOK

Driving digitalization into industrial hydraulics is clear focus topic in order to offer beneficial solutions in the environment of Industry 4.0 to the market. Besides providing products that are able to be digitally connected to superior control systems the combination with enabling these products for digital services and the operation of corresponding digital structures offers the possibility of additional data driven business models. With CytroConnect Bosch Rexroth offers a digital service platform, which allows electrohydraulic systems solutions to be integrated in the environment of the Factory of the Future. Online monitoring of operation conditions, remote diagnosis and maintenance as well as predictive services based on big data

analytics become possible. The related data driven business models like subscription, flat rate, freemium, pay per use and performance-based contracting allow advanced operation and maintenance concepts for OEMs and End-Users. The key success factor in the CytroConnect concept is the simple scalability and extension of the Hardware and Software concept on various target products, which allows consistent appearance for the user throughout the complete product portfolio. Having the well-known competition of drive technologies in mind, concepts like CytroConnect bring industrial hydraulics significantly forward and allow it to become part of the Factory of the Future.

REFERENCES

[1] https://de.wikipedia.org/wiki/Automatisierungs pyramide

[2] Bosch Internet of Things & Services Lab, St. Gallen

[3] io-link.com

INVESTIGATION OF ENERGY MANAGEMENT TOPOLOGIES FOR FORMING PRESSES WITH ELECTRO HYDROSTATIC DRIVETRAINS

Tim Reidl[1]*, Jürgen Weber[2], Steffen Ihlenfeldt[2]

[1]*Moog GmbH, Hanns-Klemm-Straße 28, 71034 Böblingen*
[2]*Institut für Mechatronischen Maschinenbau, Technische Universität Dresden, Helmholtzstrasse 7a, 01069 Dresden*
*Corresponding author: Tel.: +49 7031 622 4844; Email address: treidl@moog.com

ABSTRACT

Recent Power On Demand approaches, realized by using speed and/or displacement variable pump units, led to a significant increase of energy efficiency on hydraulic forming presses. In this paper we follow up on this development by laying the focus on the energy management and storage design of such machinery. With a derived fluidtronical model, we compare five different topologies that supply and manage the power flow for a forming press with die cushion. Our evaluation criteria are: energy consumption, minimization of the infeed power, and qualitative costs. For a representative forming cycle, the losses occurring on each of the drivetrain components and the power electronics accessory are derived in detail. We expect that this research will lead to deeper investigation of more intelligent energy management systems that use multiple storages in an optimal way and further learn and adapt during operation.

Keywords: Energy management, electro hydrostatic actuation system, peak shaving, efficiency of hydraulic forming press

1. INTRODUCTION

Machine manufacturers are obliged to further improve the energy efficiency of their machines due to increasing electricity costs, which most of the producing industry faces. The latest major improvement in the field of forming presses was the change from servo valve control to pump controlled displacement, as, for example, in [1] and [2]. Significant energy loss reductions are gained through the avoidance of throttle losses, as well as the re-use of temporally stored kinetic energy if the pump is operated in four quadrants. Research shows that up to 30% of energy can be saved by operating a deep drawing press with an electro hydrostatic die cushion instead of traditional hydraulics [2]. In [3], different control concepts — variable speed, variable displacement, or both simultaneously — were tested and compared regarding their efficiency. Using both control variables, speed and displacement, leads to an additional saving of up to 5% for a reference deep drawing cycle. Likewise, in [4], the author achieves up to 20% energy saving by implementing a loss-optimal-control strategy for a speed and displacement

variable pump. The work in [5] and [6] present significant loss reduction of 40% and 30% by using an Electro Hydrostatic Actuation System (EAS) for a ring-rolling machine and a forging press. Since this technology is only in some cases cost-equivalent to valve-based control, it is crucial to lay out all components as compact and cost-effective as possible. We expect that the paradigm of "peak shaving" will play an increasingly crucial role in the field of EAS-based machinery, as it does in the field of other machinery already. Peak power reduction is usually realized with a small power infeed in combination with different types of energy storages. The latter covers the peak power demands and stores energy in case of regenerative operation. The transformer, circuit breaker, mains switches and other inline elements may become significantly smaller and more cost effective if the peak power of the infeed is reduced. Furthermore, the authors in [7] point out that a predictable and rather constant load helps companies to gain "energetic flexibility" and participate in the future energy market more successfully. In countries with a

non-negligible amount of renewable energy plants in the power supply mix, high peak loads of factories need to be compensated with fuel based power plants due to the volatile nature of e.g. wind and solar plants. Consequently, high peak power loads are "punished" by the supplier with an additional cost, according to [8].

Peak reduction approaches have been researched and implemented, for example, in the field of electromechanical servo presses. The authors of [7] and [9] analyze different storage technologies and power supply options that limit the infeed power peak. In [10] an energy management system with reduced infeed power and local electrical storage for an electromechanical punching press is presented. In this paper, we compare five different energy management topologies (EMT), by simulation, for a 1600 kN EAS-based forming press. All studied topologies are potential solutions for handling the power flow for such a machine, each with different advantages and disadvantages. We show how much the installed power infeed can be decreased if an electric storage based on capacitors is used and how the type of topology affects the overall efficiency. Finally we will derive a rough cost indication of the investigated topologies in order to evaluate their potential in the market.

1.1. Energy management sophistication levels

In order to classify how advanced a certain energy management approach is we defined five levels of sophistication (SL). These are valid for EAS-based forming presses and for other machinery, where multiple axes act on the same machine or where several machines are coupled via the direct current (DC) link.

1. A common non-active front end supplies all axes. The axes exchange power over the DC bus. When the total regenerative-power is too high, it is dissipated over a bleed resistor.
2. An active front end powers all axes and feeds back current into the grid if power is regenerative. Axes exchange power over the DC bus. Infeed needs to cover peak power requirement of all axes at all times.
3. Infeed charges the passive capacitor storage and both power all axes. Regenerative power is stored in the DC bus. Infeed can be

significantly downsized since peak power is provided by the capacitors.
4. Controllable storages like active capacitor units or servo flywheels are additionally coupled into the DC bus. A model-based algorithm on a controller generates command values for the infeed and the storages.
5. Like in SL 4, but the model adapts/learns on a cyclic basis and changes the available control outputs according to optimization criteria.

2. MACHINE MODEL

The press and cushion axis of the built model, which can be seen in **Figure 1**, consist of a cylinder (a), a radial piston pump (b), a permanent magnet synchronous motor (c), a DC/AC Drive (d), the power infeed (e), and an external DC bus capacity (f). The cylinders are stiffly coupled to the ram mass (g) and the cushion (h). The strong simplified model of the drawing force is represented by a damper (i) and the fluid compressibility and frame stiffness by an equivalent spring that acts between the dies (j).
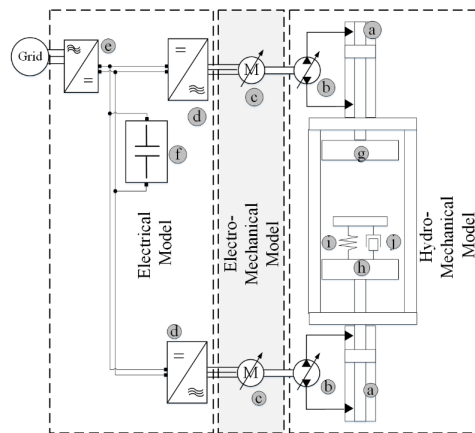

Figure 1: Schematic of the model (here with capacitor storage)

The simulation model consists of an ideal model and a loss model of each component that interact from the process backwards until the grid, as we show in **Figure 3**. The losses are added to the effective power flow, where then both need to be covered by the next component. The only closed loop model is the one from the infeed, as

shown in **Figure 2**. It controls the DC bus voltage whereas all power flows into or out-of the DC bus act as disturbances. Since different energy management topologies are simulated, we built an infeed model that is suitable for all scenarios. Depending on the infeed type, the bus voltage and current are actively controlled; therefore the upper branch of the control scheme is active. In this case, the voltage and current controller requires tuning as well as the positive and negative current limit need to be set. In case that the infeed works passively with a bridge rectifier, the lower branch is active and, depending on actual DC bus voltage U_{dc} and supply voltage U_{sup}, the supply current I_{sup} flows in an open loop way. Both electro-hydrostatic axes pull or supply power from/to the DC bus, depending on whether they accelerate, brake, press, travel, or stand. All losses from all components, including the brake choppers in case of too high voltage, dynamically take power from the bus and diminish the voltage level.

2.1. Loss models

The main losses that occur up to the cylinders input are:

- hydro mechanical friction and leakage loss at the pump,
- current and speed related iron loss at the motors,
- insulated-gate bipolar transistor (IGBT-) switching-, DC link- and extra-losses in the DC-AC drive,
- rectifier-, inductor-, and extra-losses for the passive infeed respectively IGBT switching losses instead for rectifier losses for the active front end,
- losses in the capacitors,

Since in this work we focus on the energy management part, mechanical friction- and fluid decompression-losses are neglected.

Pump losses

The pumps' hydromechanical friction and leakage model consist of two high dimensional lookup tables (LUT) that approximate between

Figure 2: Ideal Infeed and capacitor model

Figure 3: Architecture of the simulation model

measured working points. The friction torque at the shaft is given out as

$$T_{fr} = LUT_{fr}(\Delta p, n, \alpha, \upsilon), \tag{1}$$

depending on the actual motor speed n , pressure Δp and displacement α. The viscosity υ is assumed as constant. The pumps leakage flow

$$Q_l = LUT_l(\Delta p, n, \upsilon, \alpha) \tag{2}$$

is the approximated output of a second LUT with the same inputs as in equation (1). The pumps total losses are then derived as

$$P_{lp} = Q_l \cdot \frac{\Delta p}{600} + \frac{n \cdot 2 \cdot \pi}{60000} \cdot T_{fr} . \tag{3}$$

Motor losses

As derived in [15] a permanent magnet synchronous motor consists of current dependent copper losses and iron losses. The copper losses are calculated as

$$P_{cu} = 3 \cdot I_m^2 \cdot R_s. \tag{4}$$

Whereby, the current I_m is the root mean square value of the AC current in one phase and R_s is the phase resistance of the motors' windings. The total current of a permanent magnet synchronous motor, that is operated in field oriented control, consists of the torque building I_q − and a direct-current I_d. The total current is derived as

$$I_m = \sqrt{I_q^2 + I_d^2} . \tag{5}$$

The amount of d-current that is needed, if the motor operates in the field weakening area, depends on the actual DC bus voltage, and so do consequently the motor losses.

Hysteresis-, Eddy current- and non-magnetization losses can be summarized as iron losses since they all depend linearly or quadratically on the velocity of the rotating electrical field and thus of the motors speed.

$$P_{fe} = f_1 \cdot n^2 + f_2 \cdot n \tag{6}$$

The constants f_1 and f_2 can be derived from thermal tests at stall and at nominal condition. The total motor losses are then

$$P_{lmot} = 3 \cdot I_m^2 \cdot R_s + f_1 \cdot n^2 + f_2 \cdot n. \tag{7}$$

Drive losses

A complete and detailed loss model of a drive is derived and verified in [11]. However, the used model requires a lot of parameters, which would go beyond the scope of this investigation. Instead we build a model that only needs the rating values from the datasheet and power consumption measurement at idle condition. Since we want to see the effect of a fluctuating bus voltage on the losses of the components, the drive model also needs to take this into consideration. The complete losses consist of the idle-operation losses P_{ldrv0} when the drive is switched on but not controlling any current. The factor f_3 can be calculated out of the nominal current and nominal voltage. The term under the square root takes the actual voltage level into consideration,

$$P_{ldrv} = P_{ldrv0} + f_3 \cdot I_{dc} \cdot \sqrt{\frac{U_{dc}}{U_{nom}}} \tag{8}$$

with I_{dc} as the actual bus current and U_{dc} the actual bus voltage. **Table 1** shows the calculated losses at given rating points of current and voltage. Equation (8) estimates the losses in the range where the DC bus mainly operates. The error, comparing the calculated losses and the nominal drive losses P_{ldrvn}, is acceptably small.

Table 1: Ratings of the Moog Servo Drive G397 450

Voltage [Vdc]	Nominal current [Arms]	P_{ldrv} [W]	Error [%] $P_{ldrv}(I_{dc}, U_{dc})$ − P_{ldrvn}
565	450	5400	0
650	416	5361	1
678	405	5335	1.2

Active front end losses

The active front end (AFE) losses consist of the constant part P_{lafe0}, similar as in the drive model, and a current dependent part. This term inherits the nominal losses P_{nafe} of the electrics and the losses P_{lLCL} of the LCL filter at nominal condition and scales it linearly according to the grid current I_{grid}.

$$P_{lafe} = P_{lafe0} + \frac{I_{grid}}{I_{nom}} \cdot (P_{nafe} - P_{lafe0} + P_{lLCL}) \tag{9}$$

AC/DC/DC losses

The AC/DC/DC converter rectifies without boost function and controls the current on the DC bus side. The loss model consists again of a

constant part P_{lacdc0} and a term that depends linearly on the actual grid current. Since the chokes are now on the DC side, the losses P_{nch} depend on the DC current.

$$P_{lacdc} = P_{lacdc0} + \frac{I_{grid}}{I_{ninf}} \cdot (P_{nacdc} - P_{lacdc0})$$
$$+ \frac{I_{dc}}{I_{nch}} \cdot P_{nch} \qquad (10)$$

Capacitor losses

A strongly simplified model of the used aluminium electrolytic capacitors basically consists of an equivalent series resistance (ESR) which induces ohmic losses when a current flows. This value depends on the dissipation factor $tan\,\delta$, the capacitance c, and the current ripple's frequency ω

$$ESR(\omega) = \frac{tan\,\delta}{\omega C}. \qquad (11)$$

The total loss of one capacitor unit can then be derived as

$$P_{lcp} = ESR(\omega) \cdot I_{dc}^2 + I_{leak} \cdot U_{dc}, \qquad (12)$$

Whereby, I_{leak} is the leakage current that is characteristic for electrolytic capacitors. The dependency of the capacity and the leakage current of the actual temperature are neglected here. We assume that the ripple currents induced by the infeed's switching and the reactive power that travels between DC bus and motor are much smaller in amplitude and much higher in frequency than the active power related current. Since the losses grow quadratically with increasing current and the ESR value dilutes with increasing frequency, these small amplitude/high frequency currents are ignored. The frequency of the active power related current is set to 2 Hz for the ESR calculation since most of the acceleration and deceleration phases are conducted in times around 250 milliseconds.

2.2. Model Parameters

Table 2 shows the parameters of the hydro-mechanical model. Due to the high number of required parameters for the electromechanical and electrical model, we refer at this point at the datasheets of the components, listed in **Table 3**.

Table 2: Hydromechanical Model Parameters

Ram parameters	Value [unit]
Cylinder area A_{ur}	510 [cm²]
Cylinder stroke s_{ur}	320 [mm]
Ram mass m_{ur}	3500 [kg]
Cushion parameters	
Cylinder area A_{dc}	510 [cm²]
Cylinder stroke s_{dc}	160 [mm]
Die mass m_{dc}	3500 [kg]
Fluid parameters	
Viscosity	46 [cSt]
Bulk Modulus	$1 \cdot 10^4$ [bar]

Table 3: Datasheet parameters

Component	Product number	Data from:
Pump unit	S-EHA 250xHOW	[12]
Drive	MSD G397 450 xx	[13]
Supply	MSD G396 026 xx	[13]
Capacitors	VFHR2G153YF230	[14]

3. ENERGY MANAGEMENT TOPOLOGIES

The most cost-effective and simplest topology consists of a non-active front end (NFE) that powers the DC-AC drives and dissipates excessive occurring regenerative power over a bleed resistor. From an environmental standpoint, this is obviously not a satisfying solution. On the economic side, depending on the amount of energy that is transferred to heat, a more energy efficient solution might amortize in a decent time range (less than 2 years) and is worthwhile to consider. The press systems presented in [5]and [6]use an AFE and DC-bus coupling so that power is exchanged between the axes and in case of too much regen-power it is fed back on to the grid. However, the total maximum power that is required in the machine cycle needs to be covered by the infeed since no energy storage is present. Note that in some cases, it is not desired that any power is fed back to the factory grid. Consequently, it is mandatory to store energy or to dissipate it.

3.1. Simulation scenarios

In this paper, we compare five different energy management topologies in scenarios A to E, summarized in **Table 4.** In scenario A, B, and C the nominal power of the infeed is reduced significantly. Due to the presence of a passive energy storage device they correspond to sophistication level (SL) 3, as defined in **1.1**. The topology in scenario D is able to feed back power to the grid but does not use storage, thus it belongs to SL 2. The system in scenario E needs to provide the maximum power needed by the axes directly from the grid and is not able to store or feed back power. Consequently it falls under SL 1.

All scenarios are simulated and sized in such a way as to cover the needed performance, whilst remaining cost effective and compact as possible. During the sizing and simulation process, we took care that none of the components' limitations were violated and that there was a reasonable margin for uncertainties. The motor's winding turns, which define the motors torque constant and thus also the drive size, are kept as high as possible by design. By doing so, the drives remain compact but the technique of field weakening is needed in order to still achieve high rotary speed.

Table 4: Energy management scenarios

Type	Infeed type	Extra capacity [F]	Current limit [Adc]	Bus Voltage [Vdc]
A	ACDCDC 35 kVA	0.24	50	650
B	ACDCDC 35 kVA	0.27	50	540
C	AFE 35 kVA	0.24	50	700
D	AFE 250 kVA	0	320	700
E	NFE 250 kVA	0	400	540

Scenario A

The infeed of scenario A, shown in **Figure 4**, rectifies the supply voltage to a DC bus voltage

of $U_{dc} = 1.35 \cdot U_{sup}$. Since the supply voltage was boosted by the step up transformer from 400 Vac to 480 Vac, the resulting DC bus voltage is
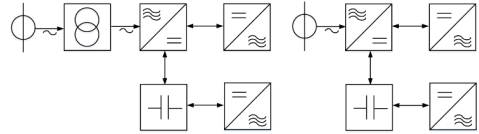
Figure 4: Topology of scenario A (left) and B (right)

650 Vdc. This topology keeps all energy in the capacitors and is not able to feed power back to the grid.

Scenario B

The topology is the same as in scenario A, with the difference that the supply voltage is not transformed but directly fed in with a level of 400 Vac. The resulting DC bus voltage is thus 540 Vdc.

Scenario C

The AFE is supplied by 400 Vac. Due to the internal boost functionality the DC bus voltage can be elevated to 700 Vdc. The infeed is able to feed back power to the grid; however, the idea in this scenario is to keep all energy in the
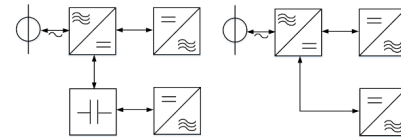
Figure 5: Topology of scenario C (left) and D (right)

capacitors. Hence, the regen current limit is set to zero. The lower limit where the AFE works in a controlled way is the rectifying voltage of 540 Vdc. The topology can be seen in **Figure 5**.
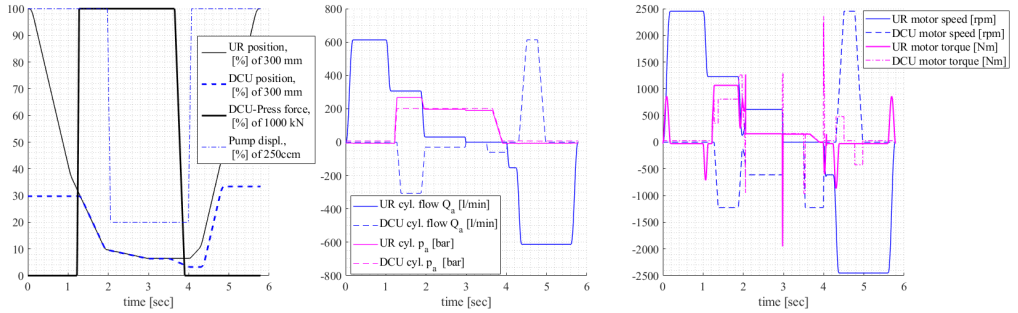
Figure 6: Upper Ram (UR) and die cushion (DCU) movement, press force and pump displacement (left). Flow and pressure at both cylinders (middle). Motors resulting speed and torque profiles (right)

Scenario D

The AFE covers the maximum needed power of all axes. In case that one or both axes run in regenerative mode, the power is fed back to the factory grid. The nominal DC- bus voltage is 700 Vdc.

Scenario E

The non-active infeed rectifies the 400 Vac supply voltage to 540 Vdc. The complete power demand needs to be covered by the power supply. In case of regenerative power inflow to the DC bus and a rise of the voltage to more than 850 Vdc, the brake chopper starts shorting the brake resistor. Consequently, part of the regen-power dissipates as heat until the voltage drops back down.
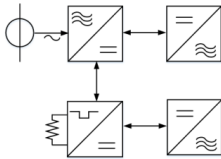
Figure 7: Topology of scenario E

3.2. Sizing and simulation methodology

During the sizing process, a special focus needs to be laid on the motor's torque and speed characteristic under a fluctuating bus voltage. If the voltage drops too much, the required torque at a certain speed might not be feasible, or it results in a high field weakening current which induces additional losses in the motor and drive. The graph in **Figure 8** shows the duty cycle of the upper ram axis in a voltage-torque-speed phase diagram. The maps show the maximum achievable torque with and without field

weakening under a varying bus voltage. The diagram shows that the required torque is not limited at any time by the motors maximum torque. However, there are phases of high speed where field weakening is necessary. The used sizing and simulation methodology respects those dynamic limits at all times and also takes the field weakening current into consideration in the overall loss balance.
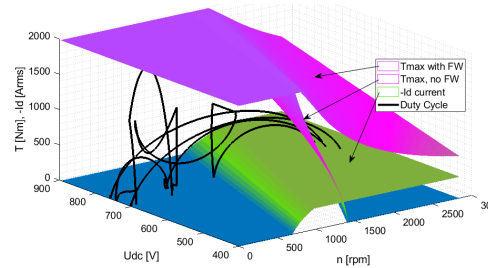
Figure 8: Duty cycle and maximum torque envelopes with and without field weakening (FW)

4. SIMULATION AND RESULTS

The reference duty cycle is shown in **Figure 6** (left). After the ram starts moving down, the die cushion contacts with it and two different drawing velocities are realized. In order to reduce the motors' torque, the pump displacement is decreased to 20% during the low speed pressing phase. The resulting flow and pressure at the cylinders A-site are shown in the graph in the middle. The difference in pressure of the two axes is provoked by the forming force which works, together with die cushion force, against the upper die. Looking at the motors
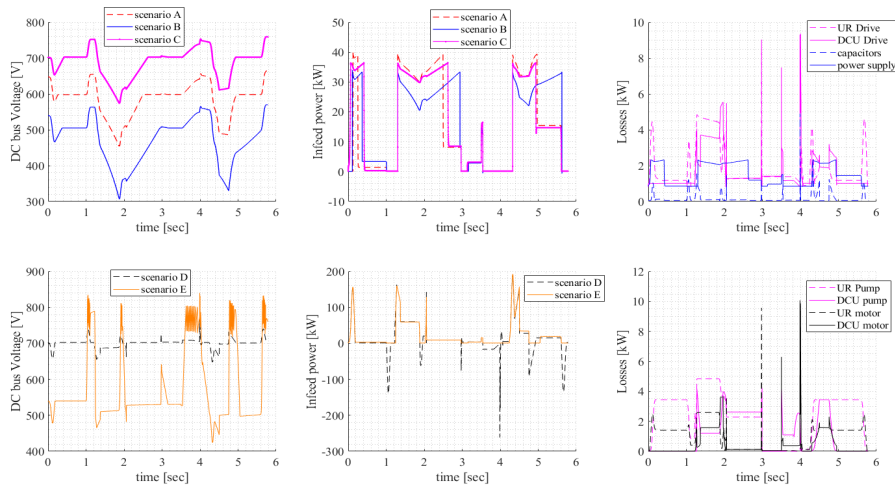
Figure 9: DC-bus voltages for all scenarios (upper left, lower left), Infeed power of all scenarios (upper middle, lower middle), Loss for all components exemplary from scenario C (upper right, lower right).

torque (right graph) we can see that during the acceleration and decceleartion phases relatively high torque peaks occur in order to speed up the motors and pump inertia.The resulting power peaks in these phases are shown in **Figure 10.**

During the pressing process, the DCU axes runs regenerative and part of the energy that the UR axes requires for pressing and moving down, is recuperated. The effective power demand of the axes and the losses in the pumps are always the same in all scenarios. The losses of the motors, as well as all components connected to the DC bus, are voltage dependent and consequently

vary in each scenario. Looking at the DC bus voltage for the different scenarios in **Figure 9** we can see that most of the energy is needed during the pressing phase and during the backwards movement of both axes, thus the voltage level decays the most during these stages. For the scenarios with lower DC reference voltage this decay is much more drastic, since with limited current inflow, the incoming power diminishes due to the voltage drop. In scenario E, the voltage rises five times over 800 Vdc and is dissipated by the resistor of the brake chopper. This happens in all four
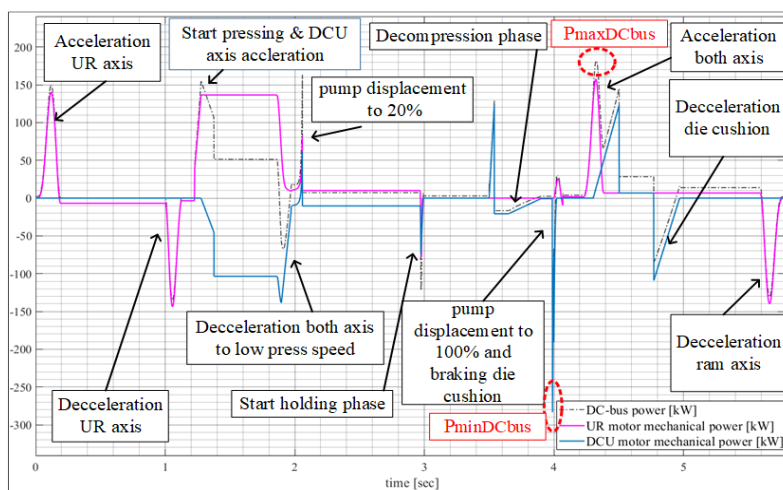
Figure 10: Power flow, process phases of the duty cycle

deceleration phases of both axes (combined), as well as during the fluid decompression phase. Here, the compression energy is transformed to electrical energy trough a power flow over pump, motor and drive into the DC bus.

4.1. Peak shaving

Looking at the DC bus power flow over time, shown in **Figure 10**, we observe that the peak power demand in that specific forming cycle is 183 kW in the acceleration phase of the upward movement of the upper ram (t=4.3 sec). There are other power peaks of around |100| to |150| kW mostly during acceleration and deceleration of one or both axes. The average power of the cycle, however, is only around 13 kW. This high ratio of maximum required power to average power already indicates that using a peak shaving approach is likely to lead to beneficial results. Indeed, the topologies from scenario A, B and C reduce the power infeed to:

$$\frac{P_{maxIn}}{P_{maxDCbus}} = \frac{35\,kW}{183\,kW} = 19\,\% \qquad (13)$$

from the maximum occurring value $P_{maxDCbus}$. Looking at the same ratio for the regenerative power, in the case of scenario D, the savings are even more drastic with:

$$\frac{P_{maxIn}}{|P_{minDCbus}|} = \frac{35k\,W}{276\,kW} = 13\,\% \qquad (14)$$

4.2. Energy consumption and losses

Figure 9 (upper right, lower right graph) shows the occurring losses of the different components for
scenario C over time. For a better overview, we calculated the average losses over the cycle as

$$P_{lavg} = \frac{1}{T}\int_0^T P_l(t)dt \qquad (15)$$

for each component in each scenario and list the values in **Table 5**. Roughly, in scenario A to E, the share of losses is about one third for the pumps, one third for the drives, and the last third for the motors, infeed and capacitors. Unsurprisingly, the topology in scenario E with a brake resistor and no storage or feedback possibility has the highest energy intake. The most efficient topology is scenario C, followed by scenario A, then D, B, and E.

Table 5: Average loss in [kW] for scenario A-E

Scenario	A	B	C	D	E
Pumps	3.4	3.4	3.4	3.4	3.4
Motors	1.67	2.33	1.45	1.44	1.82
Drives	3.84	4.22	3.52	3.48	4.03
Capacitors	0.21	0.26	0.17	0	0
Infeed	0.43	0.56	0.86	1.42	1.69
Chopper	0	0	0	0	5.28
Total	**9.59**	**10.81**	**9.45**	**10.1**	**17.3**

Working with a higher DC bus voltage clearly leads to less drive and motor losses, just like the comparison of the 480 Vac supply in scenario A and 400 Vac in scenario B indicates. Since energy management topologies similar to scenario D were recently used for EAS-based machinery, we set the energy consumption of this scenario to 100% in **Table 6.** We split the comparison in two categories, with and without pump, each scenario's losses compared relatively to the ones from scenario D. For end users certainly the first value is of interest: how much energy is consumed less by the machine as a whole. When comparing energy management topologies on a broader basis, the second value might be the more meaningful one. The differences in energy consumption of scenarios A to D are all in all rather small. Due to potential model and parameter uncertainties a sharp judgment lower than a 10% level might not be justifiable. Nevertheless, the topology from scenario A and C are certainly in the same range in terms of energy consumption as the one in scenario C, or slightly better. The solution with a lower operating voltage in scenario B is equal or slightly less efficient.

Table 6:   Relative total loss, normalized to scenario D

Scenario	A	B	C	D	E
Loss [%] with pump:	95	107	93	**100**	171
Loss [%], no pump:	92	111	90	**100**	208

4.3. Cost estimation

A complete cost of ownership analysis requires a lot of details e.g. the exact cabinet design and lifetime and maintenance considerations of all components. This goes well beyond the scope of this first investigation. However, we provide a rough indication how the energy management topologies compete in terms of cost, since this is

a crucial point in a technology's potential market acceptance.

In **Table 7** we show the qualitative costs for all EMTs, with the EMT for scenario D set to 100%. The topology in scenario E is clearly the most inexpensive solution with 50% to 60% compared to the active front end solution. All peak power limiting topologies from scenario A, B and C are cost competitive, they even seem to be slightly cheaper compared to scenario D. The energy storage in these EMTs roughly take one third of the total cost, but the infeed share becomes rather small with around 10 %. In scenario D around 60 % of the costs are the large active front end supply and the LCL Filter.

Table 7: Qualitative cost comparison EMTs

Scenario ▶ Component ▼	A	B	C	D	E
Infeed	10	10	12	40	11
Filter & Choke	8	8	6	23	5
Capacitors	27	31	27		
Chopper					11
Pre-charger			4		
Cabinet	38	38	38	32	32
Transformer	14				
Total	96	86	88	**100**	59

5. CONCLUSION AND OUTLOOK

In this paper, we modeled an electro hydrostatic drivetrain based forming press, powered by five different energy management topologies. The results indicate that a topology consisting of a supplying infeed and a well-sized amount of passive capacitors coupled into the DC-bus is a very suitable option. The installed power is significantly reduced to **less than one fifth of the peak power**. The differences between the scenarios A to C regarding the efficiency compared to scenario D are rather small. However, we certainly can state that the solutions from the scenario A, B and C are in the same range of efficiency than scenario D. Through further verification of the models, especially the capacitor loss model, we want to refine the energy consumption analysis.

Looking at the costs, we made a rough estimation of all main components of each of the five energy management topologies. We found that the systems in scenarios A to C are at least equal, possibly even around 10 % more cost effective than scenario D. All energy management topologies are competitive to scenario E — the most cost effective solution — since the amortization periods to recover the large difference in losses are rather short. In this work we focused on a small machine and showed how much the peak power can be reduced at stable or even declining costs, without any trade off in power consumption. Looking at larger forming presses of several thousand tons and Megawatts of peak power, the detailed simulation and analysis of a satisfying and cost effective EMT becomes more important. The authors from [9] reduced the installed peak power on servo presses with the help of capacitors, above a certain press tonnage with an additional kinetic storage. Likewise, in [16], the author states that the use of kinetic storage becomes beneficial for servo presses larger than 600to. The author also claims, without further specifics, that the same peak shaving approach is valid for hydraulic presses. Where the "break evens" of different storage technologies are for EAS-based press systems — if they exist at all — is something that still needs to be investigated. In any case, the use of active storage, like DC-controlled capacitor units or the aforementioned servo flywheels add complexity and demand the presence of an advanced control strategy.

The approaches presented in this paper cover the energy management sophistication levels from one to three, as defined in section **1.1**, and focus on a passive electrical storage**.** We showed that those solutions are competitive in terms of efficiency and costs. The integration of active storages into the topology leads to more degrees of freedom and possibilities of optimization. Inevitably, this will lead into a non-linear optimization problem with several degrees of freedom and competitive cost functions, e.g. efficiency versus maximum infeed current. Once this is well understood we further plan to penetrate energy sophistication level five where an online learning approach will identify sub-optimality regarding the actual cost function(s) and adapt the control outputs in a way to further optimize the total performance over the cycle. Looking towards the (not that far off) future with machines having internet of things (IOT) interfaces, a smart energy management system can certainly play an interesting and important part. Machines might (a)synchronize their production cycle to others trough self-

organization in the same factory or even in the same grid. Power could be drawn in and stored whenever low-priced, peak power could be fed back when advantageous for the common grid.

NOMENCLATURE

U_{dc}	DC bus voltage	[V]
U_{sup}	AC-Supply voltage, 3x phase	[Vrms]
I_{sup}	Supply current, rectified to DC	[Idc]
T_{fr}	Friction torque pump	[Nm]
Δp	Pressure difference	[bar]
n	Motor and pump velocity	[rpm]
α	Pump displacement factor	[ ]
υ	Fluid viscosity	[cSt]
Q_l	Pump leakage flow	[l/min]
P_{lp}	Pump losses	[kW]
P_{cu}	Motor copper losses	[kW]
I_m	Total motor current	[Arms]
R_s	Motor phase resistance	[Ω]
I_q	Torque building current	[Arms]
I_d	Flux weakening current	[Arms]
P_{fe}	Iron losses, motor	[kW]
f_1	Loss factor	[kW/rpm]
f_2	Loss factor	[kW/rpm²]
P_{lmot}	Motor total loss	[kW]
P_{ldrv}	Drive total loss	[kW]
P_{ldrv0}	Drive total loss at zero current	[kW]
f_3	Loss factor	[V/√V]
I_{dc}	Actual DC bus current	[A]
U_{nom}	Nominal DC voltage	[Udc]
P_{ldrvn}	Drive nominal loss	[kW]
P_{lafe0}	Idle state losses AFE	[kW]
P_{nafe}	Nominal losses AFE	[kW]
P_{lLCL}	Loss LCL Filter	[kW]
P_{idle}	Drive loss at zero current	[kW]
I_{grid}	Grid current 3x phase	[Arms]
I_{nom}	Nominal grid current 3x phase	[Arms]
P_{lacdc}	Loss AC\DC\DC	[kW]
P_{lacdc0}	Loss AC\DC\DC at zero current	[kW]
P_{nacdc}	Nominal losses AC\DC\DC	[kW]
I_{ninf}	Nominal current infeed	[kW]
I_{nch}	Nominal current choke	[kW]
P_{nch}	Nominal losses choke	[kW]
$ESR(\omega)$	Equivalent series resistance	[Ω]
$tan\delta$	Capacitor dissipation factor	[ ]
ω	Current ripple frequency	[rad/s]
C	Electrical capacitance	[F]
P_{lcp}	Capacitor loss	[kW]
I_{leak}	Capacitor leakage current	[A]
A_{ur}	Area cylinder, upper ram	[cm²]
s_{ur}	Cylinder stroke, upper ram	[mm]
m_{ur}	Die mass, upper ram	[kg]
A_{dc}	Area cylinder, die cushion	[cm²]
s_{dc}	Cylinder stroke, die cushion	[mm]
m_{dc}	Die mass, die cushion	[kg]
P_{maxIn}	Maximum incoming power	[kW]
$P_{maxDCbus}$	Maximum DC bus power	[kW]
$P_{minDCbus}$	Minimum DC bus power	[kW]
P_{lavg}	Average losses	[kW]
P_l	Generic losses	[kW]

REFERENCES

[1] Rüger H (2012) Energieeffiziente Hydraulikpressen durch Servodirektantrieb. In: 19. Sächsische Fachtagung Umformtechnik SFU Chemnitz, 13.-14. November 2012. Proceedings/Tagungsband 66, Verlag Wissenschaftliche Skripten, Chemnitz, S.365-378

[2] Lohse H, Weber J, Neumann S, Händle W, Klug D (2015) Investigation and improvement of the energy efficiency of hydraulic deep drawing presses. Presented at the 14th Scandinavian international conference on fluid power, Tampere, Finland, 20-22 Mai 2015

[3] Schenke C, Weber J (2018) Steigerung der Energieeffiziens, Verdrängersteuerung senkt den Energiebedarf hydraulischer Tiefziehpressen. O&P Fluidtechnik 9/2018:54-59

[4] Willkomm J (2016) Modellprädiktive Optimierung drehzahlvariabler Verstellpumpen. Dissertation, Technische Universität Dresden

[5] Händle W, Kirch K (2017) Case Study – Electro hydrostatic actuation system. Industrial – Moog, Inc. https://www.moog.com/content/dam/moog/literature/ICD/Moog_The_Best_of_Both_Worlds.pdf Accessed 01 Oct 2019

[6] Siemer E, Kluge A. (2016) Ecoplant Design – Moderne Antriebskonzepte für Schmiedepressen. O&P Fluidtechnik 11-12/2016:72-75

[7] Putz M, Blau P et al (2016) Energy storage in drive systems of servo presses for reduction of peak power and energy recovery. Paper presented at the Institute of Electrical and Electronics Engineers –IEEE- EPE, ECCE Europe, 18th European Conference on Power Electronics and Applications, Fraunhofer Institute for machine tools and forming technology, Karlsruhe, 5-9 September 2016

[8] Henning V, Garretson I et al (2018) Peak Power Load and Energy Costs Using the Example of the Startup and Idling of a Grinding Machine. Paper presented at the

25th CIRP Life Cycle Engineering (LCE) Conference, Copenhagen, 30th April -2nd May 2018

[9] Kaiser S, Kaever M, Budig P.-K, Ecorchard G et al (2011) Effizienz im Energiemanagement mit elektrischer Energiespeicherung in der Umformtechnik (E4U). In: Schlussbericht Verbundsprojekt http://publica.fraunhofer.de/documents/N-203362.html 25 March 2019

[10] Ristic S, Wahler M (2018) Electrification of Hydraulics opens new ways for intelligent energy-optimized systems. In: 11th IFK Proceedings 2018 Vol 2

[11] Arnivouior L, Laurila, L (2007) Loss calculation of a frequency converter with a fixed-step circuit simulator. In: Proceedings of the European Power Electronics and Applications Conference 2007

[12] Moog Inc. (2018) Electrohydrostatic Pump Unit, Revision G, October 2018 https://www.moog.com/content/dam/moog/literature/ICD/Moog_Actuator_EPU_Catalog_en.pdf Accessed 07 Mar 2019

[13] Moog Inc. (2017) Modular Multi-axis Servo Drive System MSD, Revision J, November 2017 https://www.moog.com/content/dam/moog/literature/ICD/Moog-ServoDrives-MSDSeries-Catalog-en.pdf Accessed 07 Mar 2019

[14] Hitachi Chemical Company Ltd. (2016) Screw terminal type aluminum electrolytic capacitors VFHR Series 161201 http://www.hitachi-chem.co.jp/english/products/sds/files/e_vfhr_161201.pdf Accessed 07 Mar 2019

[15] Krishnan R (2010) Permanent magnet synchronous and brushless DC motor drives, Electrical and Computer Engineering Department Virginia Tech Blacksburg, Virginia, U.S.A.

[16] Dietz B, Reichl G (2018): Der Last die Spitze nehmen, Umformtechnik https://www.umformtechnik.net/fachartikel/der-last-die-spitze-nehmen-%7C-umformtechnik_34886_de/ Accessed 12 Nov 2019

GROUP 5
Components

STATE OF THE ART DIGITAL ON-BOARD-ELECTRONICS VS. POTENTIALLY DISRUPTIVE CONTROL ARCHITECTURES FOR HYDRAULIC VALVES

Achim Richartz

Bosch Rexroth AG, Partensteiner Strasse 23, 01069 Dresden
Tel.: +49 9352 183314; E-mail address: achim.richartz@boschrexroth.de

ABSTRACT

Currently discussed trends and new technologies regarding cloud or edge computing imply that even most recent designs and functionalities of digital on-board-control electronics may be outdated and eventually will totally disappear. Additionally, those new technologies attract potential users by promises like new use cases e.g. predictive maintenance or a simplified architecture and reduced installation efforts. On the other hand, automation levels and subsequent requirements are often mixed up or discussed too generally. Nevertheless, what is the rue situation today and in the upcoming years? This paper elaborates the potentials of both approaches – state of the art on-board-control electronics and potentially disruptive control architectures for hydraulic valves in order to take the right decision and reflect the pros and cons for each topology by:

Architecture of automation: In Terms of strongly hierarchical or multidimensional connected systems.

Requirement of installation: By reflecting the dedicated ecosystems, on levels like plant, machine, subsystems.

Maturity of technology: Looking on the user's perspective.

Safety and security: From legal and conformity aspects.

Performance needs by specific task: In comparing standard to demanding real life applications.

Keywords: digital on-board-electronics, hydraulic valves, control architectures

1. INTRODUCTION

The Bosch Rexroth AG is for sure known as one of the leading manufacturers of hydraulic control components such as proportional valves or electrohydraulic controlled pump systems. While todays widely used analogue electronics still perform well in many applications, they are limited functionality and connectivity. While analogue electronics by technology have "built in real time performance", first digital controllers sometimes suffered from performance lags. Today's state of the art generations crossed that bridge. Cycle times below 0.1ms are the required standard and met. Performing as required, mostly Ethernet-Based solutions are implemented since years in industrial and mobile applications. With upcoming technical possibilities of connectivity solutions, the question is: Will edge or cloud based systems replace those existing solutions?

Figure 1: Bosch Rexroth servo solenoid directional control valve with IFB technology (IFB= integrated field bus) with Multi Ethernet communication.

2. ARCHITECTURE OF AUTOMATION

Side a side the architectural differences between todays majority of industrial automation architectures are obvious. Key difference is an additional IT infrastructure to manage data exchange to e.g. a cloud.
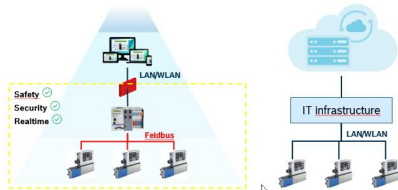
Figure 2:   Architecture comparison; hierarchical vs. cloud connected

While Fieldbus based architectures show solved solutions for safety, security and real time already today, a fully installed LAN or WLAN installation mostly lags those requirements.

3. REQUIREMENTS OF INSTALLATION

As can be seen clearly from figure 2, a very much different installation is required. As Ethernet based field busses are today's standard solutions, new other than today's IT-Infrastructure's need to be installed and maintained. This also leads to other competences for setup respectively commissioning and maintenance. While bigger companies with own IT departments may have these resources, small and mid size companies may have to install that or buy for that from external.

4. MATURITY OF TECHNOLOGY

Wireless and well-proven installations of full compliance can be found today in fun industry applications. Requirements there are demanding, even safety of humans for different SIL levels are in place, but for real time, this is not the case today.
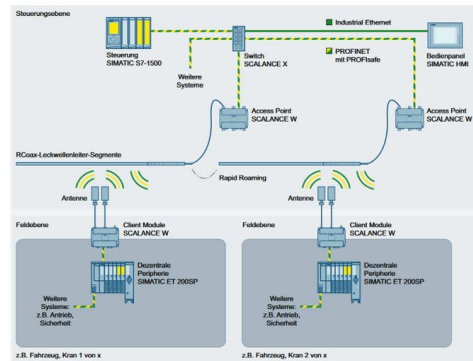
Figure 4:   Bosch Rexroth servo solenoid directional control valve with IFB technology (IFB= integrated field bus) with Multi Ethernet communication.

5. SAFETY AND SECURITY

With reference to IEC/TS 62443-1-1, the term "security" is considered here to mean the prevention of illegal or unwanted penetration, intentional or unintentional interference with the proper and intended operation, or inappropriate access to confidential information in IACS (Industrial Automation and Control Systems). Safety requirements are covered e.g. generically with IEC 61508, DIN EN ISO 13849-1 or product respectively application related to DIN EN ISO 16092 (Pressen), EN 62061.

While on shop flow level and non real time applications, those solutions already exist (Figure 3), for more demanding requirements, at least in industrial automation, these solutions are not wide spread.
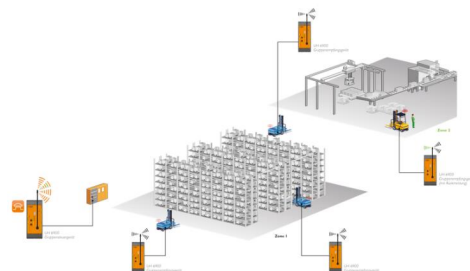
Figure 5:   Dold Safemaster W illustration / FTS application example

6. PERFORMANCE NEEDS BY SPECIFIC TASK

Solutions or applications e.g. monitoring of oil cleanliness, power consumption, or data management and trend analysis, could based solutions are already implemented. Following minimum requirements, even under best conditions only lead to ten times less performing installations.
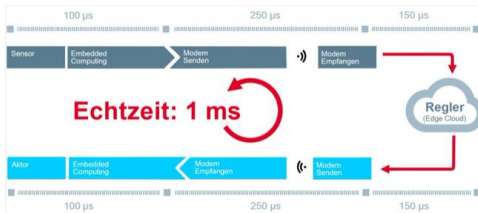
Figure 6: Best case cycle time for 5G based cloud control. [1]

7. CONCLUSION AND OUTLOOK

For the time being, cloud based installation and even edge computing will not fulfil the demanding requirements of real time hydraulic control circuits like dynamic hydraulic valves or electrohydraulic pump controls with pressure and flow control. They are for sure an upcoming solution especially for condition-monitoring ore even cloud based services on data interpretation.

REFERENCES

[1] https://www.oup-fluidtechnik.de/der-einfluss-von-5g-auf-elektrohydraulische-regelungen/

OPTIMIZATION OF DIRECTIONAL CONTROL VALVES THROUGH DOWNSTREAM COMPENSATION APPROACH

Davide Mesturini[1*], Cesare Dolcin[1], Ulderico Busani[1], Pietro Marani[2], Antonella Bonavolontà[3], Emma Frosina[3]

[1]*Walvoil SpA, via Adige 13/D, 42124 Reggio Emilia, Italy*
[2]*C.N.R.-IMAMOTER, Via Canalbianco 28, 44124 Cassana (FE), Italy*
[3]*UniNA FPRG, Università degli Studi di Napoli "Federico II", via Claudio 21, 80125 Napoli*
*E-mail address: mesturini.d@walvoil.com

ABSTRACT

Various academic studies show that in the use of common ICE Off-road Vehicles only about 10-15% of the available power at fuel level is actually transformed into useful energy for the actuators. Particularly the Directional Control Valves are responsible for the dissipation of about 35-40% of the hydraulic energy available at the pump level.

The machine electrification trend makes it even more urgent to optimize the hydraulic system to ensure greater performance and higher battery autonomy.

Traditional Directional Control Valves design solutions neglect important opportunities for reducing losses and improve internal regeneration. Especially, energy recovery is rarely applied and in any case by means of important superstructures which considerably increase the costs of the system. This paper presents an innovative Directional Control Valve layout, based on the Downstream Compensation approach that, in a simple and cost-effective design, allows to recover a considerable amount of energy from both the inertial loads and the simultaneous use of multiple actuators at different pressure level.

The proposed layout performance and efficiency are studied through lumped element simulation and laboratory experimental tests.

Keywords: Directional control valve; Energy recovery; Accumulator; Efficiency; Downstream Compensation.

1. PREMISES

Energy optimization and consumption reduction are the trends that have been driving the evolution of the off-highway sector over the last few years. On the one hand, the regulations set increasingly stringent limits for ICE pollutant emissions. On the other hand, the growing market attention and the increasingly widespread limitations on the use of diesel engines in urban and protected areas are driving the electrification success, as its cost of ownership is getting more and more convenient.

Much effort has been taken into the electrification of machines driveline, but still few solutions have been successfully implemented for the optimization of the hydraulic circuit; many electrified or hybrid vehicles simply change the primary energy source from ICE to electric motor without reconsidering the large possibilities to improve the hydraulic system.

New needs and more demanding machines performance probably require today a new generation of optimized and focused hydraulic components.

In fact, as many studies demonstrate, the traditional hydraulic circuits are responsible for dissipating a huge percentage of the available energy. The advantage of a simple hydraulic system is always connected to the disadvantage of large energy losses [1]. Different Hybrid solutions [2][3] and new operating strategies [4][5] have been realized through the years. However, from these studies emerged that for construction machinery, only a 10-15% of the available energy is converted into useful work. According to Lodewyks et al. [1] the directional control valve is one of the main responsible for

this energy waste: the distribution of a single pump flow to multiple users and the control of the speed of overrunning loads are the principal causes. This aspect also emerged in [6], in which the valve group contributes to 35-40% of the energy dissipation in the hydraulic circuit. Additional energy is lost in the pump efficiency, in the hoses and in the cylinders friction.

Academic literature has proposed as a solution to this problem the "valveless" circuits, removing the directional control valve and providing a dedicated hydraulic energy source for each actuator [1][4][7]. The solution, although brilliant from the theoretical point of view, has to deal with high costs and system complexity and, on balance, it appears to have a difficult implementation.

The directional control valve therefore turns out to be the component with greater opportunity to recover a part of this energy loss.

According to [8], through a comparison of different recovery systems for hydraulic mobile machines emerged in the last years, the greatest opportunity for energy saving lies in the recovery from available energy sources, particularly from inertial loads control [9][10] and from compensation in simultaneous movements.

2. SYSTEM ARCHITECTURE

Figure 1 shows the hydraulic schematic of the new proposed solution.

The new concept derives from a typical Load Sensing directional control valve layout. The main spool selects along its stroke the LS signal from user's ports. The highest LS signal is then delivered to a conventional variable Load Sensing pump, which supplies flow at delivery pressure p equal to LS plus a fixed margin Δp_{IN}. The meter in notches area A_{IN} in the main spool define the flow Q_{IN} delivered to the user.

$$Q_{IN} \propto A_{IN} \cdot \sqrt{\Delta p_{IN}} \qquad (1)$$

2.1. Downstream compensator

According to the suggested design, the local compensator spool of every working section is located downstream of the main spool meter out notches A_{OUT}.

Analogous compensator configurations have been presented in recent studies [11], but with different pump control logic and energy recovery strategy.

The downstream position of the compensator allows to control the return flow Q_{OUT}: the compensator guarantees a fixed pressure drop Δp_{OUT} across the main spool discharge notches
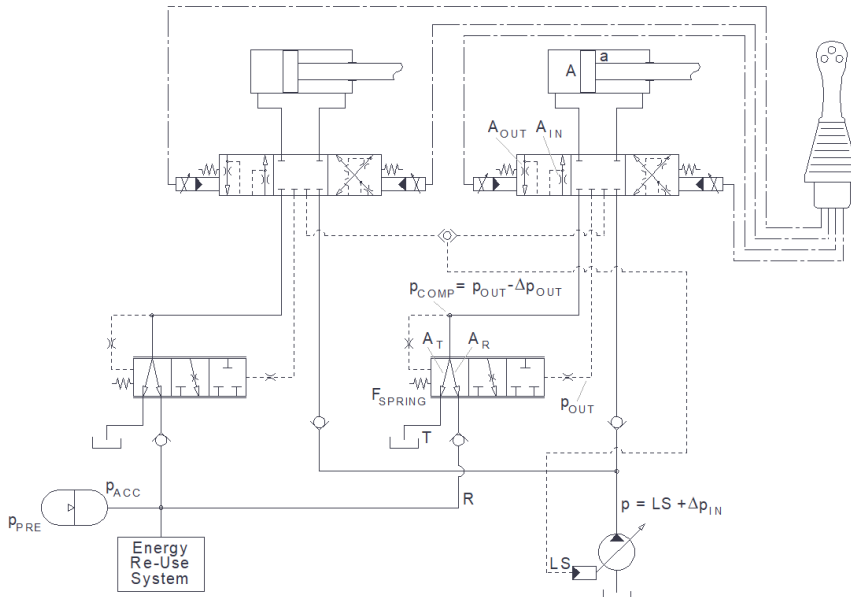
Figure 1: Complete hydraulic schematic

A_{OUT}. Thanks to a couple of pilot pressure signals, acting on identical areas A_{PIL} and taken before (p_{OUT}) and after (p_{COMP}) the main spool, the pressure drop is controlled according to the spring force F_{SPRING}:

$$p_{COMP} \cdot A_{PIL} + F_{SPRING} = p_{OUT} \cdot A_{PIL} \qquad (2)$$

$$Q_{OUT} \propto A_{OUT} \cdot \sqrt{p_{OUT} - p_{COMP}} \qquad (3)$$

The particular embodiment of the compensator is characterized by the presence of three ways, which allow the main spool discharge line to be connected respectively to the system tank T or to an energy recovery line R (typically feeding a hydraulic accumulator).

The compensator spool rest position has both ways (A_R and A_T) open. Along its stroke (x_{COMP}), it first closes the notch A_T and then the notch A_R, so as to achieve a throttling function which preferably conveys the meter out flow towards the energy recovery line R.
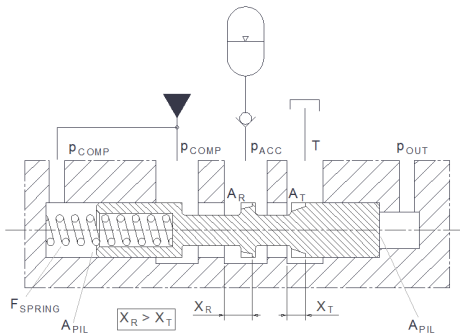
Figure 2:   Downstream compensator concept

It is interesting to notice that the compensator does not need additional devices or pressure signals to provide for the correct regulation of the meter out flow: in case the R line cannot accept further flow due to the high accumulator pressure level (p_{ACC}), the discharge flow will be redirected to the system tank, without compromising the actuator speed.

It is also worth to highlight that the whole system is achieving its functionality with a completely mechanical design, without the support of any electronic control. The valve section design is quite simple, consisting in a main spool and in a compensator spool as the most of typical Load Sensing valves. It follows that the additional costs of the system reside in the Re-Use System, which is not in the purpose of this paper, but is briefly discussed in paragraph 6.

2.2. System tuning

The system as described above is based on the serial connection of two flow control systems, working respectively on meter in Q_{IN} and meter out Q_{OUT} flows: the first characterized by the pump margin and the second characterized by the downstream compensator margin.

In some respect it can be assimilated to an Independent Metering system, where the delivered flow and the discharged flow have to be correctly managed and matched, in order to allow the correct behavior and avoid unexpected pressure increase [12].

In this case, a simple and cost-effective solution is given by providing a precise tuning of meter areas A_{IN} and A_{OUT} and of pressure drops Δp_{IN} and Δp_{OUT}.

Feeding, for instance, the bottom side of a cylinder actuator with A/a areas ratio, the following equation must always be respected for any position x_{SPOOL} of the main spool:

$$A_{IN} \cdot \sqrt{\Delta p_{IN}} \cdot {a}/{A} \leq A_{OUT} \cdot \sqrt{\Delta p_{OUT}} \qquad (4)$$

Whenever a section is actuating a positive opposing load, the pump margin control (meter in) prevails.

Whenever a section is actuating a negative overrunning load, the downstream compensator margin control (meter out) prevails.

In case of simultaneous operations, the compensator of the lower pressure section will throttle the meter out line, in order to set the correct flow.

The described system tuning inevitably involves a slight difference in the regulated flow, according to different working conditions. However, simulations and experimental tests have shown that this difference can be contained in values that are more than acceptable for the normal needs of operating machines.

The three ways compensator design allows to recover energy from both overrunning loads control and compensation of simultaneous operations at different working pressures.

Looking at typical p-Q hydraulic power diagrams for a load lifting/lowering operation

and for a two actuators simultaneous operation, it is possible to identify the potential recovery.
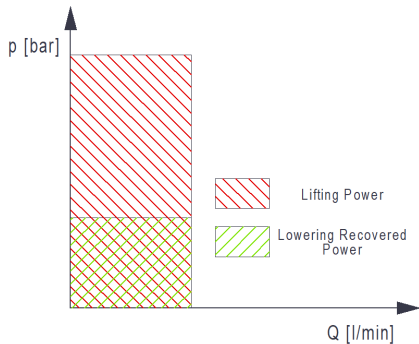
Figure 3:   Recovery from overrunning loads
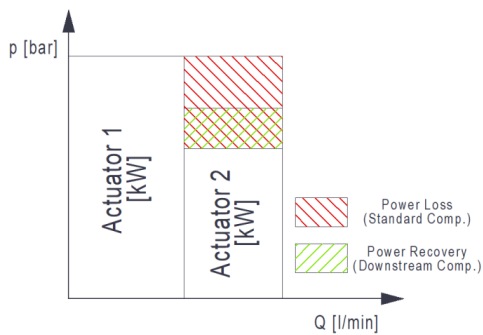
Figure 4:   Recovery from simultaneous operations

Recovery from negative loads and from simultaneous operations have been studied separately through simulation and laboratory tests to evaluate the respective contribution to energy saving.

3.   ENERGY RECOVERY FROM NEGATIVE LOADS (OVERRUNNING)

3.1.   Simulation Model

A simple circuit has been simulated by a lumped parameter model to study the downstream compensator behavior and its capability to recover energy from overrunning loads.

The effect of the external overrunning load is simulated through a pump, feeding the directional control valve and through a main relief valve to set the load pressure on meter out line.

The simulation consists in displacing the main spool, opening the A_{OUT} notches to a fixed value and verifying the accumulator filling effect (the filling is typically fast enough to be considered adiabatic) and the speed control consistency when the accumulator has reached its maximum capacity and the out flow is diverted to tank.
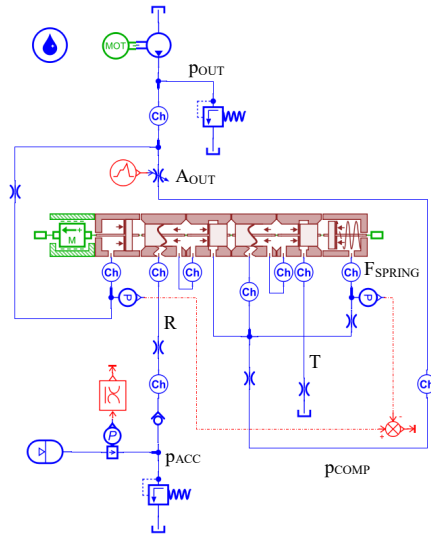
Figure 5:   Simulation model overrunning loads

3.2.   Experimental tests
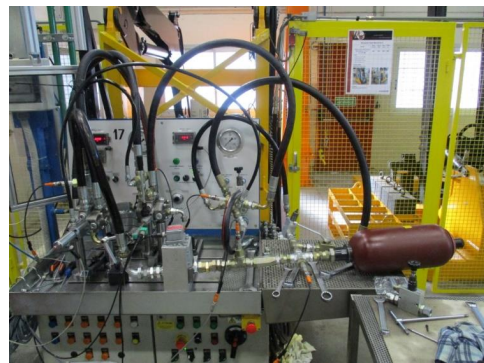
Figure 6:   Experimental test setup for overrunning loads

The simulated system has been recreated in laboratory through the use of existing components and through the manufacturing of a dedicated manifold for the compensator subsystem.

A 6 L accumulator with 35 bar precharge has been used during the test.

The test demonstrates the system capability to recover energy, without any effect on actuator speed.

The following diagrams show the result of experimental activity (continuous line) compared with simulation outputs (dotted line).
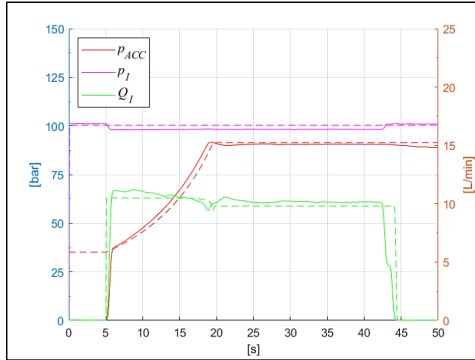
Figure 7: Controlled flow, load pressure and accumulator pressure

Figure 7 shows the pump pressure set at the constant value of 100 bar, the 10 L/min controlled flow and the increasing pressure of the accumulator. The transition from the recovery position to the tank position is smooth and does not affect the speed control and the movement continuity.
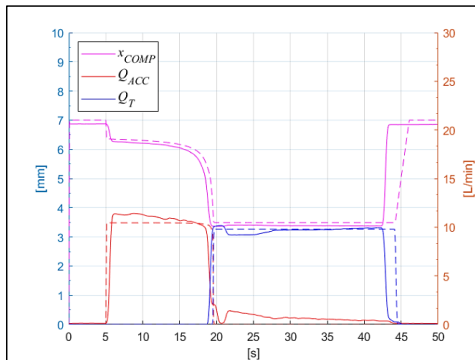
Figure 8: Compensator displacement, flow to R line, flow to T line

Figure 8 shows the compensator displacement and the consequent change of discharged flow from R line to T line. The test also confirms that the speed control depends on the main spool stroke and not on the load pressure level.

4. ENERGY RECOVERY FROM SIMULTANEOUS OPERATIONS (COMPENSATION)

4.1. Simulation Model

The complete system, given by the combination of two sections driving two actuators, has been simulated by a lumped parameter model.
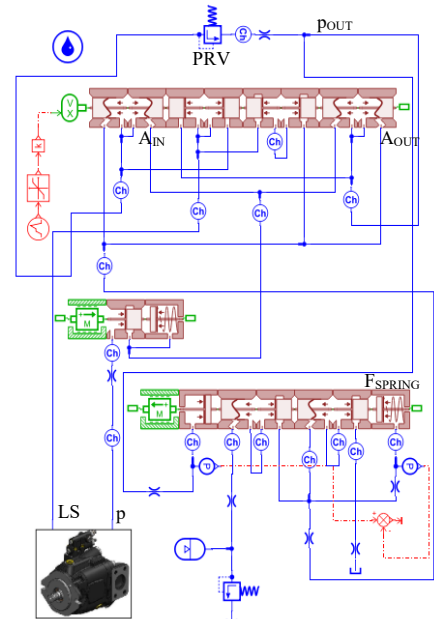
Figure 9: Single section model

The single section model shown in **Figure 9** is composed by the main spool and its check valve model, the compensator model and the pump model, which has been kept quite simple for simulation time convenience.

The single section model has been then duplicated in a larger model for the simultaneous operations analysis.

The load is applied by means of a pressure relief valve (PRV) simulating a motor type actuator.

Basic analysis and attempts have been run on this model to prove the correct behavior of the system and to optimize some of the components dimensioning and design.

4.2. Experimental tests

The two sections system has been eventually recreated on a test bench for experimental test. A preliminary testing work was necessary to match the real set up and the simulation model parameters and sizing.

After finding a complete correspondence of the basic functions, several concept-proving tests have been run.
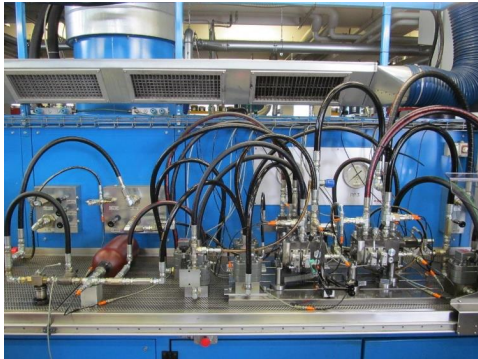
Figure 10: Experimental test setup for simultaneous operations

The system has been equipped with specific directional control valves and with a 6 L and 35 bar precharged accumulator to store the recovered flow. Moreover, different pressure and flow sensors have been inserted to thoroughly analyze the behavior of every single component. Unfortunately, the complexity of the piping has resulted in additional pressure drops that can be easily avoided in an optimized circuit. Furthermore, a structural limit of the components has limited the system maximum test pressure to 120 bar.

This paragraph explains one of the most interesting experimental tests: the cross compensation test.

Two sections are operated simultaneously. Section 1 is actuated to deliver a constant 40 L/min flow (Q_{IN-1}) at a constant 40 bar load (p_1); Section 2 is actuated to deliver a constant 40 L/min flow (Q_{IN-2}) at a load pressure (p_2) increasing from 15 bar to 110 bar.

After 27 s test time, the loads cross is happening: before this point Section 1 has the higher load and therefore its compensator is fully open; after this point Section 1 has the lower load and its compensator starts throttling. The opposite is happening for Section 2.
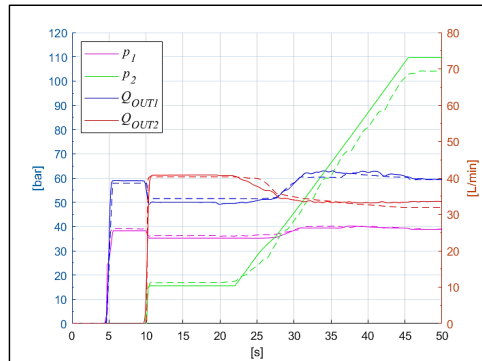
Figure 11: Delivered flows and load conditions

Figure 11 shows Section 1 and Section 2 delivered flows and loads condition. It also shows in dotted line the result from lumped parameter simulation and in continuous line the results of experimental testing.

The difference in the delivered flows during the compensating work depends partially on the system tuning explained in paragraph 2.2 and partially on high distributed pressure drops occurring in the non-optimized prototype layout. **Figures 12** and **13** show other significant details during the same test.
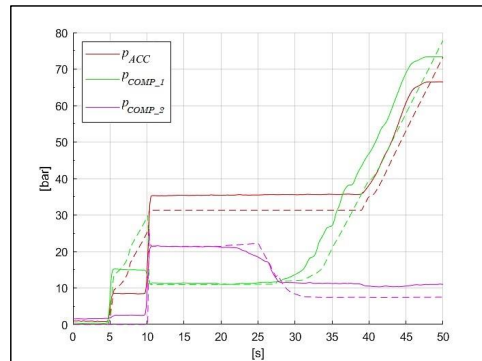
Figure 12: Compensators regulated pressure and accumulator pressure

Figure 12 shows the downstream compensators work: the p_{COMP-1} and p_{COMP-2} pressures indicate that the relative compensators are throttling to control the actuators speed. The diagram also shows the increasing pressure of the accumulator over the test time.
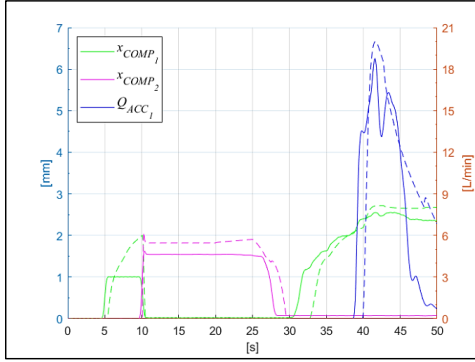
Figure 13: Compensators displacement and flow to accumulator

Figure 13 shows the compensators stroke x_{COMP-1} and x_{COMP-2} and the amount of recovered flow redirected by the compensators to the R line and to the accumulator.

5. EFFICIENCY ANALYSIS

The contribution to energy recovery for the two operating modes (overrunning load and simultaneous operations) can be studied separately.

5.1. Efficiency with overrunning loads

In case of overrunning loads, we will consider the efficiency with reference to the energy required to lift a given cylinder load during a time T.
The lift energy is ideally considered identical to the potential energy stored in the lifted cylinder:

$$\int_0^T p \cdot Q_{IN}\, dt \tag{5}$$

The recovered energy can be calculated as:

$$\int_0^T p_{ACC} \cdot Q_{ACC}\, dt \tag{6}$$

The efficiency results as:

$$\eta_{low} = \frac{\int_0^T p_{ACC} \cdot Q_{ACC}\, dt}{\int_0^T p \cdot Q_{IN}\, dt} \tag{7}$$

The recovered energy can also be calculated as the difference between the potential available energy of the lifted cylinder minus the distributed system losses, the energy losses in the main spool

tank notch (A_{OUT}) and the energy losses in the compensator throttling restrictions (A_R and A_T):

$$\int_0^T p_{ACC} \cdot Q_{ACC}\, dt = \tag{8}$$

$$= \int_0^T p \cdot Q_{IN}\, dt - E_{System\ Losses} +$$

$$- \int_0^T (p_{OUT} - p_{COMP}) \cdot Q_{OUT}\, dt + \quad \text{(DP\textsubscript{LOSS})}$$

$$- \int_0^T (p_{COMP} - p_{ACC}) \cdot Q_R\, dt + \quad \text{(AR\textsubscript{LOSS})}$$

$$- \int_0^T p_{COMP} \cdot Q_T\, dt \quad \text{(AT\textsubscript{LOSS})}$$

For some specific configurations, in which the accumulator is properly sized accordingly to the specific cylinder and load condition, a recovery efficiency over 60% has been found.

In real working conditions the recovery efficiency is limited by the following aspects:

- The accumulator is not big enough to further receive discharged flow and it starts to divert the flow to tank
- The accumulator is too big and, due to the low pressure level reached, the recovered energy is less
- The accumulator precharge pressure is too high and does not allow to recover from low loads
- The accumulator precharge pressure is too low and the compensator generates high pressure drop to control the flow

The diagram in **Figure 14** shows the simulations at different loads. It displays the contribution of **Equation 8** losses, considering a system with a 12 L accumulator and with 35 bar precharge.
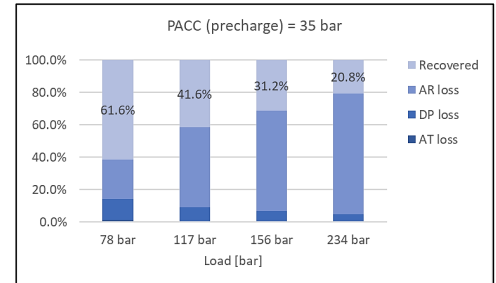
Figure 14: 35 bar precharge, various loads simulation

In this scenario the accumulator is big enough to receive the complete flow from the cylinder (almost no flow toward tank and no losses through the A_T notch in the compensator are

occurring); the distributed system losses are omitted; the pressure drop (DP loss) across the main spool A_{OUT} notch has a constant value (due to the same Q_{OUT} flow at the same Δp_{OUT}), even though its per cent relevance is decreasing as the whole energy amount is increasing.

The recovered energy is decreasing as the load increases, due to the fact that the loss through the A_R notch of the compensator is increasing.

Figure 15 shows the results in case the accumulator precharge is raised to 70 bar:
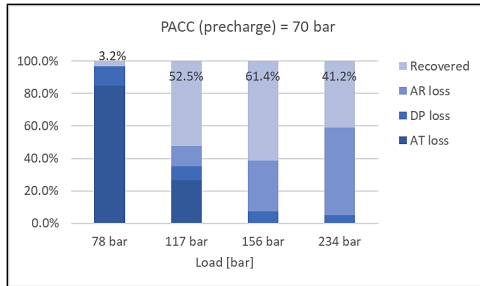
Figure 15: 70 bar precharge, various loads simulation

The high value of precharge does not allow the correct lowering speed with 78 bar and 117 bar loads, so that a considerable amount of energy is wasted through the A_T compensator notch.

When the load is high enough to allow the correct speed with 70 bar precharge, the behavior resembles to the previous case: the system efficiency is having a maximum over 60% and then it decreases again as the load increases. In real application on mobile machines, a compromise configuration that maximizes the recovery in the different and most usual working conditions has to be found.

It should also be noticed how the maximum efficiency about 60% is given by some fixed losses in the circuit: the piping distributed loss, the localized pressure drop through the main spool notch A_{OUT} and the localized pressure drop through the compensator A_R notch. A better layout, a different choice for the ΔP_{OUT} pressure drop and especially an improved dimensioning (A_R and A_T) and phasing (x_R and x_T) of the compensator notches can sensibly increase this maximum efficiency value.

5.2. Efficiency with simultaneous operations

When considering simultaneous actuations, the best is to evaluate the recovery potential with regards to the energy loss that a traditional Load Sensing compensated system is generating to keep the speed control of the less charged actuator.

Considering a Section 1, delivering a flow Q_{IN-1} with a high load p_1 and a Section 2, delivering a flow Q_{IN-2} with a lower load p_2, the energy loss in traditional LS systems can be calculated as follow:

$$\int_0^T (p_1 - p_2) \cdot Q_{IN-2} \, dt \tag{9}$$

While recovered energy is still represented by the equation:

$$\int_0^T p_{ACC} \cdot Q_{ACC} \, dt \tag{10}$$

The efficiency results as:

$$\eta_{comp} = \frac{\int_0^T p_{ACC} \cdot Q_{ACC} \, dt}{\int_0^T (p_1 - p_2) \cdot Q_{IN-2} \, dt} \tag{11}$$

In this case as well, the amount of recovered energy can be sensibly different depending on the parameters: approximately the same sizing problems described in the case of overrunning loads are the reasons for a reduction in efficiency. The recovery efficiency is strongly reduced by the throttling of compensator when the loads p_1 and p_2 are sensibly different.

The recovery efficiency is further reduced when the accumulator improper sizing forces the compensator to divert the flow toward tank.

5.3. Efficiency of tested layouts

Considering the two systems tested in experimental activity described in paragraphs 3.2 and 4.2, it must be clarified that main focus was to verify the functionality and practical feasibility of the innovative system.

The system efficiency optimization, as a secondary target, was limited by non-optimized components, complex piping and instrumentation. Nevertheless, interesting results have confirmed the expectations of simulation activity:

- Overrunning load test described in paragraph 3.2 showed a recovery of 60% of the equivalent lifting energy. The simulations allow to identify the optimal dimensioning of the accumulator volume (indicatively two times the cylinder volume to be discharged) and its precharge

pressure (indicatively 2.5/3 times lower than the applied load).

- Simultaneous movements test described in paragraph 4.2 showed a recovery of 16% of the energy normally wasted in analogous compensation work in traditional LS system. Additional simulations have shown that the correct accumulator precharge level and volume can increase the recovery up to 65%.

6. STORAGE SYSTEM

An accumulator is provided to store the recovered energy; check valves on R lines prevent the possibility of flow back.

The methods to re-use the hydraulic energy stored in the accumulator are not covered in this paper. However, some solutions have been evaluated, envisaging the use of a hydraulic motor connected to the ICE shaft in order to sustain the torque required by the system [2]. A second solution involves a hydraulic motor connected to an electric generator aimed to the battery recharge in a hybrid or totally electrified machine [13][14].

To a first approximation, the hydraulic accumulator could be omitted, although the simulations have shown that the presence of a hydraulic buffer allows to manage in a more efficient way the high and discontinuous power typically recovered from machine operations. It further allows to reduce the size of the components dedicated to re-use.

It should obviously be pointed out that the energy Re-Use system itself could reduce the whole system efficiency.

7. CONCLUSION

The paper presents an innovative directional valve layout for the control of the flow to the actuators of a mobile machine, in which a "downstream compensation" system allows to intercept hydraulic energy flows from inertial movements and from the simultaneous activation of loads at different values of pressure.

A first benefit is the possibility to control overrunning loads speed as a function of main spool displacement.

The experimental tests have proved the controllability of the system and the correct and smooth behavior of the downstream compensator.

Furthermore, the system allows for a substantial energy recovery, which has been experienced on test bench.

The amount of recovered energy is strongly dependent on the complete hydraulic circuit parameters and on the machine use mode: several analyses have brought to find the rules for optimal sizing, which can be consequently applied to different types of machine.

8. OUTLOOK

The next activities will concern the analysis of the energy benefits of the system applied on specific types of machines and in realistic work cycles. Especially the method to provide the correct and best compromise sizing of the system will be approached.

At the same time, an industrialized and commercially viable form of the concept will be developed. Furthermore, particular attention will be paid to the methods to re-use the stored energy: different concepts are going to be proved and evaluated in terms of whole system efficiency.

FUNDING

NOMENCLATURE

a/A	Cylinder areas ratio
A_{IN}	Main spool metering in area
A_{OUT}	Main spool metering out area
A_{PIL}	Compensator piloting area
A_R	Compensator way to recovery line
A_T	Compensator way to tank line
Δp_{IN}	Pressure drop through metering in area
Δp_{OUT}	Pressure drop through metering out area
F_{SPRING}	Compensator spring force
LS	Highest Load Sensing pressure
p	Pump pressure
p_{ACC}	Accumulator pressure
p_{COMP}	Pressure between main spool and compensator
p_{OUT}	Pressure on actuator meter out line
p_{PRE}	Accumulator precharge pressure
Q_{ACC}	Flow direct to the accumulator
Q_{IN}	Flow to the user (meter in flow)
Q_{OUT}	Flow from the user (meter out flow)
Q_R	Flow on the recovery line

Q_T	Flow on the tank line
x_{COMP}	Compensator stroke
x_{SPOOL}	Main spool stroke
x_R	Underlap way to recovery line
x_T	Underlap way to tank line
η_{low}	Efficiency in lowering test
η_{comp}	Efficiency in simultaneous operations test

REFERENCES

[1] Lodewyks J, Zurbrügg P (2016) Decentralized energy-saving hydraulic concepts for mobile working machines, 10th International Fluid Power Conference, Dresden, Germany

[2] Casoli P, Riccò L, Campanini F, Dolcin C, Lettini A (2016) Hydraulic Hybrid Excavator: Layout Definition, Experimental Activity, Mathematical Model Validation and Fuel Consumption Evaluation, 10th International Fluid Power Conference, Dresden, Germany

[3] Vukovic M, Leifeld R, Murrenhoff H (2016) STEAM – Hydraulic hybrid architecture for excavators, 10th International Fluid Power Conference, Dresden, Germany

[4] Schneider M, Koch O, Weber J, Bach M, Jacobs G (2014) Green Wheel Loader – Development of an energy efficient drive and control system, 9th International Fluid Power Conference, Aachen, Germany

[5] Inderelst M, Weidner F, Dongdong N, Stammen C (2018) Quantification of Energy Saving Influencers in a 21t Excavator Hydraulic System – A Holistic Investigation, 11th International Fluid Power Conference, Aachen, Germany

[6] Salomaa V, Mattila J, Minav T, Pietola M (2018) Efficiency Study of an Electro-Hydraulic Excavator, 11th International Fluid Power Conference, Aachen, Germany

[7] Busquets E, Ivantysynova M (2016) Toward Supervisory-Level Control for the Energy Consumption and Performance Optimization of Displacement-Controlled Hydraulic Hybrid Machines, 10th International Fluid Power Conference, Dresden, Germany

[8] Bonavolontà A, Dolcin C, Marani P, Frosina E, Senatore A (2019) Comparison of Energy Saving and Recovery Systems for Hydraulic Mobile Machines, 74rd Conference of the Italian Thermal Machines Engineering Association, ATI 2019, Modena, Italy

[9] Siebert J, Geimer M (2016) Reduction of System Inherent Pressure Losses at Pressure Compensators of Hydraulic Load Sensing Systems, 10th International Fluid Power Conference, Dresden, Germany

[10] Marani P, Ansaloni G, Paoluzzi R (2008) Load Sensing with Active Regeneration System, Proc.s Of The 7th Japan International Fluid Power Symposium, Toyama, Japan

[11] Marani P, Milani M, Mesturini D, Busani U. (2018) Experimental Evaluation of the New Meter Out Sensing Architecture, 11th International Fluid Power Conference, Aachen, Germany

[12] Sitte A, Weber J (2013) Structural design of independent metering control systems, The 13th Scandinavian International Conference on Fluid Power, Linköping, Sweden

[13] Tianliang Lin, Qingfeng Wang, Baozan Hu, Wen Gong (2010) Development of hybrid powered hydraulic construction machinery, Automation in Construction 19 (2010)

[14] Lei Ge, Long Quan, Xiaogang Zhang, Jaihai Huang, Bin Zhao (2018) High Energy Efficiency Driving of the Hydraulic Excavator Boom with an Asymmetric Pump, 11th International Fluid Power Conference, Aachen, Germany

EVOLUTION MIKRO – MICRO-DOSING IN THE HIGH-PRESSURE RANGE THANKS TO INNOVATIVE DRIVE TECHNOLOGY

Bernd Freissler

ProMinent GmbH, Im Schuhmachergewann 5-11, 69123 Heidelberg
Tel.: +49 621 842507; E-mail freissler.bernd@prominent.com

ABSTRACT

Oscillating positive displacement pumps are used in many industrial sectors. Mechanical stroke generators / drives such as crank drive, spring-cam drive etc have reached a high technological level, but to which are set mechanical limits. Especially in the smallest dosing range <1 l/h at a pressure range from 100 … 400 bar considerable optimisation is still required with regard to precision and continuity / control range of the dosing flow. In order to expand the current application possibilities for the diaphragm metering pump technology, it is necessary to use new drive systems such as linear motor technology. A linear motor is an electric drive unit which transmits the oscillating delivery movement of the dosing pumps directly to the displacer (hydraulic piston, diaphragm, etc.) without any mechanics, so that highly dynamic movements can be carried out with maximum precision, an individual kinematic profile and a control range of 1:200. The examples of gas odorization and filling processes show how the linear motor drive can be used to technologically solve and even optimize the customer's process requirements. The linear motor pump can realize an integrated 3-parameter control and is therefore suitable for almost any kinematically solvable dosing task.

Keywords: metering pump with linear-motor drive, integrated 3-parameter-control

1. INTRODUCTION

Mechanical stroke generators have a wide range of applications across all branches of industry. From simple lifting bow saws to windscreen wiper drives to tool drives (shapers) for machining or as piston compressors and pumps. One of the most important applications are oscillating positive displacement pumps.

In the following article, I would like to discuss the functional groups of oscillating positive displacement pumps with adjustable stroke length and ask the possibly most important question "Which drive/pump system is capable of optimally adapting to a dosing task?”

2. BASICS

2.1. Definition and operation of dosing pumps

The influence of fluctuations in process parameters on the flow rate is lowest in the oscillating positive displacement pump, as **Figure 1** and **2** show.

Most dosing pumps have a linear dependence between the manipulated variables (stroke length h and stroke frequency n) and the dosing current Q. They can therefore be easily integrated into automated processes.
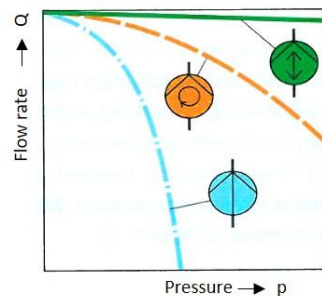
Oscillating displacement pump

Centrifugal pump

Rotating displacement pump

Figure 1: Dependence of the flow rate Q on the discharge pressure p of the dosed fluid
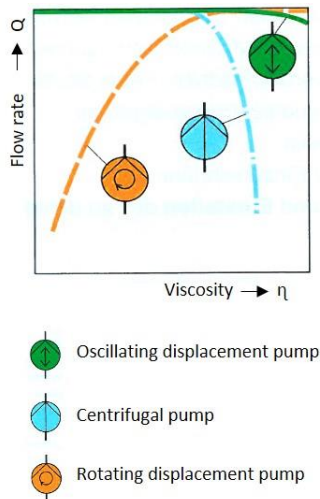
Figure 2: Dependence of the flow rate Q on the viscosity η of the dosed fluid

Therefore, and also because of its principle of action, it is particularly suitable for dosing tasks - supplemented by some additional functions:

- It delivers and increases the pressure level like any other pump.
- It measures by repeatedly displacing a given stroke volume (measuring cup principle).
- Its flow rate can be adjusted by continuously changing the stroke length, stroke volume or stroke frequency.

Apart from some special designs, dosing pumps are equipped with automatic valves which are controlled by the pressure change in the pump working chamber. **Figure 3** explains the operating principle of the classic dosing pump.
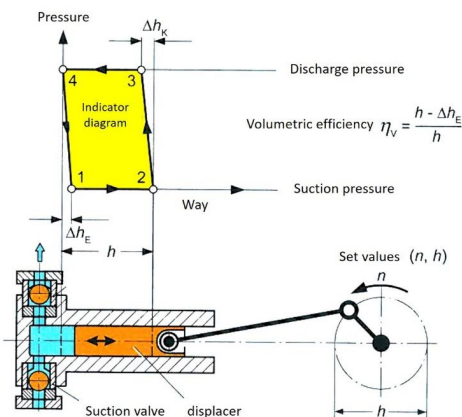
Figure 3: Function of the dosing pump

2.2. Mechanical drive units

The kinematic principles of the best-known stroke-adjustable dosing pump drives, such as straight slide crank drive, rotary crank or spring-cam drive, etc. are shown in **Figure 14**.

There are basically two parameters available for setting the flow rate in these drives.

- Stroke length: The mechanical setting of 0-100% is possible by means of a handwheel or an electric stroke length setting or control motor.
- Stroke frequency: The flow rate is set with the number of strokes per time unit (strokes/min), e.g. by means of a frequency converter control of the drive motor.

A special form of the oscillating positive displacement pump is the electromagnetic linear drive, as **Figure 4** shows. The solenoid generates the discharge stroke with its energy field, whereas the suction stroke is executed with a mechanical force such as a return spring. This is a widely used system in the low power range up to 100 watts.
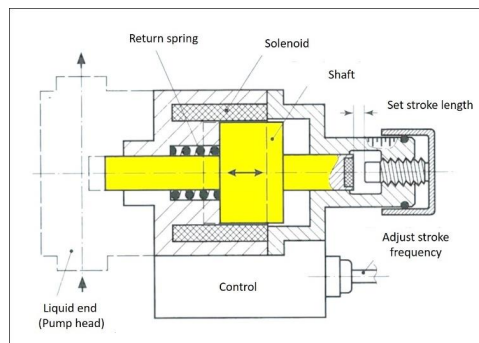
Figure 3: Function of the dosing pump

2.3. Liquid ends

The dosing units/liquid ends are essentially differentiated according to the displacement type, whereby only the diaphragm systems are dealt with here (**Figure 5b** and **5c**).
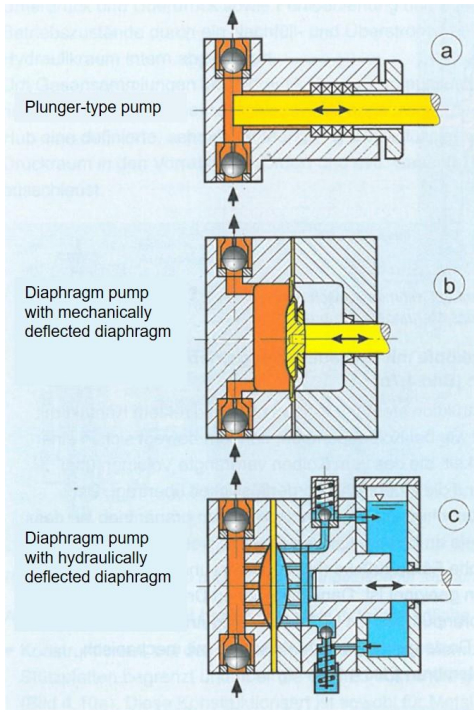
Figure 5:   Different types of liquid ends

Mechanically deflected diaphragm version

The mechanically deflected diaphragm (**Figure 5b**) is typically used in the low-pressure range up to 20 bar (occasionally up to 25 bar).
Advantages:
- Hermetically tight
- Simple design (cost-effective)
- Accuracy at ±2%, with a stroke length adjustment range of 1:4

Disadvantages:
- Not suitable for medium and high pressures
- No integrated overpressure protection in the liquid end

Hydraulically deflected diaphragm version

The hydraulically deflected diaphragm (**Figure 5c**) is very frequently used in the process industry (oil, gas, chemicals, etc.) in the pressure range up to 400 bar (occasionally up to 3,000 bar).
Advantages:
- Hermetically tight
- Accuracy at ±1%, with a stroke length adjustment range of 1:10

- In the liquid end integrated hydraulic pressure relief valve as overpressure protection.

Disadvantages:
- Technically complex solution (cost-intensive)

2.4. Characteristic transfer features

The oscillating movement of the displacer results in a digital/pulsating transfer characteristic (**Figure 6**) with a pressure-stable curve (**Figure 7**) and a simple linear dependence (**Figure 8**) of the dosing quantities on the setting parameters stroke length and stroke frequency.
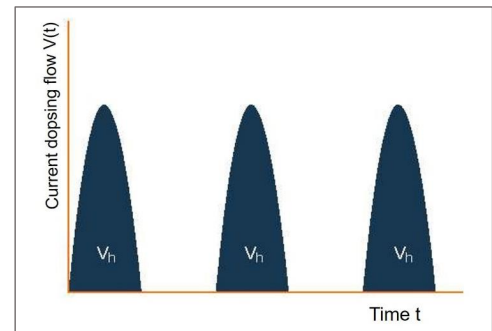
Figure 6:   Pulsating characteristic of transfer
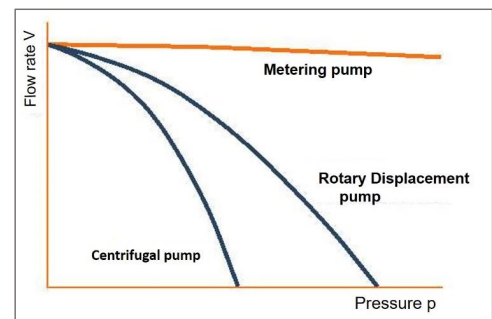
Figure 7:   Pressure-resistant curve
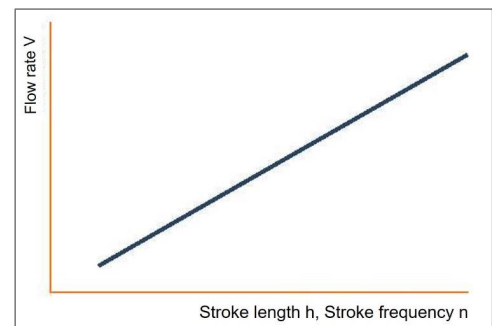
Figure 8:   Simple linear dependence

When it comes to hydraulic efficiency, oscillating displacement / dosing pumps with typical values of 75 - 95% are the most efficient system among the feed pumps.

3. CHALLENGE – OVERCOMING MECHANICAL LIMITS OF DRIVE

3.1. The process step dosing

Many process engineering procedures require precise and reliable dosing of material components to ensure that the end product produced meets the requested quality requirements. As more and more production processes have been fully automated in recent decades (**Figure 9**), dosing equipment is needed that can be integrated into the workflow of an overall process as simply and efficiently as possible. It has been shown that this is most easily achieved if the substances to be dosed are flowable, because this not only simplifies the process sequence, but also enables high dosing accuracies to be realized. Solids are therefore often prepared in fine-grained form and suspended or dissolved in a suitable carrier liquid. Each dosing process consists of three individual steps:

- Transfer (convey)
- Measure and
- Adjust the dosed flow rate Q
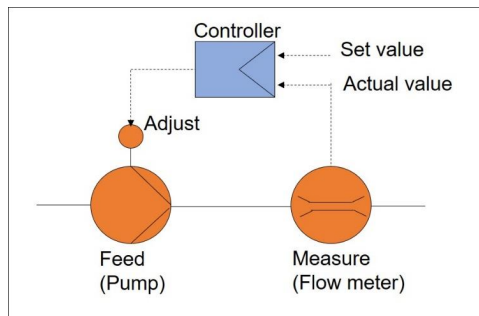
Figure 9: Dosing in the control circuit

3.2. Dosing parameters

Especially with regard to the drive technology of motor-driven dosing pumps, it can be stated that the kinematic principles of dosing movement (path-time profile, etc.) have virtually not changed in recent decades (see **Figure 10**).

Although there are already some systems such

as vector-controlled frequency converter pumps or controlled solenoid drives that modify the path-time diagram, these are still far from a true free definition of the complete motion profile.
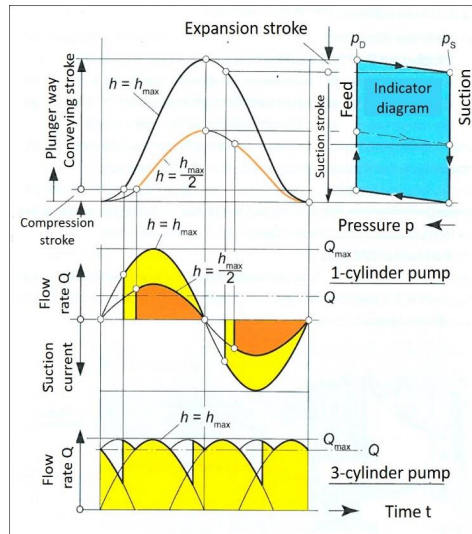
Figure 10: Flow rate pulsation Q(t) of a dosing pump with harmonic kinematics and volumetric efficiency η_V=0.9

The process of dosing still essentially includes the classic 1 or 2 parameter control:

- Stroke volume/stroke length control
- Stroke frequency/frequency converter for controlling the motor speed

Parameter 1 – stroke volume / stroke length control

Classically, the stroke length is set between 0-100 % (either mechanically or electrically supported). This process is typically carried out with a separate device for mechanical stroke length adjustment (adjusting eccentric, remote cam drive, etc.) or by means of an electric rotary drive. In practice, a typical control range of up to 1:10 is implemented here.

Parameter 2 – stroke frequency / frequency converter for drive motor

The speed of the electric drive motor in the control range 1:3 to 1:5 is usually controlled by a frequency converter.

Parameter 1 and 2 in combination

In order to realize a larger overall control range, it is necessary to use both parameters in combination. In practice, control ranges from 1:20 to 1:30 can be reliably realized (theoretically 1:50). The control ranges of the individual parameters are either connected in series (via process control system) or are linked to two independent control circuits.

3.3. Future requirements on dosing technology

Ideally, the operator would like to have a dosing solution for his application that is individually adapted to his needs.

In the best case, this means a 2-parameter control with a variable motion profile (parameter 3), which is exactly matched to the requirements during the injection of the pump into the process (discharge stroke) and, considered separately, also to the design of the suction stroke.

The properties of the liquids to be dosed, such as viscosity, chemical resistance, etc. must be taken into account, as must the hydraulic characteristics of the dosing stroke. These include, for example, minimising the spraying behaviour at the nozzle and preventing post-dripping in filling processes.

4. SOLUTION WITH LINEAR MOTOR TECHNOLOGY

4.1. Basics

The actual dosing movement required is the oscillating dynamic stroke in both directions. Therefore, a drive unit that executes a directly controlled/regulated oscillating movement for discharge and suction stroke without any movement and force deflection would be optimal. The linear motor fulfils exactly this requirement. The supplied electrical energy is converted directly into an oscillating movement. By this construction the complete drive unit contains only one moving part (**Figure 11**).
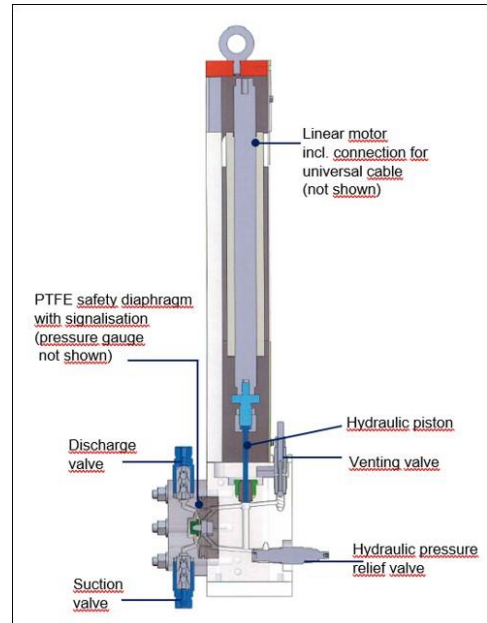
Figure 11: Structure of the linear motor pump

The structure and function of the linear motor are shown in **Figure 12**. The stator length with the coil and solenoid pairs is proportional to the force. The excess length of the solenoid package generates a constant force over the entire process range.
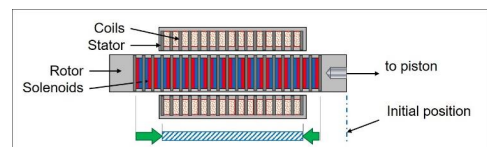
Figure 12: Structure and function of the linear motor

In comparison, the movement of the electric rotary motor is reduced from the motor speed (e.g. 1400 rpm) to the required stroke frequency for dosing pumps (e.g. 1:10 which corresponds to 140 strokes/min.) by means of a gear reduction. This is then converted into a usable oscillating movement via a crank drive with adjustable eccentric. Three changes are therefore ultimately necessary in order to obtain the actually usable, adjustable oscillating movement type. **Figure 13** shows the replacement of these components in linear motor technology.
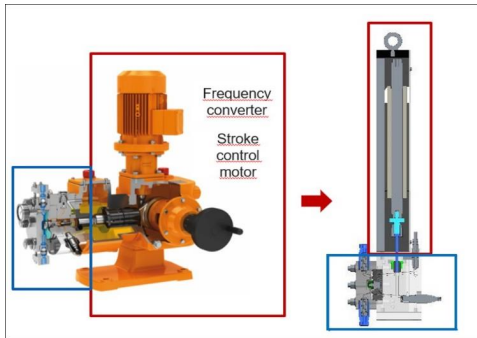
Figure 13: Comparison of mechanical stroke generator and linear motor

The advantages of the linear motor are obvious:

- The gearless design allows operation without deflection. This reduces components, making the design relatively wear-resistant. Costs and installation space can also be saved.
- Due to the high dynamics (velocity/ acceleration) inadequacies in the hydraulics, e.g. in the valves, can be actively compensated.
- The "stepper motor characteristic" with integrated path detection is well suited for the control of dosing profiles (see **Figure 15 - 17**).
- Unlike solenoids, the force is proportional to the current and can be applied in both directions.

Disadvantages:

- Low drive power, currently only up to 1 kW is possible.
- A drive control is always required for operation.
- Realisation

During the practical implementation, it should of course be noted that the combination of

- long stroke,
- highly dynamic motion and speed sequences and
- relatively low rod force

is best used in combination with a hydraulic diaphragm dosing unit (**Figure 5c**). Despite the low rod force of the linear motor, the hydraulic piston/force ratio makes it possible to achieve high conveying pressures such as 400 bar.

Due to the large stroke length, a useful stroke volume is possible despite the small piston diameter. Furthermore, the large stroke length also enables very precise positioning of the piston, which is reflected in a very high accuracy

of the dosing flow.

4.2. Parameter control 2+1

A linear motor is usually combined with its own individual control unit, so that the typical operating modes for 1 or 2 parameter control can be selected variably. These are e.g.

- Manual / permanent operation
- Contact activation
- Analogue control
- Fieldbus control (e.g. ProfiNet)

It is also possible to program a fixed or dynamic dosing profile for the discharge and (separately) for the suction stroke as a third parameter.

This means that the pump controller is on the one hand able to combine the stroke length and stroke frequency parameters optimally (e.g. 60% stroke length with 40% stroke frequency) and on the other hand at the same time to change/adjust the path-time profile according to requirements.

The linear pump can implement an integrated 3-parameter control and is therefore **suitable for almost any kinematically solvable dosing task.**

The best way to demonstrate the advantages of linear motor technology is to use the dosing profiles. **Figure 14** shows the kinematics of the classic crank drive/spring cam drive.
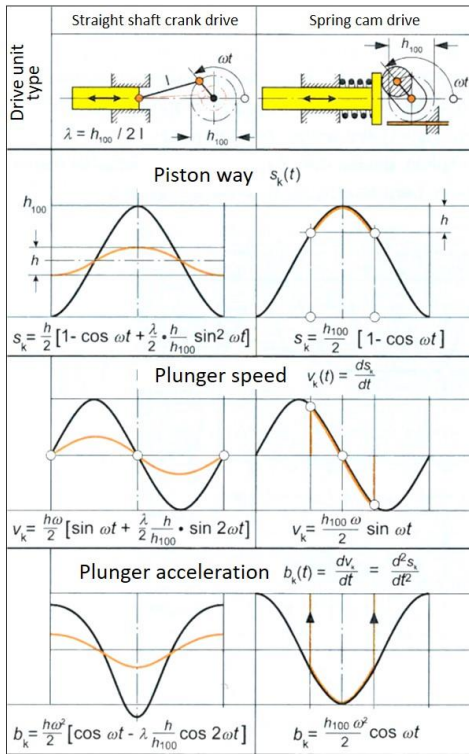
Figure 14: Kinematics of the straight shaft crank and spring cam drive at full stroke and reduced stroke length

In comparison, **Figures 15** to **17** show the flexibility of the linear motor on the basis of different speed-time profiles of single-head pumps. These are classified in the following chapter by means of application requirements and application examples.

5. APPLICATION EXAMPLES

5.1. Continuous dosing

Dosing task

Optimum mixing by means of almost continuous dosing

Application:

For gas odorization it is requested that the dosing quantity of odorant (e.g. mercaptans) is introduced as evenly as possible into the gas flow. This means that the suction stroke takes place in short time intervals (< 0.5 sec.) and the pressure stroke in as long time intervals as possible (up to

30 sec.). A linear motor drive can carry out the suction and discharge sides completely independently of each other without any problems and thus carry out the corresponding dosing profiles.
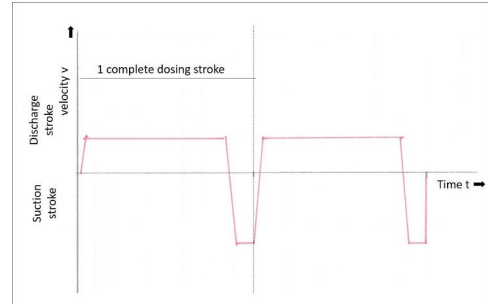
Figure 15: Linear motor dosing pump Evo mikro – nearly continuous dosing with minimum dosing pause

5.2. Dosing of high viscous fluids

Dosing task

Dosing of highly viscous fluids e.g. polymers with 1,000 mPas in water treatment

Application:

In order to achieve optimum dosing of highly viscous media, it is important that the liquid is sucked in during the suction stroke with the displacer moving as evenly and relatively slowly as possible. Furthermore, the pressure stroke must be performed much faster in order to reduce the backflow leakage at the valve. A linear motor drive can easily execute the suction and discharge sides completely independently of each other and thus execute the corresponding dosing profiles.
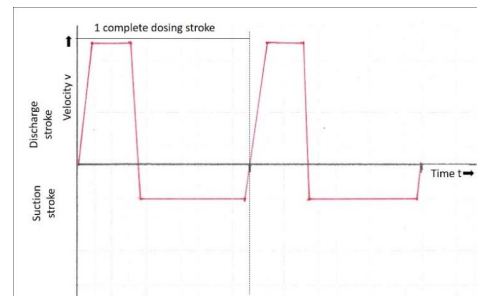
Figure 16: Linear motor dosing pump Evo mikro – dosing of high viscous fluids, optimized with long suction stroke

5.3. Dosing in the filling process

Dosing task

Dosing of additives in measuring cups with high accuracy, variable cycle times and absolutely drip-free

Application:

In the laboratory, individual test samples of various fluids are required for various processes, i.e. for every possible combination of process and fluid it is necessary to adapt the filling process (dosing profile). **Figure 17** shows the filling of a viscous additive.

1. Phase - Pressure stroke
   Start at medium speed to open all valves quickly and set the liquid in motion.
2. Phase 2 - Constant speed
   To continuously fill the fluid into the measuring cup.
3. Phase 3 - Gentle speed reduction
   To prevent dripping
4. Phase 4 – Suction
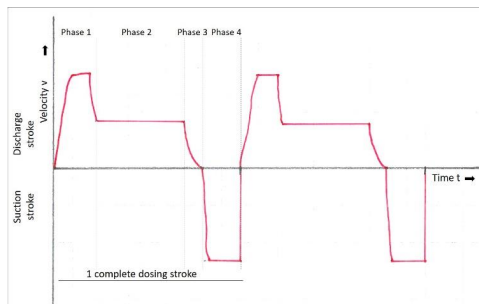
Figure 17: Linear motor dosing pump Evo mikro – filling process with nozzle due to individual and optimized speed profile with drop-free effect

6. CONCLUSION

Returning to the question: "Which drive/pump system is capable of optimally adapting to a dosing task?", we have found a new answer. By using a highly dynamic and precise linear motor as drive for oscillating positive displacement pumps, you have all degrees of freedom to adapt the pump kinematically to the dosing task.

Such an individual/application-optimised kinematic profile is particularly important in the field of small and very small quantity dosing in combination with medium and high pressures.

Consequently, the next question is: "What do the kinematic dosing profiles for the most varied fluids (high viscosity, solvents, etc.) and the various processes (filling quantity, continuity, dosing profile, etc.) have to look like in order to maintain an optimum?

With linear motor technology, we will systematically determine the different profiles and thus contribute to plant optimization.

REFERENCES

[1] Dulger V (Hrsg.), 2020 Richtig Dosieren, Vogel Business Media, Würzburg, Germany
[2] Fritsch H (1989) Die Bibliothek der Technik Bd. 50, Dosierpumpen - Grundlagen, Konstruktionen, Anwendung, verlag moderne industrie, Landsberg/Lech, Germany
[3] Vetter G (Hrsg.), 1994 Handbuch Dosieren, Vulkan Verlag, Essen, Germany

CFD-AIDED OPTIMIZATION OF CUSTOMER-SPECIFIC TANK SYSTEMS USING AN INNOVATIVE LABYRINTH DEAERATOR

Karl Wartlick*, Matthias Baumann, Andras Veres, Roman Weidemann

ARGO-HYTOS GmbH, Industriestrasse 9, 76703 Kraichtal, Germany
* Corresponding author: Tel.: +49 0 7250 76 -0; E-mail address: K.Wartlick@argo-hytos.com

ABSTRACT

This paper introduces the comprehensive approach of ARGO-HYTOS in developing and optimizing hydraulic tanks. Starting with a detailed analysis of the application, the tank design was optimized and an innovative deaerator was developed. In a first step, various Computational Fluid Dynamics (CFD) -based analyzing methods are presented, which are used to support the optimization process of tank development with regard to complex flow conditions and unexpected influences. The main topic of this paper is the introduction of an innovative labyrinth deaerator, causing coalescence of air bubbles, slower subsequent flow conditions and finally a better deaeration. A further focus is on a customized deaeration test rig, which is used to validate improved components and tank designs on the one hand and to learn more about the complex deaeration effects on the other hand.

With this comprehensive optimization approach and the innovative, compact and patented labyrinth deaerator, the size of the tank and the amount of oil can be reduced to a minimum, without impairing air separation, but on the contrary, even improving the air separation behavior.

Keywords: CFD, Tank optimization, Hydraulik Tank, Deaeration

1. INTRODUCTION

Increasingly complex construction space, the need for harmonization, integration of functions, as well as the pursuit of efficiency and a minimum usage of resources – all of these factors keep challenging the development of hydraulic systems. In order to meet these requirements and the fundamental objective of cost reduction, as well, reducing tank volume seems to be a main target for redesigns or new developments. However, this method bears a risk. The reduction of oil and tank volume lead to less heat exchange, as well as to increasing fluid aeration, both of which accelerate the oil aging process and cause a loss of performance, efficiency and component durability. Without a detailed analysis, optimization and validation of the tank system, an initial cost reduction may be negated by unforeseeable secondary costs and risks. To compensate for the shortened oil dwell time, an optimized tank volume utilization and a fast oil deaeration is vital.

The optimization of hydraulic oil reservoirs is sparsely treated in basic literature. The remarks on this issue are limited to design advice without further explanations. Technical literature merely deals with stationary applications, the examples being welded steel boxes across the board [1], [2], [3].

The recommendations and advice given regard deceleration of the flow, such as keeping a maximum distance between return and suction ports, separating them by position as well as geometrically by baffle, and avoiding abrupt changes of flow cross sections. Another advice is to make sure that the minimum distance to walls and oil surface is always observed, as this leads to deceleration and less turbulences, which are good conditions for a better deaeration behavior. Therefore, these tips are applicable to all reservoirs, whether they are stationary or mobile, made from steel or polymers, and independent of the manufacturing process. However, these recommendations are component-based and aim to improve flow conditions for each component, not the entire system. That optimizing individual components also improves the tank as a system is only implied. What is more, the interrelation of the components as a system and their influence on the system flow can only be abstracted for less complex geometries with a small amount of elements, such as a rectangular steel box.

Especially in mobile applications, the shape, weight and integration of functions are more important. For example, the weight of a stationary tank has no impact on the efficiency of a hydraulic press but it would have a major effect on mobile machinery. Tank designs in mobile applications are usually more complex, which makes a comprehensive consideration of a hydraulic tank system very challenging.

In this paper, the possibilities of supporting the optimization of hydraulic tanks by means of computational fluid dynamics within the development process is discussed, as well as the opportunity to improve deaeration behavior by applying a new type of labyrinth deaerator.

2. HOW CFD CAN SUPPORT TANK DEVELOPMENT AND OPTIMIZATION

With their experience in hydraulic systems – beyond their main expertise in filtration, valves and applications – ARGO-HYTOS also develop and manufacture hydraulic tanks. For quantities of less than hundred or several thousand pieces, the company offers the Hybrid Integrated Tank (HIT) technology or proprietary injection-molded solutions.

By using Computational Fluid Dynamics (CFD), any complex geometry and constellation can be mathematically modeled. Loaded with operating conditions, the system can be simulated and the results can be used to assess its behavior. CFD is used as a tool to analyze the oil volume in order to optimize the tank geometry. In addition, dead zones, vortexes and unintended increased velocities within internal flow channels formed by secondary streams and fluid movements can be detected. In the same way, the simulation helps to evaluate the deaeration behavior of a newly designed tank; being aware of the flow conditions is absolutely beneficial. Even small modifications in the geometry, such as unfavorably placed cutouts, rips, slants or other shapes obtruding the stream can change the flow conditions. With CFD simulation, the changes can be identified and their influence analyzed.

To implement the optimization process early on, the first model of the tank concept is reviewed based on the results of the CFD simulation. With the approach to regard a steady state one-phase flow under maximum conditions, it is the goal to get quick valid results and to evaluate whether the tank concept is going in the right direction.

Therefore, several post-processing features are considered. Streamlines visualize the paths of an arbitrary amount of fluid and give a general overview of the total flow movement. The color of the lines provides additional information, such as velocity or dwell time or any other physical parameters the simulation has calculated. By extracting bubble tracks from the simulation, illustrated in **Figure 1**, an initial statement on the tank's deaeration behavior can be made. In this context, similar to the streamlines, the paths of bubbles are shown according to their density and size. Depending on the simulation's boundary conditions, bubbles can be evaluated as deaerated by reaching the oil level or remaining in the system when they pass the suction outlets. In addition, a look at the pressure distribution of the oil level indicates possible vertical movements. Supported by two-dimensional velocity plots, predictions concerning potential optimization areas can be made and considered in further development. In a subsequent step, by comparing the simulation results of an optimized design with the former design, the improvements can be verified or previously undetected negative effects can be figured out and avoided in an additional development loop.
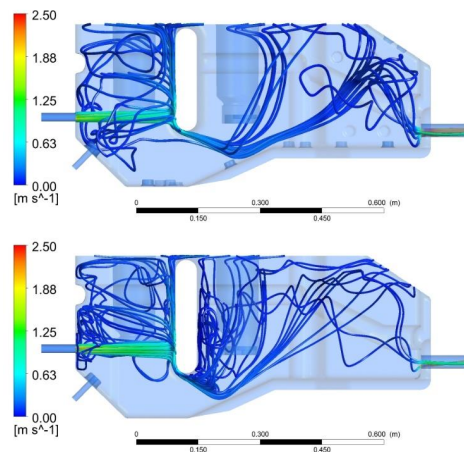
Figure 1: Simulated bubble tracks of a polymer tank with a shorter (upper fig.) and an extended baffle (lower fig.)

In the following example, this process led to a successful revision of an existing steel tank. The result is a new, optimized polymer construction with benefits in costs and deaeration, shown in **Figure 2**, under less oil volume.
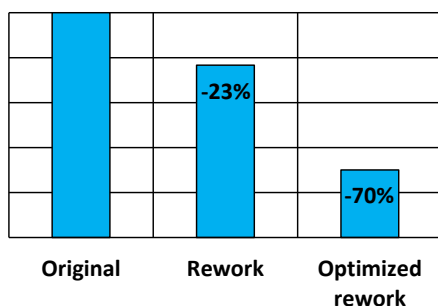
Figure 2: Comparison of the remaining dissolved bubbles depending on the stage of development

After analyzing the initial state, the concept was newly arranged with respect to the tank advice given in literature and the polymer design information. The review with the CFD simulation showed an obviously better deaeration behavior. Concerning the possibility to have major impact with little changes in geometry, the extension of the baffle wall led to a better separation between return and suction area, resulting in even better deaeration, as shown in **Figure 2**. Previously, the main return was not distributed but unfortunately deflected by the baffle and a subsequent slope. That led to a nearly unrestricted bypass channel to the outlet. However, this has been avoided during the concept phase without any major delay by using CFD to analyze, evaluate and decide how to move on.

On one hand, the potential spots for optimization without disturbing the tank functions can be identified before a redesign is executed; on the other hand, the new design can be analyzed and compared to the former shape. Thus, the process of new development, as well as rework, can be supported by the experience of ARGO-HYTOS to meet tougher requirements while improving functionality.

While these methods are conducted to improve the flow conditions with the aim of achieving better deaeration, developments by not only modifying the oil but also the air are followed up.

3. LABYRINTH DEAERATOR

Once the limits of tank optimization and tank size reduction with the help of CFD and design changes are reached, an innovative labyrinth de-

aerator (**Figure 3**) offers new possibilities and degrees of freedom to further optimize or to further reduce the size of tank concepts, without impairing air separation within the tank. The deaerator was developed with the aim of combining it with return filters, while making sure that this combination requires only slightly more space. Due to this reason, it is small and compact; it can be adapted to fit current return filter ranges and it can be integrated into virtually all existing, as well as newly designed tank systems without any problems. With this – in addition to various functions that can already be integrated into the tank (HIT concept) –another essential feature is available, which allows tank solutions to be successful even if installation space is limited.

Comparing the labyrinth deaerator with alternative solutions and approaches available on the market, among others, cyclones [4] can be found. With these, the idea is to create a centrifugal field induced by rotational flow, in which phase separation or an accumulation of air bubbles occur. At first glance, this is an obvious approach. However, the flow must first be accelerated to high velocities, which results in an additional pressure loss in the return line that cannot be disregarded. If the flow is accelerated too much, this will also lead to elongational flows and, in conjunction with turbulences, to air bubble disintegration. This, in turn, counteracts the actual goal of air separation. What is more, it is neither easy nor cost-efficient to adjust a cyclone to larger flow ranges or operating states. The labyrinth deaerator has no such disadvantages. It presents a very stable deaeration behavior across a wide range of operating conditions, while keeping differential pressure at a negligible level.

Another approach in the market is air discharge into the tank directly via openings in the bowl of a return filter; among other things, the air can be discharged closer to the oil surface, thus shortening the air bubbles' way to the surface. However, in mobile hydraulic applications, especially, the oil volume may vary considerably depending on the given operating condition. If the openings are above oil level, this is extremely counterproductive and with high flow rates, in particular, more air enters the hydraulic system than is separated. In contrast, the labyrinth deaerator can always be reliably mounted below oil level and, if required, it can be placed even lower in the tank with the help of a tube extension.
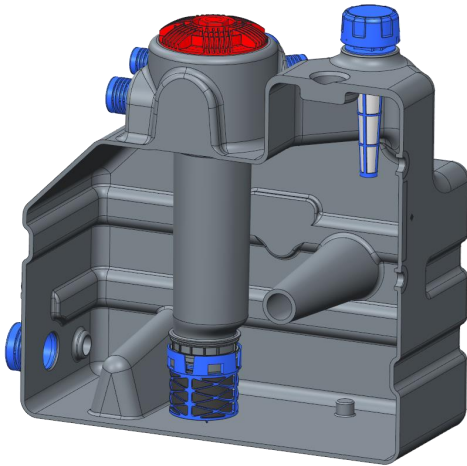
Figure 3: The labyrinth deaerator integrated into a Hybrid Integrated Tank (HIT)

3.1. Function

The key idea on which the labyrinth deaerator is based and for which a patent application has been registered is to have the air bubbles pass through a 3D labyrinth structure before they enter the tank; within this 3D labyrinth structure, smaller air bubbles can merge and form into larger bubbles. Moreover, the deaerator reduces the air entrance velocity into the tank, thus acting as a diffusor at the same time. Due to the reduced flow velocities in the tank, there is less turbulence, which might prevent air bubbles from ascending. **Figure 4** is a simplified representation of the function of the labyrinth deaerator.
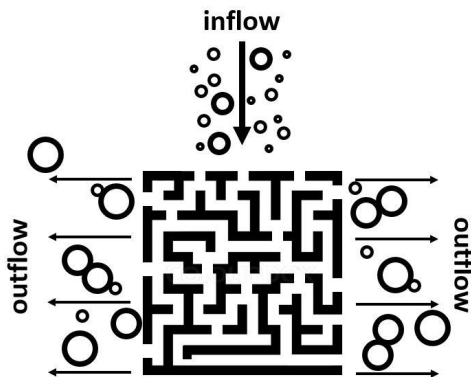
Figure 4: Functional principle of the labyrinth deaerator

The air bubbles entering the deaerator are constantly being redistributed and redirected with the flow through the material structure. This significantly increases the likelihood of air bubble collisions and the coalescence of air bubbles with it.

3.2. Test results

The labyrinth deaerator was developed and tested for a wide range of conditions to ensure that it works well in the most diverse operating conditions. In the process of development, a multitude of tests were performed with the deaerator, which were based on and performed in comparison with a reference system using a return filter without labyrinth deaerator. The following parameters were examined, among others:

- temperature (oil, viscosity)
- flow rate
- air content and type of air injection
- dwell time in the tank (15-35 sec)
- tank size reduction of up to 30%

In principle, two types of air injection were selected for these tests; the first type was air injection in blasts, as it might occur in practice after a filter element removal (adding a defined amount of air within 30 seconds). The second way was to add air over a longer period (15 minutes) in a lower concentration.

It is especially interesting that the labyrinth deaerator can substantially contribute to realizing a tank size reduction, without this having any negative effect on the air separation qualities of the tank.
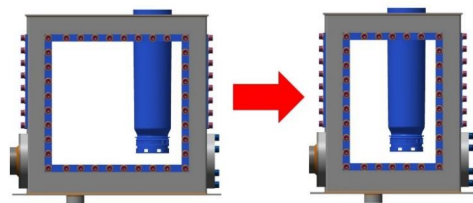
Figure 5: Test rig tank before and after 30% reduction

As can be seen in **Figure 5**, the test rig tank was narrowed down in one dimension and the oil quantity was adjusted accordingly. **Figure 6** shows the measuring results for the tank reduced by 30% in size, with labyrinth deaerator, compared with the reference system without size reduction and without labyrinth deaerator. The tests were performed with an air injection of 3% (over a period of 15 minutes) at 45°C and at 75% of

nominal flow rate of the filter. What can be seen is that the air concentration decreases much faster with the deaerator once air injection ends than it does in the reference system without the deaerator – this even though tank size and oil quantity were significantly reduced.
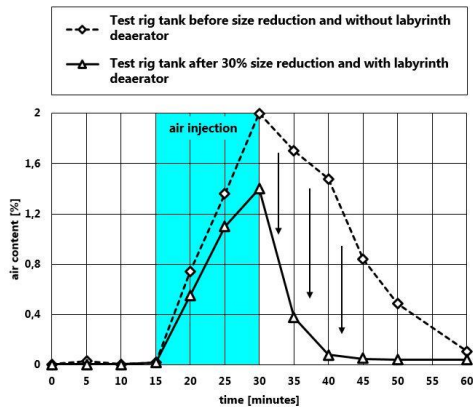
Figure 6: Deaeration of the test rig tank with return filter before and after 30% reduction

It is also quite interesting how the labyrinth deaerator performs in comparison with the solutions by competitors mentioned above. Comparative tests have definitively confirmed that the labyrinth deaerator works better than all other solutions tested. **Figure 7** shows a comparative test.
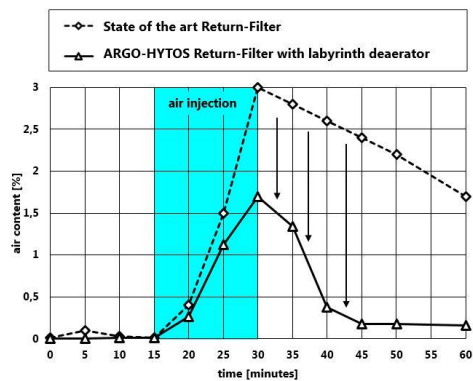
Figure 7: Deaeration of a state of the art return filter and an ARGO-HYTOS return filter with labyrinth deaerator

A state of the art return filter (which is supposedly optimized for air separation, in particular) was tested against an ARGO-HYTOS return filter with labyrinth deaerator. The test was performed at nominal flow rate with 3% air injection

(over a period of 15 minutes). In this test, the labyrinth deaerator could clearly demonstrate its virtues and achieved very good results. The advantages could be noticed already during air injection – the maximum concentration at the end of air injection was considerably lower than it was in tests of the solutions offered by the competition.

4. TEST RIG

For development of the labyrinth deaerator but also for other projects a multifunctional test rig was built. The test rig is supposed to make extensive and comprehensive testing and assessment of the air separation performance in hydraulic tanks possible. Achieving a high level of reproducibility was one of the most important requirements. **Figure 8** shows the test rig's schematic.
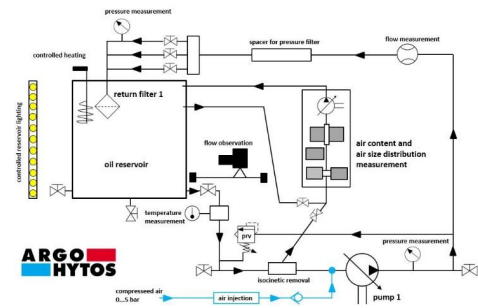
Figure 8: Schematic diagram of the deaeration test rig

Multifunctional means that the test rig can be converted quickly to test and compare various tank concepts, tank size reductions, filters or other components/installations and devices in tanks. Among other things, the following is possible:

- reduce test rig tank size by up to 30%
- tank exchange (customized tank)
- filter exchange (size, fineness, …)
- several return line connections
- pump for a large flow range

Another objective of building a multifunctional test rig was to be able to validate CFD simulation results. At the same time, the test results and sensor data of the test rig also help in setting useful parameters for the CFD simulation. This results in improved and more realistic CFD simulation, especially when considering air separation.

5. SENSOR AND MEASURING TECHNOLOGY

It is a challenge to detect air content and air bubbles in oil by means of sensor technology [5]. For this purpose not only different sensors are used and measuring solutions as well as evaluation methods to better assess and understand the problem „air in oil" in the test rig are developed. In addition to measurements and evaluation of number and size of the air bubbles, the air content can also be measured continuously, or it can be determined based on measuring data. The measuring technology for determining air content and air bubble size distribution integrated in the test rig can be used independent of the test rig, as well, for on-site measurements in mobile applications at the customer's (see **Figure 9** & **Figure 10**).

Figure 9:   Measurement system for air content and air size distribution

Figure 10: On-site measurement system

On-site measurements can help to find useful optimization approaches and to verify them not only in a simulation but in the actual machine, as well.

With the help of the evaluation method, valuable information on air content, separation times, separation efficiency/rate and general air separation performance based on the size and number of air bubbles can be gained. **Figure 11**, for example, shows a three-dimensional visualization of deaeration.
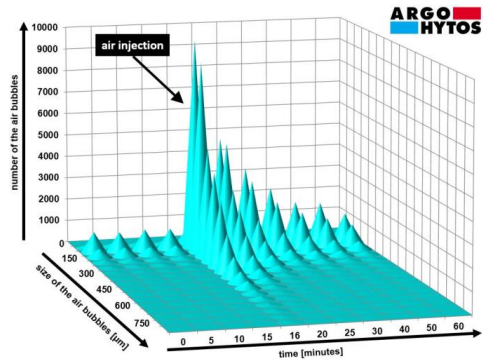
Figure 11: 3D diagram of the deaeration of a return filter

Figure 12 presents a measured bubble size distribution and a simulated distribution adapted to it. In this way, much better application- and customer-specific CFD simulations can be performed.
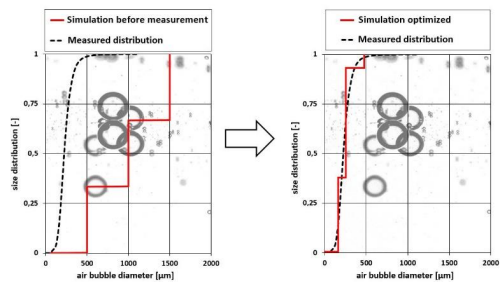
Figure 12: Adapted bubble size classes for more realistic CFD calculation based on measurement data

6. CONCLUSION AND OUTLOOK

Within the framework of CFD simulation, the issue „air in hydraulics", development of an innovative deaerator and building of a multifunctional test rig to validate this deaerator have been addressed, among other things. The test rig contains sensor and measuring technology for analysis purposes that can also be used at the customer's location. What is more, ARGO-HYTOS manufacture hybrid integrated tank systems (HIT) themselves, and the experience and knowledge gained are taken into account in the development and optimization phases of each new tank system. The company is thus well-equipped to offer comprehensive and competent support in optimizing

tank systems according to customers' specific needs.

Air in hydraulic fluids will remain an important and interesting issue. Whether it is about improving simulation options, finding new approaches to tank optimization, or further enhancing deaeration concepts, better solutions will be continued to come up with here, in close cooperation with customers.

REFERENCES

[1] D. Findeisen und S. Helduser, Ölhydraulik - Handbuch der hydraulischen Antriebe und Steuerungen, Berlin Heidelberg: Springer Vieweg, 2015.

[2] H. J. Matthies und K. T. Renius, Einführung in die Ölhydraulik, Wiesbaden: Vieweg+Teubner Verlag, 2011.

[3] D. Will und N. Gebhardt, Hydraulik - Grundlagen, Komponenten, Schaltungen, Berlin Heidelberg: Springer-Verlag, 2011.

[4] S. Sakama, Y. Tanaka, H. Higashi, H. Goto und R. Suzuki, „Air Bubble Separation and Elimination from Working Fluids for Performance Improvement of Hydraulic Systems," in *IFPE 2014*, Las Vegas, USA, 2014.

[5] K. Schrank, H. Murrenhoff und C. Stammen, „Investigation of different methods to measure the entrained air content in hydraulic oils," in *ASME/BATH 2014 Symposium on Fluid Power & Motion Control*, Bath, United Kingdom, 2014.

GROUP 6

Predictive maintenance

VALIDATION OF A SOFT SENSOR NETWORK FOR CONDITION MONITORING IN HYDRAULIC SYSTEMS

Jakob Hartig, Christian Schänzle, Peter F. Pelz[*]

Institut für Fluidsystemtechnik, Technische Universität Darmstadt, Otto-Berndt-Straße 2, 64287 Darmstadt
* Corresponding author: Tel.: +49 6151 1627100; E-mail address: peter.pelz@fst.tu-darmstadt.de

ABSTRACT

With increasing digitization, models are more important than ever. Especially their use as soft sensors during operation offers opportunities in cost saving, easy data acquisition and therefore additional functionality of systems. In soft sensor networks there is redundant data acquisition and consequently the occurrence of inconsistent values from different soft sensors is encouraged. The resolution of these data-induced conflicts allows for the detection of changing components characteristics. Hence soft sensor networks can be used to detect wear in system components.

In this paper this approach is validated on a test rig. It is found, that the soft sensor network is capable to determine wear and its extent in eccentric screw pumps and valves via data induced conflicts with relatively simple models.

Keywords: soft sensor, condition monitoring, wear, hydraulic system

1. INTRODUCTION

Increasing automation and digitization provide sensor data in a unified architecture and thus encourage the usage of soft sensors. Soft sensors are models of components that use easily accessible auxiliary quantities to estimate target quantities that are difficult to measure. [1]

Soft sensors are not isolated, however. The development of communication standards like OPC-UA allow for easy information transfer between soft sensors for different components. [2] An interconnected soft sensor network is formed. In soft sensor networks there is redundant data acquisition and consequently the occurrence of data-induced conflicts is encouraged.

Different methods have been developed to deal with conflicting data sources. On the one hand, conflicts can be seen as part of the systems normal behavior. Then data from multiple sources can be used to reduce uncertainty and to improve the overall level of data quality. Simple methods for data reconciliation of conflicting sensor data are voting systems. [3] More elaborate fusion methods are the Bayes method [4, 5], Dempster-Shafer method [6, 7], and heuristic methods [8, 9]. In the process industry for the estimation of process states data reconciliation methods are implemented. The

goal is to fuse the conflicting data, i.e. reconcile the state of the system with the conservation laws of mass and energy. With a quadratic minimization method, the measured system states are changed until the values satisfy the conservation laws. [10] On the other hand conflicts between data sources can be seen as part of erroneous system behavior. Thus different methods use conflicting data for fault detection and fault isolation [10, 11]. Fault diagnosis methods generally consist of a dynamic process model which is used to generate features. The chronological sequence of features and the difference of these features to features in normal operation lead to symptoms which are used for a diagnosis of faults. There is a vast literature on fault diagnosis systems and predictive maintenance to recognize a changing flow rate. A survey of methods for fault diagnosis systems can be found in [12].

In this paper a soft sensor network approach for condition monitoring [13–15] is validated where data-induced conflicts are used to derive additional information about the hydraulic system.

2. CONDITION MONITORING BASED ON A SOFT SENSOR NETWORK

In this paper a simple soft sensor network for a hydraulic system is considered (c.f. **Figure 1**). The hydraulic system consists of a pump and a valve where the valve represents any hydraulic resistance. This case example considers the perspective of a pump manufacturer whose pump is used in an unknown fluid system. Regarding the pump, the complete environment, e.g. valves, filters or similar, can be described as one generalized resistance. The pump and the resistance are each represented by a soft sensor which is subject to uncertainty and lack of knowledge e.g. component characteristic changes due to wear. Measured quantities in the system are the pump speed as well as temperature and pressure differences over the components.

The purpose of the soft sensor network is to generate redundant data of the volume flow from two different sources, firstly the soft sensor of the pump and, secondly, the soft sensor of the resistance, i.e. valve. In this way, the soft sensor network enables the occurrence of data-induced conflicts which are inconsistent values calculated by two different sources. The aim is to generate additional information about the system based on the data-induced conflicts.

Data-induced conflicts may result from, firstly, the breakdown or defect of a measuring sensor, secondly, model uncertainties of the soft sensors and, thirdly, change of component characteristics, e.g. due to wear. [15] The resolution of these data-induced conflicts either leads to greater confidence in the model-based system quantities or allows for the detection of changing components characteristics.

In the following data-induced conflicts caused by changing component characteristics are considered to detect wear in system components. To validate this approach three research questions need to be answered:

1. What is the error and uncertainty for the two soft sensors? Error is the deviation of the computed flow rate from the true value and uncertainty describes an interval around the computed value which contains estimates that can be reasonably attributed to the true value.
2. Can wear be determined via data-induced conflicts?
3. Is it possible to isolate the worn component?

In the following these three questions are discussed based on an experimental investigation.

3. METHOD

3.1. Test rig for simulated wear

Wear in pumps, valves and other components leads to a change in the flow characteristics. Therefore, at a given pressure, the detection of wear with soft sensors requires the detection of small changes in the flow rates. This is the motivation for an experimental analysis of the flow rate variations on redundant soft sensor outputs and their use for wear detection. [16]

Hence a test bench was set up on which a leakage of the components can be adjusted representing wear. For this reason, bypasses for the positive displacement pump and the valve were in integrated into the test bench (c.f. **Figure 2**).

Figure 1: Soft sensor network for wear detection in hydraulic systems.
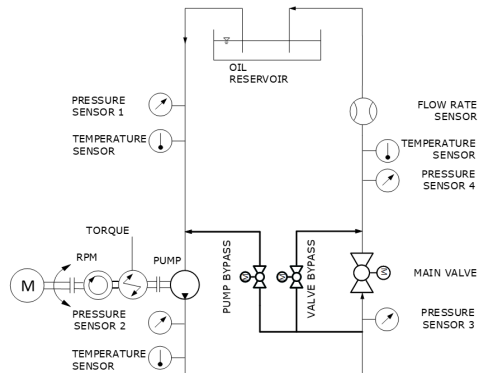
Figure 2: Test rig for simulating wear in a hydraulic system.

The pump used in the test rig is a progressive cavity pump and the valve is represented by a ball valve. The eccentric screw drive pump with a geometric volume of $V = 0.0723\,l$ is driven by an asynchronous motor with $18\,kW$. The resistance of the system is mainly determined by the main ball valve. The bypass flows are controlled with electric ball valves. All measured points are approached from lower degrees of opening to avoid mechanical play in the valves.

A torque meter with built-in speed sensor measures the rotational speed of the pump. The volume flow rate Q_{main} after the valve is measured with a screw type flow meter. Pressures are measured with piezo resistive sensors and temperatures are measured with Pt100 resistance thermometers.

The oil is of the type Shell Tellus 10. The temperature of the oil during experiments was held at $30° \pm 1°\,C$. The temperature was measured before and after the pump and the results were averaged for calculating oil density and viscosity. The soft sensor network was tested for the rotational speeds 200 rpm, 300 rpm and 400 rpm of the pump.

3.2. Soft sensors

Since the volume flow is a conservation quantity it needs to be identical in the considered pump and valve. Hence the purpose of both soft sensors, the pump and the valve, is to generate redundant data of the volume flow rate.

For the valve the well-known and simple K_v model is used. The flow rate is determined by

$$Q_{valve} = K_v(\alpha) \sqrt{\frac{\Delta p_{valve}}{\Delta p_0} \frac{\varrho_0}{\varrho}}, \tag{1}$$

where $\Delta p_0 = 1$ bar and $\varrho_0 = 1000$ kg/m^3 and the pressure difference over the valve $\Delta p_{valve} = p_2 - p_4$ and ϱ is the fluid density.

For the calibration of K_v as a function of valve opening α a third degree polynomial was used. The parameter identification was done with a robust nonlinear least squares method. The results for the fit for different rotational speeds for the pump can be found in **Figure 3.**
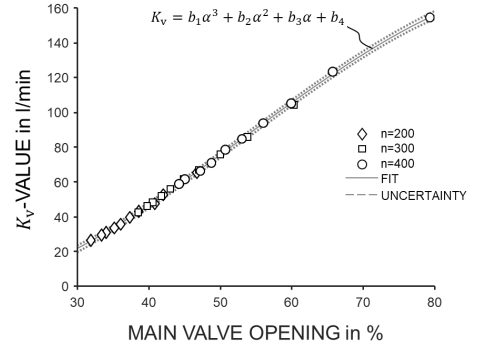
Figure 3: Calibration curve for the valve model.

The soft sensor of the pump is based on a type independent efficiency model for positive displacement pumps [17]. The flow is determined by the geometric volume V and the rotational speed n less the gap losses Q_L.

$$Q = nV - Q_L = nV - Q_{L+}vV^{\frac{1}{3}} \tag{2}$$

The gap losses are modelled by

$$Q_{L+} = L_{\Delta p+} \cdot \Delta p_+{}^m, \tag{3}$$

where $L_{\Delta p+}$ and m are model parameters that need to be calibrated. Δp_+ is the dimensionless pressure difference given by

$$\Delta p_+ = \frac{\Delta p\, V^{2/3}}{v^2 \varrho}. \tag{4}$$

Measured quantities are the rotational speed n and pressure difference Δp. The fluid density ϱ and kinematic viscosity v are derived from a calibration curve via temperature measurements.

The results for the fit for the pump model can be found in **Figure 4.**
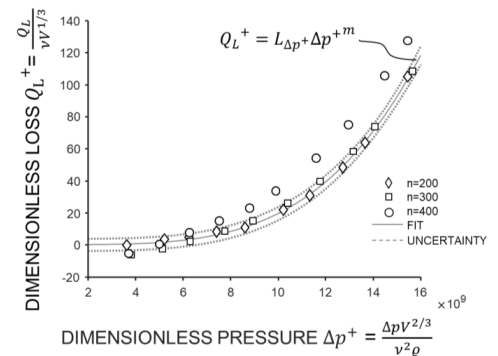
Figure 4: Calibration curve for the pump model.

3.3. Propagation of Uncertainty

Soft sensors should be considered as sensors. Uncertainties should therefore be included in their calculated values. In the following two sources of uncertainty in soft sensors are considered: the systematic and stochastic uncertainty from the measurements e.g. pressure measurement as well as the systematic uncertainty from the calibration procedure (c.f. **Figure 5**).
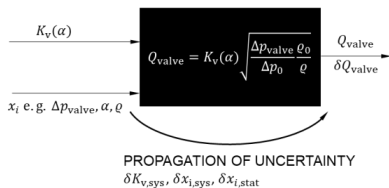

Figure 5: a) Calibration and b) soft sensor measurement with propagation of uncertainty.

The uncertainty from the calibration and from the measurement is propagated through the model to yield the soft sensor uncertainty. Stochastic and systematic uncertainty is propagated independently.

4. RESULTS

In the following the results for closed bypass valves (i.e. no wear), wear in one component and simultaneous wear in both components are discussed.

4.1. Function of the soft sensors

To check whether the soft sensors reflect the volume flow in the hydraulic system, soft sensor outputs and flow rate measurements for closed bypass valves are compared. It is found that the relative deviation from the true value (relative error) for the valve soft sensor is < 2 % and < 0.5 % for the pump soft sensor. However, in an application the true flow rate is not known and therefore the relative error is not relevant. To assess whether the soft sensors are useful for

determining the true flow rate and detecting wear, the uncertainty of the soft sensors has to be determined. The relative uncertainty for the valve soft sensor is < 5 % and < 1 % for the pump soft sensor.

4.2. Wear in one component

To check how the soft sensors react to wear and whether a data-induced conflict can be determined the bypass is opened during measurement. For pump wear the volume flow is plotted above the opening degree of the pump bypass represented in **Figure 6**. The speed and pressure difference were kept constant at all operating points by controlling the main valve opening (pressure controlled system).

The measurement point with a nearly closed bypass resembles the results from section 4.1. The two soft sensors calculate the actual volume flow within their uncertainties

With increasing wear (i.e. with increasing opening degree of the pump bypass), the actual volume flow decreases. Since the valve is not exposed to wear, the valve soft sensor shows the actual flow rate. Only the pump soft sensor deviates from the actually volume flow with increasing wear. This is because the volume flow of the pump soft sensor is determined by the speed and the pressure difference. Since these two variables are kept constant, a constant volume flow is calculated despite wear. The actual volume flow is not constant due to a backflow through the bypass.

The valve soft sensor, in turn, calculates the reduced volume flow, since the valve soft sensor takes the pressure difference and the valve opening degree of the main ball valve into account.
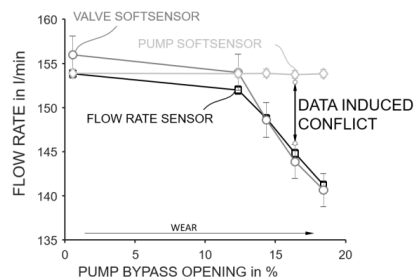
Figure 6: Soft sensor outputs for wear in pump.

The soft sensor network shows data induced conflicts between the calculated flow rates of the two soft sensors. Where the errors of the two soft sensor outputs do not overlap (c.f. **Figure 5**) a data induced conflict of type (iii) occurs.

The data induced conflict is the result of pump characteristics changes. In the results, the size of the data induced conflict increases with increasing bypass flow, i.e. the simulated wear. The same was found for wear in the valve.

Hence the proposed soft sensor network can be used to detect wear in the pump. However, due to the uncertainty of the two soft sensors, a difference of 6 % between the two soft sensor outputs indicates wear. Thus, wear in early stages cannot be identified.

4.3. Combined wear in pump and valve

In fluid systems wear is caused by particles and is consequently propagated through the system. This leads to combined wear. [18] To investigate this the flow rates for pump and valve bypasses are varied simultaneously.
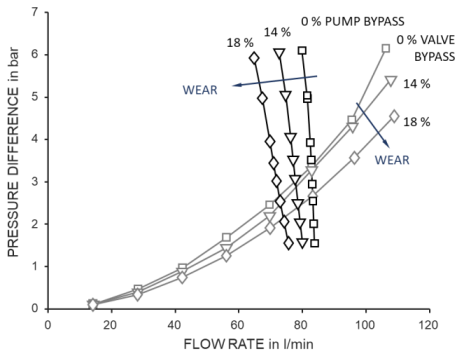
Figure 7:   Characteristic curves for pump and valve with varying opening degree for bypass.

In **Figure 7**, the pressure is plotted above the volume flow at different bypass openings for valve and pump. For each bypass flow the pump- and valve characteristics are shown as lines. As soon as the pump wears out, its characteristic curve shifts to lower flow rates. With the same pressure difference at the pump, less volume can be pumped due to internal leakage. When the valve is worn, the characteristic curve shifts to lower pressures so that at the same pressure difference, more volume flow can flow through the valve due to the enlarged valve cross-section.

The characteristics intersect at the respective operating point.

To investigate combined wear further, different bypass openings are set for the pump. In this series of measurements, the speed and pressure difference and the opening of the valve bypass remains constant at 16 % (c.f. **Figure 8** left). The volume flow trend of flow meter and valve soft sensor is the same. The absolute values have a relatively constant difference which corresponds to the constant bypass opening degree of 16 %. At 0 % bypass opening degree, the pump soft sensor initially outputs the actual volume flow. Only with increasing wear a larger deviation occurs.

For valve wear, conversely, the opening degree of the pump bypass remains constant at 16 % and the opening degree of the valve bypass varies from 0 to 18 %. (c.f. **Figure 8** right). The pump soft sensor outputs a constant deviation from the actual volume flow, since the pump bypass opening degree is constant at 16 %. The volume flow of the valve soft sensor deviates from the actual volume flow after initial overlapping with increasing wear.

It still remains to be clarified whether the defective component can be determined using the two soft sensors. For this purpose, we consider the same graphs of combined wear and tear, which corresponds most closely to the real, unknown system state.

Comparing both soft sensor outputs in **Figure 8** we find that the characteristics of the two wear patterns are very similar and regardless of the wear condition in the system, the volume flow from the valve soft sensor is always smaller than that of the pump soft sensor. Hence, without further information we are not able to determine which component is defective.

5. CONCLUSION

It is found, that the soft sensors, despite being relatively simple can predict the systems flow rate with a relative error lower than 2 % and an uncertainty lower than 5 %. Consequently, the soft sensor network consisting of the soft sensors for the pump and the valve can reliably detect differences of 6 % in flow rate between two soft sensor outputs. Thus, the network is capable to determine wear and its extent in eccentric screw pumps via data induced conflicts. To isolate the
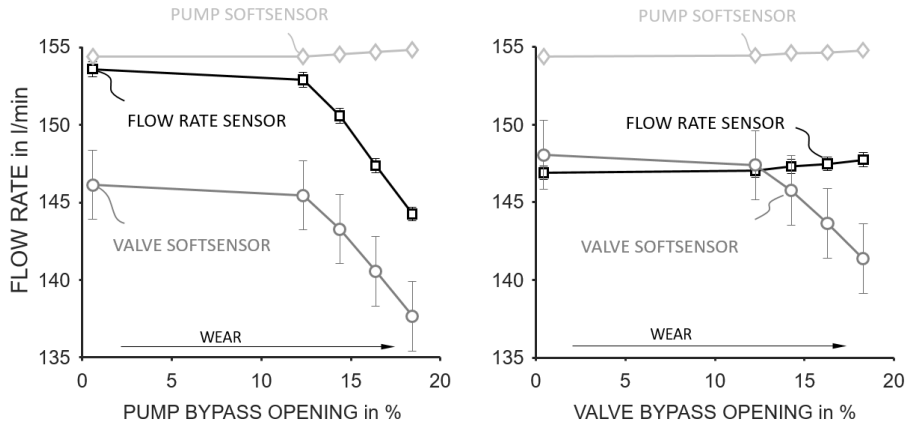
Figure 8: Results for combined wear with varying wear in pump (left) and varying wear in valve (right).

worn component additional information (e.g. temperature) is necessary.

Furthermore, the application of the proposed method shows, that the determination of the uncertainty of soft sensors is inevitable to reliably classify unavoidable data-induced conflicts in redundant data acquisition.

In future studies the concept should be tested with more complex systems. In addition to that, the transient behavior of the soft sensor network should be investigated.

ACKNOWLEDGEMENTS

NOMENCLATURE

α	valve opening in %
K_v	valve parameter
$L_{\Delta p+}$	pump parameter
m	pump parameter
n	rotational speed
Δp	pressure difference
Δp_+	dimensionless pressure
Δp_{valve}	valve pressure difference
Δp_0	atmospheric pressure
p_2	pressure sensor 2
p_4	pressure sensor 4
Q	volume flow rate
Q_{main}	main volume flow rate
ϱ	fluid density
ϱ_0	density of water
V	geometric volume
ν	kinematic viscosity

REFERENCES

[1] Fortuna L, Graziani S, Rizzo A, Xibilia MG (2007) Soft Sensors for Monitoring and Control of Industrial Processes. Advances in Industrial Control. Springer, London, Berlin, Heidelberg

[2] Hannelius T, Salmenpera M, Kuikka S (2008) Roadmap to adopting OPC UA 6th IEEE International Conference on Industrial Informatics, 2008. INDIN 2008 ; Daejeon, South Korea, 13 - 16 July 2008. IEEE Service Center, Piscataway, NJ, S 756–761

[3] Fischer MJ (1983) The consensus problem in unreliable distributed systems (a brief survey). In: Karpinski M (Hrsg) Foundations of computation theory. Proceedings of the 1983 International FCT-Conference, Borgholm, Sweden, August 21 - 27, 1983, Bd 158. Springer, Berlin, S 127–140

[4] Kumar M, Garg DP, Zachery RA (2006) A generalized approach for inconsistency detection in data fusion from multiple sensors American Control Conference, 2006. 14 - 16 June 2006,

[Minneapolis, MN. IEEE Operations Center, Piscataway, NJ, 6 pp

[5] Castanedo F (2013) A Review of Data Fusion Techniques. ScientificWorldJournal 2013. doi:10.1155/2013/704504

[6] Yager RR (1987) On the dempster-shafer framework and new combination rules. Information Sciences 41(2):93–137. doi:10.1016/0020-0255(87)90007-7

[7] Khaleghi B, Khamis A, Karray FO, Razavi SN (2013) Multisensor data fusion: A review of the state-of-the-art. Information Fusion 14(1):28–44. doi:10.1016/j.inffus.2011.08.001

[8] Steinhorst W (1999) Sicherheitstechnische Systeme. Zuverlässigkeit und Sicherheit kontrollierter und unkontrollierter Systeme. Aus dem Programm Naturwissenschaftliche Grundlagen. Vieweg+Teubner Verlag, Wiesbaden

[9] Kreß R, Crepin P-Y, Kubbat W, Schreiber M (2000) Fault Detection and Diagnosis for Electrohydraulic Actuators. IFAC Proceedings Volumes 33(26):983–988. doi:10.1016/S1474-6670(17)39273-X

[10] Grimble MJ, Johnson MA, Sbárbaro D, del Villar R (2010) Advanced Control and Supervision of Mineral Processing Plants. Springer London, London

[11] Isermann R (2006) Fault-Diagnosis Systems. An Introduction from Fault Detection to Fault Tolerance. Springer-Verlag Berlin Heidelberg, Berlin, Heidelberg

[12] Isermann R (2005) Model-based fault-detection and diagnosis – status and applications. Annual Reviews in Control 29(1):71–85. doi:10.1016/j.arcontrol.2004.12.002

[13] Hartig J, Schänzle C, Pelz PF Concept validation of a soft sensor network for wear detection in positive displacement pumps 4th International Rotating Equipment Conference - Pumps and Compressors, Wiesbaden, Sep 24-25, 2019

[14] Pelz PF, Dietrich I, Schänzle C, Preuß N (2018) Towards digitalization of hydraulic systems using soft sensor networks. 11th International Fluid Power Conference 2018, S 40–53

[15] Schänzle C, Dietrich I, Corneli T, Pelz PF (2017) Controlling Uncertainty in Hydraulic Drive Systems by Means of a Soft Sensor Network Proceedings of the 35th IMAC, a Conference and Exposition on Structural Dynamics, Volume 5

[16] Park H (1994) Fehlererkennung und Rekonfiguration von redundanten Ölhydraulikversorgungssystemen. Dissertation, Technische Hochschule Darmstadt

[17] Schänzle C, Ludwig G, Pelz PF (2016) ERP Positive Displacement Pumps – Physically Based Approach Towards an Application-Related Efficiency Guideline 3rd International Rotating Equipment Conference (IREC) 2016, Düsseldorf

[18] Lehner S, Jacobs G (1997) Contamination Sensitivity of Hydraulic Pumps and Valves. In: Totten GE (Hrsg) Tribology of hydraulic pump testing. ASTM, Philadelphia, Pa., 261-261-16

PREDICTIVE MAINTENANCE WITH A MINIMUM OF SENSORS USING PNEUMATIC CLAMPS AS AN EXAMPLE

Wolfgang Gauchel*, Thilo Streichert, Yannick Wilhelm

Festo AG & Co. KG, Ruiter Straße 82, 73734 Esslingen, Germany
* Corresponding author: E-mail address: wolfgang.gauchel@festo.com

ABSTRACT

In standard pneumatics, the available signals for data analytics are very limited. As a rule, no continuous status information is available. Usually only the reaching of the end position is indicated - by means of a digital signal of a proximity sensor. This paper examines whether these limited data can be used to derive usable and useful information for predictive maintenance. Pneumatic clamps in body-in-white construction were chosen as application example. The paper describes a continuous run to investigate the basic feasibility of predictibility. In the following chapters, possibilities for error classification are discussed. Finally, the implementation of the findings in a field test is described.

Keywords: Predictive Maintenace, Clamping Units, Pneumatics

1. INTRODUCTION AND PROBLEM DESCRIPTION

In the course of digitization the automation world, predictive maintenance is becoming more and more important. Thanks to continuous measurement and analysis, predictive maintenance makes it possible to forecast the remaining service life of machine components [1].

One of the most promising approaches to realize predictive maintenance is machine learning. Machine learning deals with algorithms, that learn from data and predict outcomes that will occur with a certain probability [2].
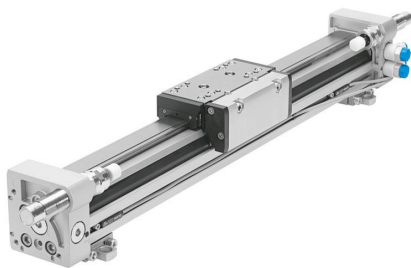
Figure 1: Typical sensor equipment in pneumatics: Linear drives DGC with two proximity sensors SMT.

This paper focuses on the question, whether a maintenance requirement for pneumatic standard systems using a minimum of sensors can be predicted with the help of machine learning algorithms. A double acting cylinder is normally equipped with an proximity sensor in every end position (cp. **Figure 1**). Does such a system with a minimum of sensors generate enough data, containing sufficient information about the health state of the underlying process and component so that is applicable for predictive maintenance?

From the perspective of control engineering, this is rather not possible. A system consisting of two limit switches cannot be observed.

A system is called observable if the initial value of the system state at the beginning of the time interval can be calculated from the temporal course of the output and input signals in a finite period of time [3]. If this holds for any initial state and not only for a limited set of initial states, the system is called complete observable [3, 4]. (Föllinger [4] supplements this definition by a "no matter where this [initial state] lies").

It is obvious that this definition is not fulfilled by a pneumatic cylinder with only two proximity sensors. If, for example, the initial state is somewhere in the motion phase, the first information one receives about the system state is reaching the next end position - i.e. location information at a defined point in time. With this information however, it is not possible to calculate in which position the cylinder has started or even which pressures were prevailing in the cylinder chambers at the start time. An

observability of the considered pneumatic system is therefore not given. The "free flight" between the end positions without any sensor information makes observation impossible.

However, it should be noted that this definition of observability is based on a classical control engineering understanding of a system model. This assumes, that state variables such as pressure or position can be described continuously over time. Another type of model, in which e.g. only the average travel speed is described, can be derived from the existing digital signals. This raises the question whether a prediction of possible failures is possible based on such rudimentary observability.

To investigate this, chapter 2 describes the state of the art in predictive maintenance. In chapter 3, the selected application example - pneumatic clamps in body-in-white construction - is explained. Chapter 4 describes an endurance run with pneumatic clamps in order to fulfill the basic proof of predictibility. To generate useful information for maintenance personnel in addition to a simple "there is a risk of failure", chapter 5 deals with possibilities for fault localization. Finally, chapter 6 describes a field test in automotive production. The paper ends with a summary and outlook in chapter 7.

2. STATE OF THE ART IN PREDICTIVE MAINTENANCE TECHNOLOGY

Predictive maintenance is a subgroup of condition-based maintenance, in which known operating conditions, that can lead to condition changes, are preferentially monitored and corrected after detection with the objective of preventing machine failures. The changing operating conditions are identified by root cause analysis. Before faulty operating conditions can be diagnosed, anomalous process states and failures must be detected by comparing them to a normal reference condition (fault detection) [5, 6].

Subsequently the fault diagnosis identifies the type of the fault, localizes the fault in the system and quantifies the magnitude of the fault effect [5, 6].

Fault detection and fault diagnosis for pneumatic actuators using sensor systems is a well-known topic in scientific literature. In [7] the dynamic performance of an industrial globe control valve unit is monitored via a temperature sensor, a pressure transducer, a displacement sensor and a flow transmitter. For fault diagnosis they analyze waveform characteristics based on main statistical properties of the data, captured by the sensors. Subbaraj and Kannapiran investigated fault detection in pneumatic actuator valves for cooler water spray systems in cement industry by using principle component analysis for input feature dimension reduction [8] and an artificial neural network (ANN) model for classification [8, 9]. Further investigations on fault detection for pneumatic actuators in control valves using ANNs are described in [10, 11]. In [12] three different types of cylinder leakages are considered by an ANN approach to predict the leakage orifice. The input features are captured by two proximity sensors, one working pressure sensor, two pressure transducers in each cylinder chamber and a differential pressure transducer for air flow determination. Mahmoud et al. [13] use sensor-detected acoustic emissions of micro-structural changes in the material of pneumatic cylinders for condition monitoring. The average energy of the acoustic emission signal is used as metric for fault detection. None of these works investigated a minimal sensor use, consisting of only two proximity sensors at the end positions of a linear pneumatic cylinder towards the practicability of predictive maintenance.

Predictive maintenance is not only a relevant topic in the scientific world, also many companies have already presented solutions or offer corresponding products. Examples at component level are the monitoring of roller bearings [14], plastic plain bearings and drag chains [14] as well as pumps [16] or electric motors [16, 17]. What all these examples have in common is, that sensors are available for condition monitoring, some of which are even supplemented separately. An example is the addition of a sound sensor [18].

Pneumatic companies also have shown first examples for predictive maintenance, e.g. the monitoring of shock absorber functions or cylinder speeds based on an electro-pneumatic valve system [19]. In this case, only the digital information of a standard pneumatic system is used.

3. APPLICATION EXAMPLE PNEUMATIC CLAMPS

Pneumatic clamping systems were selected as an application example to investigate whether sufficient data is available in standard pneumatics that allow statements about the operating conditions of the drive system. Such clamps are widely used in body-in-white construction (cp. **Figure 2**). From a pneumatic point of view clamps are double acting cylinders with oval piston. The piston is part of a toggle joint mechanism (cp. **Figure 3**).

Clamps are an interesting example, because the price pressure for such pneumatic components is very high. The willingness of automobile manufacturers to pay for additional sensor technology for the clamps tends towards zero. That's why in the foreseeable future the minimum sensor technology will be installed only. On the other hand, a plant shutdown is very expensive for manufacturers due to the loss of production.
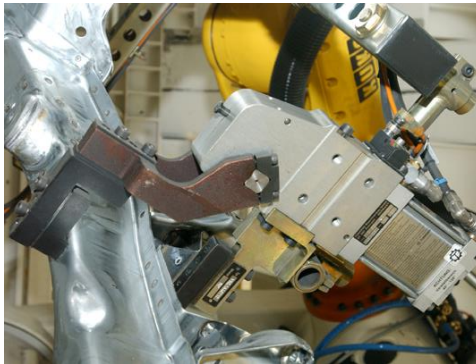
Figure 2: Pneumatic clamps in body-in-white construction [20].
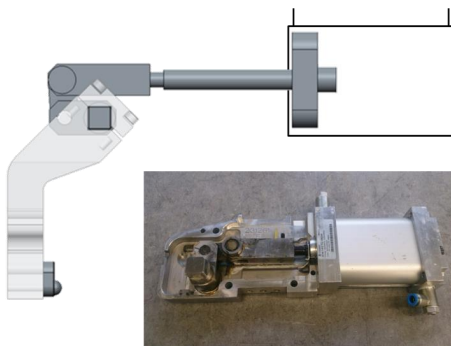
Figure 3: Structure of a pneumatic toggle level clamp.

Furthermore, clamping units offer relatively clearly defined conditions: All clamps perform a very similar movement, the main differences in the clamps lie in the size, the angle range and the clamping arm used. Thus, the application example is very suitable for investigating and generalizing the feasibility of predictive maintenance for pneumatic linear actuators with a minimal sensor use.

4. ENDURANCE TEST WITH CLAMPING UNITS

In a first step, an endurance run was started in which a total of six clamps were tested until end of life (cp. **Figure 4**). The recorded data was used to determine whether any changes in the available data could be detected before a failure. And if so, how far in advance.

Figure 4: Picture of endurance test with six clamps.

In **Figure 5** the corresponding circuit diagram of the endurance run is depicted. It shows that the six clamps are only controlled by three valves. The first valve switches one clamp, the second valve switches two clamps and the third valve switches three clamps. This is quite common in real body-in-white production. Here, one valve controls a number of 1 to 7 clamps.

Only the valve shifting signal and the two signals from the proximity sensors are included in the signal evaluation for each clamp. Two times each for closing and opening the clamp can be derived from these three digital signals, thus in sum four times (cp. **Figure 6**).
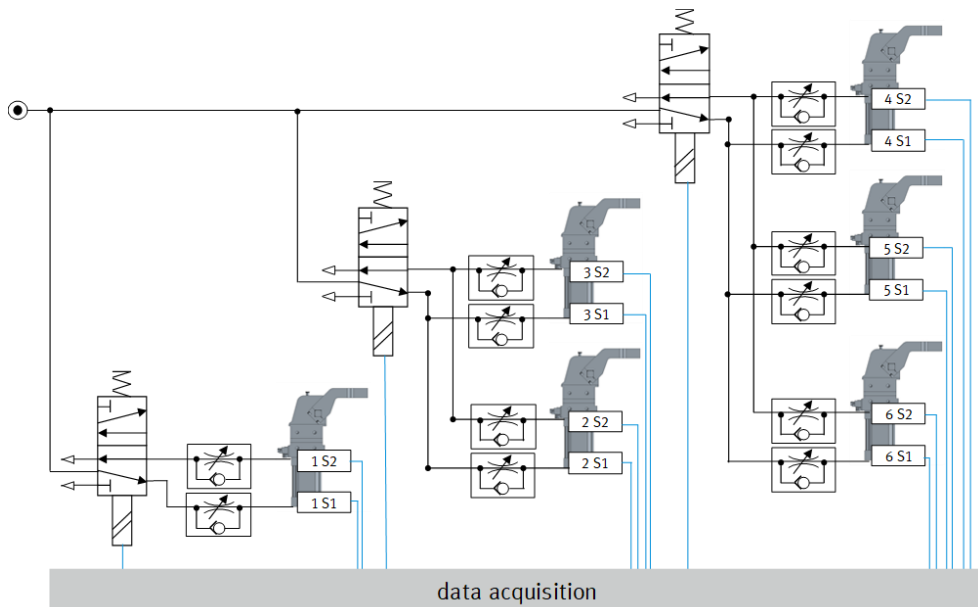
Figure 5: Circuit diagram and data acquisition of endurance test.

- The **reaction time** is the time between the valve signal and leaving the first end position.
- The **travelling time** is the time between leaving the first end position and reaching the second end position.

The results of this endurance run can be summarized as followed: With a lead time of 2 to 4 days changes occur in the four times described. As an example, **Figure 7** shows the signal characteristics of the travelling times for closing (extracting of clamp) and opening (retracting of clamp) before failure. Minimum, maximum and mean values are given for each direction.

The endurance run was operated at a higher frequency than actually occurs in a production line in automotive engineering. Thus, there is a chance to make a maintenance recommendation sufficiently early by monitoring the clamps.

Furthermore, the results underline why a machine learning approach for clamp monitoring makes sense. Although the design was very similar for each clamp e.g., same installation position and same lever arm, there are individual times for each clamp which must be learned separately.
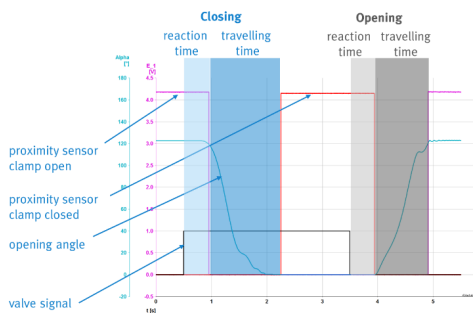
Figure 6: Time definitions.
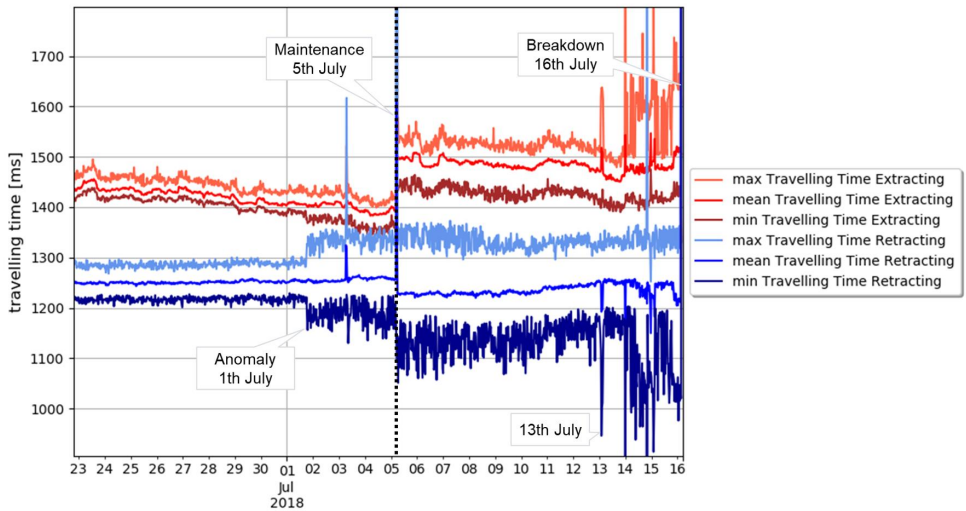
Figure 7:   Exemplary signal characteristics of the travelling time in case of failure of a clamp.

5. FAULT CLASSIFICATION

The endurance run has shown that one can (hopefully) derive information from the digital signals in time, that the operating conditions have changed compared to the normal process states at the beginning of data recording. The next step is to ask in the sense of fault diagnosis whether one can also read from the data what is the root cause of the changing in the operating condition be-haveior. This aimed at fault localization and/or fault description, both of which can be helpful for targeted and faster maintenance.

First of all, fault classification takes place at component level. Using known information from the circuit diagram, it can be concluded which of the components involved is out of order. If, for example, all clamps connected to the same valve extend with a delay, this is probably due to a cause affecting the whole pneumatic drive system, e.g., the valve, the pressure supply or leakage. If only one of the clamps extends with a delay, it is probably due to a problem with this specific clamp.

Furthermore, fault classification is possible at function level of the clamp or the valve. To investigate this, a test bench with a single clamping unit was created (cp. **Figure 8**) where defined errors easily can be added to the system.
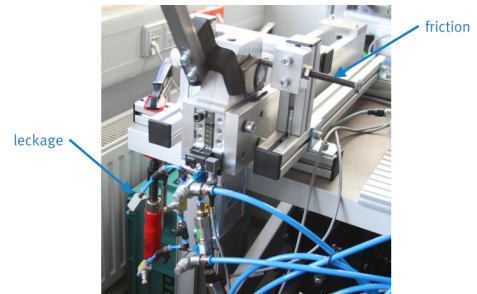
Figure 8: Test bench to add defined errors.

This is a procedure well-known from condition monitoring investigations (cp. [6, 21, 22]).

In the following subsections, two faults are described as examples: A leakage at the upper cylinder chamber (chapter 5.1) and a friction at the clamping arm (chapter 5.2). The conclusions of the test bench results are presented in chapter 5.3.

5.1. Leakage at the upper cylinder chamber

Leakage is one of the well-known possible faults of pneumatic systems. Leakage can theoretically occur in all pneumatic components: In tubes, fittings, valves, one-way flow control valves and cylinders. In cylinders (and valves), a distinction can be made between internal leakage from one

Table 1: **Influence of a leakage at the upper cylinder chamber on reaction and travelling time (normalized)**

	closing		opening	
	reaction time	travelling time	reaction time	travelling time
leakage 0 %	100 %	100 %	100 %	100 %
leakage 6 %	94 %	93 %	103 %	99 %
leakage 36 %	77 %	72 %	111 %	97 %
leakage 100 %	62 %	51 %	137 %	89 %

Table 2: **Influence of friction at the clamping arm on reaction and travelling time (normalized)**

	closing		opening	
	reaction time	travelling time	reaction time	travelling time
friction 0 %	100 %	100 %	100 %	100 %
friction 25 %	136 %	97 %	99 %	107 %
friction 50 %	216 %	99 %	104 %	115 %
friction 100 %	225 %	133 %	115 %	130 %

chamber to another and external leakage from one chamber to the environment.

As an example, external leakage at the upper cylinder chamber of a clamp is investigated below. For this purpose, a precisely adjustable throttle is integrated between the cylinder chamber and the associated throttle check valve, which vents the chamber into the environment (cp. **Figure 9**). For the measurements, the throttle is set to a desired leakage flow at a given inlet pressure.

The changes in the four times considered for different leakages are shown in **Table 1**. The results are explained below.

In the open position of the clamp (cp. **Figure 9**), the upper cylinder chamber is connected to the supply pressure, the lower cylinder chamber to the environment. The added leakage slightly reduces the pressure in the upper cylinder chamber in this position. If the valve is switched, the upper cylinder chamber is exhausted. The leakage causes a larger amount of air flowing out of the chamber, the pressure drop is faster. Thus, the cylinder movement starts faster, i.e. the reaction time when closing is reduced. During the movement, the leakage acts here like a larger opening of the throttle check valve, too. The movement time when closing the clamp is therefore also reduced.

In the closed clamping position (cp. **Figure 9**), the upper cylinder chamber is exhausted, and the

lower chamber is filled with supply pressure. After shifting the valve, the upper chamber must
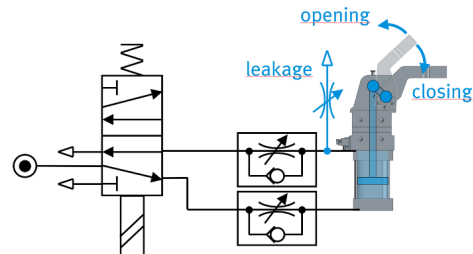
Figure 9: Leakage at the upper cylinder chamber.

be filled with pressure. This pressure build-up is slowed down due to the leakage, so the reaction time during opening is slightly increased. However, as long as the leakage remains limited, the travelling speed hardly changes. Because of the supercritical flow through the exhaust air throttle, the movement is initially independent of fluctuations in the drive pressure. If, however, the leakage in the upper chamber is increased to such an extent that the cylinder breaks away much later, the chamber pressure in the lower chamber drops further and further. This significantly increases the movement speed at the beginning of the return stroke, which results in a shorter travelling time.

5.2. Friction at the clamping arm

Changes in friction behavior is a second category of possible defects that is important in practice. Changes in friction can essentially occur at the valve spool or at the dynamic seals of the cylinder (clamp). Furthermore, the clamping arm can grind, which corresponds to increased friction on the load side of the toggle lever gear. This case is described in more detail now. On the test bench, a screw is placed on the clamping arm so that it grinds past the screw (cp. **Figure 8**). Even if this looks rather rough, a grinding of the clamping arm is still a case of damage, which occurs in rare cases in automobile production.

It should be noted that the change in friction force cannot be adjusted as precisely with the test setup as the change in leakage. For this purpose, a force sensor and an additional drive would have had to be integrated. This effort has not been made. Accordingly, the results of the friction change shown in **Table 2** are to be considered rather qualitatively.

The increased friction on the clamping arm has the greatest effect at the start of the closing movement of the clamp. The closing movement does not begin until the increased static friction has been overcome. In order to generate the necessary pressure difference, a reaction time that increases with increasing friction is necessary. With lower friction forces, the travelling time is then initially independent of the friction; only with very high friction forces does the travelling time increase. This is the result of the supercritical pneumatic movement, which is at first approximation independent of the load.

The influence on the reaction time during opening is considerably lower than during closing. At the beginning of the opening movement, the main load of the drive is the overcoming of the toggle lever. Therefore, noticeable changes in reaction times only occur when friction forces are high. The following movement shows a clear dependence: the higher the friction, the longer the travelling time. The difference between opening and closing travelling times can be explained, among other things, by the different influence of the weight force depending on the direction of movement. This means that the mounting situation of the clamp has a relevant influence on the travelling times.

5.3. Conclusion of the test bench results

As the description of the two test cases leakage at the upper cylinder chamber and increased friction at the clamping arm have shown, the introduced errors have a very different effect on the four considered times resulting from the few available digital signals. The result is an error-typical pattern in the times that can be used for predictive maintenance. In the same way as for the two example errors, a pattern can also be identified for other faults such as leakage or friction elsewhere, obstructed throttle or changes in supply pressure. Fortunately, these are indeed specific patterns that can be explained using mechanical and pneumatic expertise.

The example also shows, that condition-based monitoring with limit and trend checking of just single sensor signals cannot provide an appropriate and exact fault discrimination for fault diagnosis.

Due to the large number of faults, the intensity of the effect depending on the degree of error as well as the fault interdependencies between various sensor signals, more complex methods of fault detection and diagnosis are needed to describe the anomaly and failure behavior. And this is exactly what machine learning can guarantee. The strength of this data analytic techniques lies in learning complex patterns and assigning them to normal and anomalous states.

6. FIELD TRIAL

Due to the promising results, a pilot project was started at a car manufacturer to investigate the feasibility of the laboratory results in practice. Details of the results are subject to confidentiality. The tests are still ongoing. In the following section, however, the concept for implementing data acquisition and machine learning can be briefly discussed.

Acquiring data can be done on several system levels with a different granularity (see **Figure 10**). On the very lowest level – the field level – data like shifting time of limit switches and valves can be directly read from a valve terminal via the field bus. This could be a solution for retrofitting scenarios where the PLC should not be modified. If this restriction does not exist, it is also possible to directly contact the PLC for acquiring the necessary data. In both cases, a so-called edge-device or IoT-Gateway is typically

capable in receiving this data. On the other hand, a plant PC is typically installed close to a machine cell which receives data from the PLC.

With this in mind, two possible targets exist for executing analytic models, i.e. an edge-device/IoT-gateway or the plant PC.

While the edge-device can be installed without interference of the machine, some software installations are necessary at the plant PC. In our approach, we distinguish between model execution and training. The training phase requires large data batches with historical data and the model execution typically has real-time constraints and requires streaming data from the machine. Therefore, the configuration and training of analytic models is implemented on an engineering PC or in a cloud platform. This has the advantage that only during a training phase data needs to be sent to the cloud and later on, only analytic results from e.g. the edge-device will be transmitted. This reduces the cost for data transmission because the high-frequent traffic is processed close to the machine.

Once the model is trained and loaded to the computational resource close to the machine, it can be executed and will produce results. In such a setup, several methods exist for providing results to the operator:

1. via dashboards in a cloud,
2. via a PLC to an MES system or
3. via a panel installed to the machine cell.

7. CONCLUSION AND OUTLOOK

The paper shows that even with the limited number of data from a minimum of sensor use in standard pneumatics, valuable information about the operation process states can be derived. The acquired data is sufficient for accurate fault detection and fault diagnosis. An endurance run with pneumatic clamps has shown that changes can be seen in the reaction and travelling times about 2 to 4 days before failure. In addition, a test bench was used to prove that typical faults in the pneumatic system lead to different patterns in the four calculated times. Thus, these data can be used for a more detailed fault description and localization. Finally, a current field test was described in which the findings are tested in practice. If the practical test is successful, the predictive maintenance of the clamps will be commercialized.
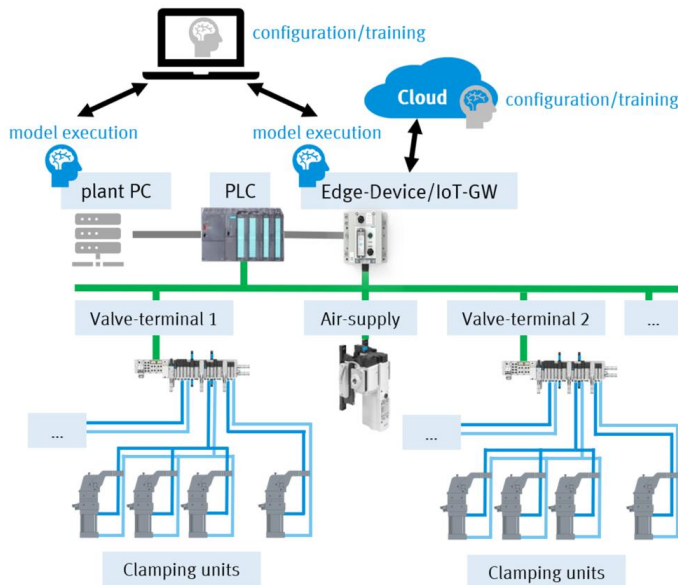
Figure 10: Concepts for data acquiring.

REFERENCES

[1] Predictive Maintenance - Servicing tomorrow - and where we are really at today, VDMA, April 2017

[2] Quick Guide Machine Learning in Mechanical and Plant Engineering, VDMA, 2018

[3] J. Lunze, Regelungstechnik 2. Berlin, Heidelberg: Springer Berlin Heidelberg, 2014.

[4] O. Föllinger, „Regelungstechnik", 11. Auflage, 2013, VDE Verlag, Berlin Offenbach

[5] DIN/VDI-Normenausschuss Akustik, Lärmminderung und Schwingungstechnik, „Condition monitoring and diagnostics of machines – General guidelines (ISO 17359:2018)", DIN ISO 17359:2018-05, 2018

[6] S. Fritz, "Verfahren zur Erkennung sowie Diagnose von Fehlern in pneumatischen Systemen und Komponenten", PhD Thesis, RWTH Aachen, 2011

[7] M. A. Sharif und R. I. Grosvenor, „Sensor-based performance monitoring of a control valve unit", Proc. Inst. Mech. Eng. Part E J. Process Mech. Eng., Bd. 213, Nr. 2, S. 71–84, Mai 1999.

[8] P. Subbaraj und B. Kannapiran, „Artificial Neural Network Approach for Fault Detection in Pneumatic Valve in Cooler Water Spray System", Int. J. Comput. Appl., Bd. 9, Nr. 7, S. 43–52, Nov. 2010.

[9] P. Subbaraj und B. Kannapiran, „Fault Diagnosis of Pneumatic Valve Using PCA and ANN Techniques", in Trends in Computer Science, Engineering and Information Technology, 2011, S. 404–413.

[10] J. F. Gomes De Freitas und I. M. Macleod, „Neural Networks For Pneumatic Actuator Fault Detection", Trans. South Afr. Inst. Electr. Eng., Bd. 90, 1999.

[11] M. Karpenko und N. Sepehri, „Neural network classifiers applied to condition monitoring of a pneumatic process valve actuator", Eng. Appl. Artif. Intell., Bd. 15, Nr. 3–4, S. 273–283, Juni 2002.

[12] Ž. Nakutis und P. Kaškonas, „Application of ANN for pneumatic cylinder leakage diagnostics", S. 6, 2005.

[13] H. Mahmoud, P. Mazal, F. Vlasic, und M. Jana, „Condition Monitoring of Pneumatic Cylinders by Acoustic Emission", in Applicaion of Contemporary Non-Destructive Testing in Engineering, Bernardin, Slovenia, 2017, S. 8.

[14] A. Tiede, „Der spannende Weg von Predictive Maintenance zu Industrie 4.0", Accessed 05/08/2019 https://www.easyfairs.com/fileadmin/groups/9/maintenance/Dortmund_2018/PDF/17_Tiede_Schaeffler.pdf

[15] IGUS GmbH, „Smart plastics", Accessed 05/08/2019, https://www.igus.at/_Product_Files/Download/pdf/DE_smart_plastics_2019_screen.pdf

[16] Phoenix Contact, „Predictive Maintenance - Lösungen für die Überwachung von Pumpen und Motoren", Accessed 05/08/2019, https://www.phoenixcontact.com/assets/downloads_ed/global/web_dwl_promotion/1065451_DE_DE_PumpMonitor_LoRes.pdf

[17] R. Näther, „Vernetzte Elektromotoren für Predictive Maintenance", Accessed 05/08/2019, https://www.elektrotechnik.vogel.de/vernetzte-elektromotoren-fuer-predictive-maintenance-a-774056/

[18] Neuron Soundware, „Machine Whisperer", Accessed 05/08/2019 https://www.neuronsw.com/machine-whisperer-neuron-soundware-presents-three-world-firsts-at-hannover-messe/

[19] Aventics, "Intelligent Pneumatics Drives Predictive Maintenance Forward", Accessed 05/08/2019 https://www.aventics.com/media/about_us/AVENTICS_at_a_glance/Press/Pressemitteilungen/Aventics_PI_005_17_HMI_Predictive_Maintenance_EN.pdf

[20] Tünkers, "Standardspanner", Accessed 18/12/2019 https://www.tuenkers.de/publish/binarydata/service/download/standardspanner_de.pdf

[21] S. Mundry, „Zustandsüberwachung an Prozessventilen mit intelligenten Stellungsreglern", PhD Thesis, RWTH Aachen, 2002

[22] R. Gutiérrez González, "Development of a diagnostic concept for pneumatic systems and components", PhD Thesis, RWTH Aachen, 2012

DEVELOPMENT OF A LUMPED PARAMETER MODEL OF AN AEROSPACE PUMP FOR CONDITION MONITORING PURPOSES

Geneviève Mkadara*, Pr. Jean-Charles Maré

Institut Clément Ader, INSA de Toulouse, 3 rue Caroline Aigle, 31400 Toulouse, France

* Corresponding author: Tel.: +33 442 858190; E-mail address: mkadara@insa-toulouse.fr

ABSTRACT

This paper presents the development of a helicopter axial piston pump model with condition monitoring in mind. Industrial constraints and needs ask for modelling with a lumped-parameter approach and require model architecture to be addressed with care. The aim of the proposed model is to assess the merits of pump leakage monitoring through measurement of case pressure. Once reviewed the state of the art in pump modelling, the slipper/swashplate interface is taken as an example to propose and implement in Simcenter AMESim a variable gap height model. The simulation results show that commonly used lumped-parameter models overestimate leakage. It also points out that average leakage at slipper may reverse at high pump displacement.

Keywords: Axial piston pump, Helicopters, Modelling, Model architecting

1. MOTIVATION

In the current years, as an increasing interest has been brought to the industry on costs reduction and client satisfaction, maintenance has been under scrutiny for all the benefits that its improvement can bring. One of the main potential of advances is to transit from scheduled maintenance to predictive maintenance. This change of paradigm significantly increases product availability through a prediction of its remaining functional life-time. Steps to switch from planned to predictive maintenance are condition-based maintenance and condition monitoring. This trend is being considered by the authors' industrial partner, a rotorcraft manufacturer.

1.1. Industrial needs

For helicopters (H/C), maintenance of hydraulics is mainly scheduled with resort to the definition of time between overhauls (TBO), in particular for pumps and servoactuators. Flight controls of medium and heavy class H/C involve non reversible servoactuators that are hydraulically supplied. Therefore any pump failure is safety-critical and leads to rotorcraft grounding or mission aborting (and unscheduled landing) if failure happens in flight. A previous paper [1] has reported reliability considerations for axial piston

pumps that are installed on Airbus Helicopter fleet. Degradation of pump performance can be detected through observation of several measurements, e.g. acceleration [2] or discharge pressure [3]. As pump degradation often leads to increased internal leakage, an attractive solution consists in measuring the case drain flow, as addressed in [4]. In order to investigate the interest of the latter option, the reported work aims at developing an axial pump simulation model that is sufficiently realistic regarding the real internal leakage.

Two main schools of thoughts can be highlighted for general modelling: data-driven against physics-based. Data-driven approaches identify patterns from measured data and do not necessitate any knowledge on the modelled system. On the contrary, physics-based approaches rely on detailed internal system knowledge. When this latter approach is applied to engine-driven, variable-displacement, and pressure-compensated axial piston pumps, two types of models have been developed: distributed-parameter (sometimes called 3-D) models [5, 6] and lumped-parameter (sometimes called 1-D) models [7, 8].

Not being a hydraulic pumps Original Equipment Manufacturer (OEM), the rotorcraft manufacturer does not have access to extensive pump test data, which leaves out the data-driven

approach for pump modelling. On the other hand, the authors' industrial partner does not need very detailed 3-D models which generally require high computation loads and a lot of supplier proprietary information. In practice, the company needs a system-level pump model that can be interfaced with other sub-models of the H/C hydraulic systems. These reasons have favoured the adoption of a lumped-parameter approach for modelling the pump under study. Leakage being the focus of the monitoring approach, it is mandatory that the 1-D model includes the pump leakage paths. This contribution reports how the internal leakage can be modelled more accurately in the lumped-parameter frame, considering the gaps as varying quantities instead of fixed input parameters, as always assumed in this frame.

1.2. Industrial constraints

From the industrial point of view, the monitoring approach shall be sufficiently generic to be applicable to most axial piston hydraulic pumps of the fleet, throughout all H/C categories and flight operation types. In this light, the sensors used for monitoring shall not be pump intrusive, in order to not require any alteration of already certified pumps. The number of sensors added to the existing ones has to be minimized for cost and weight considerations. Moreover, the pump case drain flow cannot be measured directly on helicopters due to safety issues. This is why measuring the pressure directly at pump case port is used as an alternative in the present work. In our application the reservoir is opened to atmospheric pressure and there is no equipment prone to clogging on the return line. The hydraulic system at case port can then modelled as a fixed impedance. Finally, the monitoring approach shall be robust against temperature and atmospheric pressure variations induced by the wide operational domain of helicopters

(temperatures ranging from -40°C to +50°C, and altitude as high as 7000m).

This paper presents the development of a lumped-parameter simulation model of an axial piston pump meeting the above constraints. First, the model architecture is discussed. Then the pump model, its implementation and some simulation results are described with focus on the slipper/swashplate interface model that includes a variable gap height. Shortcomings of the presented model and ways to improve it conclude this publication.

2. ARCHITECTURE OF PUMP MODEL

The pump model is developed to meet an industrial need – assess the merits of case drain pressure measurement for monitoring the H/C pump through analysis of its internal leakage. As such, the model shall meet the requirements defined in **Table 1**. These requirements are either linked to the project purpose, or to the long-term durability of the model. The first requirement category is to be answered through modelling, while most of the second category can be managed through a proper model architecture.

Model architecture is of primary interest in an industrial context, where models need to be easily modified and reused by different actors. It consists in representing blocks (or super components, or sub-models) in a structured manner, including how they interconnect at their ports with other blocks or with the full model environment. When possible, explicit distinctions should be made to indicate whether the interconnections are considered as power or signal type. Several colours can also be used to differentiate technological domains. Defining an appropriate architecture is a necessary prerequisite to meet the durability requirement for an industrialized model (a model to be used in an industrial context). Not taking it into account

Table 1: List of requirements for the pump model

Project Purpose	
Rq1	Shall simulate accurate behaviour of internal leakage, as well as suction and discharge pressure and flow
Rq2	Shall be ready for simulation of pump degradation leading to increased internal leakage
Rq3	Shall enable to assess the monitoring approach
Durability	
Rq4	Shall be as generic as possible for further modifications, easy to assemble and modify (e.g. changing the number of pistons)
Rq5	Shall allow for parameters and mathematical expression modifications
Rq6	Shall grant easy access to the basic components of the model
Rq7	Shall be usable as a digital twin, also as "plug and simulate" (only applicable to the whole pump model)

leads to prototype-like models, with poor readability, capitalization and even potential for re-use of extension for anyone who was not in charge of the first model issue.

Model architecting is seldom discussed in the literature, because it initially stems out of overall shared pragmatism. Data-driven or 3-D models generally do not need to be architected. For lumped-parameter models, architecture is usually managed implicitly thanks to modellers' experience. Several published papers dealing with 1-D modelling of axial piston pumps show structured model, however without any discussion on architecting or structuration methodology, e.g. [8, 9]. Some lumped-parameter software editors now propose applications for automatic generation of pump models, following a pre-defined topologic architecture, e.g. [10]. Maré and Akitani [11] described the modelling of an electro-mechanical actuator and its associated architecture. In their work, the model architecture is derived from the product topology itself. In [12], Maré proposed a set of standard requirements for models, two of these requirements being "Workshare" and "Capitalization". It is there emphasized that an architecture based on the real product topology helps the understanding and reuse of the model, allowing to partially meet both requirements. It is the authors' opinion that model architecture should be defined during the first phases of a project, anticipating future modifications, extension or reuse of the model.

In practice, this task is iterative because it requires the interfaces between the blocks and their environment to be identified exhaustively. Once done, the blocks themselves can be filled with models which level of detail depends on the current engineering task needs. Depending on this level, some interconnections can remain (partially or totally) unused. The example of the pump block on **Figure 1** is used to illustrate this last statement. This pump block shows every pump ports and interfaces:

- For hydraulics: Suction (s) , Discharge (d), and Case ports (c) with pressure (P) and volume flow rate (Q) at each port;
- For mechanics: Torque (Γ) and angular velocity (ω), at drive shaft (m) and base (b);
- The thermal port with temperature (T) and heat flux (Φ).
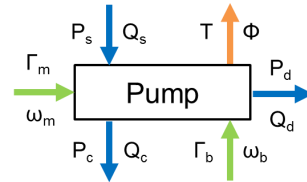
Figure 1: Schematics of pump model ports and interconnections to its environment

If the modeller wants to make a purely hydraulic model, both thermic and base ports will be totally unused. In this use case, the driving port will be partly used, as only the rotating speed is necessary for the modelling of the pumping effect.

Considering the practical implementation of the architecture, the authors present here two architecting approaches for an axial piston pump model The topology of such pump is shown on **Figure 2-a**, adapted from an EATON document. The first architecting approach, highlighted on **Figure 2-b**, defines blocks from pump inner functions which come in four: pump fluid, distribute fluid, regulate flow, and collect leakages. On **Figure 2-c** the model is structured per pump part as a second. Both **Figure 2-b** and **Figure 2-c** make the distinction between mechanical and hydraulic interconnection through the use of colours. Thermal interconnections are not shown for the sake of clarity.

Durability requirements of **Table 1** are used in order to choose between these two candidate model architectures. Except for Rq7 which is only applicable to the full pump model, the consequences of the durability requirements on architecture are the following:

- Rq4 – At least one block per pump part should be defined, the interconnections with other blocks shall be straightforward and the architecture prepared for future modifications;
- Rq5 – The blocks should be modifiable white-boxes;
- Rq6 – The architecture should be less than two-blocks deep, i.e. the models shall be available opening two block boxes at most, including the pump block.

These considerations, regarding Rq4 in particular, speak in favour of the topology-based architecture of **Figure 2-c**.
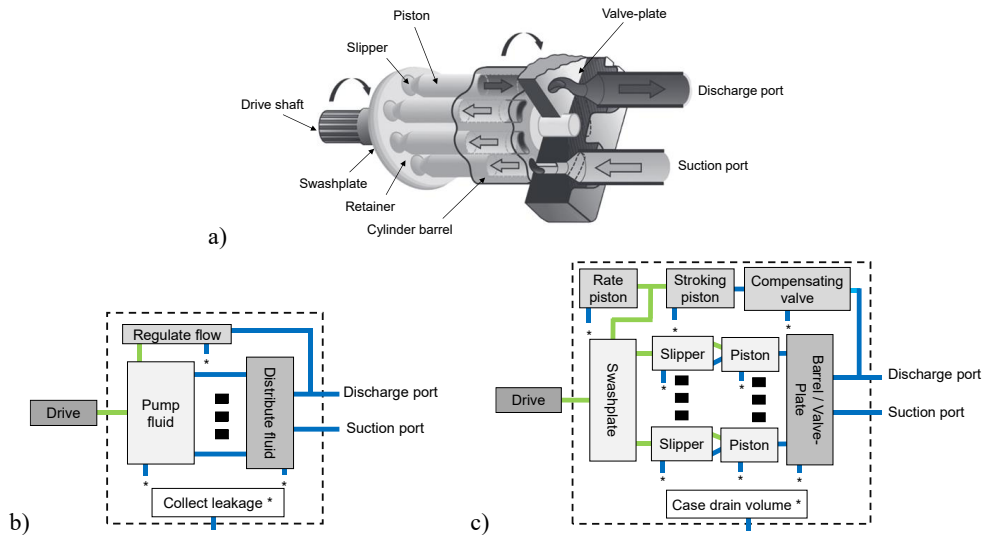
Figure 2: Pump topology and proposed architectures – a) pump cut, b) architecture by function, c) architecture by pump part

3. PUMP MODEL

In **Table 1**, Rq1 requires the simulation of leakage, case drain pressure, as well as pressure and flow at discharge and suction ports. An extensive work has been done to propose analytical models of pump main leakage paths, an interesting entry point being [13]. The synthesis of literature review is given in **Table 2**, considering both lumped and distributed-parameter models. The review focusses on the considered physical effects at leakage interfaces. When the interface is not considered in the paper, cells are coloured in grey. If there is no explicit mention to a given physical effect, the cell is left blank. The last column highlights the contribution of the model described in this communication.

Each listed source meets a particular need, favouring one model type. References [14], [5] and [6] describe in a very detailed way Computational Fluid Dynamics (CFD) models developed to study the influence of the pump design on its performance. Reference [15] discusses the slipper/swashplate interface from a lubrication point of view. Reference [7] aims at deriving lumped-parameter analytical equations of the pump flows. Reference [16] develops a 1-D model to study the influence of the hydraulic system on the pump behaviour, while reference

[17] highlights the AMESim software capacities for pump modelling. **Table 2** highlights the discrepancy between lumped and distributed-parameter modelling approaches. The first type of approaches considers far fewer physical phenomena compared to the second one. Pure lumped-parameter models of axial piston pumps only consider leakage with constant gap heights. On its part, this paper deals with the way to introduce variable gaps in a 1-D modelling paradigm. After having introduced generic lumped-parameter models of leakages, it focusses on the slipper/swashplate interface shown on **Figure 3**.
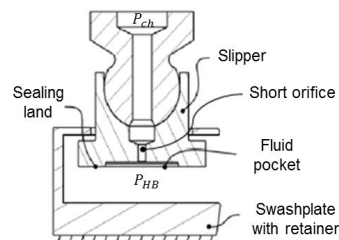
Figure 3: Slipper interface schematics adapted from [18]

Table 2: **Synthesis of main contributions relative to leakage modelling of axial piston pumps**

Interface	Physical effect considered	[14]	[5]	[6]	[15]	[7]	[16]	[17]	Presented model
(1) : Piston/barrel type	Tilt	O	**O**						
	Axial relative velocity	O	**O**			*Δ*	Δ		Δ
	Eccentricity	O	**O**				Δ		Δ
	Spin	O	**O**						
	Hydrodynamic forces	O	**O**						
	Varying gap length	O	**O**					Δ	Δ
	Variable gap height	O	**O**						
	Solid to solid contact	O	**O**						
	Local thermal effects	O	**O**						
	Elastic deformations	O	**O**						
(2) : Slipper/ swashplate	Tilt	O			O	*Δ*			
	Relative velocity	O			O	*Δ*			
	Spin				O				
	Hydrodynamic forces	O							
	Variable gap	O			O				Δ
	Solid to solid contact	O							Δ
	Local thermal effects	O							
	Elastic deformations								
(3) : Barrel / valve-plate	Tilt	O		O		*Δ*	Δ		
	Relative velocity	O		O		*Δ*	Δ		Δ
	Timing grooves	O				*Δ*			N/A
	Hydrodynamic forces	O		O					
	Variable gap	O		O					
	Solid to solid contact	O							
	Local thermal effects	O		O					
	Elastic deformations			O					

Legend:			
Δ	Lumped-parameter	O	Distributed-parameter
Bold	Compared to experiments	*Italic*	Compared to CFD models

3.1. Generic 0D leakage pair models

The **Table 3** summarizes the well-known lumped-parameter models relative to the generic leakage sources that appear in pressure compensated, axial piston pumps [13]. Although several leakage paths exist at barrel/valve plate interface, only the leakage from a valve plate port to the case is considered in the table.

When used for the slipper/swashplate interface of the pump considered in the present work, this provides the numerical values of **Table 4** if the pressure drop from piston chamber to slipper pocket is neglected. A constant gap height of 17 microns is used for the computation. This gap height is the one obtained from hydrostatic lift at 160 bar. To compute the total leakage $Q_t{*}$ for nine pistons, it is considered here that four piston

chambers are at discharge pressure while the other five are at suction pressure.

For the pump used in this study, the supplier specified maximum allowed leakage is 1.5L/min, but the result of the leakage computation for the slipper alone gives 97.5% of this maximum flow rate, without considering transient effects. This simple calculation shows that using the generic leakage model at slipper/swashplate interface leads to an unrealistic result.

In the current study, the authors aim at developing a lumped-parameter model with correct representation of the pump leakage. In order to improve the current state of the art for 0D models of the leakage interfaces, many physical effects can be taken into account. In the following part, a step forward to a more accurate model of the swashplate/slipper leakage through a variable gap height using a lumped-parameter approach is discussed.

Table 3:   **Generic pump leakage lumped-parameter models with pump cut adapted from [14]**
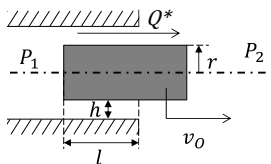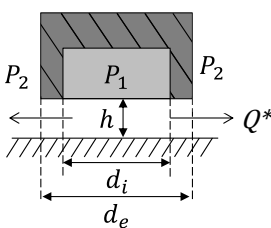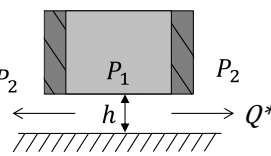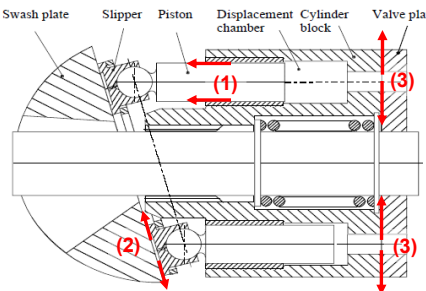
Leakage	Generic form of the leakage	Analytical formulation [13]
(1) Annular leakage with variable length: Pistons / housing		For a centred piston with speed and no spin : $Q* = \frac{\pi}{6\mu}\frac{P_1 - P_2}{l} rh^3 + \pi r v_0 h$ Where r is the piston radius, h the gap height, and v_0 the piston velocity, P_1 and P_2 the chamber and case pressures respectively.
(2) Hydrostatic bearing: Slippers		Laminar flow and logarithmic variation of the pressure along the radius, without spin or tangential velocity: $Q* = (P_1 - P_2)\frac{\pi h^3}{6\mu \ln\left(\frac{d_e}{d_i}\right)}$ Where h is the gap height, d_e and d_i the bearing external and internal diameter respectively, P_1 and P_2 the internal and external bearing pressures respectively.
(3) Valve-plate / barrel		Laminar flow, barrel not tilted and relative speed not considered: $Q* = (P_1 - P_2)\frac{\pi h^3}{12\mu}\int\frac{1}{l}d\lambda$ Where p_1 is the port pressure, p_2 the case pressure, h the gap height and l and λ geometrical features depending on barrel angular position.

Table 4:   **Total leakage from slipper/swashplate interface using the generic leakage model**

Variable	Pp [bar]	Pc [bar]	h [μm]	$Q*$ [L/min]	Q_t* [L/min]
Value	160 1.8	3	17	0.37 -0.0034	1.463

3.2. Proposition of a slipper/swashplate variable gap model

It is today well known from experiments [19] and 3-D simulation, e.g. [14], that the effective geometries of the gaps are not as ideal as the ones that enable formal calculations. The facing surfaces are not parallel and affected by parasitic additional motion, e.g. tilting and spinning of the slipper. However, the lumped-parameter models of axial piston pumps in literature only considered constant gap heights, and/or parallel surfaces, e.g. [7, 9, 16, 17]. In the particular case of the slipper/swashplate, there is very little consideration to the action of the retainer and to the pumping effect in the case domain.

As a step forward, the variable gap is proposed for the slipper/swashplate interface, with the following assumptions:

- There is no tilt of the slipper, slipper axis remains perpendicular to the swashplate plane;
- Hydrodynamic forces are neglected;
- Only 1-D displacements are considered, null component of the slipper/swashplate relative speed in the swashplate plane;
- All forces out of piston or slipper axial direction are neglected (no lateral friction, windage, centrifugal effect…).

Model

The gap height can be seen as the consequence of slipper and swashplate relative movement, which is constrained by the retainer. The kinematics without retainer is shown on **Figure 4**, where h is the gap height and $\vec{y}$ is the axis of the piston. Considering that there is no play between slipper and piston at pivot point A, the geometric parameters and variables are linked by:

$$l' = y_0 \cos \alpha - R \sin \alpha \qquad (1)$$
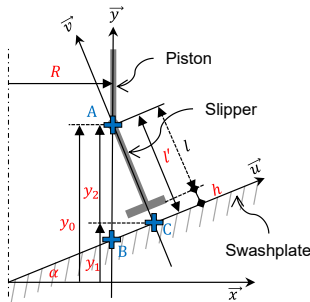
Figure 4:   Schematics for the slipper/swashplate gap kinematics

where y_0 is the piston axial position, and α the swashplate tilt angle. R is the horizontal distance between the piston and the swashplate tilting axis defined as:

$$R = -\frac{t_d}{2} \sin \theta \qquad (2)$$

with t_d being the diameter of the piston trajectory along the barrel rotation, and θ the angular position of the piston axis with respect to the pump frame. Then the gap height temporal variation is:

$$\dot{h} = \dot{l}' = \dot{y}_0 \cos \alpha - \dot{R} \sin \alpha - \dot{\alpha}[y_0 \sin \alpha + R \cos \alpha] \qquad (3)$$

The position y_0 is linked to the force balance on the piston. Hydrostatic and friction forces due to chamber and case pressures, as well as the force applied by the slipper are considered. Friction losses and backlash at slipper/piston ball joint are neglected. The pressure forces and contact forces applied on the slipper on swashplate and retainer, applied on piston axial direction, give $F_{sl/p}$, the force applied on the piston by the slipper:

$$F_{sl/p} = \left(F_{hb} + F_{cont} - F_{c/sl}\right) \cos \alpha \qquad (4)$$

The contact force F_{cont} is modelled as an elastic end-stop model for both swashplate and retainer sides. Consequently, it can be either negative or positive depending on which solid is reached. $F_{c/sl}$ is the pressure force applied by the case fluid on the slipper back, and is written as:

$$F_{c/sl} = \frac{\pi d_e^2}{4} P_c \qquad (5)$$

where P_c (P_2 in **Table 3**) is the case pressure. Considering laminar flow in the gap, the pressure force F_{HB} on the slipper is:

$$F_{HB} = P_{hb} S_{eq} = P_p \frac{\pi(d_e^2 - d_i^2)}{8 \ln d_e/d_i} \qquad (6)$$

with d_e and d_i the external and internal diameters of the slipper bearing, respectively. The pressure P_{hb} in the slipper pocket (P_1 in **Table 3**) is calculated from the mass conservation, from the flow from piston to slipper pocket (through the fixed short orifice), and from slipper pocket to pump case (through the slipper/swashplate gap), considering the fluid compressibility. The leakage flow in the gap is computed as expressed in **Table 3**.

The torque generated on the swashplate by the pressure force at slipper interface and by contact forces is also modelled. It is assumed that the

slipper trajectory on the swashplate is circular, and that of the swashplate tilting axis passes through the centre of this trajectory.

Model implementation

The model is implemented in the Simcenter AMESim environment (v14) that is based on power bonds. However, due to the approach taken to express the gap height, a signal view is also taken to integrate the barrel rotating speed. The implemented model is given on **Figure 5**. The pressure force from the gap is considered through a piston ❶ with the equivalent section S_{eq}. The gap height is bounded with an end-stop model ❷ that also supplies the $F_{contact}$ force. The influence of the case pressure on the slipper is taken into account through the piston model ❸. The projection of the forces on the slipper axis is made at ❹. The leakage from the piston to the case flows through the first short orifice ❺, then through the slipper/swashplate gap ❻ which is implemented as a variable orifice.

Results

In order to compare the simulation results from the model to that of the generic equations presented in part **3.1**, a simulation of a single piston/slipper subassembly is made. **Table 5** lists the numerical results for the mean simulated slipper leakage over one pump shaft revolution, computed with the same pressure boundary conditions as in **Table 4**. The total leakage at slippers Q_t is compared to the generic model Q_t^* through relative error (Er) computation ($Er = 100(Q_t^* - Q_t)/Q_t^*$). The total leakage at slippers Q_t is at least 19.34% lower than that of the generic model Q_t^* (which is independent from swashplate yoke) whatever the pump

displacement. It is interesting to note that at maximal pump displacement, the simulated leakage becomes negative, meaning that the slipper averagely sucks from the pump case.

Table 5:   Comparison of total leakage at slipper/swashplate interface for 1 rev.

Variable	α [deg]	Q_t^* [L/min]	Q_t [L/min]	Er [%]
	0		1.18	19.34
Values	5	1.463	0.9	38.48
	15.15		-0.29	119.82

In order investigate this, the simulated slipper/swashplate clearance over two pump shaft revolutions is shown on **Figure 6**. The simulated gap height variation from this figure complies with measurements made in [19]. **Figure 6** highlights two phenomena at low pump displacement. Firstly, the discharge (high) pressure generates slipper lift as predicted by hydrostatic bearings theory. The second phenomena is linked to case pressure. This last point is specific to the present application where forces from case pressure are implemented on slippers and pistons back sections. The parameterized slipper back section is larger than that of the piston, which leads to piston/slipper subassembly displacement towards the swashplate during the suction phase.

For high displacement, **Figure 6** shows that the modelled pressure force under the slipper does not allow to lift it hydrostatically during the discharge phase. During the suction phase, the slipper is lifted up until it makes contact with retainer. As the case pressure is greater than the piston chamber pressure in this simulation, this movement leads to fluid intake at slipper. Both facts (no lift at discharge phase and fluid intake
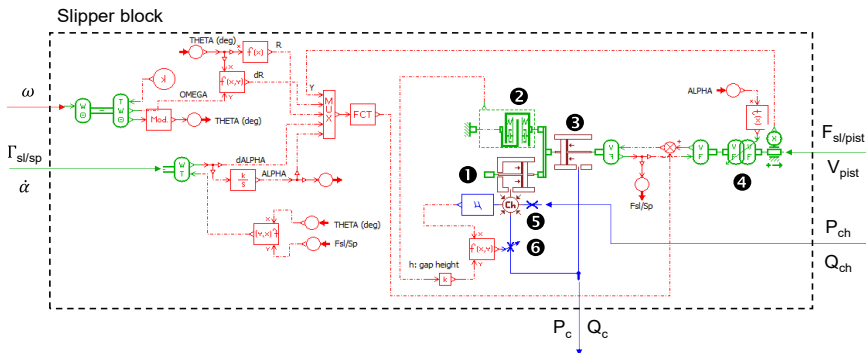
Figure 5:   Implementation of the slipper model in Simcenter AMESim (v14)
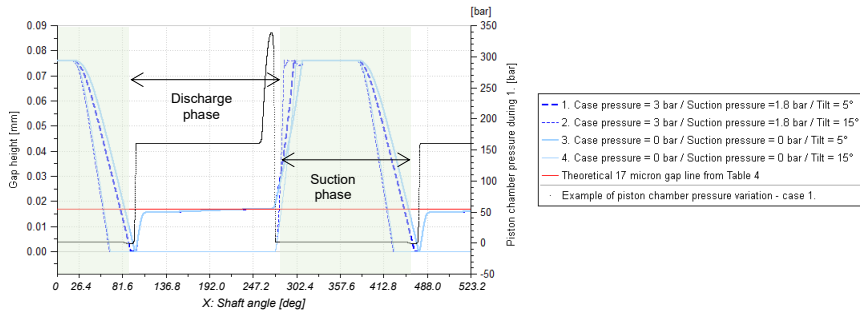
Figure 6:   Slipper/swashplate gap height over pump rotation in several simulation cases

during suction phase) explain the overall negative slippers leakage. Considering this result and the presence of contacts between slipper and swashplate, hint at the need to develop, integrate and validate a more detailed model that includes additional degrees of freedom.

4. CONCLUSION AND OUTLOOK

The development of a lumped-parameter model of an axial piston pump under industrial constraints has been presented. The model aims at assessing the feasibility of leakage monitoring through the measurement of the pump case pressure, leading to the need of pump leakage paths accurate modelling.

The model architecting in the industrial context has been addressed in order to facilitate the building of a durable and capitalized model. This lead to select an architecture based on the pump topology.

The state of the art in axial piston pumps modelling has been summarized to point out the well-established or missing knowledge. Then, a slipper/swashplate lumped-parameter model with variable gap height has been proposed to improve the representativeness of the current 1-D models, which are lacking in accuracy compared to distributed-parameter models. It has been shown that the proposed model shows less slipper-due leakage over a pump revolution than the generic model. However, the variable gap model is highly dependent on the case and suction pressures as well as pump displacement. Simulation results show that the slipper and the swashplate enter into contact at high pump displacement, which is not realistic.

Several improvements to the variable gap model are foreseen. One of them consists in introducing the slipper tilt. To this end, forces in every direction must be taken into account, leading to a 3-D lumped-parameter model. Another option consists in generating metamodels from CFD simulation, to supply the gap height to the model as a function of operating conditions. This approach would also enable introducing hydrodynamic effects that are currently missing in the presented model. Both options will be studied and compared in terms of final computation time and physical representativeness.

ACKNOWLEDGEMENTS

NOMENCLATURE

α	Swashplate tilt [rad or deg]
θ	Piston axis angular position [rad]
μ	Fluid dynamic viscosity [Pa.s]
$\omega_{b,m}$	Rotating speed (base or motor) [rad/s]
$\Gamma_{b,m}$	Torque on pump (base or motor) [N.m]
Φ	Thermal flux [W]
d	Slipper bearing diameter [m]
t_d	Piston circular trajectory diameter [m]
d	Slipper bearing diameter [m]
F	Force [N]
$h, \dot{h}$	Gap height and temporal variation [m, m/s]
$l', \dot{l}'$	Variables defining slipper kinematics [m, m/s]
P	Pressure [Pa or bar]
Q	Flow [m³/s or L/min]
Q^*	Theoretical leakage flow at one slipper [L/min]
$R, \dot{R}$	Variables defining slipper kinematics [m, m/s]
S_{eq}	Equivalent hydrostatic surface on slipper [m²]
T	Pump temperature [°C]
$y, \dot{y}$	Piston displacement and velocity [m, m/s]

Recurrent subscripts

c	Case
ch	Piston chamber
cont	Contact
d	Discharge
e	External
hb	Hydrostatic bearing
i	Internal
p	Piston
s	Suction
sl	Slipper
t	Total due to slippers (over 1 rev)

REFERENCES

[1] Paulmann G, Mkadara G (2018) Condition Monitoring of hydraulic pumps – lessons learnt. 11th Int. Fluid Power Conf., March 19-21, Aachen, Germany

[2] Torikka T (2001) Evaluation of Analysis Methods for Fault Diagnosis on Axial Piston Pumps. Proc. of the Twelfth Scandinavian International Conf. on Fluid Power (SICFP), Tampere, Finland, 18–20 May

[3] Gao Y, Zhang Q (2006) A wavelet packet and residual analysis based method for hydraulic pump health diagnosis. Proc. of IMechE, vol. 220 Part D: J. Automobile Engineering, pp. 735-745

[4] Kwan C, Xu R, Zhang X (2003) Fault Detection and Identification in Aircraft Hydraulic Pumps using MCA. Proc. of IFAC Symposium on Fault Detection, Supervision and Safety for Technical Processes, Washington, D.C., USA

[5] Pelosi M, Ivantysynova M (2009) A Novel Fluid-structure Interaction Model for Lubricating Gaps of Piston Machines. Proc. of the Fifth Fluid Structure Interaction Conf., eds. C.A. Brebbia, WIT Press, Southampton, pp. 13-24

[6] Ivantysynova M, Baker J (2009) Power Loss in the Lubricating Gap between Cylinder Block and Valve Plate of Swash Plate Type Axial Piston Machines, International Journal of Fluid Power, 10:2, 29-43

[7] Bergada J M, Kumar S, Davies D Ll, Watton J (2012) A complete analysis of axial piston pump leakage and output flow ripples. Applied Mathematical Modelling, Vol. 36, Iss. 04, pp 1731-1751

[8] Poole K, Raeth M, Thielecke F, Mädige C (2011) Leakage Diagnosis for Electric Motor Pumps in Aircraft Hydraulic Systems. Deutscher Luft - und Raumfahrtkongress, September 27-29, Bremen, Germany

[9] Mancò S, Nervegna N, Lettini A, Gilardino L (2002) Advances in the simulation of axial piston pumps. Proc. of the Fifth JFPS International Symposium, Nara, Japan

[10] Deléchelle O (2019) From CAD to Simulation - A Smooth Workflow to Model Axial Piston Pumps for EDP/EHA Systems, SIEMENS Digital Industry Software, Presentation at SAE A-6 meeting

[11] Maré J-C, Akitani S (2018) Foundation for Virtual Prototyping of Mechanical Power Management Functions in Actuators. Proceedings of the BATH/ASME 2018 Symp. on Fluid Power and Motion Control FPMC2018 September 12-14, Bath, UK

[12] Maré J-C (2019) Best practices for model-based and simulation-aided engineering of power transmission and motion control systems. Chinese Journal of Aeronautics, Elsevier, 32(1), p.186-199

[13] Ivantysyn J, Ivantysynova M (2003) Hydrostatic Pumps and Motors: Principles, Design, Performance, Modelling, Analysis, Control and Testing. Tech Book International

[14] Wieczorek U, Ivantysynova M (2002) Computer Aided Optimization of Bearing and Sealing Gaps in Hydrostatic Machines—The Simulation Tool Caspar. Int. Journal of Fluid Power, 3:1, 7-20

[15] Chao Q, Zhang J, Xu B, Wang Q (2018) Discussion on the Reynolds equation for the slipper bearing modeling in axial piston pumps, Tribology International, Vol. 118, pp 140-147

[16] Aaltonen J (2016) Interaction of Bootstrap Reservoir and Hydraulic Pump in Aircraft Hydraulic Systems. PhD Dissertation, Tampere University of Technology, Finland

[17] Simcenter AMESim demo TwoDOFSwash. Model of a pressure compensated axial piston pump of the swash plate design. Available via software help menu

[18] Schenk A T (2014) Predicting lubrication performance between the slipper and swash-plate in axial piston hydraulic machines. Open Access Dissertations. 359. Available at http://docs.lib.purdue.edu/open_access_dissertations/359

[19] Chao Q, Zhang J, Xu B, Wang Q (2018) Multi-position measurement of oil film thickness within the slipper bearing in axial piston pumps. Measurement, Vol. 122, pp 66-72

CONDITION MONITORING SYSTEMS FOR HYDRAULIC ACCUMULATORS – IMPROVEMENTS IN EFFICIENCY, PRODUCTIVITY AND QUALITY

Christian Nisters*, Dr.-Ing. Frank Bauer, Marco Brocker

HYDAC Technology GmbH, Industriestraße, 66280, Sulzbach/Saar, Germany

* Corresponding author: Tel.: +49 6897 5099555; E-mail address: christian.nisters@hydac.com

ABSTRACT

This paper addresses the necessity of a correct hydraulic accumulator pre-charge pressure for the optimum performance and in some cases even the essential function of the corresponding hydraulic application.

In this context HYDAC has developed a smart product for predictive monitoring of the pre-charge pressure without any need to do a measurement on the gas side of the accumulator – the p0-Guard. The paper gives an overview on the conventional way of checking the pre-charge pressure, the function of the monitoring device and points out the benefits of a predictive monitoring of the accumulator pre-charge pressure. The benefits are clearly depicted by an analytical view as well as on practical example.

Keywords: Efficiency, Hydraulic accumulator, Pre-charge pressure, Predictive monitoring, p_0-Guard

1. INTRODUCTION

In various hydraulic applications hydraulic accumulators are used for energy and performance support as well as for emergency functions. Due to the fact that the hydraulic medium is practically incompressible (and therefore unable to store energy) the hydraulic accumulator introduces the benefits of a compressible gas to the hydraulics. The capacity of energy storage is directly affected by the pre-charge pressure of the nitrogen gas (p_0) inside the accumulator [1]. The hydraulic accumulator consists of a separation element (bladder, piston, diaphragm) which separates the gas section from the fluid section connected to the hydraulic system (see **Figure 1**). HYDAC Accumulator Technology has many years of experience in research and development, design and production of hydraulic accumulators. As the only manufacturer of all four types of hydraulic accumulators HYDAC is suitable to supply all types of accumulators, from bladder accumulators and piston accumulators to diaphragm accumulators and also the metal bellows accumulators for special fields of application. The product range of HYDAC Accumulator Technology is completed by

various types of accumulator accessories and safety equipment which makes the hydraulic accumulator ready for essential future requirements in automation and safety.
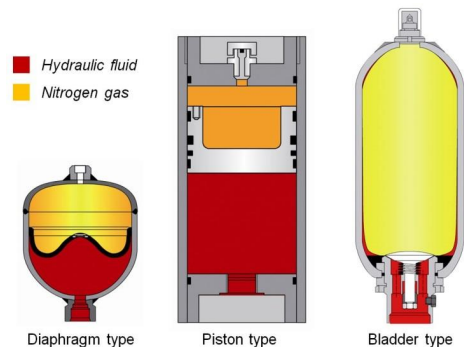
Figure 1: Different types of hydraulic accumulators

As the performance and availability of hydraulic applications is strongly depending on the correct function of the hydraulic accumulator the correct pre-charge pressure condition is essential. Illustrated using the example of a hydraulic press application the pre-charge pressure of the accumulator is affecting the performance of the press in both quality and quantity of the output product.

This paper first gives an introduction to the relation between pre-charge pressure and the usable energy in an analytical way as well as on a simulation example. In this context the importance of a correct pre-charge pressure condition is outlined. Furthermore the risks of conventional methods of checking the pre-charge pressure and the benefits of the predictive approach by the implementation of the p_0-Guard are described.

2. THEORETICAL RELATION BETWEEN PRE-CHARGE PRESSURE AND USABLE ENERGY

The hydraulic energy supplied to the accumulator is going to be supplied to the gas as pressure-volume works:

$$W = - \int p dV \tag{1}$$

It is stated, that most relevant hydraulic applications are pressure controlled. Therefore in the following we focus on the energy/performance potential of a hydraulic accumulator under the restriction of a fixed operational pressure range. This means that the operating pressure varies between the minimum pressure p_1 and the maximum pressure p_2. In this context **Figure 2** depicts the terms of usable and non-usable energy in the p-V-diagram.
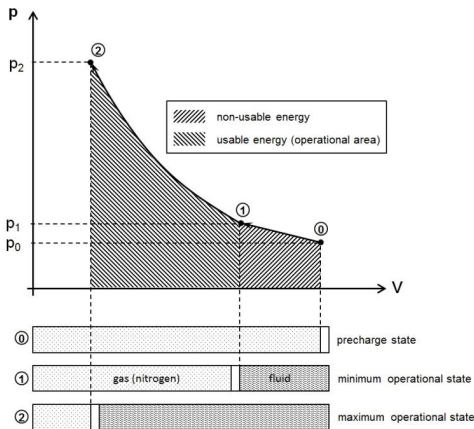
Figure 2: Operating range of a hydraulic accumulator supporting a pressure controlled system

Under the assumption of an ideal gas there are two limiting cases how to describe the thermodynamic behavior of a hydraulic accumulator:

- Isothermal
- Adiabatic

The energy equation for isothermal change of state

$$W_{12,iso} = p_1 \cdot V_1 \cdot ln\left(\frac{p_2}{p_1}\right) \tag{2}$$

with an isothermal compression from state 0 to 1

$$V_1 = \frac{p_0}{p_1} \cdot V_0 \tag{3}$$

shows a direct proportional relation between the pre-charge pressure p_0 and the usable energy in the operational range:

$$W_{12,iso} = p_0 \cdot V_0 \cdot ln\left(\frac{p_2}{p_1}\right) \tag{4}$$

For adiabatic change of state the corresponding energy equation shows the same relation:

$$W_{12,adi} = p_0 \cdot \frac{V_0}{k-1} \cdot \left[\left(\frac{p_2}{p_1}\right)^{\frac{k-1}{k}} - 1\right] \tag{5}$$

The energy quotient β is introduced in relevant literature on the calculation of hydropneumatic accumulators as the ratio between usable energy and a pV-product representing the given energy capacity of the accumulator [2]. For the considerations in this paper the energy quotient is stated as:

$$\beta = \frac{W}{V_0 \cdot p_2} \tag{6}$$

Under the assumption of an ideal gas **Figure 3** and **Figure 4** show the characteristic curves of the energy quotient as a function of the operating pressure ratio p_1/p_2 in dependence of the loss of pre-charge pressure, normalized to the ratio p_0/p_1.
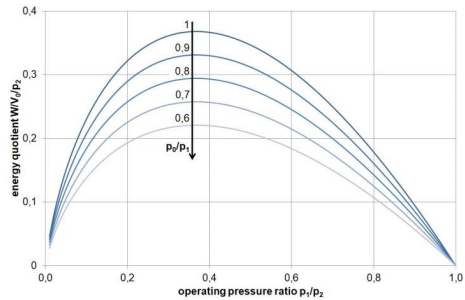
Figure 3: Energy quotient vs. operating pressure ratio (isothermal change of state)
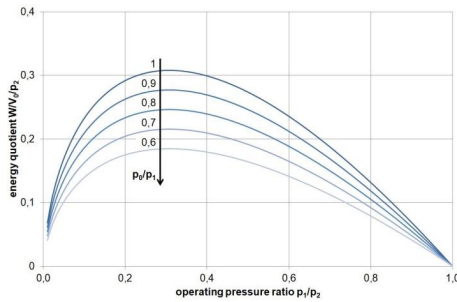
Figure 4: Energy quotient vs. operating pressure ratio (adiabatic change of state)

The figures above show an optimum operating pressure ratio $p_1/p_2 = 0,368$ for an isothermal change of state and 0,308 for an adiabatic change of state. As already shown in Equation 4 and Equation 5 the loss of pre-charge pressure p_0/p_1 reduces the energy quotient (and the usable energy of the accumulator) in a direct proportional behavior. For this reason it is mandatory to check the pre-charge pressure continuously during the operation, otherwise it leads to an inefficient use of the accumulator.

3. EFFICIENCY DECREASE BY PRE-CHARGE LOSS

In the following section the effects of a precharge pressure loss are shown by a dynamic simulation, exemplary on an energy supporting accumulator for the hydraulics of a tool clamping system. The tool clamping system is driven by an auxiliary HYDAC Compact Power Unit CO1. The corresponding hydraulic circuit diagram is shown in **Figure 5**.
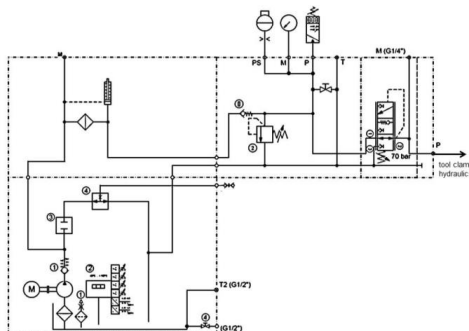
Figure 5: Hydraulic circuit diagram of HYDAC Compact Power Unit CO1

In terms of energy efficiency the pump of the power unit is controlled by an electronic pressure switch to realize a hydraulic accumulator charging function. When the accumulator pressure drops below a minimum pressure $p_1 = 100$ bar the pump charges the accumulator up to a maximum pressure $p_2 = 150$ bar. The charged accumulator supports the hydraulics of the tool clamp as long as the pressure drops below p_1 again. In this case the energy (volume) of one accumulator filling is sufficient to carry out four working cycles of the tool clamp.

As already shown in section 2 the usable energy of an accumulator decreases with a decreasing pre-charge pressure. A real gas simulation with HYDAC in-house Accumulator Simulation Program ASP illustrates this for the given application example of a tool clamp.
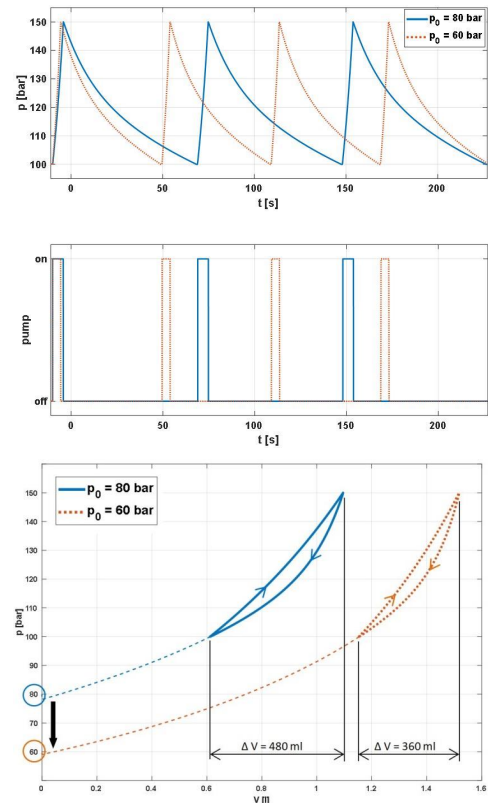
Figure 6: Simulation study of volume/energy capacity at decreased pre-charge pressure

Due to a 25% pre-charge loss from 80 bar to 60 bar the simulation results in **Figure 6** predict a limitation from four to three working cycles

operated by one accumulator filling. Concerning the operation of the power unit this means that the pump switch-on frequency increases by 25%. Due to increased efficiency losses the temperature of the power unit increases. This has an effect on:

- Pump & Valves:
  Increased mechanical wear due to increased operation cycles.
- Seals:
  Increased ageing due to increased operating temperatures (pump shaft seal).
- Fluid:
  Increased ageing due to increased operating temperatures.

The following Table 1 gives an overview on the simulation parameters.

Table 1: Parameters of the simulation

Parameter	Value
Max. accumulator pressure p_2	150 bar
Min. accumulator pressure p_1	100 bar
Pre-charge pressure p_0	80 bar
Accumulator volume	2,8 l
Displacement volume	120 ml/cycle
Constant pump flow rate	5 l/min

4. MONITORING THE PRE-CHARGE PRESSURE

There are two main reasons to illustrate why a correct pre-charge pressure is so important:

- Important for **function and performance** of the system - to ensure the optimal accumulator performance in the operating pressure range and thus maintain the machine output.
- Important for **availability** of the system - to avoid destruction of the accumulator's separating element (bladder, diaphragm, sealing system of the piston) due to a permanent malfunction and thus optimise the machine service life.

The most conventional way to check the pre-charge pressure of a hydraulic accumulator is to measure the pressure on the gas side. The check can be carried out by permanent devices like pressure gauges or pressure transducers or by non-permanent devices like the HYDAC charging and testing unit FPU. Some major examples of conventional ways to check the pre-

charge pressure by permanent pressure gauges are given in **Figure 7**.

Figure 7: Examples on conventional ways to check the pre-charge pressure

On the one hand the check on the gas side is the easiest and most direct measurement method, e.g. the use of gauges gives a direct and visual indication of the gas pressure. But on the other hand there are some disadvantages and risks which should be considered:

- A comfortable accessibility of the gas side to carry out the measurement is not always ensured. It may even be necessary to use a ladder to reach the gas side of the accumulator (see **Figure 7** a).
- By using permanent gauges or pressure sensors the risk of potential leakage points on the gas side has to be taken into account. In terms of better visibility the pressure gauges may be installed at eye level of the operating staff (see **Figure 7** b). The additional piping increases the essential costs and further the technical risk of leakage.
- The accumulator fluid side has to be non-pressurized and thermal stabilized during the pre-charge check in order to get a representative and comparable measurement result.

5. P₀-GUARD

The preventive maintenance strategy already described leads to excessive maintenance and machine downtimes and is therefore quite time and cost intensive for the operator.

In this context HYDAC has developed a smart product for predictive monitoring of the accumulator pre-charge pressure without any need to measure the pressure on the gas side – the p_0-Guard EDS 3400 **(Figure 8)**. By monitoring and evaluating the oil side pressure gradients the p_0-Guard detects any significant drop of the pre-charge pressure and activates a output signal in case of a critical pre-charge value.

Figure 8:   HYDAC p_0-Guard

5.1. Measurement principle

The measurement principle of the p_0-Guard is based on the physical conditions of the different bulk modulus of a hydraulic fluid / system and the gas medium inside the accumulator. The physical context of the measurement principle is shown in **Figure 9**. According to [3] the gas pressure has to be at a value of $p \approx 10^4\ bar$ or higher to reach the same bulk modulus as the bulk modulus of a hydraulic fluid. Due to the fact that in common hydraulic operating pressure areas the bulk modulus of the hydraulic system is much higher than the bulk modulus of gas, there is a significant gradient change in the characteristic curve on pressurizing and depressurizing the accumulator.

$$K_{hydr.} \gg K_{gas} \tag{7}$$

With regard to the accumulator fluid side pressure this gradient change occurs during depressurization when the separation element sets down on the fluid side bottom of the accumulator. The related pressure is called closing pressure p_0' and is directly dependent on the gas pre-charge pressure p_0. At pressures lower than the closing pressure the accumulator gas pressure is not any more supporting the hydraulic system and the bulk modulus of the hydraulic fluid $K_{hydr.}$ is defining the system stiffness. The value of p_0' is detected by the p_0-Guard on every

discharge process and the deviation from a reference p_0'-value is monitored.
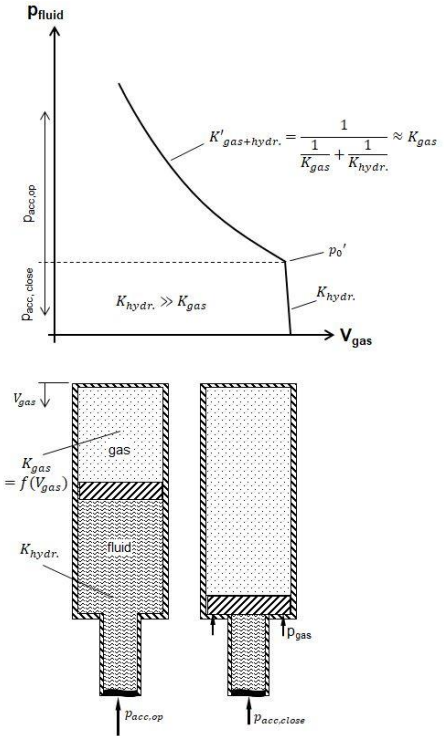
Figure 9: Measurement principle of the p_0-Guard

5.2. Validation

The function, reliability and stability of the p_0-Guard algorithm were validated in various tests at HYDAC in-house test department. **Figure 10** gives an overview over the functional tests carried out to validate the accuracy and reliability of the p_0-Guard on detecting the closing pressure under different discharge flow rates. On this test setup a piston accumulator with a pre-charge pressure $p_0 = 80$ bar was installed on a test rig with a p_0-Guard next to the accumulator. The result shows that the p_0-Guard reliably detects the closing pressure at low as well as at high discharge rates. Even on high discharge flow rates with only a slight change in pressure gradient the p_0-Guard is able to detect the closing pressure with a high accuracy (see **Figure 10** b).
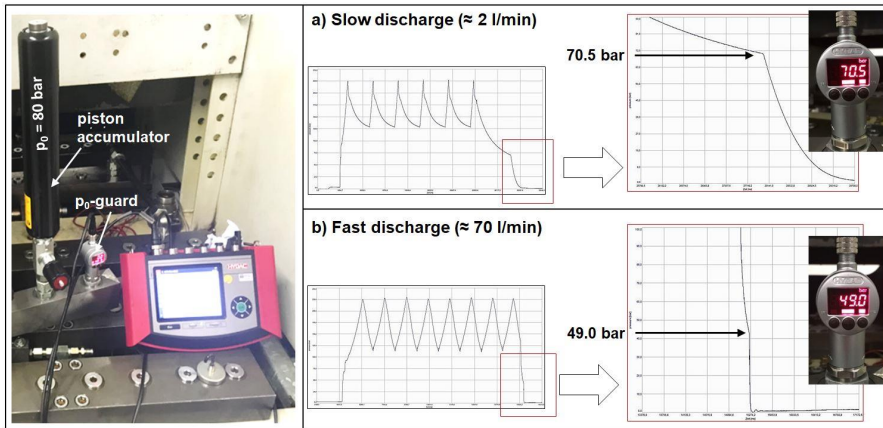
Figure 10: Validation test of the p_0-Guard

It can be noticed that in both discharge processes (at slow discharge p_0' = 70.5 bar; at fast discharge p_0' = 49.0 bar) the value differs in general from the static pre-charge setting of the accumulator. This can be explained by the thermodynamic effects during accumulator discharge. On discharging the accumulator the compressed gas inside the accumulator expands and cools down the nitrogen and its surrounding. Depending on the dynamics of this change of state the closing pressure deviates more or less from the (static) pre-charge pressure [4].

This effect is examined separately on a measurement series shown in **Figure 11**. In this test setup a hydraulic accumulator is discharged with different flow rates under the conditions of a constant ambient temperature and a constant pre-charge pressure. The results show a nearly linear dependence between the discharge flow rate and the change ratio of the closing pressure. For a proper installation of the p_0-Guard it is recommended to keep the discharge flow rate of the accumulator nearly constant on each pre-charge pressure detection cycle. In the simplest way by a separate bypass valve with a fixed throttle setting – what is already given in most industrial applications.

In another test setup like shown in **Figure 12** five accumulators with descending pre-charge pressures from 100 bar to 80 bar were installed in parallel on a test rig. On discharging the test rig it is shown, that the p_0-Guard detects the lowest closing pressure on the rig. Implied that there are several accumulators with the same nominal pre-
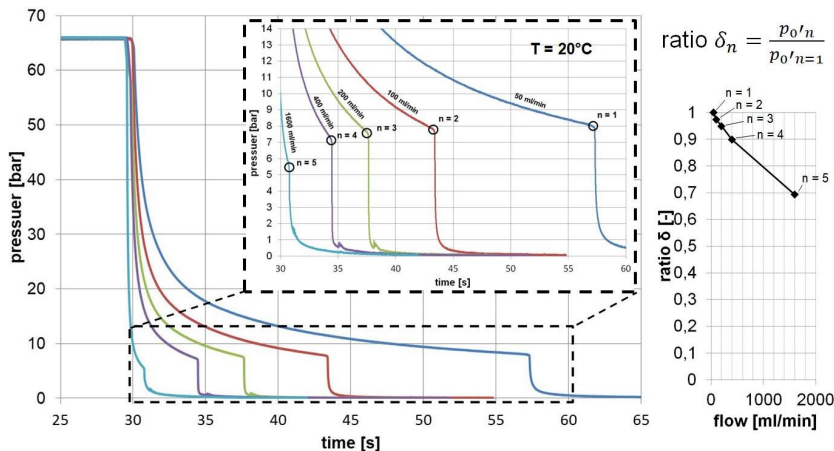
Figure 11: Study on discharge flow rate affecting the closing pressure
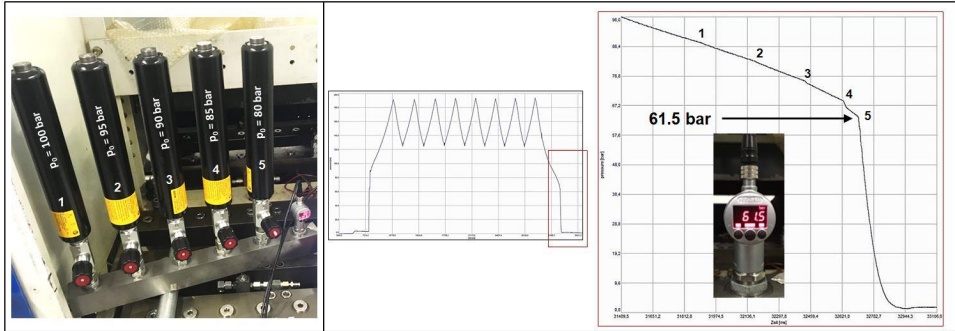
Figure 12: Validation test of the p_0-Guard (multiple accumulators)

charge pressure installed on a hydraulic system, the test results show that it is possible to monitor the overall status of the accumulators pre-charge pressure with only one p_0-Guard.

5.3. Product connectivity

To realize the detection of the closing pressure HYDAC has developed a monitoring algorithm which works even stable under the influence of disturbances like ripples or shocks on the hydraulic pressure signal. Due to the fact, that the p_0-Guard is based on the hardware of a HYDAC pressure switch, the user can benefit from the advantages of a long term proven product as well as a high sampling rate (which is essential for accurate function of the implemented algorithm).

The monitoring function of the p_0-Guard can either be realized in the standard switching mode or IO-Link mode. In the switching mode the output for pre-charge pressure monitoring switches off when the detected closing pressure drops below the defined minimum value. In the IO-Link mode the p_0-Guard is able to communicate bi-directional with the connected IO-Link master. The master is able to change setting parameters or to read the relevant values. Beside its main function of monitoring the pre-charge pressure the p_0-Guard has an additional output, which can either be used as a switching output for an accumulator charging function or as an analog output for the actual hydraulic pressure signal.

6. P_0-GUARD IMPLEMENTED IN HYDAC APPLICATION

As a manufacturer of hydraulic accumulators, HYDAC of course uses the benefits of accumulators in their own production plants. Since the company's own requirements on efficiency, productivity and quality are very high, HYDAC uses the p_0-Guard on most accumulators operated in their production plants. This gives HYDAC the possibility to monitor the actual pre-charge condition of all hydraulic accumulators, ensuring always the optimum performance. Furthermore it is now possible to generate historical trend data from which predictive data and maintenance forecasts are derived.

The benefits are shown by an example of a hydraulic clamping system working in a HYDAC production plant (see **Figure 13**).
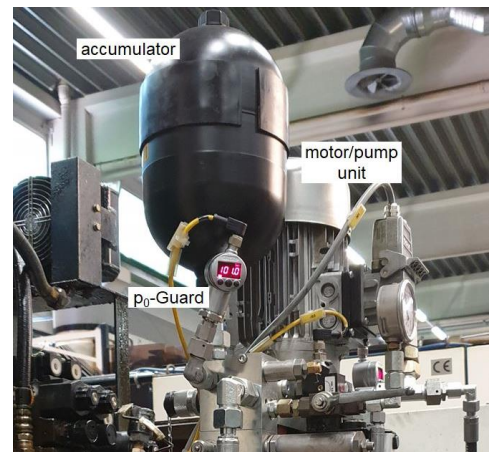
Figure 13: HYDAC Compact Power Unit CO1

The hydraulic functions driven by an auxiliary power unit are the chuck clamping, table clamping and pallet clamping (see **Figure 14**).
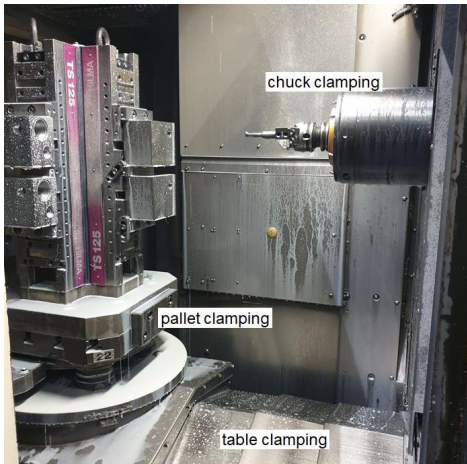
Figure 14: Hydraulic clamping functions

As a standard pressure switch only controls the accumulator charging function, the p_0-Guard replaces this function and additionally introduces the pre-charge monitoring function.

The pressure curves during the standard working cycles (**Figure 15**) show that there is a periodic volume/energy consumption of the hydraulic clamping functions supported by the accumulator. On time periods when the accumulator support is not needed or even on machine downtimes (e.g. maintenance) the closing pressure is automatically detected and monitored by the p_0-Guard.
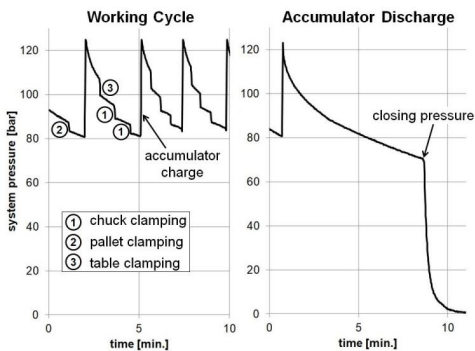
Figure 15: Pressure curves of clamping system

Due to the fact that the p_0-Guard is connected to the company network via IO-Link, the detected closing pressures are periodically stored on a server. In this context **Figure 16** shows the trend data of the p_0' detected on every discharge process, collected over a period of 21 weeks.
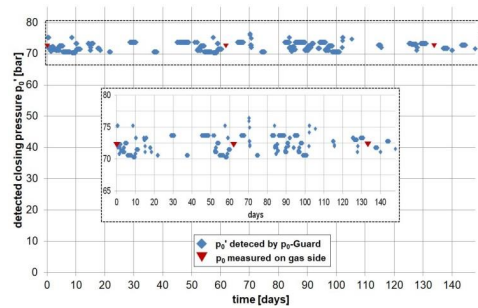
Figure 16: Detected closing pressure - trend data

Depending on the the slightly varying boundary conditions like ambient/fluid temperatures the detected closing pressures are stably scattering between 71 bar and 74 bar. For validation of the results a regular pre-charge check on the gas side confirms that there is no significant pre-charge loss on the hydraulic accumulator. So the given example shows that the energy supporting function of the accumulator is still ensured and there is no need for any pre-charge pressure service upcoming.

7. CONCLUSION AND OUTLOOK

This paper points out the importance of a correct accumulator pre-charge pressure condition and its impact on efficiency, productivity and quality of the hydraulic application. In this context the p_0-Guard provides a smart monitoring tool for the pre-charge pressure, which can be used as stand-alone device as well as embedded in an industrial network system. Compared to the conventional methods to check the pre-charge pressure the p_0-Guard offers a number of major advantages / benefits like:

- Installation on the fluid side of the accumulator. So it is easy to retrofit and install without any need to access the gas side of the accumulator. In the easiest way the existing HYDAC pressure switch can be exchanged by the p_0-Guard. This is even important in terms of accessibility, leakage and approval.

- No need to wait for thermal stabilization of the accumulator after discharge. Depending on the operating cycle and the size of the accumulator this process can take up to 30 minutes to stabilize. The p_0-Guard detects the pre-charge pressure loss directly after a defined discharge.

- The algorithm of p_0-Guard works independent on the accumulator type and therefore can be used for diaphragm, metal bellow, bladder and piston accumulators also including backup gas bottles.
- The p_0-Guard works on hydraulic circuits with multiple accumulators in parallel. The lowest pre-charge pressure is detected.
- Predictive planning of maintenance intervals to support and optimize a preventive maintenance philosophy.

NOMENCLATURE

W	Energy (pressure-volume works)	[J]
β	Energy quotient	[-]
k	Specific heat ratio of N2	[-]
V_0	Accumulator effective gas volume	[m³]
p_1	Minimum operating pressure	[bar]
p_2	Maximum operating pressure	[bar]
V_1	Accumulator gas volume at p_1	[m³]
V_2	Accumulator gas volume at p_2	[m³]
V_{gas}	Accumulator gas volume	[m³]
p_{gas}	Accumulator gas pressure	[bar]
$p_{acc,op}$	Hydraulic pressure on operating accumulator	[bar]
$p_{acc,close}$	Hydraulic pressure on accumulator non-operating/closed	[bar]
p_0	Accumulator pre-charge pressure at 20°C	[bar]
p_0'	Accumulator closing pressure	[bar]
$K_{hydr.}$	Bulk modulus of hydraulic fluid/system	[Pa]
K_{gas}	Bulk modulus of gas	[Pa]
$K'_{gas+hydr.}$	Superposed bulk modulus of gas and fluid	[Pa]
Δp_0	Loss of pre-charge pressure	[bar]
$\Delta p_0'$	Loss of closing pressure	[bar]

REFERENCES

[1] Korkmaz F. (1981) Hydrospeicher als Energiespeicher. Springer, Berlin.

[2] Rotthäuser S. (1993) Verfahren zur Berechnung und Untersuchung hydropneumatischer Speicher. Dissertation, RWTH Aachen

[3] Murrenhoff H. (2011) Grundlagen der Fluidtechnik Teil 1:Hydraulik. 6. neu bearbeitete Auflage

[4] Rist, D. (1996) Dynamik realer Gase. 1. Auflage

GROUP 7

Electro-hydraulic actuators

GENERAL LECTURE:

ELECTROHYDROSTATIC ACTUATION SYSTEM – AN (ALMOST) COMPLETE SYSTEM VIEW

Dr.-Ing. Dirk Becher

Moog GmbH, Hanns-Klemm-Straße 28, 71034 Böblingen
Email: dbecher@moog.com

ABSTRACT

Electro-hydrostatic Actuation Systems (EAS) successfully combine the advantages of electro-mechanical actuation - such as high-energy efficiency and low noise emission - with the benefits of electro-hydraulic technology –which include robustness and the precise handling of large forces. This paper defines keywords like EAS and Electro-hydraulic pump unit (EPU), and provides a comparison of the two technologies. Given the wide range of EAS technology topics, it is only possible to briefly introduce and discuss these in this paper. This technology has reached a level that renders it a strong mechanism for machine manufacturers to support existing and future motion control requirements.

Keywords: Electrohydrostatic Actuation System (EAS), Electrohydrostatic Pump Unit (EPU), Motion Control, Digitalization, Energy Management, Condition Monitoring

1. DEFINITION AND TECHNOLOGY COMPARISON

What exactly is an Electrohydrostatic Actuation System? **Figure 1** shows the principle means of controlling flow in a hydraulic application. A common approach is to use a variable displacement pump to operate it, with constant rotational speed. The displacement of this pump is varied in order to meet the flow and/or pressure requirements of the application. This approach works successfully, but generates losses and high noise levels when in part load or idle condition. Over the last decade, there has been a growing trend toward speed controlled pumps where largely, but not exclusively, a fixed displacement pump is used. Flow control is performed by a speed variable electrical motor. The advantages of such a concept are lower losses and sound emission, especially in part load and under idle condition. As the number of controlled cylinders is typically greater than one, both systems require additional proportional or servo valves to control the movement of the cylinder. The speed variable pump (SCP) system still requires a relatively large tank to provide the appropriate flow for all machine axes.

An EAS is a system combining at least one fixed or variable displacement machine, driven by a speed controlled electrical motor controlling the movement of a cylinder in both directions, without the need for any additional control valve. Both ports of the hydrostatic machine are directly connected to the ports of the cylinder.
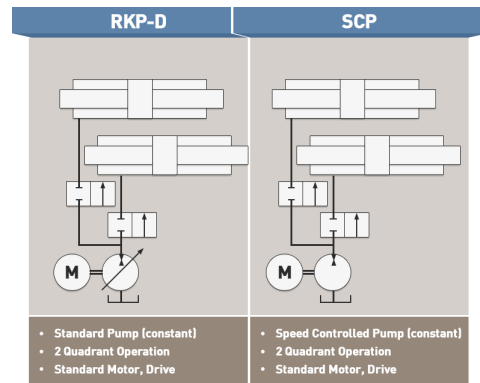
Figure 1: Adaption of flow by pump control

Among the many, main advantages of the EAS are:

- High energy efficiency;

- A small footprint and greater environmental cleanliness (low amount of hydraulic fluid, no or a small reservoir and less tubing);
- Low sound emission (sound only occurs under operation);
- High forces, robustness, simple overload protection as general features of hydraulics;
- Decentralized drive and control architecture;
- Easy installation and commissioning;
- Seamless integration in motion control systems with a mix of different technologies.

The EAS is a technology that will not replace existing drive and control technologies completely, but provides machine builders with an attractive, additional option that can realize a certain movement task.
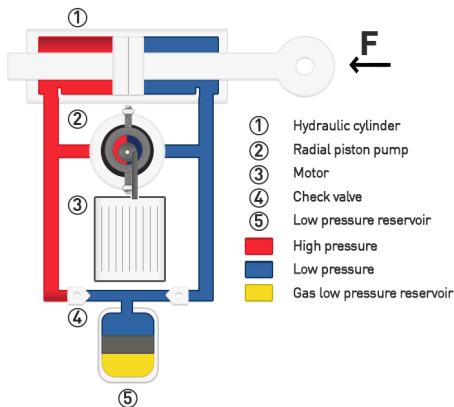
Figure 2: Self-contained axis, balanced cylinder

Figure 2 shows an EAS as a self-contained design that makes use of a balanced hydraulic cylinder. The fluid volume in this case is always constant – and independent of the stroke of the cylinder. This requires only a small sized low-pressure reservoir.

The most common actuator in hydraulics is the unbalanced cylinder, as shown in **Figure 3**. The size of the low-pressure reservoir should be larger compared to a system with a balanced cylinder. Besides the function to pre-pressurize the system, the accumulator should also provide the volume difference of the unbalanced cylinder.

A brief comparison of different drive and control technologies is shown in **Figure 4.**

In electro-hydraulic actuation (EH) a hydraulic power unit (HPU) consists of a reservoir, a flow variable pump (variable displacement and/or speed variable) and auxiliary devices for filtering and cooling the fluid. The actuator's motion control is performed by means of a proportional or servo valve. The controllability and the dynamics of such an axis are outstanding. The critical points are the losses of energy due to throttle losses, the large hydraulic footprint mainly by the HPU and - if not speed controlled – the permanent noise level of the motor/pump unit.
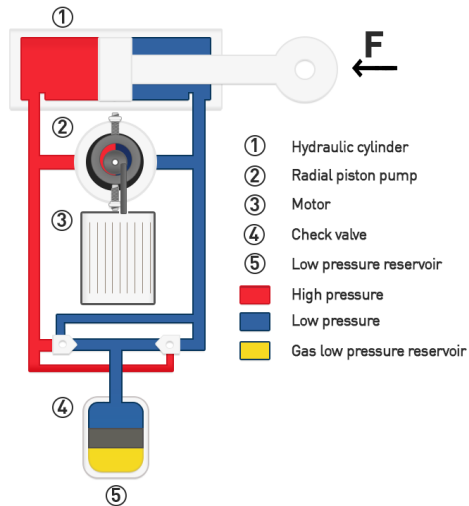
Figure 3:   Self-contained   axis,   unbalanced
              cylinder

In electro-mechanical actuation (EM), electric energy is transformed to a speed variable electrical motor that transforms its rotation, via an optional gearbox and a rotary to linear conversion (i.e. ball screw) into a linear movement. This technology delivers energy efficiency, a small footprint and low noise that only occurs if the axis is under operation. High forces are not the primary domain of EM.

The EAS combines all the benefits of both EH and EM technology. A hydraulic displacement machine can be coupled to a speed variable electrical motor, and the flow at the pump outlet directly drives and controls the movement of the attached cylinder. Robustness, long endurance and the capability to handle large forces and loads, are without doubt the DNA of the hydraulic part of such a system. Energy

efficiency and a generally smaller footprint are the key strengths that EM adds to this solution.
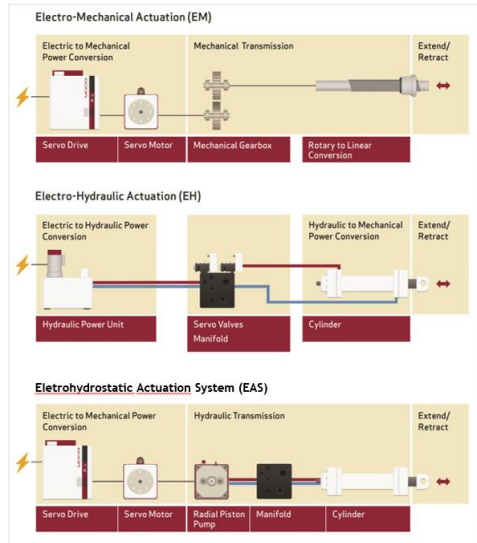
Figure 4: EH, EM, EAS - technology

2. DEMANDS ON THE EAS

2.1. Electrohydrostatic Pump Unit (EPU)

The EPU forms the central element of an EAS. It consists of a combination of electrical motor and hydrostatic machine, either with direct coupling or with a more traditional system with bell housing and coupling between both elements. The requirements on a speed controlled electrical motor are not special: it has to generate a certain rotational speed in combination with the torque needed, controlled by a drive. Continuous torque, maximum torque and field weakening of the motor over the rotational speed, should be designed to fit the behaviour of the hydrostatic machine and the application.

Industrial pumps are operated at constant speed, and mainly optimized for pump or motor operation. EAS requirements are different: As the cylinder speed is proportional to the rotational speed of the pump, a low cylinder speed requires low rotational speed and vice versa. Load holding requires high pump pressure with almost zero speed. To move the cylinder in and out, the hydraulic machine must be able to operate in both directions of any rotation. A pushing load requires pump operation, whereas a pulling load uses hydraulic motor operation.
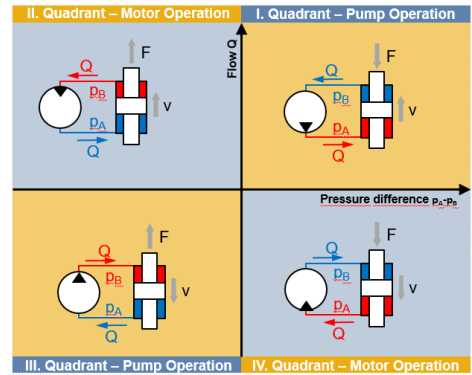
Figure 5: 4Q requirements for an EAS

Depending on the application, the hydrostatic machine should be able to operate in all 4 Quadrants. To reach a high dynamic, it is preferable to remove bell housing and coupling, and to connect motor and pump in a more direct way. In general, this also leads to a more compact design. An example of such an integration is shown in **Figure 6.**
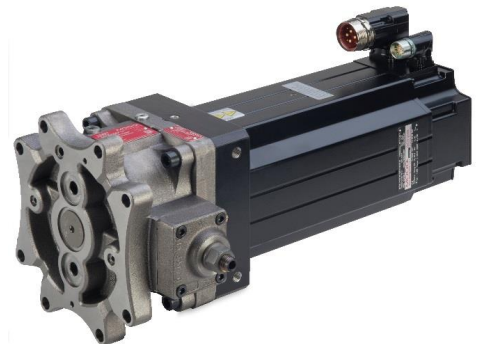
Figure 6: Moog EPU [8]

The Electrohydrostatic Pump Unit (EPU) is very compact. It also features a single hydraulic interface: all hydraulic ports are located in a single plane. By connecting the EPU to the manifold by 8 screws, the hydraulic connection is done in parallel.

2.2. EAS Architecture - circuits

Even though the task for an EAS seems to be clear and simple – to move a cylinder directly out of the pump in both directions – there are a couple of options that can optimize the EAS to meet the requirements of a specific application (**Fig.7**).
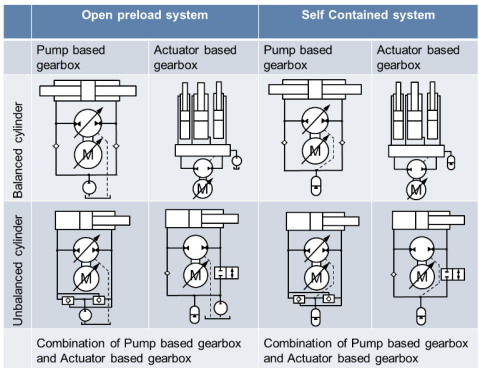
Figure 7: EAS Design options (incomplete)

The easiest option for the actuator is a balanced cylinder. In this case, the flow to and from both piston chambers is equal, and therefore so is the flow at both pump ports. A situation where the flow in and out of the pump is equal can be achieved by a single balanced cylinder, or by the combination and linking of two or three unbalanced cylinders. An example of an integrated EAS consisting of three unbalanced cylinders to create a balanced cylinder is shown in **Figure 8**.
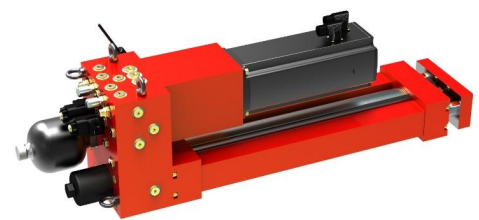
Figure 8: EAS with 3 cylinders by Bucher Hydraulics

The most common option for cylinders however, is the unbalanced one. As the flows on both chambers are different, this option needs additional valves and an accumulator to handle the flow difference. A basic circuit to handle the different flows of pump and cylinder is shown in **Figure 3**. An adaption of different flows on both ports of the cylinder can also be achieved by using two pump stages of different sizes. In such cases, the displacement ratio of both units should be adapted to the area ratio of the cylinder. Such a solution, which combines an integrated design with a two-pump stage solution, is shown in **Figure 9**.
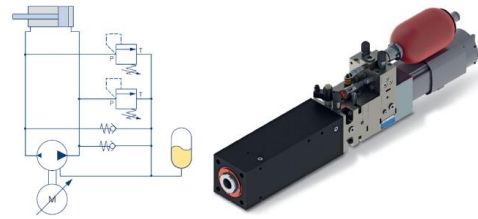
Figure 9: CLDP by Voith [7]

In general, an EAS consists of the following parts:

- A hydrostatic machine to generate a fluid flow;
- A motor as electromechanical transformer;
- A manifold for circuit structure and auxiliary functionality (pressure relief, rapid motion/force motion switching);
- An actuator (balanced/unbalanced cylinder).

The number of components can be assembled as a motion system in various ways (**Fig. 10**). An integrated design is the best option wherever a solution needs to be fitted in a well-defined, small envelope on an application. The compact approach makes use of more or less standard, off the shelf components, and combines them in a way that achieves a compact solution with a lower requirement for external tubing or housing. The distributed approach allows the larges degree of freedom for an integration in a machine structure and may be the best approach for a retrofit in existing applications.
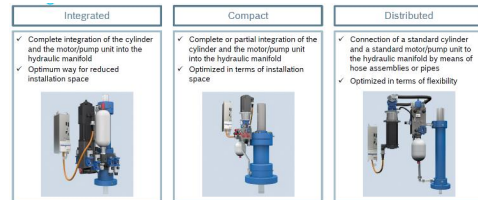
Figure 10: Integrated, compact, distributed design [9]

Many stationary hydraulic applications are featured by a movement consisting of a phase with high velocity/flow and low force/pressure

(rapid motion), and a phase with low velocity/flow and high force/pressure (force motion), for instance on metal forming and pressing applications. For such applications, it makes sense to adapt the power train components during the cycle of the machine. The main goal is to reduce the size of electrical motor and drive. The EAS offers this flexibility by way of a gearbox, which can be actuator based or pump-operated or a combination of both.

Figure 11 shows an example of an actuator-based gearbox. An actuator-based gearbox in this context means that switching between rapid and force motion is done via the interconnection of (generally) cylinders in the application. In Fig. 11, the unbalanced cylinder on the right side acts as a reservoir for the flow difference of the main (unbalanced) cylinder on the left. The upper picture represents the force movement, while the lower picture demonstrates rapid movement. Switching between both movements is performed by means of two simple switching valves.

A pump-based gearbox necessitates use of a variable displacement machine, or at least two machines with different displacements.
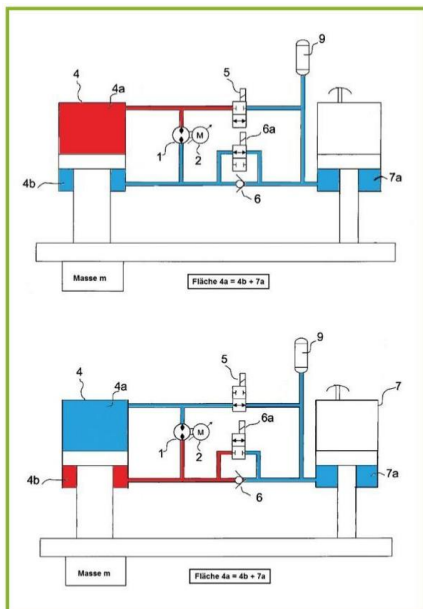
Figure 11: Actuator based gearbox [16]

A simple approach is the utilization of a variable displacement machine and to switch between maximum and a minimum displacement (dual displacement). With a given motor/drive, it is now possible to achieve a force movement with maximum force, or alternatively it is possible to reduce the motor/drive size combination by at least one size. A proportional displacement machine offers the maximum degree of freedom. In such cases, the full horse- power capability, as a product of pressure and flow, can be used to apply a maximum force/velocity ratio on the machine axis.

Figure 12: Pump based gearbox

Another advantage of the proportional adjustment is the proportional behaviour between the transitions of both movements. In the case of dual displacement and actuator/based gearboxes, the transition is undertaken by switching elements, which also leads to unsteady control behaviour. To reach maximum dynamics with switching gearboxes, an appropriate switching strategy needs to be applied [12].

2.3. Motion Control

An EAS is a controlled system/axis. The hydraulic machine is driven by a speed controlled electrical motor. The flow at the outlet of the hydrostatic machine is – at constant displacement - almost linear to the rotational speed. The slight nonlinearity is the result of the leakage of the hydrostatic machine, which increases more or less in line with pressure. The steady state characteristic diagram in **Fig. 13** shows this

behaviour for an EAS, with an unbalanced cylinder for all 4 quadrants. This is different to a valve driven axis with a strong nonlinear, root-shaped correlation (**Figure 14**) and makes the controller design somewhat simpler.
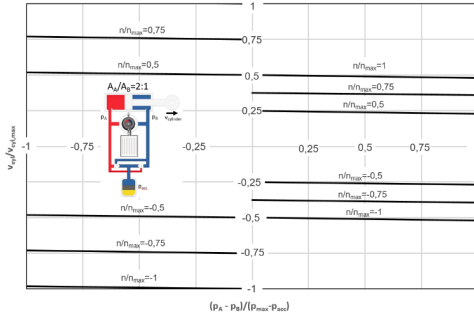

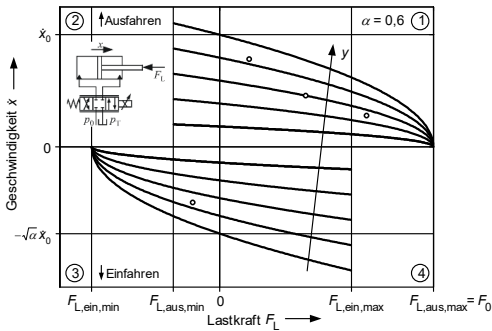**Figure 13:** Steady state characteristic of EAS

Figure 14: Steady state characteristic of valve axis [13]

The cylinder as hydraulic actuator is either position, flow/speed or pressure/force controlled or a combination of these. For this reason, an EAS consists of at least one position/speed sensor to measure the position and/or speed of the cylinder, two pressure sensors to determine the pressure in each piston chamber and a speed sensor in the motor to measure the rotational speed of the motor/pump combination.

A simple controller structure for a position controlled EAS is shown in **Figure 15**, which is in comparison to a valve driven cylinder. The inner control loop for the EAS is the current controller. Overlaid to the current controller is the speed controller of the motor, which controls the rotational speed at the shaft of the motor. Overlaid to the speed controller is the position controller of the cylinder. This controller receives the position signal from the sensor integrated in

the cylinder. The controller structure of a valve-controlled axis looks similar: the inner control loop is again a current controller, which in this case controls the current of the valve motor - in most cases a proportional solenoid or linear force motor. The current leads to a linear movement of the armature, which is connected to the spool. The motor/spool position is measured by an LVDT, and this signal is used to close the control loop of the spool position. On proportional/servo valves with integrated on-board electronics, booth control loops are closed inside the valve electronics. Depending on the spool position and the difference in pressure over the valve ports, a flow streams to the cylinder and leads to a movement of the cylinder. The position signal is again used to close the cylinder position controller. The cylinder position controller is normally closed in the machine PLC. On the other hand, there are so-called axis control valves (ACV) available, which can close the external control loop inside the valve electronics.
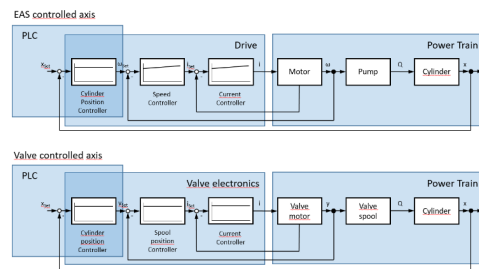

Figure 15: Simple valve axis and EAS control loop

The general electric infrastructure of an EAS offers the opportunity to operate different controllers on different hardware platforms. The drive itself is predetermined for the internal current control and the speed control and torque limitation of the motor. Beside this basic functionality, it is also possible to integrate a basic control loop for alternating position and force in the drive. Demand values for position, speed and force are generated by the PLC (**Figure 16**).

Figure 16: Simple EAS control via drive.

As the drive is limited in memory and operating power, it makes sense to use a different hardware platform if seeking to achieve more sophisticated control demands. Additional functionality for the EAS could come in the form of pressure ripple compensation, fine positioning or an enhanced control loop for the axis (**Figure 17**). In cases where a synchronisation of multiple machine axes is necessary, it is more advantageous to realize this motion control on a separate hardware platform.

Figure 17: Enhanced EAS control

Figure 18 shows how axis control functionality for a single EAS can be achieved. The EAS in this example uses the "motion block controller (Fahrsatzregler)" functionality, which is included in the drive. With this function, it is possible to create a motion profile, which consists of a limited number of motion tasks for a single axis on a machine. Each motion block defines a motion task (for instance, moving from A to B with speed v). After the motion task is completed successfully, the PLC/drive moves onto the next motion tasks in the series. Ultimately, once the blocks of a cycle are complete, the PLC/drive starts a new cycle.
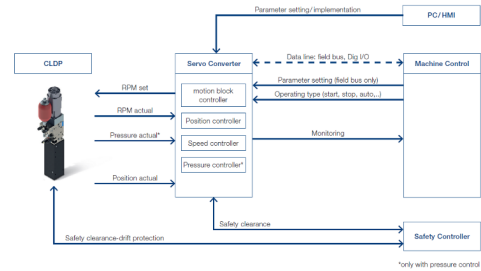

Figure 18: Motion block functionality [7]

2.4. Energy Management

The need to reduce overall energy consumption and the infeed power of machines is an ongoing concern for machine manufacturers. The use of the EAS on applications such as metal forming and pressing machines addresses this demand. On the one hand, an EAS is a 'power on demand' system that only consumes energy if it is operated. On the other hand, the machine's integration in the power bus or shop floor is possible via an electrical motor and drive, and offers enhanced opportunities for energy management. An example of such an integration is shown in **Figure 19.** The die cushion is realized as an EAS. During the deep drawing process, the hydrostatic machine in the EAS works as a hydraulic motor. The hydraulic motor drives the electrical motor, which in this case functions as an electrical generator. Over the DC bus between the die cushion drives and the press cylinder, electrical energy generated by the die cushion axis is used to support the press cylinder axis. This relatively simple approach offers a potential energy reduction of up to 40% on press/die cushion machinery.

An advanced approach for the energy management of presses is described and discussed in [6]. The energy management scenarios described in this paper can be used for machines and applications where all axes are EAS, in machines with a mix between EAS and EMS (electromechanical system) or purely EMS driven machines. In order to classify how advanced any given energy management approach is, the author defines five levels of sophistication (SL):

- A common non-active front end supplies all axes. The axes exchange power over the DC bus. When the total regenerative-

power is too high, it is dissipated over a bleed resistor.

- An active front-end powers all axes, and feeds back current into the grid if power is regenerative. Axes exchange power over the DC bus. Infeed needs to cover the peak power requirement of all axes at all times.
- Infeed charges the passive capacitor storage, and both power all axes. Regenerative power is stored in the DC bus. Infeed can be significantly downsized give that peak power is provided by the capacitors.
- Controllable storage, such as active capacitor units or servo flywheels, are additionally coupled onto the DC bus. A model-based algorithm on a controller generates command values for the infeed and the storages.
- As above, but the model adapts/learns on a cyclical basis, and changes the available control outputs according to optimization criteria.
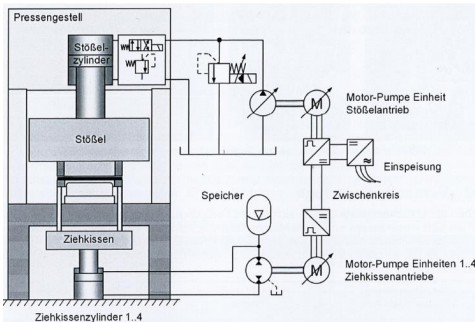

Figure 19: Press with energy management [5]

The five concepts highlighted above belong to SL1, SL2 and SL3. Beginning with a system that shares only the energy over the DC Bus (which already has the potential to save approximately 40% of all energy compared to a traditional hydraulic system), further investment in system hardware can further reduce machine energy losses in a range of additional 40-50%. Moreover, for the solutions with energy storage, the installed power could be reduced to less then 20 % of the peak power requirement of the axes. Consequently the inline elements of the infeed become much smaller and cost effective.

In components terms, the distribution of losses in almost each scenario is roughly 1/3 for pumps, 1/3 for drives and 1/3 for motors, infeed and

capacitors. Each component offers the potential for further energy reduction.
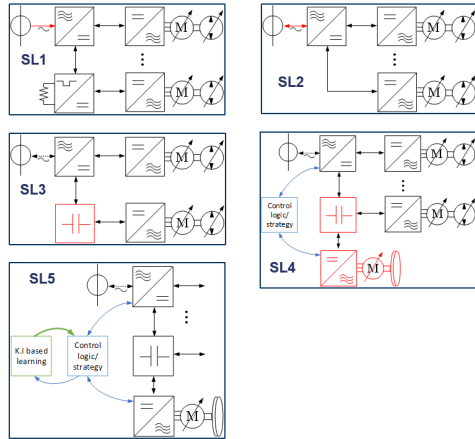

Figure 20: Description of sophistication levels

2.5. Digitalization, IoT, I40

Communication

Communication between the EAS and the PLC is provided by the drive. These components normally consist of a broad variety of digital fieldbus interfaces that offer a seamless integration with modern machine structures. Standard fieldbus interfaces such as EtherCAT, ProfiNET, Powerlink or OPC UA TSN based communication, are normally standard options.

Condition Monitoring/Predictive Maintenance

On components or at axis level - like EPU and EAS - CM and PrM becomes especially important, as they mainly influence machine performance. However, what should be monitored, and what could happen?

One answer to this question is shown in **Figure 21.** It is an approach based on two steps: First, it is necessary to collect data from an existing application/machine. For data collection, existing machine sensors can always be combined with additional sensors (e.g. vibration sensors). All data should be transferred within a cloud environment where the predictive analytics software is running. For this purpose, the installation of an IoT Gateway is necessary. The IoT gateway itself connects the machine sensors to the cloud, and transforms the data to a cloud compatible format (i.e. MQTT). In the first learning phase, the data is used to teach in a

neural network based machine model. This model describes the behaviour of the new machine. After the teaching phase, the data are used to identify anomalies that may occur while operating the machines. Any anomalies should be evaluated by an expert, who subsequently recommends any further necessary steps to the customer. This could take the form of a maintenance recommendation enabling the maintenance of the machine or/and the substitution of machine components. The service includes analytics via the ODiN platform, operation of the user interface (account), monitoring, reporting, consulting and recommendations.
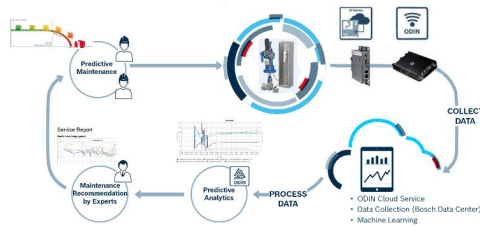

Figure 21: CM/PrM on system level [10]

Another approach is more focussed on single components that are part of the axis (**Fig. 22**). The hydrostatic machine is one of the most loaded parts of the EAS. High loads on tribological contacts may lead to wear over time. There are a number of approaches for dealing with this, but chiefly sensors (vibration, temperature, pressure) should be added on or near the pump.

The approach described here uses the existing sensors in an EAS. The main task of a pump is to deliver a certain flow proportional to displacement and rotational speed. However, the flow at the pump outlet – and therefore the leakage - is also influenced by the operating pressures at both ports. The fluid viscosity is a function of the fluid used, and of the temperature of the fluid.

To describe and calculate the flow at the hydrostatic machine outlet depending on these parameters (p_A, p_B, V_1, n_1, ν), an appropriate pump/flow model is necessary. The model itself can be based either on a physical model, or a collection of equations parametrized by measurement data. Alternatively, it can be based on a neural network, which is also trained by measurement data. The main goal of the model adopted is to reach a good approximation of the real behaviour of the hydrostatic machine, and the ability to integrate the software based algorithm on an appropriate hardware platform.
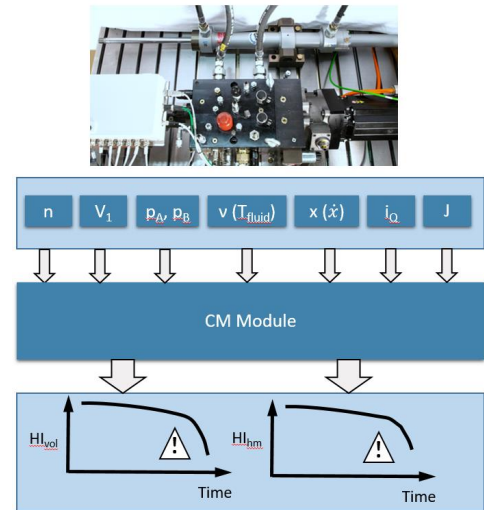

Figure 22: CM on Component Level

On the other hand, a sensor is required to measure real flow at the pump outlet. The cylinder can act as a sensor for flow: the dimensions are well known, and the position or the velocity respectively are accessible via the cylinder position/velocity sensor.

With this information, a health index acts as a ratio between delivered (measured) flow and a theoretical flow for a brand new pump, and allows the operating parameters to be derived. This value demonstrates the flow that should be delivered by the pump (out of the model), and the flow that moves the cylinder. Unfortunately, leakage does not only occur in the pump but also in the manifold, over the valves or between the chambers of the cylinder. In any case, this approach gives at least a value for the flow performance of the whole EAS. To detect the hydrostatic machine's wear a second value should be considered. As the first health index describes the volumetric efficiency of the pump (EAS), a second value considers the hydraulic/mechanical efficiency of the pump. The basis again is a model describing the torque needed on the shaft of the hydrostatic machine depending on the operating parameters. As is the case with the volumetric health index, the torque

mainly depends on the system pressures, machine displacement, speed and viscosity (p_A, p_B, V_1, n_1, v). During phases of acceleration and deceleration that torque also has to be taken into consideration. The inertia of the system (motor, hydrostatic machine) can be derived from design parameters, or by performing an appropriate test cycle on the axis.

In general, the determination of a health index does not have to occur in real time at a high sampling frequency. It is sufficient to start the algorithm for a longer period (once per hour/day/week). This provides the opportunity to place the necessary data collection in a part of the cycle where the quality of the measurement is high (i.e. constant velocity, constant load).

The implementation of such an algorithm can be realized on different hardware platforms. As the memory requirements and computing power of such an approach is less, it can run on the axis' drive, the machine PLC or it can be implemented in a cloud environment. In addition, the algorithm can also be implemented later on a constantly operational machine: as the models calculate the behaviour of a new hydrostatic machine and compare it to the actual state, they will always give a correct value for the health indexes even if installed in an already functioning machine.

Moreover, an additional expert, who analyses the CM data permanently, is not necessary: if a certain value for the health indices is fallen below a defined limit, this generates a clear signal to take action accordingly.

Tools

To fit an EAS to a certain application it needs to size the electrical and hydraulic components like hydrostatic machine, electrical motor and drive, and in case of multiple axes to consider the interaction between. **Figure 23** shows an example of such a sizing tool. Basis in this example is a commercial sizing tool (ServoSoft) which is developed for electrical drive technology originally (drives, electrical motors). The tool is enhanced by the characteristic of hydrostatic machines (size, speed and pressure range, efficiency characteristics). The sequence on the hydraulic output (flow, pressure) over the cycle forms the input parameters to size the hydrostatic machine, electrical motor and drive. A library of existing products supports to find the proper components.
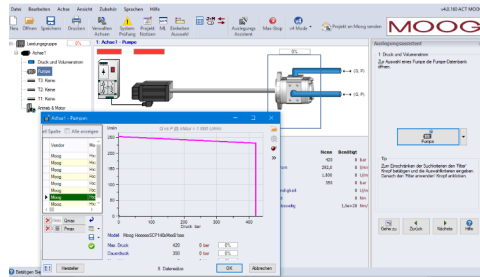

Figure 23: CM on Component Level [17]

3. APPLICATIONS

A look at the application use of the EPU/EAS shows that this technology is currently used solely in the industrial sector.

Figure 24 shows a structure durability test rig equipped with Voith's CLDP (closed loop differential pump) described above. The purpose of the machine is to perform structural tests of motor vehicle springs and stabilizers. The CLDP achieves a maximum stroke of 600 mm, and can apply a load of up to 60 kN. In comparison to a traditional hydraulic axis, this technology offers energy savings of up to 70%. Energy stored in the compression of the spring can be generated back into the electrical bus/grid for use on a parallel machine working in opposite movement.

Figure 24: Test Application [11]

A similar application is shown in **Figure 25**. An EPU powered by the Moog EAS is used for the structural testing of truck axes. The EAS acts as a self-contained axis with an unbalanced cylinder. The test frequency is up to 3 Hz at a stroke of 50 mm. Other test machines have been running with up to 10 Hz.
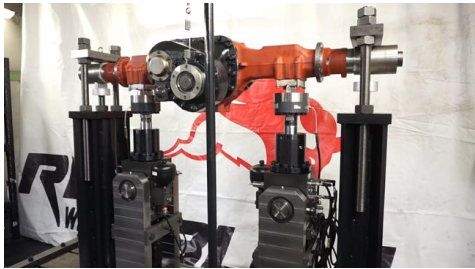

Figure 25: Test Application with MoogEPU/EAS

Figure 26 shows a calibration press equipped with a Bosch-Rexroth self-contained SHA axis. The hydrostatic machine works with an operating pressure of up to 315 bar. It reaches a precision in position control of 1 μm. The machine itself needs up to 60% less energy, and emits less noise.
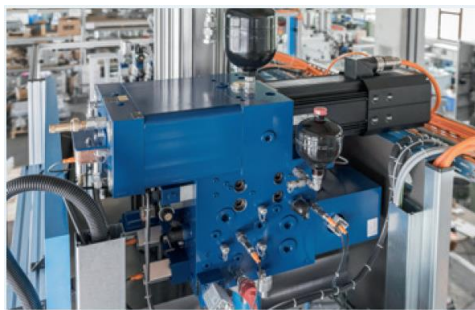

Figure 26: Axial Press [15]

A last example (**Figure 27**) shows the scalability of the EPU/EAS technology. It shows a pre-press that calibrates parts which are formed to large rings in a next step. The pre-press is equipped with 14 Moog EPU250s, achieving a maximum flow in the range of 6.000 l/min. The maximum force of the cylinder is 63.000 kN. For such an application, an open preload system is the better solution. It offers a better way to deal with fluid maintenance, such as cooling and filtering.
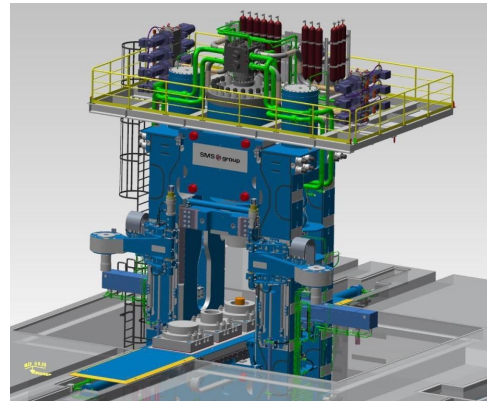

Figure 27: Hydraulic Press [14]

4. CONCLUSION AND OUTLOOK

EPU/EAS technology is an enhancement of drive and control technology, and combines the advantages of electro-mechanical and electro-hydrostatic actuation. It gives machine builders an attractive additional option in achieving a certain movement task. Scalability in terms of architecture and size offers a motion control solution for a broad number of markets and applications.

Certainly, there is room for optimization across all the fields outlined in this paper. Potentially, the next step in the development of hydrostatic machines could be an increase of rotational speed as they enhance the power range of an EPU fitted with speed controlled electrical motors. In addition, it is not a mistake to keep an eye on the reduction of losses on the hydraulic side in general.

However, there is also further potential in reducing the overall energy consumption and infeed power of machines that are running as part of a network of other machines.

All in all the rapid growing number of applications show that this technology is accepted, and will play a more important role in the future.

REFERENCES

[1] Brahmer, B: On Adaptive Electro Hydrostatic Actuators, 11th IFK Aachen, 2018

[2] Brahmer, B: CLDP – Hybrid Drive using Servo Pump in Closed Loop, 8th IFK Dresden, 2012

[3] Helbig, A, Boes, C: Electric Hydrostatic Actuation - modular building blocks for industrial applications, 10th International Fluid Power Conference, Dresden, 2016

[4] Boes, C. & Helbig, A. Electro Hydrostatic Actuators for Industrial Applications, 9th International Fluid Power Conference, Aachen, 2014

[5] Weber, J.: EFB-Forschungsbericht Nr 451, Energieeffizienz verdrängergesteuerter Pressen-hydraulik, 2017

[6] Reidl, Tim.: Energy management systems for electro hydrostatic propulsion based forming presses, Proceedings of 12th IFK Dresden, 2020

[7] Voith Group: Self contained servo drive CLDP, Technical data sheet, Product Brochure

[8] Moog GmbH: Electro-Hydrostatic Pump Unit: Modular Electro-Hydrostatic Pump Unit for Industrial Applications, Product Brochure, Rev. H, 2020

[9] Bosch Rexroth AG: Servo Hydraulic Actuator SHA, Customer Information, DC/ESS21 24.09.2019

[10] Gellner, T.: Servo-Hydraulic Actuator – SHA, Presentation of 16th Scandinavian International Fluid Power Conference – SICFP19

[11] Fluid 09/2019: Prüfen wie geschmiert, CLDP-Servoantriebe für Betriebsfestigkeitsprüfungen

[12] Kolks, G.: Electro-hydrostatic compact drives with variable transmission ratio, proceedings of 12th IFK Dresden, 2020

[13] Murrenhoff, H.: Servohydraulik – Geregelte hydraulische Antriebe, Umdruck zur Vorlesung, Aachen, 2012

[14] https://www.linkedin.com/posts/hong-zhao-86a7b8161_new-investment-in-wuxi-paike-china-7000t-activity-6595840832140611584-HDhe

[15] Bosch Rexroth AG: https://dc-corp.resource.bosch.com/media/general_use/industries_2/machinery_applications_and_engineering/pressing_and_forming/BR_Success_Frey_AE_RZ_1015_media.pdf

[16] Siemer, E.; Kluge, A: Ecoplant Design – Moderne Antriebskonzepte für Schmiede-pressen, o+p Fluidtechnik, 11/12 2016, http://digital.oup-fluidtechnik.de/o-p-fluidtechnik-11-2016/56259823/72

[17] ServoSoft: https://www.controleng.ca/servosoft/

FLEXIBLE AND EASY TO ENGINEER SERVO-HYDRAULIC ACTUATORS USING 3D PRINTING MANUFACTURING PROCESS

Stefan Thienen*, Thomas Gellner

Bosch Rexroth AG, Zum Eisengießer 1, 97816 Lohr am Main, Germany,
* Corresponding author: E-mail address: stefan.thienen@boschrexroth.de

Already since some time, Bosch Rexroth offers solutions as compact servo hydraulic actuators (SHA). Because there are lot of requests from the market, we thought about reducing the inquiry processing time and delivery time by designing a kit system for the SHA solutions. This system should be flexible enough to cover different technical solutions (e.g. cylinder), functionalities and design styles.

After some investigation, we decided to use an innovative casting block, made with a 3D printed sand core. By using this technology, we got a compact and lean design for our block and the entire hydraulic system. This shows the usage of modern production methods in series production in relatively new hydraulic systems, like the SHA.

Further, we created an online configuration tool, which will help our sales team to choose and validate a solution that fulfills our customer requirement within very short time. To be ready to place an order the tool includes the pricing process. All is build in a user-friendly way with all necessary calculations in the background.

The benefits for the customer are the fast configuration, evaluation with all available options and the required installation space. Because of optimizations of the product, we are able to deliver such axis within short time, even if it is only one single axis.

The product with the described features will be available for customers in 2020.

ELECTRO-HYDROSTATIC COMPACT DRIVES WITH VARIABLE TRANSMISSION RATIO

Giacomo Kolks*, Jürgen Weber

Institut of Mechatronic Engineering, Technische Universität Dresden, Helmholtzstrasse 7a, 01069 Dresden
* Corresponding author: Tel.: +49 351 46339932; E-mail address: giacomo.kolks@tu-dresden.de

ABSTRACT

Electro-hydrostatic compact drives are an emerging technology within a range of industrially available translational drive solutions, combining the specific advantages of hydraulic and electromechanical screw drives. Compared to electromechanical screw drives, hydrostatic drives can vary their transmission ratio with comparably little effort, giving them the key advantage of downsizing the electric drive components for a given load cycle.

This paper provides a guideline on how to calculate the downsizing potential of electric motors and inverters arising from variable transmission ratio based on the load regime of a given application. Furthermore, a comprehensive systematisation of the actual switching process is described for systems that are switched by means of switching valves. The presented set of methodology is applied to demonstrators in order to validate the general findings.

Keywords: electro-hydrostatic compact drive, variable transmission, switching hydraulics

1. INTRODUCTION

Machine manufacturers are increasingly in demand of modular and self-contained drive solutions with high energy efficiency – without abandoning the traditional benefits of hydraulic cylinder drives, such as robustness and high force density. Electro-hydrostatic compact drives (ECD) provide substantial benefits in these aspects and are therefore an emerging technology in the hydraulic sector. ECD are displacement controlled cylinder drives with variable-speed pumps in a compact unit with an enclosed oil circuit. Alongside the advantage of improved ease-of-use compared to conventional hydraulic systems, ECD come with high robustness, high force capability and freely implementable fail-safe-behaviour compared to electro-mechanical screw drives (EMD). ECD are therefore primed to be a competitor to EMD, which have been replacing classical distributed hydraulic systems in many applications over the past years, mainly for modularisation reasons.

ECD with double-acting cylinders can generally be categorised in open hydrostatic circuit (OHC) and closed hydrostatic circuit (CHC). OHC refers to structures that connect one chamber of the cylinder to the baseline pressure of a reservoir or accumulator, while the other chamber is hydrostatically connected with one pump port. In order to create a system capable of operation in four quadrants of load, typically electric or hydraulic actuated valves are needed, see **Figure 1a**. CHC on the other hand means that both cylinder chambers are constrained with both pump ports, creating a closed kinematical chain, as depicted in **Figure 1b**. A requirement for CHC is a pump structure whose flow asymmetry matches the cylinder area ratio. Furthermore, suction valves are needed in order to define the minimum pressure in the circuit.
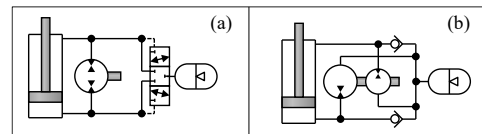

Figure 1: Exemplary circuitry structures for OHC with inverse shuttle valve (a) and CHC (b) drive solutions

In addition to the previously mentioned benefits of hydraulic cylinder drives compared to EMD, hydraulic circuits allow for variable transmission ratio by either varying effective pump displacement or effective cylinder area. This effect can be

conceived as variable pitch of a screw, if the analogy to electromechanical drives is sought [1]. In applications with a distinct separation between high load and rapid traverse strokes, such as hydraulic presses, variable transmission ratio enables downsizing of the electric drive. This effect is illustrated in **Figure 2** by means of single operation points: Assuming fixed transmission ratio, for speed stroke and force stroke the motor needs to be able to deliver both high rotational speed and high torque at different times of the cycle. If high force is only requested at low speed, by shifting to a higher transmission ratio the operation point of force stroke can be shifted towards high rotational speed and low torque. Thus, a motor with a lower specified torque can be used.
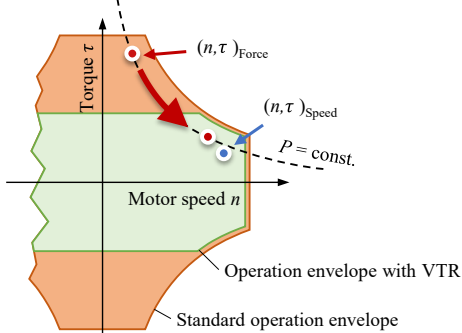

Figure 2: Illustration of motor downsizing through variable transmission ratio

It has previously been stated that in order to alter the transmission ratio, either variation of effective pump displacement (pump-based switching) or variation of effective cylinder area (actuator-based switching) can be applied. Pump-based switching can either be achieved by physically changing the displacement of a variable pump (continuous variation), or by combining multiple fixed displacement units by means of valves and manipulating output flow by activating or deactivating flows of single units (discrete variation). Actuator-based switching lacks the possibility of continuous variation of cylinder area for technological reasons, thus only variation of effective cylinder area by means of combination of different areas of a cylinder is possible (discrete variation). The resulting solution space of ECD with variable transmission ratio is described in **Table 1**. With reference to the system structure it can further be refined as to whether the individual transmission stages are implemented in OHC or CHC. Solutions with discrete pump-based

switching comprise a minimum of two pumps, solutions with discrete actuator-based switching at least to cylinder chambers.

The research project, which the paper at hand is based on, concentrated on ECD with at least one transmission stage in CHC using single rod cylinders. This configuration cannot be achieved with a single variable displacement pump, leading to neglecting continuously variable solutions.

Table 1: Solution space of ECD with two transmission stages

circuit type CHC/OHC	pump-based switching		actuator-based switching
	continuous	discrete	discrete
both stages OHC	PC0	PD0	AD0
one stage OHC/ one stage CHC	PC1	PD1	AD1
both stages CHC	PC2	PD2	AD2

Creating solutions with CHC structure in both transmission stages is a design problem within tight constraints concerning pump displacements and cylinder areas. A comprehensive approach to describe the subspace of these solutions is given by the authors for discrete pump-based switching [2] and discrete actuator-based switching [3], as well as state-of-the-art in switching linear drives.

Pioneer work on displacement controlled cylinder drives has been carried out by Sprockhoff [4] and Berbuer [5], dealing with OHC structures and valves to ensure a minimum pressure level in the cylinder and oil exchange with a reservoir. Important foundations for asymmetric single rod cylinders with displacement control in CHC structure have been laid by Lodewyks [5]. More recent research by Michel examined both OHC and CHC types, proving that OHC tend to be more energy efficient, while CHC having the better controllability [6, 7]. It has been shown that OHC structures with inverse shuttle valves exhibit discontinuities and instabilities when the load pressure is around zero or changes directions. Instability issues through pressure-piloted switching valves in this context have been investigated in further research [8, 9]. A good overview over the current state of the art in ECD is included in the work by Ketelsen et al. [10].

2. DOWNSIZING POTENTIAL

2.1. Dimensioning of electric drivetrain

Choice of electric motors and servo inverters are crucial to ECD drives, since they are strongly related with their static and dynamic properties as well as total costs. In the following, dimensioning is carried out with relation to typical combinations of servo inverters and synchronous servo motors.

Usually, servo motors are dimensioned so that they withstand the thermal load over a specific cycle and the maximum dynamic torque that occurs over time. The **maximum torque criterion (MTC)** can be formulated as the following:

$$\max(\tau(t)) < \tau_{\text{M,max}} \tag{1}$$

As a thermal criterion, a motor exhibits an S1-line $\tau_{\text{M1}}(n)$ in the torque-speed plane, which has to lie towards the outside of operating point of equivalent load $(n_{\text{eq}}, \tau_{\text{eq}})$ of the motor during its load cycle. It is often an acceptable simplification to assume the S1-curve to be parallel to the speed axis, thus for generalisation purposes this will apply. The torque value of the horizontal S1-line will be referred to as the nominal torque τ_{N}. Thus, the thermal criterion (**equivalent torque criterion, ETC**) reads

$$\tau_{\text{eq}} < \tau_{\text{M,nom}} \tag{2}$$

with the equivalent torque

$$\tau_{\text{eq}} = \sqrt{\frac{1}{T} \int_T \tau(t)^2 \, \mathrm{d}t}. \tag{3}$$

This equivalent torque formulation correlates the electric losses of the motor to the square of the torque according to the following:

$$P_{\text{loss}}(t) \propto I(t)^2 \propto \tau(t)^2 \tag{4}$$

Any electric motor has to fulfil both maximum torque and equivalent torque criterion that are calculated based on the torque regime $\tau(t)$ of the load cycle.

2.2. Choice of transmission ratios

ECD can be regarded as transmission that transform rotational mechanical input power into translational mechanical output power. The transmission ratio can be defined as

$$i = \frac{\omega}{\dot{x}} = \frac{2\pi n}{\dot{x}} \tag{5}$$

Neglecting losses, conservation of energy results

in

$$i = \frac{F}{\tau}. \tag{6}$$

For the simplified and idealised ECD structure shown in **Figure 3**, the transmission ratio yields

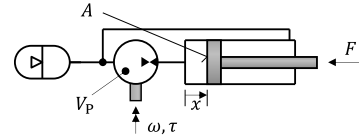$$i = \frac{2\pi \, A_{\text{eff}}}{V_{\text{P,eff}}}. \tag{7}$$

Figure 3: Simplified structure of ECD

It is obvious that, by changing effective cylinder area A_{eff} or effective pump displacement volume $V_{\text{P,eff}}$, the transmission ratio can be varied.

Let i^{F} be the transmission ratio in force stage, and i^{S} the transmission ratio in speed stage of any drive with variable transmission ratio. The transmission range is defined as

$$\alpha_i = \frac{i^{\text{F}}}{i^{\text{S}}} \tag{8}$$

and from eqs. (5)-(6) we can derive

$$\alpha_i = \frac{\tau^{\text{S}}(F)}{\tau^{\text{F}}(F)} = \frac{n^{\text{F}}(\dot{x})}{n^{\text{S}}(\dot{x})}. \tag{9}$$

For calculation of downsizing potential, following hypothesis is used:

The size of an electric servo drive is minimal if the required torque is minimal.

Thus, a drive dimensioning minimises the drive size, whenever it maximises the rotational speed. In direct-driven hydraulics, pumps are typically the limiting factor of rotational speed, thus the goal is to reach the maximum pump speed in both force and speed stage:

$$\left| n^{\text{S}} \right|_{\text{max}} = \left| n^{\text{F}} \right|_{\text{max}} = n_{\text{max}} \tag{10}$$

Neglecting leakage, the rotational speed is

$$n(t) = \begin{cases} \dfrac{i^{\text{S}}}{2\pi} \cdot \dot{x}(t) \text{, in speed stage} \\[2mm] \dfrac{i^{\text{F}}}{2\pi} \cdot \dot{x}(t) \text{, in force stage.} \end{cases} \tag{11}$$

Thus, an optimal transmission range can be derived as the ratio of maximum speed in speed stage over maximum speed in force stage:

$$\alpha_i = \frac{\left| \dot{x}^{\text{S}} \right|_{\text{max}}}{\left| \dot{x}^{\text{F}} \right|_{\text{max}}} \tag{12}$$

Neglecting friction losses, the torque yields

$$\tau(t) = \begin{cases} \dfrac{F(t)}{i^S} & \text{, in speed stage} \\ \dfrac{F(t)}{i^F} & \text{, in force stage.} \end{cases} \tag{13}$$

2.3. Downsizing potential for electric motors

For a reference, an ECD with fixed transmission ratio is dimensioned in a way that it reaches the maximum pump speed. The equivalent torque is

$$\tau_{eq,Ref} = \sqrt{\frac{1}{T_{tot}} \int_{T_{tot}} \left(\frac{F(t)}{i_{Ref}}\right)^2 dt} \tag{14}$$

while maximum torque yields

$$\tau_{max,Ref} = \frac{F_{max}}{i_{Ref}}. \tag{15}$$

The load cycle is divided in a speed stage T_S and a force stage T_F, see **Figure 4**, and the transmission of the switching drive is chosen accordingly.
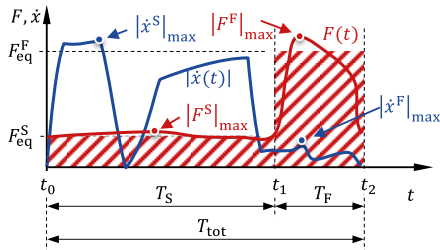

Figure 4: Exemplary machine cycle

According to the findings in eq. (12) and an optimally dimensioned reference transmission ratio, following transmission ratios can be assumed:

$$i_{Ref} = i^S = \frac{i^F}{\alpha_i} \tag{16}$$

With this definition, we can calculate the ratio between the equivalent torque of the reference drive over the equivalent torque of the switching drive $\alpha_{\tau,eq}$:

After introducing proportional parameters

$$\alpha_F = \frac{F_{eq}^F}{F_{eq}^S} \tag{17}$$

$$\alpha_t = \frac{T_F}{T_S} \tag{18}$$

and with definition of an equivalent force

$$F_{eq} = \sqrt{\frac{1}{T} \int_T F(t)^2 \ dt} \tag{19}$$

the equivalent torque ratio results in

$$\alpha_{\tau,eq} = \frac{\tau_{eq}}{\tau_{eq,Ref}} = \sqrt{\frac{1 + \dfrac{\alpha_F^2 \cdot \alpha_t}{\alpha_i^2}}{1 + \alpha_F^2 \cdot \alpha_t}}. \tag{20}$$

The ratio of maximum torques is

$$\alpha_{\tau,max} = \frac{\tau_{max}}{\tau_{max,Ref}} = \min\left(\alpha_i, \frac{|M^E|_{max}}{|M^K|_{max}}\right). \tag{21}$$

With these parameters $\alpha_{\tau,eq}$, $\alpha_{\tau,max}$ an assessment of downsizing potential can be made. If both reference fixed drive and variable transmission drive are limited by the equivalent torque criterion, the downsizing parameter concerning rated torque is equal to the equivalent torque ratio $\alpha_{\tau,eq}$. However, this is not always the case, thus differentiation has to be made.

Whether a motor is limited by maximum torque or equivalent torque depends on its overload capacity, meaning the ratio of maximum torque to nominal torque:

$$\alpha_{OL} = \frac{\tau_{Mot,max}}{\tau_{Mot,nom}} \tag{22}$$

For generalisation, we assume that all feasible motors that are within the choice range share the same overload capacity α_{OL}. Under this circumstance, downsizing factors with respect to torque specifications are listed in **Table 2**. The downsizing factor means the ratio of reduction of required nominal motor torque that can be achieved by means of transmission switching against a fixed transmission reference drive:

$$\alpha_{\tau,Mot} = \frac{\tau_{M,nom}}{\tau_{M,nom,Ref}} \tag{23}$$

The resulting calculation schedule for downsizing potential is thus:

1. Choose force stage intervals and speed stage intervals according to the load cycle.
2. Calculate transmission range with eq. (12) and $\alpha_{\tau,eq}$ using eqs. (17)-(20).
3. Choose a realistic overload capacity α_{OL}
4. Select case and calculate downsizing factor $\alpha_{\tau,Mot}$ according to Table 2.

Table 2: Calculation of downsizing factors depending on load conditions

	Limiting criteria	Condition	Downsizing factor
Case 1	Reference → MTC Switching drive → MTC	$\dfrac{F_{max}}{\alpha_i \cdot F_{eff} \cdot \alpha_{\tau,eq}} > \alpha_{OL}$	$\alpha_{\tau,Mot} = \alpha_{\tau,max}$
Case 2	Reference → MTC Switching drive → ETC	$\dfrac{F_{max}}{F_{eff}} > \alpha_{OL} > \dfrac{F_{max}}{\alpha_i \cdot F_{eff} \cdot \alpha_{\tau,eq}}$	$\alpha_{\tau,Mot} = \dfrac{\alpha_{OL} \cdot F_{eff} \cdot \alpha_{\tau,eq}}{F_{max}}$
Case 3	Reference → ETC Switching drive → ETC	$\alpha_{OL} > \dfrac{F_{max}}{F_{eff}}$	$\alpha_{\tau,Mot} = \alpha_{\tau,eq}$

Switching transmission ratio also has an effect on the choice of servo inverters. These are often dimensioned to withstand the maximum current during the cycle, which correlates with maximum torque. Thus, the downsizing factor can be considered to be

$$\alpha_{I,Inv} = \alpha_{\tau,max} \qquad (24)$$

This methodology is applied to an idealised cycle of a hydraulic press brake in the following. The cycle data is given in **Figure 5** (left) by means of cylinder position and speed as well as load force curves over time. The resulting motor torque and speed are shown in the diagram in the middle of the same figure, for a reference drive with fixed transmission and an ECD with variable transmission. Switching is carried out at the times t_a and t_b. By evaluating the cycle in the described manner, the downsizing factor of the motor results in $\alpha_{\tau,Mot} = 0.22$ (case 3) and $\alpha_{I,Inv} = 0.19$ for the inverter. Using an exemplary model range of synchronous servo motors and inverters in the power range of 1 to 10 kW, the benefits of variable transmission in terms of weight and cost savings are given in Figure 5 on the right.

3. DEMONSTRATOR DRIVES

In order to validate the findings from the project, two demonstrator ECD that arose from the systematic scan of solution space [3, 2] have been set up – one for each switching principle – as depicted in **Figure 6**.

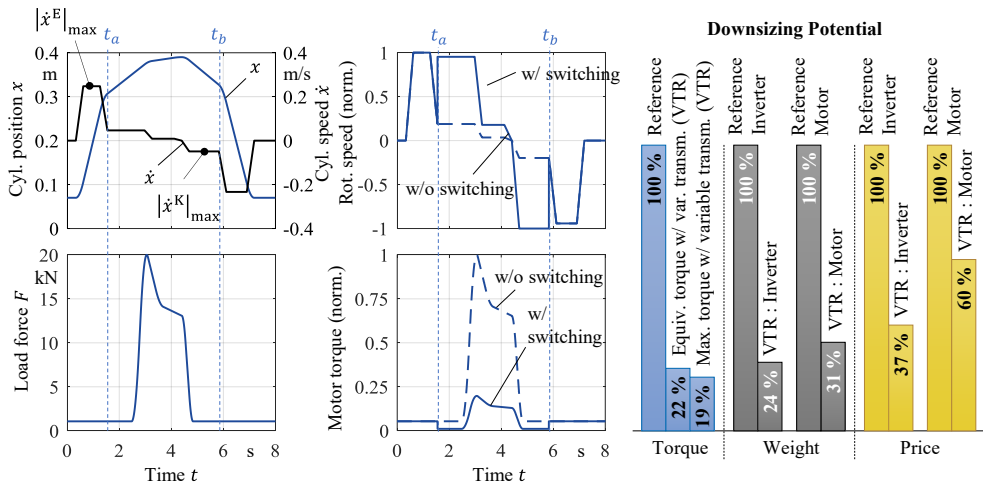The pump-based switching demonstrator (PBD) makes use of a CHC structure in speed

Figure 5: Cycle of an idealised press brake with motor torque and speed with and without switching transmission, and downsizing in terms of weight and cost of exemplary commercially available component.
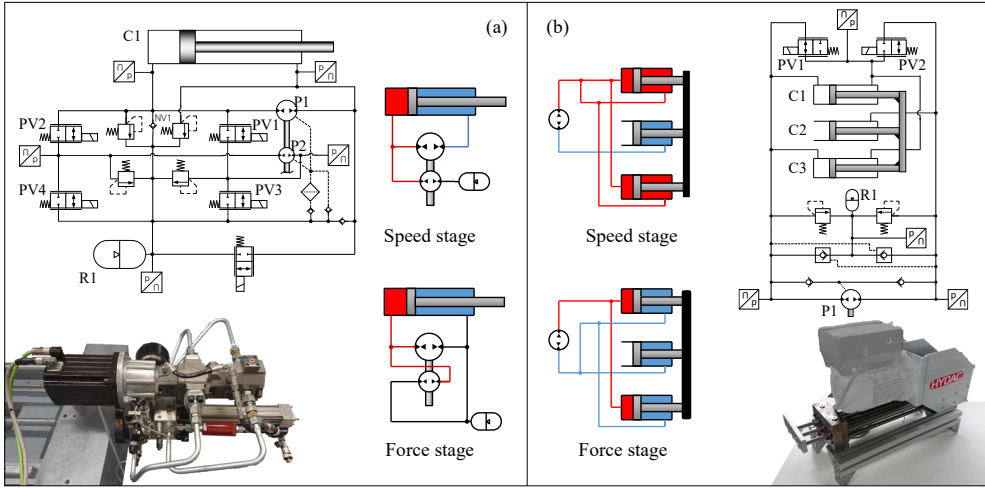
Figure 6: Demonstrators PBD (a) and ABD (b)

stage, where the sum of two pump outflows is connected to the head-side cylinder chamber while the rod-side chamber receives the flow only from the larger pump. Due to CHC, the ratio of pump displacement volumes has to be related to the cylinder area ratio. In force stage, an OHC is applied such, that the rod-side chamber is connected with the reservoir. The head side chamber receives a flow that results from the difference of both pump outflows. Torque reduction is due to one unit working in pump mode, and the other working in motoring mode on the same shaft. Switching is carried out via five 2/2 directional proportional solenoid cartridge valves. For details see [2].

The actuator-based switching demonstrator (ABD) comprises three parallel, identical single rod cylinders with mechanically coupled piston rods. In force stage, one pump port acts on the three rod-side chambers, while the other pump port acts on the two outer head-side chambers. The centre head-side chamber is constantly vented. In speed stage, the two outer rod side chambers are switched to the other pump port. Since the cylinders are dimensioned in a way that the cylinder unit acts as a statically symmetrical consumer in both stages, it can be operated in CHC with a single pump. However, in order to avoid any undesired pressure increase, pilot operated check valves are used to define the minimum pressure in the used system. Switching valves are two valves identical to the ones used in PBD. More details on this demonstrator can be found in [3].

In terms of the systemisation shown in Table 1, PBD can be considered PC1 and ABD can be considered AD2.

Significant parameters for both systems are listed in **Table 3**.

Table 3: Demonstrator dimensioning parameters

	PBD	ABD
Pump displacement	$V_{P1} = 10,8$ cm^3 $V_{P2} = 6,9$ cm^3	$V_{P1} = 5$ cm^3
Cylinder dimensions	ø(40mm/25mm) x 450 mm	ø(25mm/14,43mm) x 400 mm
Reservoir	$V_{tot} = 1,4$ l	$V_{tot} = 80$ ml
transm. range	1 : 4.5	1 : 3

4. SWITCHING STRATEGY

The aim of the switching process is to change the transmission. Obviously, a discontinuous switch to a different transmission ratio will lead to a disturbance of the system, similar to a step in the primary command signal of the prime mover.

In order to allow a smooth transition, valve trajectories are generated such that the transmission ratio is a smooth curve from start to end of the process. Further we demand

$$i^F \geq \frac{\omega(t)}{\dot{x}(t)} \geq i^S \tag{25}$$

throughout the switching process. Since due to valve opening, the drive is no longer a hydrostatic transmission, the load has to be taken into account.

4.1. Systematisation

In previous work [3, 2], the definition of a transmission stage allocates each pump port to any cylinder port or the reservoir port in case of pump-based switching, or allocates each cylinder port to any pump port or the reservoir in case of actuator-based switching, respectively. Thus, any switching process can be thought of as a sequence of reallocations of pump ports (pump-based switching) or cylinder ports (actuator-based switching). Reallocation of one port is called an elementary switching process (ESP), which is illustrated in **Figure 7**.
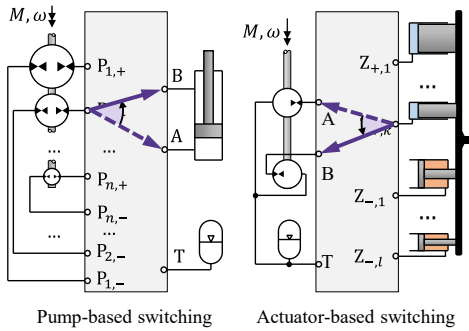

Figure 7: Examples of elementary switching processes

Any such ESP, of which global switching processes are constituted, have the logic of an electric two-way switch, or a 3/2-directional valve. A general way of realisation with one more degree of freedom is a combination of two 2/2-directional valve per ESP, as shown in **Figure 8**.
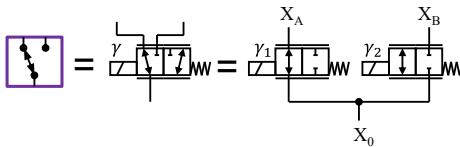

Figure 8: Valve architectures for ESP

The advantage of separating the switching process in ESP is unification of control strategies. Since all ESP can be treated similarly, even complex global switching processes can be broken down to manageable units.

The meaning of ESP in terms of the demonstrator drives is given in **Figure 9**. For PBD, there are two ESP that have to be switched consecutively. Between the two ESP, there is an intermediate state, in which the smaller pump idles at negligible pressure difference. The exact order, in which ESP1 and ESP2 are switched decide on

whether the pump idles at the pressure level of the reservoir or of the cylinder's head-side chamber. Before any switching is carried out, PV5 has to be opened in order to open the hydrostatic circuit on the rod-side chamber to reservoir. In case of ABD, only one ESP is required.
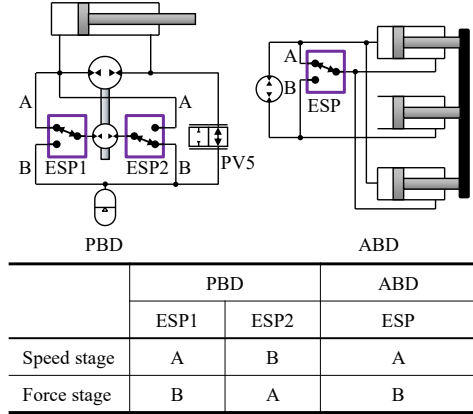

	PBD		ABD
	ESP1	ESP2	ESP
Speed stage	A	B	A
Force stage	B	A	B

Figure 9: ESP in demonstrator drives and state table

With reference to the nomenclature in **Figure 6**, ESP1 of PBD consists of valves PV2 and PV4, while ESP2 consists of PV1 and PV3. As to ABD, ESP obviously consists of PV1 and PV2.

4.2. Elementary switching process

Although all ESP have the same structure, the boundary conditions do vary between pump-based and actuator-based switching. With reference to the port labels in **Figure 8**, pump-based ESP can be considered to have an independent flow input at port X_0 due to exclusively having one pump port directly attached, and independent pressure input at port X_A and X_B depending on load. When considering actuator-based switching, flows and pressure on all ports depend on interaction of loads, pump speeds and valve positions. However, strategies developed for the simpler pump-based switching proved to work for actuator-based switching as well.

Modelling of ESP is carried out based on the system depicted in **Figure 11**. It is governed by turbulent valve flow and flow continuity:

$$Q_0 = Q_A + Q_B \tag{26}$$

$$Q_A = B \cdot \gamma_A \cdot \text{sgn}(p_0 - p_A) \cdot \sqrt{|p_0 - p_A|} \tag{27}$$

$$Q_B = B \cdot \gamma_B \cdot \text{sgn}(p_0 - p_B) \cdot \sqrt{|p_0 - p_B|} \tag{28}$$

B is the turbulent flow coefficient that accounts for nominal valve flow at a given pressure difference.
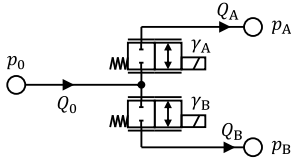

Figure 11: ESP model

Control strategies for the proportional valves of an ESP are based on a static analysis of the switching process with the boundary conditions of pump-based switching at constant motor speed and constant load. An exemplary analysis under such constraints is given in **Figure 10** in the plane over the two normalized openings of the valves involved. Any switching process requires a transition from point X to Y or vice versa across the plane. Any trajectory through the plane results in increased loss over the valve control edges. Every load and speed condition exhibits a saddle point of minimum unavoidable power loss, marked with 'M' in the given example.

Choosing a bilinear valve trajectory through the saddle point 'M' as shown in Figure 10 minimises losses and fulfils eq. (25). Moving the corner point further towards the upper right results in flow losses (short-circuit flow across the valves ($Q_A < 0$)) and thus violates eq. (25). Moving it further down towards lower γ_B results in drastic pressure increase and thus torque loss. At negative Q_0 it would even lead to serious cavitation.

With such valve trajectories, the challenge is to meet accuracy requirements using simple direct solenoid driven valves without spool position feedback. Around point 'M' the pressure p_0 is sensitive to valve spool position, leading to dynamic excitation of the system especially at actuator-based switching.

A more robust strategy therefore makes use of a p_0 pressure feedback to 'guide' one valve control signal along it correct trajectory. An overview of the strategy is given in the following, with reference to Figure 10:

Depending on flow direction of Q_0 and direction of pressure difference across the switch $p_A - p_B$, the saddle point 'M' lies on one of the axes γ_A or γ_B. As a characteristic property of the proposed control strategy, the valve command signal on whose axis 'M' is located, is governed by a pressure feedback controller. In the example given in Figure 10, this is signal γ_B. For the exemplary transition from point X to point Y, the control strategy is given in **Figure 12** by means of state chart notation.
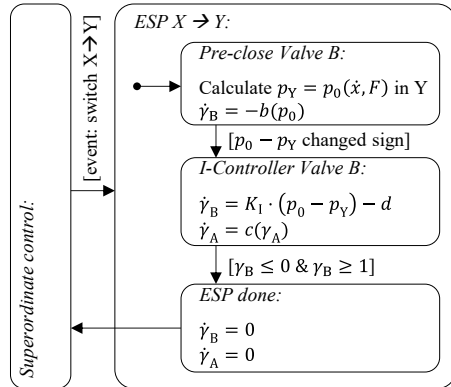

Figure 12: ESP sequence X→Y, see Figure 10

First, the valve B is closed using a trajectory that takes p_0 into account in order to prevent overshoot. During that process, the pressure p_0 corresponding to point 'Y' is constantly calculated based on measurement data. Once p_0 reaches that
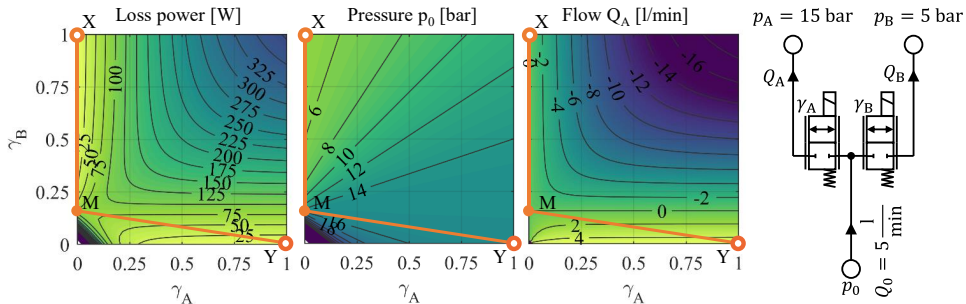

Figure 10: Static behaviour of the ESP for exemplary boundary conditions

pressure p_Y, the integral pressure feedback controller is activated to keep p_0 at p_Y while opening valve A. The term d in the pressure feedback control law makes sure that valve B closes and the switching process carries on. When the conditions of point 'Y' are met in terms of valve command signals, the ESP is completed. The parameters or functions K_I, b, c, d have an impact on the smoothness and duration of the ESP, however an optimal set is yet to be defined and depend strongly on the dynamic properties of the system and valves.

5. VALIDATION

The pump-based switching demonstrator is used to validate both the switching strategy and the downsizing potential on a load test stand. In the following, a range of experimental results will be presented. Results using ABD remain subject of future publications.

5.1. Switching strategy

The first example shown is a switching procedure from speed stage to force stage at constant motor speed of $n = 1000 \text{ min}^{-1}$ for different load forces, with result plotted in **Figure 13**. The cylinder velocity at low load force ($F = 1 \text{ kN}$) took a smooth decline over the course of switching, regardless of whether the smooth switching strategy was applied ($\Delta t = 0.25 \text{ s}$) or whether all valves were operated at the same time and as fast as possible ($\Delta t = 0 \text{ s}$). The smooth transition at discrete switching operation may be due to low response of the valve, but cannot be verified since spool position measurement is not implemented.
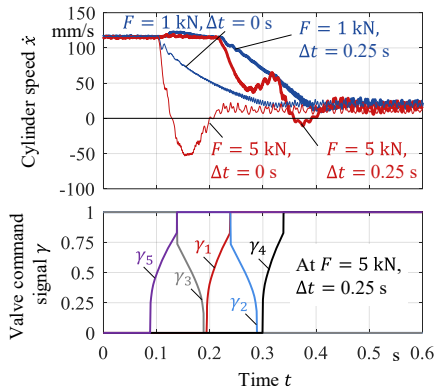

Figure 13: Switching from speed stage to force stage at $n = 1000 \text{ min}^{-1}$ at constant load force F

At higher load, the smooth switching strategy yields a smoother transition and less overshoot than discrete switching. When all valves are actuated at one time, uncontrolled short-circuit flow makes the mass accelerate in direction of external load, which is prevented using the above described valve trajectory.

The bottom diagram of Figure 13 shows the valve command signals during the controlled switching process. Integral-dominated pressure feedback control lets both valves be closed at the same times ($t = 0.19 \text{ s}$ and $t = 0.29 \text{ s}$) in both ESP. That would mean the flow to be blocked and dramatic pressure increase or cavitation at on pump port. The absence of these proves that the spool positions of the closing valves lack behind their command signal significantly.

A similar switching procedure was run at a motor speed that was generated by a dynamic feedforward control to keep the cylinder speed constant. The controller calculates the motor speed according to desired cylinder speed trajectories, taking plant dynamics, load force and valve positions into account. Measurement result are shown in **Figure 14**.
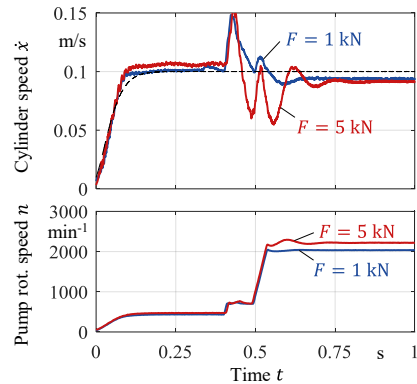

Figure 14: Switching from speed stage to force stage at constant load force F and with feedforward speed control

It becomes obvious that while switching, the trajectory cannot be tracked by the motor speed command. The reason is mainly related to deviations between valve command signal and actual spool opening. The feedforward control law receives the valve command signal and calculates required rotational speeds based on these.

5.2. Downsizing potential

Downsizing potential of the demonstrator drive

can be assessed by mapping the torque require-ment over speed and load force in speed stage and force stage. The associated measurement results are illustrated in **Figure 15**. Speed stage record-ings could not exceed a load force of 7 kN in the experiment, since the used motor was restricted to a nominal torque of 20 Nm. Linear extrapola-tion of the curves however is admissible. A torque reduction due to force stage can clearly be observed at high load force. Given a maximum torque of 20 Nm, the achievable force in force stage is about three times the achievable force in speed stage.
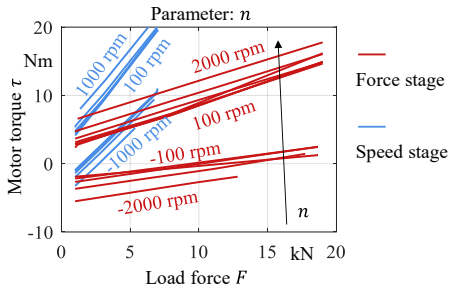

Figure 15: Measurement of torque over speed and force

As further proof of concept, the press brake cycle analysed in Figure 4 is implemented on the load test bench. The results in terms of torque are com-pared in **Figure 16** for the demonstrator in speed stage only and with switching activated. The re-sulting ratios of maximum and equivalent force are $\alpha_{\tau,\max} = 0.31$ and $\alpha_{\tau,\max} = 0.43$ respec-tively, resulting in the estimated cost reduction shown in Figure 16.
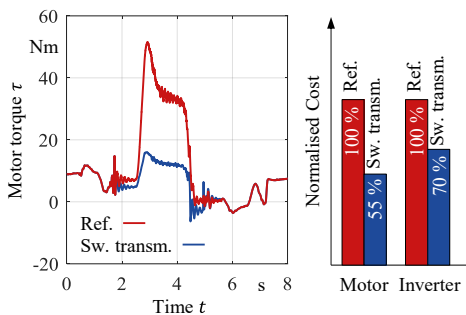

Figure 16: Measurement of torque in press brake cycle from Figure 5, for reference and switching driving

The cost reduction is lower compared to the re-ductions estimated under ideal conditions, as shown in Figure 5. This is mainly due to to

causes: Firstly, pump friction has a major impact on motor torque in force stage and, secondly, the transmission range of the demonstrator is lower than the optimal transmission range for the cho-sen load cycle, due to a restricted choice of cylin-der area ratios, as documented in [2].

6. CONCLUSION AND OUTLOOK

The paper at hand provides a guideline on how to estimate the downsizing potential of variable transmission linear drives in comparison to fixed transmission drives, depending on a given load cycle. For an exemplary press brake cycle, the maximum downsizing potential is estimated to be around 80 % in terms of torque. Using a demon-strator drive, the achievable downsizing potential was reduced to 57 % mainly due to pump friction. Even with friction related losses, substantial cost savings of the electric components can be real-ised.

A general approach to handle switching pro-cesses for discrete variable transmission drives is given and applied to the demonstrators. Switch-ing smoothness was found to be improved with valve trajectories based on pressure feedback in comparison to discrete switching, although valve accuracy proved to be crucial to attainable switching smoothness in general. When it comes to adoption of the strategy for application in pro-duction machinery, thorough measurement and characterization of the used valves is necessary to meet accuracy specifications when switching un-der load occurs.

Approaches that may be investigated in future work are ballistic switching strategies that might be applied when inertia is high in comparison to external load forces.

ACKNOWLEDGEMENT

NOMENCLATURE

ABD   Actuator-based switching demonstrator

CHC   Closed hydrostatic circuit

ECD	Electro-hydrostatic compact drive	
EMD	Electromechanical drive	
ESP	Elementary switching process	
ETC	Equivalent torque criterion	
MTC	Maximum torque criterion	
OHC	Open hydrostatic circuit	
PBD	Pump-based switching demonstrator	
VTR	Variable transmission ratio	
eff	Effective	
eq	Equivalent	
F	Force stage	
max	Maximum	
Mot	Motor	
nom	Nominal	
OL	Overload	
P	Pump ports	
Inv	Inverter	
Ref	Reference	
S	Speed stage	
T	Reservoir port	
tot	Total	
X	Port label	
X,Y	Operation points	
Z	Cylinder ports	
A	Area	m²
B	Flow coefficient	$m^3/s\sqrt{Pa}$
b	control parameter	1/s
c	control function	1/s
d	control parameter	1/s
F	Force	N
I	Electric current	A
i	Transmission ratio	-
K_I	Integral gain	1/Pa s
n	Rotational speed	1/s
p	Pressure	Pa
P	Power	W
Q	Flow rate	m³/s
t	Time	s
T	Time interval	s
V_P	Pump displacement volume	m³
x	Cylinder position	m

α	Ratio parameter	-
γ	Normalised valve command signal	-
τ	Torque	Nm
ω	Angular speed	rad/s

REFERENCES

[1] Brahmer, B.: On Adaptive Electro Hydrostatic Actuators. In: *Proceedings of the 11th International Fluid Power Conference (11. IFK)*. Aachen, Germany, 2018

[2] Kolks, G.; Weber, J.: Compact Cylinder Drives with Variable Transmission Ratio Using Multiple Pumps. In: *Proceedings of the 10th Workshop on Digital Fluid Power*. Linz, AT, 2019

[3] Kolks, G.; Weber, J.: Symmetric Single Rod Cylinders with Variable Piston Area? A Comprehensive Approach to the Right Solution. In: *Proceedings of the ASME/BATH 2018 Symposium on Fluid Power & Motion Control : FPMC 2018*. Bath, UK, 2018

[4] Sprockhoff, V.: *Untersuchungen von Regelungen im hydrostatischen Zylinderantrieb mit Servopumpe*. RWTH Aachen. Dissertation. 1979

[5] Berbuer, J.: *Neuartige Servoantriebe mit primärer Verdrängersteuerung*. RWTH Aachen. Dissertation. 1988

[6] Michel, S.; Weber, J.: Electrohydraulic compact-drives for low power applications. In: *Proceedings of the 7th FPNI PhD-Symposium on Fluid Power*. Reggio Emilia, Italy, 2012

[7] Michel, S.: *Energieeffiziente elektrohydraulische Antriebe kleiner Leistung*. Dresden, TU Dresden. Research Report. 2012

[8] Çalışkan, Hakan; Balkan, Tuna; Platin, Bülent E.: *A Complete Analysis and a Novel Solution for Instability in Pump Controlled Asymmetric Actuators*. In: *Journal of Dynamic Systems, Measurement, and Control* 137 (2015), Nr. 9, 091008-091008-14

[9] Williamson, C.; Ivantysynova, M.: Stability and motion control of inertial loads with displacement controlled hydraulic actuators. In: *Proceedings of the 6th FPNI PhD-Symposium on Fluid Power*. West Lafayette, USA, 2010

[10] Ketelsen, Søren; Padovani, Damiano; Andersen, Torben; Ebbesen, Morten; Schmidt, Lasse: *Classification and Review of Pump-Controlled Differential Cylinder Drives*. In: *Energies* 12 (2019), Nr. 7, p. 1293

ROBUSTNESS OF THE LIEBHERR-AEROSPACE EHA TECHNOLOGY FOR FUTURE FLIGHT CONTROL APPLICATION

Tobias Röben[1]*, Emmanuel Viennet[2], Henry Wider[3]

[1] *Liebherr-Aerospace Lindenberg GmbH, Pfänderstrasse 50-52, 88161 Lindenberg, Germany*
[2] *HES-SO University of Applied Sciences and Arts Western Switzerland, 1700 Fribourg, Switzerland*
[3] *Liebherr Machines Bulle SA, Rue Hans Liebherr 7, 1630 Bulle, Switzerland*
* Corresponding author: Tel.: +49 8381 46 5615; E-mail address: tobias.roeben@liebherr.com

ABSTRACT

Future more electric aircraft (MEA) architectures require a new generation of power-by-wire actuators, e.g. Electro Hydrostatic Actuators (EHA). These units have to be capable of frontline operation of safety critical flight control surfaces over the entire aircraft life. Prove of robustness becomes a challenging objective. This paper illustrates the Liebherr-Aerospace EHA technology as well as methods for validation of robustness. It gives an insight regarding the design of a robust piston pump.

Keywords: EHA, More Electric Aircraft, piston pump, robustness

1. BACKGROUND

State of the art aircraft architectures for civil aircraft embody a significant share of electrically driven systems (More Electric Aircraft) compared to the traditional importance of hydraulics and pneumatics in aviation. These more electric architectures require new equipment, e.g. power-by-wire actuators and power control electronics. For the safety critical application of primary flight controls Electro-Hydrostatic Actuators (EHA) are favored, because they still rely on hydraulic actuation (refer to **Figure 1**). However, in contrast to conventional servo-hydraulic actuators these units form a local, independent hydraulic circuit, which is powered by an electric motor and a fixed displacement piston pump. Therefore, hydraulic power is generated only, when it is needed for the actuation of the relevant flight control surface. Furthermore, these units are easy to install and maintain.

Axial piston pumps are of great importance in industrial applications. Nevertheless, this experience cannot be transferred to aviation. While pumps are usually operated in a distinctive nominal condition, e.g. to maintain a certain pressure level, EHA for flight control application are designed to provide maximum performance under worst-case condition: low temperature, high air loads and dynamics.

However, the actual dynamic and loads are less most of the time. The pump is even operated bidirectional to enable extension/retraction and in motor mode, when external loads are supporting the motion. Thus, the pump has to provide good efficiency in all these operating conditions and it must especially be robust against operation in the partial load range.
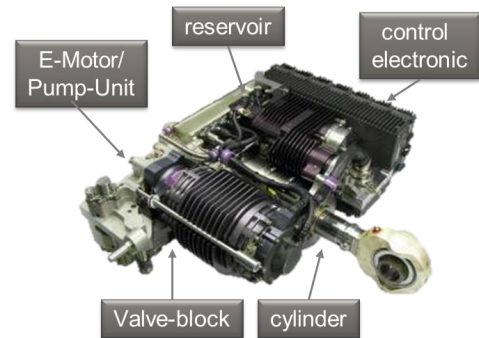
Figure 1: State of the art Liebherr-Aerospace EHA

2. ENDURANCE TESTING

Since stick-slip effects and mixed friction are critical mechanisms causing pump wear, the varying operating conditions must be considered, in order to prove the robustness of EHA for the safety critical flight control application. For this reason, Liebherr-Aerospace chose a two-way approach of testing.

2.1. Unit level tests

To prove robustness in a most representative environment, a qualification test rig of an in-series project has been re-used for long term testing considering a representative endurance cycle (**Figure 2**). Here every test hour relates to one Flight Hour (FH), but in laboratory environment.

Figure 2:   Unit level test endurance test rig

This approach is elaborative and expensive: One random sample unit was tested and operated for more than 5 years to accumulate about 35'000FH. Since it constitutes merely one sample of a given application, it only gives an idea of the robustness of this technology. Nevertheless, such a test shows the general long-term behavior of the pump design.

Basically, three interfaces of tribological contact can be distinguished (refer to **Figure 3**):

- Cylinder barrel / valve plate (yellow)
- Piston / cylinder bore (blue)
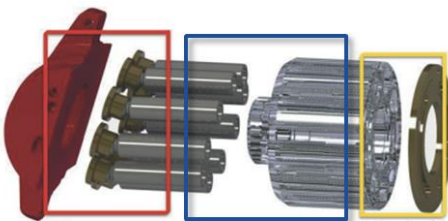- Slipper / swash plate (red)

Figure 3:   Interfaces of tribological contact within a fixed displacement axial piston pump [1]

Thanks to state-of-the-art manufacturing tolerances and surface treatments, usually the piston and cylinder bore interface is not critical in axial piston pumps [2]. The more sensitive interfaces are the valve plate interface and the swash plate interface.

To avoid jamming of contact pairs in motion

usually a weaker and a more hard material is chosen. This combination inherently causes the weaker material to wear off during operation. For all three tribological areas within the considered piston pump the material combination is brass and hardened steel.

In order to determine the pump's health state (resp. degradation) continuously, the progression of the volumetric efficiency is monitored over time (refer to **Figure 4**). For a given operating condition the volumetric losses of a system are comparable [3]. This condition is determined by the temperature resp. viscosity, the operating pressure and the displacement rate.
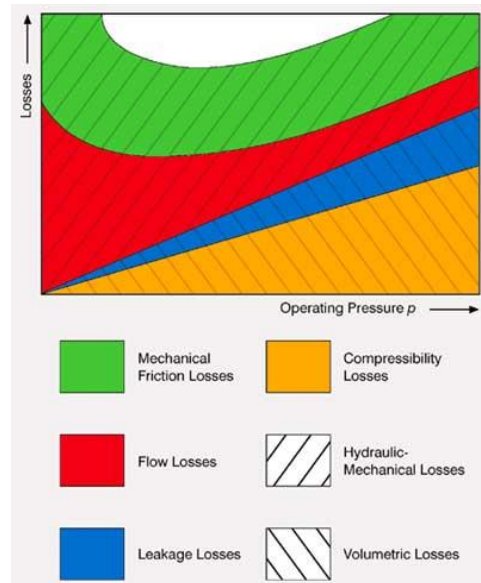

Figure 4:   Losses in a hydraulic drive [3]

Accordingly, in order to determine the volumetric losses in the closed system at hand without a flow meter, the pressure holding speed is measured. This is the rotational speed of a fixed displacement pump, which is required to maintain a defined operating pressure at a given temperature. Depending on the level of degradation, an increase of the rotational speed is expected. In **Figure 5** the progress of this speed is illustrated for the given EHA over its operating hours.

For the first 25000 operating hours the overall leakage is constant and the respective pump speed remains below 50rpm. In the following the continuous abrasion exceeds the filter capacity of the unit; the filter clogs and the increased pre-

filter pressure causes the bypass valve to open. As a consequence the wear particles are circulating within the closed hydraulic circuit unfiltered. This results in exponential wear of the pump's sealing surfaces and leakage. A maximum value of 500rpm (factor 10) is reached after 27000 operating hours (refer to **Figure 5**).
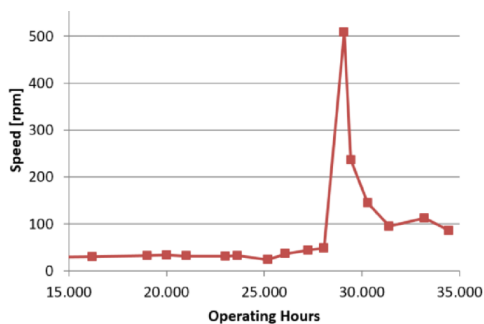

Figure 5: Progression of internal leakage over time for fluid temperature of 40°C.

A subsequent inspection of the actuator indicated that the degrading performance is related to the contamination of the hydraulic fluid. An analysis of both fluid and filter revealed steel particles, which arise from the drive shaft bearings. The bearings showed wear marks, accordingly. The pump itself showed slight wear marks, but was considered to be undamaged still. Hence, the unit has been flushed with fresh oil and reassembled with a new set of bearings and filter cartridge for test continuation.

Once the unit has been maintained, the volumetric efficiency increased again (refer to **Figure 5**). Even though the pressure maintenance speed remains higher than the initial value, it stabilizes at about 100rpm, which is still within the nominal operating range of the actuator. This value is constant until the end of testing close to 35000 operating hours.

The fact that the performance of the unit recovers after the refresh of fluid, illustrates the failure tolerance of the EHA design.

However, while the pairing of cylinder and valve plate seems to be uncritical, for the given piston pump it was rather the slipper / swashplate interface, which suffered wear later on. Solely here material removal was visible; the slippers have been worn off dramatically to the end of the endurance test at about 35000 operating hours (refer to **Figure 6**). Not only was the material removed on the slipper sealing surface. As a

consequence, from the increasing clearance between slipper, swash plate and retainer plate, shocks occurred between the slippers and the hardened retainer plate causing wear in the slipper shoulder.

Figure 6: Slipper wear after 35'000 hours of endurance testing

Nevertheless, even though the wear of the slippers is immense, the EHA was still able to provide the required performance, when the first pistons have been separated from the slipper, so that they did not provide pressure anymore. This again illustrates the pump's failure tolerance.

However, the corresponding noise and vibration lead to the conclusion that condition monitoring is a reasonable approach to detect a pump failure and might possibly facilitate predictive maintenance.

Furthermore, this endurance test creates confidence in the pump technology and the specific EHA design. Several 10'000FH are more than what is required for today's aircraft, where the EHA technology is a backup solution that operates actively merely for 100 to 1'000FH within an aircraft life.

2.2. Pump level tests

An even more efficient approach to investigate the pump wear behavior are tests on pump level. While a flight control EHA is a highly integrated and complex unit, the Liebherr-Aerospace pump test rig (refer to **Figure 7**) provides a deeper view inside the pump via additional laboratory sensors, like particle sensors and viscometers as well as a number of temperature sensors. Following the endurance spectrum of the considered actuator, sinusoidal oscillations are applied covering a representative range and amount of pressure and speed cycles (refer to **section 1**).

Figure 7: Pump level test rig at Liebherr-Aerospace Lindenberg GmbH

Thereby the influence of distinctive operating conditions (speed, pressure, temperature, fluid etc.) on the generation of wear particles can be investigated. The hydraulic schematic of the pump test rig is illustrated in **Figure 8**.
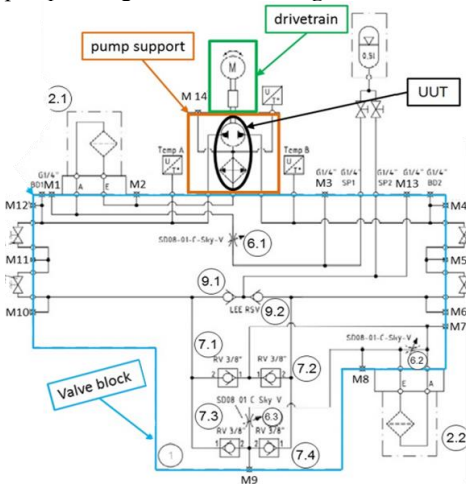

Figure 8: Pump level test (schematic)

Another purpose of the pump test rig is to reproduce the wear mechanism that has been identified during the previous unit level tests and thereby validate the test results. Furthermore, condition monitoring functions, which have been developed model based, are validated iteratively within the pump test rig environment. Finally, the goal is to facilitate and expedite the generation of reliable data that allows for the optimization of the pump design or the system architecture (choice of fluid) as well as for the online monitoring of its health condition.

Initially, the basic characteristics of the pump

have been determined. In order to measure the drag torque in different operating points a torque measuring shaft was introduced into the drive train. Subsequently the data was post-processed, in order to distinguish between the load and the relevant drag torque as follows:

$$T_{drag} = T - \frac{\Delta p \cdot D}{2\pi} \qquad (1)$$

In **Figure 9** the drag torque is illustrated for various pressure and temperature levels. Similar to the Stribeck curve dry friction occurs for low rotational speed. In case of lubricated friction at higher speed, the drag torque is reduced to a minimum at around 500rpm. For even higher speed of several 1000rpm viscous fluid friction is dominating. However, in contrast to the static friction at low speed, solid contact is avoided.
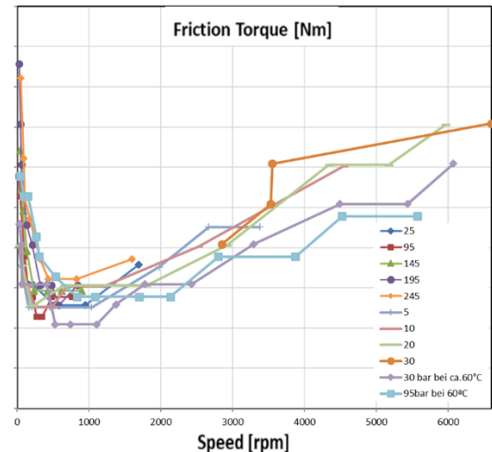

Figure 9: Calculated drag torque for varying speed and pressure level

However, it is remarkable that the drag torque is independent from the pressure level, which has been varied between 5bar and 245bar. Furthermore, the reduced viscosity at higher temperatures (violet and light blue line) results merely in a slight increase of low speed friction, but also in a reduced fluid friction at high speed.

Primary flight control actuators (e.g. aileron) perform an oscillating (corrective) motion during flight, which causes the pump to be operated bi-directionally. According to **Figure 9** every change of direction is connected to a start-stop, where lubrication is a key.

The unit level tests highlighted the major importance of the lubricant for the health condition of the EHA. Hence, on pump level the fluid condition is monitored by several means.

First, the particle contamination is identified with the aid of particle sensors according to the SAE AS4059. Depending on the particle size (2-25µm) the respective class of contamination is illustrated in **Figure 10** over time. While the sensor does not distinguish between the type of particles, the initial fluid contamination is high. Due to the integrated filter (5µm) the amount of particles in class B, C and D is reduced throughout the testing (>400h). With continuing abrasion the filter capacity is exceeded after 900h of testing. Here the fluid contamination increase rapidly, which is correlating with an increased pre-filter pressure.
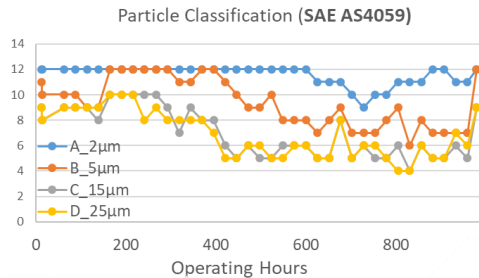

Figure 10: Generation of fluid contamination

As mentioned above, the particle sensor does not distinguish between metallic and other sources of contamination, like dust. However, especially the hard metallic materials are more harmful for the pump wear. Further, particle sensors do not detect micro-particles (<2µm). Yet, it is considered that the amount of micro-particles increase, whereas greater particles are bound within the filter.

In contrast, the fluid conductivity constitutes a more expressive characteristic (refer to **Figure 11**). Precisely because it does not differ the size of the particles, it relates to the overall amount of metallic contamination within the system; and therefore it is a significant characteristic with respect to the progressing deterioration due to tribological wear. In contrast to the complex particle sensors, the determination of the fluid conductivity is less complex and therefore more reliable.

The sensitivity of the conductivity is illustrated by the curve in **Figure 11**. It has a slightly exponential characteristic and spans over magnitudes. Similar to the particle concentration

(refer to **Figure 10**), the conductivity also increases rapidly after 900h, when the filter clogs. However, the fact that the first conductivity measurement after 13 hours of operation is merely 1.5nS/m points out that the initial fluid contamination given by the particle sensor is not resulting from metallic but rather dust particles.
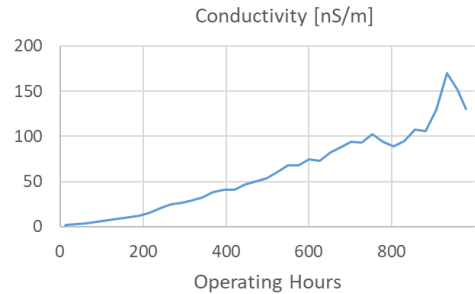

Figure 11: Generation of fluid conductivity

3. CURRENT PUMP DESIGN

Within the previous section test data was presented, which illustrates both the robustness of the current Liebherr piston pump and the wear effects related to the primary flight control application.

In the following, the current pump design is described in detail with respect to the wear findings. Design improvements are presented, which have potential of optimization with respect to long-life operation of the pump.

3.1. Operating conditions

In order to increase the power density and hence to minimize the weight, the pump used in Liebherr-Aerospace EHA has a displacement less than 1 cm^3/rev and operates on a very broad range of velocity.

In addition to that, the design of the EHA is very compact, see **Figure 1**, and it is typically encapsulated within the aircraft structure. According to [4], in spite of counter-measures at the aircraft level, for instance with openings made in the wings to improve air circulation and cooling, the heat generation within the EHA is a critical issue.

Due to these severe operating conditions, designing an EHA pump with high performance and long service time is a challenging task, which can be broken down into four main issues,

according to [5]:

- Cavitation erosion, mainly a consequence of high rotation speed and high pressure necessary for achieving a good power density
- Flow and pressure ripples, because of the difficulty to optimize a valve plate of EHA pumps on a very broad operating range
- Tilting motion of the rotating group, again a consequence of high rotation speed leading to high centrifugal forces of pistons and slippers
- Heat issue, because of high power density and compactness

3.2. Inclined-piston design

The pump under investigation, developed by Liebherr, is an axial-piston pump of swash plate type whose 7 pistons are inclined with respect to the rotation axis of the pump, see **Figure 12**.
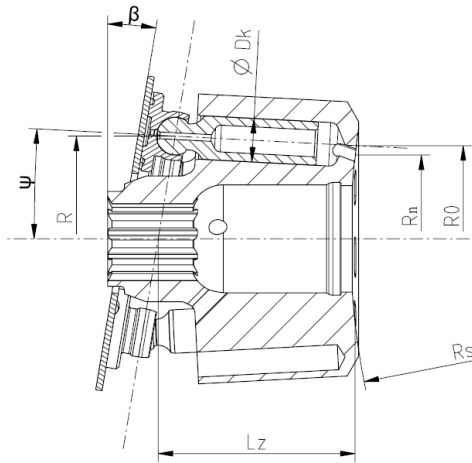

Figure 12: Sketch of the rotating group with pistons inclined with respect to rotation axis

The piston stroke for such a pump is given in [6] as follows:

$$H_K = \frac{2 \cdot R \cdot tan\,\beta}{cos\,\psi \cdot (1 - tan\,\psi \cdot tan\,\beta)} \qquad (2)$$

Where:

- β is the swash plate angle
- ψ is the inclination angle between the pistons and the rotation axis of the pump
- R is the distance from the piston sphere center to the rotation axis of the pump when the piston is at the inner dead center (furthest position within the cylinder-block)

Axial-piston pumps with inclined pistons are less common than in-line pumps and show more complicated kinematics and dynamics. Nevertheless they have a few very interesting characteristics, especially for high-speed applications.

3.3. Clamping force on the slippers

At high rotational speed, two main effects tend to separate the slippers from the swash plate. The first significant effect arises because the center of mass of the slipper does not generally coincide with the center of the piston-slipper ball joint. Therefore, the centrifugal forces acting on the slippers generates a centrifugal tilting moment that tend to tilt the slipper towards its inner edge. For inclined-piston designs like the pump under investigation, this effect is slightly higher near the outer dead center where the slipper is further from the pump rotation axis.

The second – even more – significant effect is due to the axial acceleration of piston-slipper assemblies. The resulting inertial force pushes the slipper against the swash plate during 180° of its travel on the outer dead center side while it tends to pull the slippers away from the swash plate during the other 180° on the inner dead center side.

In the region of the inner dead center, the two main effects described above add to each other and a sufficient clamping force is needed to prevent the slippers from lifting or tilting. In pumping mode, when the slipper approaches the inner dead center, it is connected to high-pressure port and a sufficient clamping force can be achieved with available pressure. However, once the slipper has passed over and goes away from the inner dead center, it is connected to the low-pressure port, hence with only a limited clamping force available from the pressure. The situation is even more critical if one considers that due to pressure losses in the inlet duct at high speed, the actual pressure in the piston chamber might be even lower than the inlet pressure.

Therefore, sufficient clamping of the slippers requires countermeasures to be taken like for instance increasing the inlet pressure and/or using a positive force retaining mechanism. However both these design changes induce extra losses, especially at low speed where this extra clamping force is actually not needed.

In this context, the design of the Liebherr EHA

pump has the benefit that the inclined pistons generate an axial component of the centrifugal force that act as an additional clamping force on the slippers. Since this force increases with the square of the rotational speed, it is mainly present at high speeds and does not cause additional losses at low speeds. For the pump under investigation, at high speed the inclined pistons generate a significant additional clamping force that is equivalent to an increase of approx. 2.5 bar in the inlet pressure.

3.4. Tilting of the cylinder-block

When an axial-piston pump operates at high pressure, the pressure in the cylinder bores typically generates a clamping force that helps maintaining the cylinder-block against the valve plate. However when the pump operates at low pressure and high speed, the inertial forces transferred from the pistons to the cylinder block tend to destabilize it by generating a tilting moment and since no clamping force is available from the pressure it is necessary to axially preload the cylinder block with the help of a spring. Again, this additional axial preload of the cylinder induces undesired extra losses, especially at low rotational speeds when this preload is not required.

Another interesting effect of the inclined pistons used in the Liebherr EHA pump is that the inertial forces acting on the piston/slipper assemblies generate an additional clamping force pushing the cylinder block against the valve plate. As for slippers, the clamping force generated on the cylinder block is only significant at high speeds and does not cause any loss at low speeds. For the pump under investigation, the inclined pistons allowed to reduce by a factor 2.0 the theoretical spring preload needed to prevent the cylinder block from tilting at high speed in comparison to a design with in-line pistons.

4. PUMP DESIGN IMPROVEMENTS

4.1. Slipper / swash plate interface

The test results presented in this article show that the slipper / swash plate interface has suffered dramatic wear after 35'000 FH, which is an indication that there is room for optimization of the lubrication of this sliding interface. The lubrication mechanism involves a complex

thermal-fluid-structure interaction that has been addressed by an impressive research effort conducted in the recent years, especially under the guidance of Prof. Ivantysynova at Purdue University, see for instance [7]. Nevertheless, the simple macroscopic approach of computing a so-called hydrostatic balance factor is still of value when comparing two designs. The balance factor of a slipper in an inclined-piston design is very seldom detailed in literature. It is obtained as the ratio of the force generated by the slipper hydrostatic bearing $F_{hydro}[N]$ to the total reaction force perpendicular to the swash plate in static equilibrium condition $F_{reac}[N]$.

The hydrostatic bearing force is the same for in-line and inclined-piston design. It is obtained as follows:

$$F_{hydro} = \frac{\pi}{8} \cdot \frac{D_{Ga}^2 - D_{Ge}^2}{ln\left(\frac{D_{Ga}}{D_{Ge}}\right)} \cdot P_{HD} \qquad (3)$$

However, the total reaction force perpendicular to the swash plate surface is specific to the inclined-piston design:

$$F_{reac} = \frac{\pi \cdot D_K^2 \cdot P_{HD}}{4 \cdot \left(\begin{array}{c} cos\beta \cdot cos\psi \\ -sin\beta \cdot sin\psi \cdot cos\phi_i \end{array}\right)} \qquad (4)$$

Where ϕ_i is the angular displacement of the considered i[th] piston (with $\phi_i = 0°$ at the outer dead center) and the diameters D_K, D_{Ga} and D_{Ge} are shown in **Figure 13**.
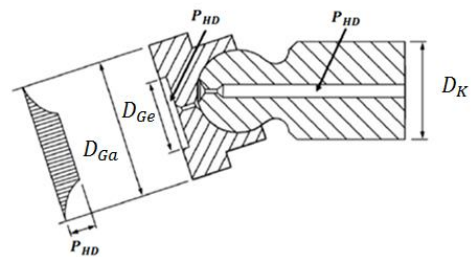

Figure 13: Hydrostatic pressure field under the slipper

It follows that the hydrostatic balance factor is slightly higher at inner dead center than at outer dead center. For the pump under investigation, this difference is, however limited to less than 2% and the balance factor of the slipper at inner dead center reaches a maximum value of approx. 90%. This indicates that a better lubrication – yet without significant increase of leakage – can be

achieved by increasing this value compared to the tested pump.

4.2. Valve plate design

The valve plate is a key component in an axial piston pump. Among others, it affects particularly the cavitation and the pump solid borne noise because it controls the pressure transients in the piston chambers. The pump under investigation does not feature any pressure relief grooves in the transition regions but rather has fixed pre- and decompression angles. While this design can give optimal results for one given operating point (working pressure and speed) this may lead to increased cavitation and/or extremely fast pressure transients for other operating points.

Therefore, the original design of the valve plate has been reviewed and a new valve plate has been proposed with pressure relief grooves. This new design aims at smoothing the pressure transitions over a relatively broad operating range. The numerical simulations conducted are based on a classical control volume approach described for instance in [8]. Example results for the obtained smoothing of pressure compression are shown in **Figure 14** and in **Figure 15**.
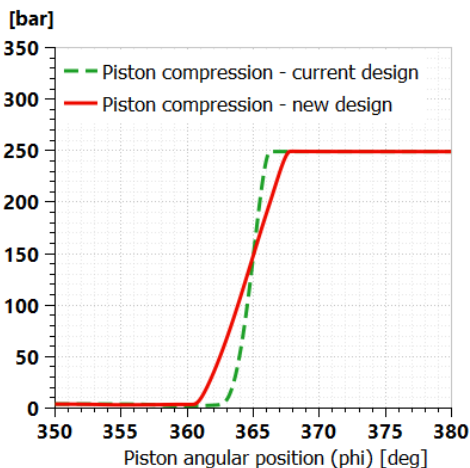
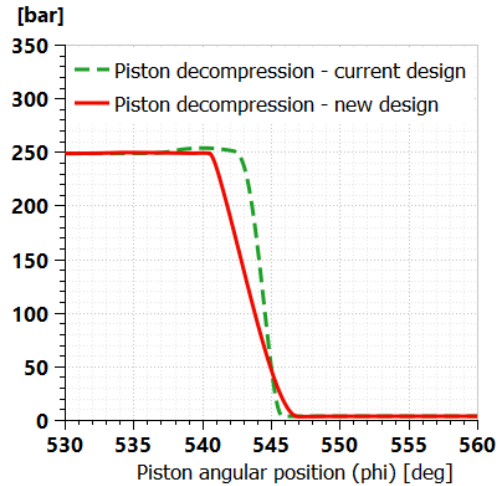**Figure 14:** Simulated pressure transients in piston chamber at outer dead center

Figure 15: Simulated pressure transients in piston chamber at inner dead center

5. CONCLUSION AND OUTLOOK

In general, this paper illustrates Liebherr's experience regarding piston pumps in primary flight control actuators, respectively EHA. The variety of data gathered by testing activities proves the robustness and failure tolerance of the current pump design. It complies with the challenging requirements of future more electric aircraft architectures. Therein the EHA could replace the conventional servo-hydraulic actuation and be operated in frontline for the whole aircraft life.

However, the test campaign also revealed the wear mechanism, which ultimately causes the piston pump to fail. Accordingly, two possible design modifications have been presented that might further increase the life time of the EHA technology. In particular the adaption of the hydrostatic balance factor of the slipper / swash plate interface is considered to be beneficial.

With the aid of the presented pump level test rig it is then possible to perform comparative test, in order to validate optimized pump designs. Moreover, innovative material combinations will be investigated. Apart from their wear behavior, hereby focus is also on materials compliant to environmental legislation, with a reduced share of lead for instance.

Furthermore, the acquired test data indicates, that despite the general robustness of the Liebherr pump design, a degradation of performance sets in, if the fluid quality cannot be assured. In case of a contamination with metallic particles the internal leakage within the system can increase exponentially. Hence, the continuous filtration of the hydraulic system is the key for long-term operation of EHA in primary flight controls.

Nevertheless, a degradation takes place over a considerably long time span and can be identified based on the monitoring of some basic features. The benefit of condition monitoring functions has been highlighted as a measure to reduce the remaining technological and financial risk constituted by today's limited maturity of EHA in civil aviation.

REFERENCES

[1] Roman Ivantysyn (2018) Investigation of the Thermal Behavior in the Lubricating Gap of an Axial Piston Pump with Respect to Lifetime, IFK2018, Aachen, Germany

[2] Gertraud Wolff (1977) Lässigkeitsverluste in Axialkolbenpumpen, Agrartechnik, Heft 5, 225-227

[3] Brendan Casey (2004) Determining Hydraulic Pump Condition Using Volumetric Efficiency, Machinery Lubrication, 9/2004

[4] Maré J-C (2017) Aerospace Actuators Vol. 2: Signal-by-Wire and Power-by-Wire, ISTE Editions Ltd., London

[5] Chao Q, Zhang J et al (2016) A Review of High-Speed Electro-Hydrostatic Actuator Pumps in Aerospace Applications: Challenges and Solutions, J of Mechanical Design, Vol. 141

[6] Ivantysyn J, Ivantysynova, M. (2001) Hydrostatic Pumps and Motors: Principles, Design, Performance, Modelling, Analysis, Control and Testing, Academia Books, Delhi

[7] Schenk A, Ivantysynova M (2011) An Investigation of the Impact of Elastohydrodynamic Deformation on Power Loss in the Slipper Swashplate Interface. In: Proceedings of the 8th JFPS International Symposium on Fluid Power, Okinawa, 2011

[8] Viennet E, Gaile A, Roeben T (2018) Noise and vibration reduction for an aerospace secondary controlled hydraulic motor, 11th International Fluid Power Conference, Aachen, 2018